Australian National University

Retinal ganglion cells: Physiology and Prosthesis

Raymond Chi Shing Wong

A thesis submitted for the degree of Doctor of Philosophy of
The Australian National University in May of 2013

Knowing is not enough, we must apply.
Willing is not enough, we must do.

- Bruce Lee

To my dear family

Declaration

I hereby declare that this thesis is composed of my original work, except where due reference has been made below. I have clearly stated the contribution of the collaborators in my thesis, and explicitly acknowledged to any assistance provided from others. I conducted all the experiments, analysed the data and wrote the thesis. The content of my thesis has not been submitted to qualify for the award of any other degree or diploma in any educational institutions.

There are four results chapters in this thesis. At the time of submission, Chapter 2 was published. The physiological data in Chapter 2-3 were used for modelling and were accepted for publication in two conferences. Chapter 4 had been partially published in conference abstracts. I have also given an oral presentation for partial results of Chapter 5 in a conference abstract and platform presentation.

Contributions:

Chapter 1: Professors William Levick (WRL) and Ted Maddess (TM) contributed to the second draft of the manuscript.

Chapter 2: Dr Brendan O'Brien (BJO) contributed to the first draft, data analysis and provided the cat data. Professor Michael Ibbotson (MRI) and Dr Shaun Cloherty (SLC) revised the manuscript. WRL and TM reviewed the modified version in the thesis. Mr Wen-Yen Wu helped on programming. Professor David Berson had given helpful comments.

Chapter 3: WRL and TM contributed to the second draft and provided advice on the data analysis.

Chapter 4: SLC contributed to the first draft for the conference paper that contained only part of the contents and was the first author for presentation purposes, he being a member of the society. BJO, MRI, Mr Alex Hadjinicolaou and Dr Hamish Meffin revised the conference paper. WRL and TM contributed to the full version of the second draft and the data analysis.

Chapter 5: BJO contributed to the experiment design. WRL and TM contributed to the second draft and the data analysis. Dr Craig Savage made the videos. Dr David Garrett provided the diamond stimulating electrodes. Associate Professor David Grayden, Dr Nicholas Price, Dr Andrew James and Professor Trevor Lamb had given helpful comments on the data analysis.

Chapter 6: WRL and TM contributed to the second draft.

Raymond C.S. Wong

May 2013

Published works:

Chapter 2:

Wong, R. C. S., Cloherty, S. L., Ibbotson, M. R., & O'Brien, B. J. (2012). Intrinsic Physiological Properties of Rat Retinal Ganglion Cells with a Comparative Analysis. *Journal of Neurophysiology*. doi: jn.01091.2011 [pii]10.1152 / jn.01091.2011

Chapter 4:

Cloherty, S. L., **Wong, R. C. S.**, Hadjinicolaou, A. E., Meffin, H., Ibbotson, M. R., & O'Brien, B. J. (2012). Epiretinal Electrical Stimulation and the Inner Limiting Membrane in Rat Retina. 2012 Annual International Conference of the IEEE Engineering in Medicine and Biology Society (EMBC), 2989-2992.

Additional published works relevant to the thesis but not forming part of it

Maturana, M., **Wong, R**., Cloherty, S., Ibbotson, M. R., Hadjinicolaou, A. E., Grayden, D. B., Burkitt, A. N., Meffin, H., O'Brien, B. J., Kameneva, T. (2013). Retinal ganglion cells electrophysiology: the effect of cell morphology on impulse waveform. The 2013 Annual International Conference of the IEEE Engineering in Medicine and Biology Society (Embc), Osaka, Japan.

Maturana, M., **Wong, R.**, Kameneva, T., Cloherty, S., Ibbotson, M. R., Hadjinicolaou, A. E., Grayden, D. B., Burkitt, A. N., Meffin, H., O'Brien, B. J. (2013). Predicting the location of the axon initial segment using spike waveform analysis: Simulations of retinal ganglion cell physiology. The Computational Neurosciences Conference 2013, Paris, France.

Wong, R.C.S., Garrett, D., Grayden, D.B., Savage, C., Apollo, N., Cloherty, S.L., Ibbotson, M.R., Prawer, S., Burkitt, A.N. and O'Brien, B., "Recreating vision with a retinal prosthesis", 33rd Annual Meeting of the Australian Neuroscience Society, Melbourne, 3-6 February 2013. Oral Presentation

Wong, R.C.S., Marginson, M., Cloherty, S.L., Ibbotson, M.R., O'Brien, B., "Can Spike waveform analysis identify some retinal ganglion cell types?", Proc. 32nd Annual Meeting of the Australian Neuroscience Society, Gold Coast, Australia, 29 January-1 February 2012. Poster Presentation.

Hadjinicolaou, A.E., Kameneva, T., **Wong, R.**, Grayden, D.B., Cloherty, S.L., Ibbotson, M.R., Burkitt, A.N., Meffin, H., O'Brien, B., "Sinusoidal stimulation of retinal ganglion cells: computational model and experimental results.", Proc. 32nd Annual Meeting of Australian Neuroscience Society, Gold Coast, Australia, 29 January-1 February 2012. Poster Presentation.

Kameneva, T., Hadjinicolaou, A., **Wong, R.**, Grayden, D.B., Burkitt, A.N., Meffin, H., O'Brien.,B., "Simulating electrical stimulation of degenerative retinal ganglion cells with bi-phasic pulse trains.", Second International Conference on Medical Bionics, Phillip Island, Australia, 20-23 November 2011. Poster Presentation.

Wong, RCS, Cloherty, SL, Ibbotson, MR & O'Brien, BJ, "Are retinal ganglion cell intrinsic physiological properties conserved?", Association for Research in Vision and Ophthalmology (ARVO), Fort Lauderdale, USA, 2011. Invest Ophthalmol Vis Sci, vol 52, E-abstract 4572. Poster Presentation.

Wong, RCS, Raj, DS, Cloherty, SL, Ibbotson, MR & O'Brien, BJ, "Intrinsic physiological properties of rat retinal ganglion cells", Proc. 30th Annual Meeting of the Australian Neuroscience Society, Sydney, February 2010. Poster Presentation.

Acknowledgements

I am still not too sure if it was altogether the right choice to leave my family for my PhD research in Australia, especially the last two years were not easy at all. Seeking knowledge has a lot of fun and full of challenges. Somehow I feel responsible to contribute to this research. Without the support from my lovely wife Suk Kwan and my family, I could not come this far. I am delighted that it is finally the time to conclude the work of the last four years. My pleasure is equal only to my appreciation for all the great help I have gotten from many people. From time to time, they gave me their helping hands without asking for a return, which meant a lot to me.

I found it easier to thank everyone in chronological order. However, first and foremost I would like to express my gratitude to my supervisors Professors Ted Maddess and William Levick. Ted is the white knight who pulled me out from the mud. His guidance has been very important for me, both in academic and personal life. If he counts the million thanks I gave him, he will be a multi-billionaire by now. I owe him big time. Bill turns my eyes on research upside down. He has an unparalleled knowledge of the literature and a very unique way of thinking. I have really enjoyed the intensive meetings with him in the past few months.

More than a decade ago, I was inspired by the work done on retinal prosthesis by Professor Nigel Lovell. Unfortunately my scholarship arrangement didn't work out at that time. However, his enthusiasm was very encouraging and it was one of the main reasons I still want to work on retinal prostheses half a decade later. Professors Philip Parker and Jim Reilly are always there when I needed advices. I thank Professor Michael Ibbotson for assisting with my admission into the Australian National University (ANU) and scholarship. I am indebted to numerous agencies for the provision of funding and resources.

Most of my research training, travel to conferences, and personal life were generously supported by the ARC Centre of Excellence in Vision Science (aka the Vision Centre). I was the part-time web-administrator for the centre. Besides earning money to survive, I also got many chances to find out about the different fields of vision researches and to get in touch with many researchers. I would like to thank the former Director Professor Trevor Lamb, the present Director Professor Ted Maddess, and the Centre managers: Ms Dorothea Huber, Dr Adnan Syed Muhammad, and Ms Bryony Webster, for

their efforts in running the centre. Trevor also helped me on my return to ANU, and taught me some of his lab techniques.

If Drs David Tsai and Ben Sivyer didn't tell me about the Australian Course in Advanced Neuroscience (ACAN), I would have kept doing my experiments in my own creative ways. Ben also taught me a few things about rabbit retinas, and he was very kind to give me a copy of his thesis. He is my role model. He has been very successful lately and I wish him all the best. ACAN made a critical change to my career. I would like to thank the ACAN Director Professor John Bekkers and everyone who contributed to the courses. They spent a tremendous effort to run the course. This course is very beneficial for junior neuroscientists to develop their skills, and lots of fun too! John also has a lot of patient to answer my immature questions from time to time. I also met Drs Sarah Etherington, Julian Choy, and Sonata Yau in the course. They became my good friends and I hope they all have a very successful careers.

At the Research School of Biology (RSB) I met a lot of friends and they were willing to share their expertise. I would like to thank Drs Ricardo Natoli and Peter Kozulin who taught me how to use the confocal microscope. Mr Wen-Yen Wu spent a lot of time to debug my lousy LabVIEW programs. Ms Catherine Stewart-Moore helped me out on administrative paper work even before I came to Australia. Mr Mark Snowball gave us excellent technical support. Ms Rizsa Albarracin found me the job at the Vision Centre. Drs Owen Carr and Matt Rutar allowed me to borrow lab supplies (thanks to their supervisors Lauren Marotte and Jan Provis too, I did return the supplies to the best of my ability). Drs Lisa Vlahos, Angeliza Querubin, and Yu-Shan Hung shared some of their discoveries with me. I have eaten Yu-Shan's share of food most of the time and she was very generous to allow me to do so. Thank to Dr Krisztina Valter-Kocsi who let me work as a teaching assistant in the system neuroscience course, what an experience!

During my lockup experiment time at RSB, Fanny gave me some of her garden fruit. The tomatoes were the best I ever had! Dr Partha Bhagavathula gave me chocolate when I was hungry and listened to my grumbles. My martial arts mate Mr Tim Yiu did some good training with me to keep ourselves healthy. Ms Mary Ann Go assisted me several times to find a place to live when I was in Canberra. Ann became a very good friend of mine and I really enjoy the time with her to learn how to play saxophone. Perhaps one day I will go to church with her to learn how to be a good person.

During my down time in Melbourne, my friends from Ving Tsun Combat Science kept me alive. I would like to give a special thanks to my sifu Darren Elvey. Darren is not just a sifu, he is also a big brother. Mark Sinclair, Paul Nguy, Gerald Lee, Amy Lin and Kim Soo also make me spiritually strong. Gerald, as my therapist, also cured my torn ligaments. Friends from Rice Bar restaurant, Wai, Shui, and Ivan always gave me discounts and fed me very well when I was broke. Dr Hung-Hsun Yen let me stayed in his place and shared some of his veterinarian experience with me. I am glad that Lala Shang left research temporarily and all the best to her and her new born baby!!!

When I came back to ANU, Ted's group members: Drs Andrew Bell, Corinne Carle, Faran Sabeti, Marconi Barbosa, and Eman Ali are always welcoming, helpful, and a fun group to interact with. I enjoyed the teatime and lunchtime with them. Also thanks to Drs Penny Oakes, Anna Cowan and Simon Bain, for straightening out my course. Dr Andrew James showed me some programming skills and I probably need more time to digest.

My parents, they have been continuously supportive to whatever I do and never asked any questions. My sisters and brother took care of the family while I was absent for many years, I will return the favour by teaching all my little nieces and nephews some solid lessons! My family-in-law always trust me and warmly welcome me whenever I am home. At the end, I should thank my wife Suk Kwan once again because I promised to take care of her but I have never done a very good job.

I really appreciate for all the help I got, thank you everyone.

Abstract

The retina is responsible for encoding different aspects of the visual world. Light enters the eyes and is converted by the photoreceptors into electrochemical signals. These signals are processed by the retinal network and proceed afferently to the brain via the axons of the retinal ganglion cells (RGCs). The RGCs outputs are in the form of action potentials (spikes), which encrypt the visual information in terms of spike shape, firing frequencies, and the firing patterns. When the photoreceptors are gone due to disease, vision is lost. The idea of a retinal prosthesis is to activate the surviving RGCs by electrical stimulation in order to recreate vision. In this thesis, I have studied the physiological properties of the RGCs, and reconstructed natural RGC spike trains by electrical stimulation.

Chapter 1 introduces the anatomy of the retina and the retinal neurons. How the RGCs respond to light. Electrical stimulation is also discussed. A brief historical summary of the receptive field properties and cell physiology is also presented.

Chapter 2 characterizes the intrinsic properties of 16 morphologically defined types of rat RGCs. The intrinsic properties include the biophysical properties due to morphology and dendritic stratification, in addition to physiological properties such as firing behaviours. These properties are also compared with the cat RGC intrinsic properties in order to investigate the variations between the morphologically similar RGCs of the two species. The results suggest that the RGCs among species, even with similar morphologies, do not have conservative intrinsic properties.

Chapter 3 examines the details of the spiking properties of the different rat RGC types. Spikes are initiated at the axonal initial segment. A 'single' spike recorded at the soma consists of an axonal spike and a somatic spike. The existence of the two spikes can be recognized by two humps in the phase plot, and further revealed in the higher derivatives of the membrane potential. A principal component analysis shows that the parameters extracted from the phase plots are very useful for a model-independent rat RGC classification.

Chapter 4 establishes the foundations for electrical stimulation of the retina. The question is to what extent optimum placement of the stimulating and reference electrodes might be affected by anatomical location. Here we placed the stimulating electrode above or below the retinal inner limiting membrane and found no statistical difference between the thresholds. In addition, reflective axonal spikes from the cut end are discussed.

Chapter 5 combines the knowledge obtained in the previous chapters for the sole purpose of reproducing natural RGC outputs when using electrical stimulation. The light responses of the eye under saccadic movements were recorded and used to form the stimulus patterns. The reconstructions were performed on the brisk-transient (BT) and the brisk-sustained (BS) RGCs. Our results suggested that BT RGCs are more capable of following the stimulus patterns over a wide range of frequencies than the BS RGCs.

Chapter 6 concludes the whole thesis.

Keywords:

Retina, retinal ganglion cell, retinal prosthesis, bionic eye, electrical stimulation, intrinsic property, phase plot, receptive field, brisk-transient, brisk-sustained

Table of Contents

List of Figures and Tables

Page

Chapter 1
Introduction

Chapter 2
Intrinsic Physiological Properties of Rat Retinal Ganglion Cells with a Comparative Analysis

Chapter 3
Spike Waveform Analysis of Rat Retinal Ganglion Cells

Chapter 4
Epiretinal Electrical Stimulation and the Inner Limiting Membrane in Rat Retina

Chapter 5
Naturalistic Vision Reconstruction in Cat Retinal Ganglion Cells by Electrical Stimulation

Figures

Tables

List of abbreviations and acronyms

A	Ampere
AIS	axon initial segment
AMD	age-related macular degeneration
BISTRAT	RGC stratification at ~40% IPL depth or bistratified
BS	Brisk-sustained
BT	Brisk-transient
CO_2	carbon dioxide
Ca^{2+}	calcium ion
C_N	input capacitance
DNA	Deoxyribonucleic acid
DS	direction selective
dV/dt	first derivative
d^2V/dt^2	second derivative
E	efficacy
E_K	potassium equilibrium potential
EGTA	ethylene glycol tetraacetic acid
ER	electrically-evoked response
FA	frequency adaptation
FS	fast spiking
GABA	gamma-Aminobutyric acid
GC	ganglion cell
GCL	ganglion cell layer
GTP-Na	Guanosine triphosphate sodium
H	Kruskal Wallis H-test
HCl	hydrogen chloride
HEPES	hydroxyethyl piperazineethanesulfonic acid
I	current
IB	intrinsically bursting
ILM	Inner limiting membrane
INL	Inner nuclear layer
INNER	RGC stratification at 40-100% IPL depth
IPI	interphase (interpulse) interval
IPL	Inner plexiform layer
IS-SD	initial segment-soma dendritic
I_D	voltage-gated potassium current
I_h	Hyperpolarization-activated cation current
I_{max}	current that evoke a spike for every stimulus in SP_{10} (max=1mA)
I_{thresh}	threshold stimulus current amplitude
K	potassium
KCl	potassium chloride
K_{Ca}	calcium-activated potassium
K^+	potassium ion
LR	light-elicited response
MEA	multi-electrode array
MΩ	megaOhm (1×10^6 Ω)
mM	milliMolar (1×10^{-3} mol/L)
mOsm	milliosmole (1×10^{-3} osmole)
min	minute
Na	sodium

NaCl	sodium chloride
$NaHCO_3$	sodium bicarbonate or sodium hydrogen carbonate
Na^+	sodium ion
Na-ATP	sodium adenosine triphosphatase
N-UNCD	ultra-nanocrystaline diamond
n	number, normally refer to number of samples
OFF	OFF-centre/ON-surround
OLED	organic light-emitting diode
ON	ON-centre/OFF-surround
ONL	outer nuclear layer
ON-OFF	ON and OFF centre-surround
OPL	outer plexiform layer
OUTER	RGC stratification at 0-40% IPL depth
O_2	Oxygen
PBS	phosphate buffered saline
PCA	principal component analysis
PPS	pulses per second
p	p (probability) value of t-test
pA	picoAmpere (1×10^{-12} A)
pH	measure of the activity of the hydrogen ion (acidity or alkalinity)
R	resistance
RGC	Retinal ganglion cell
RP	retinitis pigmentosa
RS	regular spiking
R_N	input resistance
R^2	correlation coefficient of determination
r	correlation coefficient
SEM	standard error of the mean
SP	stimulation pattern
SS	sluggish-sustained
ST	sluggish-transient
S1-S5	inner plexiform layer sublayers 1 to 5
sp/s	spike per second
t	time
t_{delay}	time from onset of stimulus to peak of evoked spike
t_{m1std}	time of mean plus one standard deviation
V	voltage
V_m	membrane potential
VGSC	voltage-gated sodium channel
xcorr	cross-correlation
µM	microMolar (1×10^{-6} mol/L)
σ	standard deviation
τ	time constant
^{o}	degree (visual angle)
^oC	degree Celsius
3-D	three dimensional
$(LR/SP/ER)_{10}$	(LR/SP/ER) - 10-pulse stimulus pattern
$(LR/SP/ER)_{mg}$	(LR/SP/ER) - moving grating test
$(LR/SP/ER)_{nv}$	(LR/SP/ER) - naturalistic video test

Chapter 1

Introduction

As you read this sentence, each word is approximately positioned at the centre of your visual field. You will be aware that there are also words at the bottom of the page, but you will not be able to tell what they mean. The inability to recognize the words at the bottom, while looking at the top of the page occurs because visual acuity diminishes greatly from the centre of your visual field to the periphery (Figure 1.1). This is also why we turn our eyes directly towards objects or events that come to our attention. This primary *line of sight*, the direction where visual acuity is maximal, intersects the retina at an anatomical arrangement called the fovea. The visual information transduced at the fovea is of primary importance in humans. The sensory experience of it is termed *foveal vision*, whereas for retinal regions outside the fovea, is called *peripheral vision*.

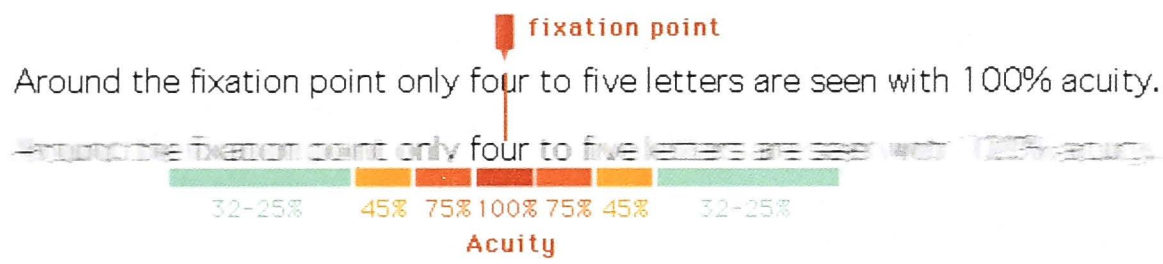

Figure 1.1 An example of the visual acuity of foveal vision in reading. Focus at the fixation point of the word 'four' in the upper line, and try to read the words away from it. The level of difficulty to recognize the words increases as visual acuity decreases (Hunziker, 2007). The progressive blurriness of the sentence imitates the fade out of visual acuity. Reproduced with permission.

As you keep reading, you are probably keeping your head stable while glancing at successive parts of each sentence, one block of words after another. During normal reading you might not be aware of the quasi-automatic jump-like movement of your eyes from place to place. Your eyes scan the line of text by a sequence of fast eye rotations called *saccades*, followed by longer intervals called a *fixation* pause. This sequence is repeated about three times per second along each line of text, for review see (Awater & Lappe, 2004). During each pause there are tiny, slow drifts of the primary line of sight in various directions followed by corrective micro-saccades, for reviews see (Hoffman & Subramaniam, 1995; Martinez-Conde, Macknik, & Hubel, 2004), that keep the fovea pointed within a tiny patch of the external visual field. Fixation pauses are the intervals when retinal ganglion cells (RGCs, see section 1.3 for details) are able to supply stable data to the higher visual centres. During each fast saccade, the retinal motion causes strong blurring of the signals transduced by the photoreceptors (see section 1.3 for details) because of their limited temporal bandwidth (Tatler, O'Carroll, &

Laughlin, 2000). The saccades serve to reposition the fovea to capture a stable image of the next packet of the scene. A more speculative idea is that the saccade (and coordinated higher circuitry) defines an interval during which successive stable 'snap-shots' can be patched together at higher cortical centres, so that an unmoving representation of the external world can be synthesized (Crespi et al., 2011; Turi & Burr, 2012). It is a remarkable observation that the external world does not appear to move, despite the sudden jerking of the retina during a saccade. This is also true for persons who display constant nystagmus (voluntary or involuntary eye movement) or oscillopsia (an effect experienced by patient in which visual objects seem to oscillate) up to quite high rates (Tkalcevic & Abel, 2005). Saccades allow us to be responsive to the changes in the surroundings. The persistent quasi-voluntary repetition of the sequence, fast saccade followed by fixation pause, is a repeated process in which the visual scene is progressively explored. 'Quasi-voluntary' could be used as a qualifier of the process of repetition, for two reasons. Sometimes, the next saccade is launched automatically in the brain to refresh a fading part of the current map of the external scene (e.g. like the sequencer of dynamic memory chips in a computer). At other times, the next saccade may be launched from peripheral retina when some new event disturbs the ongoing activity of a group of RGCs. In this case, the role of the saccade is to foveate the event for immediate refilling of the internal 'processing pipeline' for that part of the internal representation. Once novelty is detected, your head and your eyes will be repositioned, so that the fovea will be centred to the scene of interest. Being able to respond with saccades has survival value.

The visual process begins when images, in the form of patterns of light, are projected onto the retina. The photoreceptor layer transduces the visual information from light to graded (non-impulsive) electrical activity. Complex interactions between the neurons of the retinal networks filter and gate these electrical signals, eventually delivering the output to the array of the RGCs. In this output layer, the RGCs produce trains of full-sized, 'all-or-none' nerve impulses. A neuron, when excited by a stimulus that exceeds threshold, will either produce an nerve impulse with maximum magnitude (all), or does not produce any at all (none). These nerve impulses are also known as action potentials or spikes. They propagate rapidly to various destinations in the visual centres of the brain. In these locations, further neural processing is no longer constrained by the physical dimensions and other limitations of the eye and retina. The spike trains of different classes of RGCs represent different aspects of visual

information (form, color, motion, etc.) in a digitized format are directed to different parts of the brain for interaction and integration with recent history of input to construct a basis for visual reflex actions and visual perception, for review see (Wassle, 2004).

Individual spikes in retinal ganglion cells have previously been evoked by electrical stimulation of the retina (Crapper & Noell, 1963; Granit, 1946; Taira, Imazawa, & Motokawa, 1965). Despite the radical differences in the spike generation mechanisms between visually and electrically evoked impulses, they are individually indistinguishable when received by the higher visual centres of the brain. Before we ask if the brain can interpret the incoming electrically evoked spikes as vision, we need to know if we can electrically stimulate the retinal neurons to reproduce the spike patterns as they occur in normal vision. *Is the capability of spiking by electrical stimulation limited by the physiological characteristics of the RGCs*? These questions are critical to developing any retinal visual prosthesis that uses electrical stimulation, and so are central to this thesis.

Under ordinary viewing conditions, there are at least two features of the RGC behaviour that should be considered. The first is that in the absence of visual stimulation, most RGCs have an ongoing (i.e. maintained) discharge that is inherently irregular in the timing of the impulses (Kuffler, 1953). The second point is the observation that visually appreciable responses are spread out in time regardless of how brief the evoking stimulus is made (Levick & Zacks, 1970). These observations imply that an individual impulse, on its own, contributes very little to the perceptual experience of vision. Therefore it is necessary to determine whether electrical stimulation can be applied so as to emulate the pattern of many impulses as observed in the natural vision process. Finally, when an electrical stimulation is applied, a population of neurons are stimulated instead of only one. The overall production of the nonphysiologically elicited spike patterns can be very complicated. For example, activating both the ON and OFF RGCs (see section 1.4 for details) by the same electrical stimulation at the same location does not make sense perceptually and may not pass possible input filters in the brain.

1.1 Vision and Blindness

Vision is a very important component for survival in most animal species. Different visual systems have evolved to assist in the survival of these *visual* species. The capacity to survive increases if we are able to detect predators when they approach, and also to find a way to escape, to identify specific objects that are recognizable as food, and to provide the ability to estimate the position and distance of objects in our surroundings. While the other senses can play useful roles in these tasks, vision provides remarkable telemetry of distant terrain in the external world. This constitutes a valuable early warning advantage in these tasks and requirements, which give us an improved chance of survival under natural selection.

Humans appreciate the gift of being able to see for many reasons: they appreciate seeing the faces of their families, and having the ability to admire the world around them. Conversely, loss of vision is socially and psychologically devastating (Access-Economics, 2004).

In a simplified view, the overall process of vision can be conveniently partitioned into two successive stages: a *sensory* input stage in the eye together with its retina and a *perceptual* constructive stage that occurs in the brain. The initial *pre-processing* stage is responsible for continuous capture of a rich video stream from the external visual scene and performing preliminary transformations of intensity, space and time to compress the multi-channel signal stream into a narrow multiplexed digital communication channel to the brain. The *post-processing* stage in the brain engages the visual stream with other sensory streams and available memory in a pipelined history of the immediate present to provide the basis for a perceptually constructed world around us. Seeing allows us to recognize the position, motion, form, color and distance of objects in our visual field. Perception interprets what we see and converts it into tokens defining options for action.

According to the World Health Organization (WHO, 2012), among the 285 million visually impaired people worldwide, 121 million could restore their vision to normal with eyeglasses, contact lens or refractive surgery. There are 39 million people considered as totally blind due to various problems, such as physical eye damage and retinal diseases. At least 50% of all blindness is due to age-related retinal diseases. One of the most common retinal diseases that causes progressive loss of photoreceptors and lead to blindness is retinitis

pigmentosa (RP). Once the photoreceptors are gone, the retina is de-afferented and vision is lost. The loss of photoreceptors will also trigger remodeling in the retinal network: changes in neuronal structure and large-scale reorganization (Marc, Jones, Watt, & Strettoi, 2003). Postmortem morphometric analysis of retina of RP patients showed that approximately 30% RGCs might survive (Humayun et al., 1999; Santos et al., 1997; J. L. Stone, Barlow, Humayun, de Juan, & Milam, 1992). Prospects for artificially restoring vision clearly depend on the level at which the vision mechanism has been damaged. Nevertheless it is clear that RP patients might be good candidates for a retinal visual prosthesis given the survival of at least some RGCs. By contrast, in glaucoma it is the RGCs that die, leaving no means of communication between eye and brain. Along with glaucoma, macular degeneration and diabetic retinopathy are the leading causes of blindness world-wide (Quigley & Broman, 2006). These diseases often have a destructive neovascular component or the development of an atrophic retina, probably also ruling out retinal prostheses. Overall, it is essential to understand the physical structure and the physiological properties of the elements involved in the processing of visual input before we consider vision restoration with technology.

1.2 Retina

The retinas are embryologically constructed as extensions of the brain, for review see (Dowling, 1987). They are the most accessible part of the brain that can be directly inspected with an ophthalmoscope (invented by Helmholtz in 1856). Evolution might have crafted different types of eyes, but the main purpose of eyes remains the same. That is, to collect visual information from the outside world and transfer it to the brain. A diagram showing the structure of the mammalian eye is shown in Figure 1.2A.

Light-rays from the external field-of-view enter the eye through the cornea, the opening (pupil) in the iris and the biological lens. The aspheric surfaces (cornea, lens) focus the image on a (conceptual) hemispherical shell coextensive with the photoreceptor layer. The main effect of the pupil is to control aberrations in the image due to residual imperfections in the four refracting surfaces. Its light-controlling capability (about 25-fold) is miniscule

compared with the effective sensitivity control within the retina (100,000-fold) provided mainly by the photoreceptors (Lamb, Collin, & Pugh, 2007).

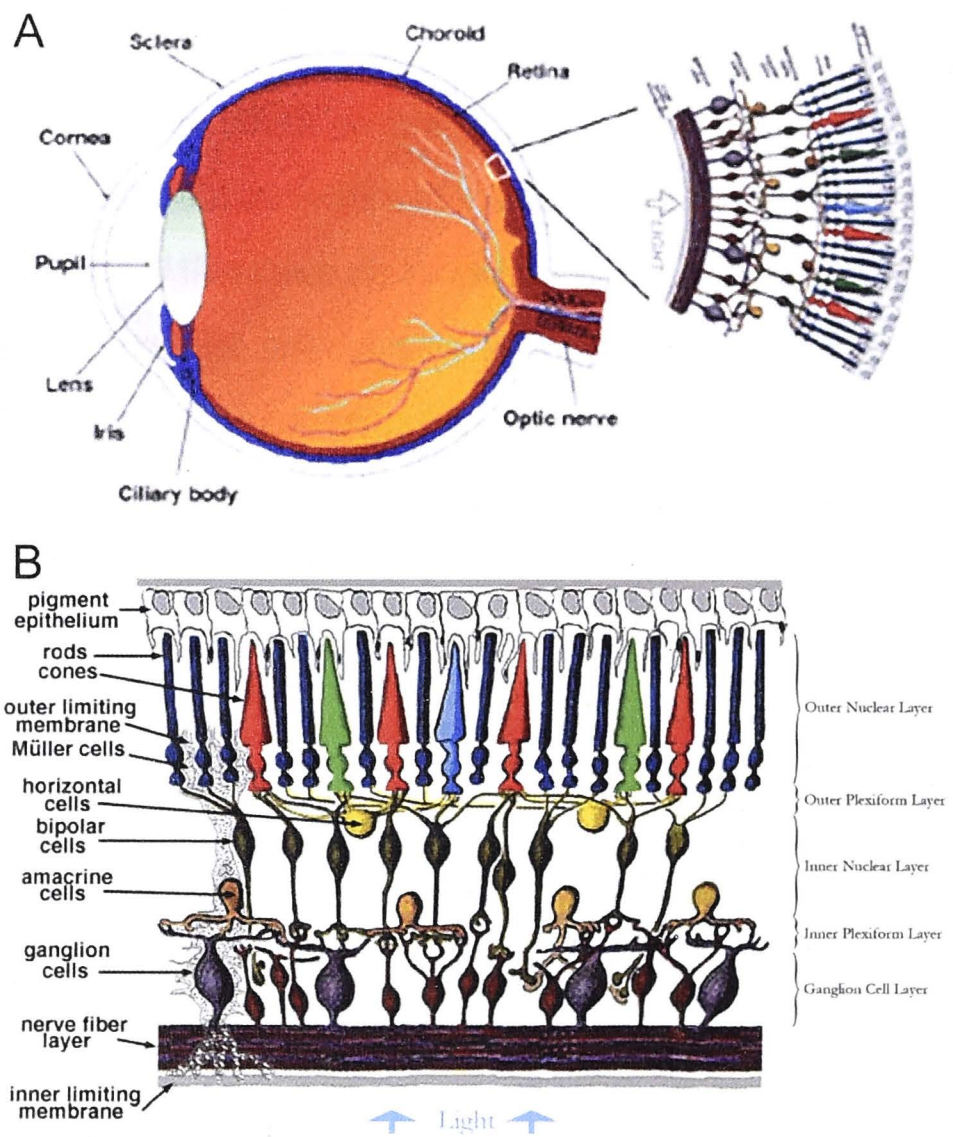

Figure 1.2 Diagrams of organization of a mammalian eye. **A**) Physical structure of the eye. **B**) The retinal organization. Reproduced with permission.
Source: http://webvision.med.utah.edu/book/part-i-foundations/simple-anatomy-of-the-retina/

The retina is the thin piece of tissue, spanning the interior surface of the eyeball as shown in Figure 1.2A. It is sometimes described as a simple anatomical structure with a complex interconnection pattern. The word 'simple' here implies the packing of cell-bodies into only 3 main cascaded cellular layers: the ganglion cell layer (GCL), the Inner nuclear layer (INL) and the outer nuclear layer (ONL) (Figure 1.2B), for reviews see (Dowling, 1987; Rodieck, 1998), far simpler than the complex organization of the brain. The 'simplicity' is deceptive: there are many different types of cell intermingled in each layer. The interconnections of cells occur by a dense network of fine processes extending from the cell bodies into the two 'synaptic affiliation' layers: the inner plexiform layer (IPL) and the outer plexiform layer (OPL), between the three cellular layers as shown in Figure 1.2B. The physical connections, known as

synapses, are miniature, specialized, close appositions between partnering processes. They are much more numerous than the neurons they interconnect (Jakobs, Koizumi, & Masland, 2008). These anatomically 'simple' arrangements of neurons and synapses form a very complex network to pre-process visual information entering the brain that later constructs the experience of visual perception. More detail on the assorted cell types in the retina is given in Section 1.3 below.

Vertical sections of the retina show retinal neurons in more detail as in Figure 1.3, the schematic drawing by Santiago Ramon y Cajal at around 1900 (left) compared to a rat retina slice (right).

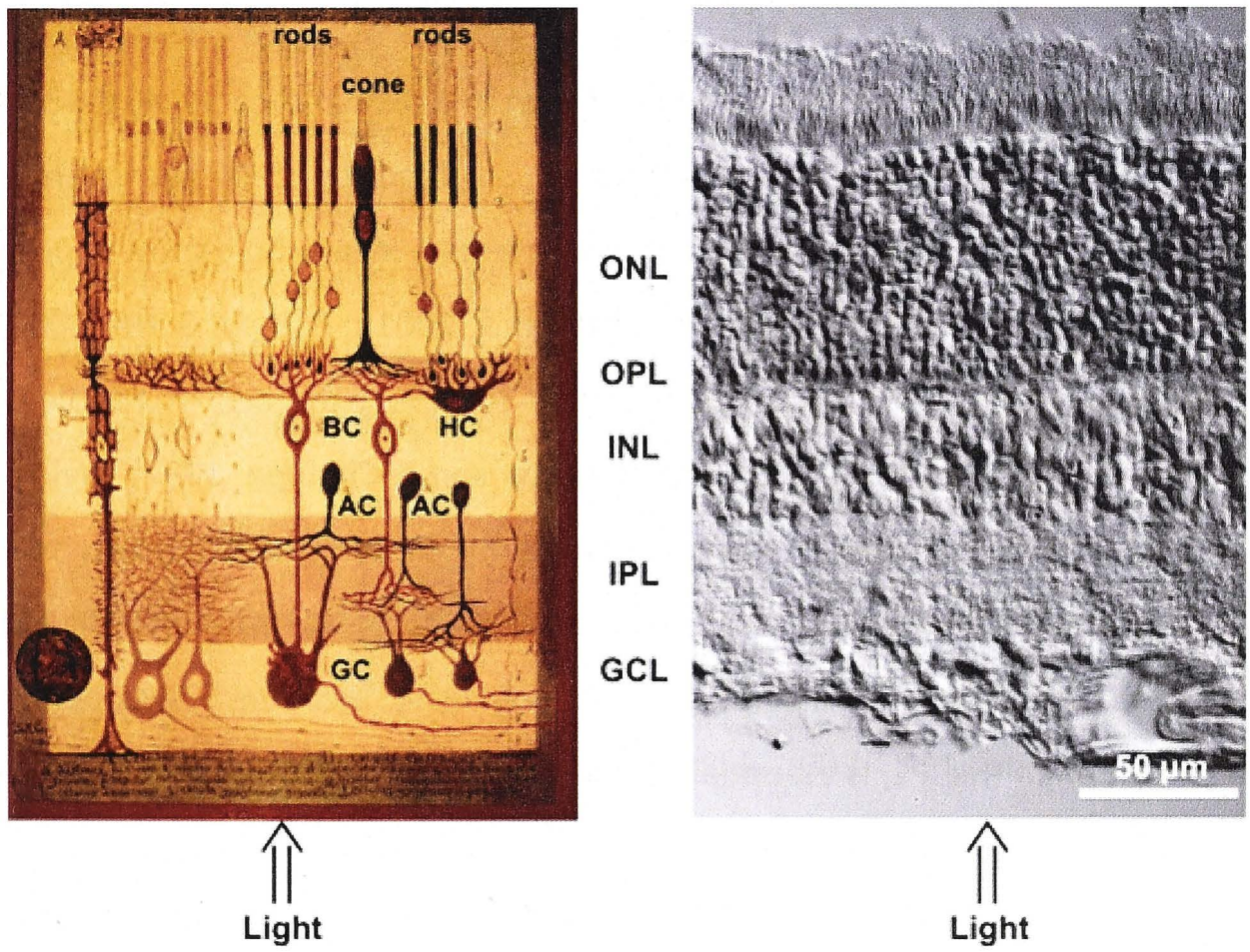

Figure 1.3 Anatomy of retinal neurons and layers. The schematic drawing (left) by Santiago Ramon y Cajal *circa* 1900 compared with a rat retina slice (right) showing: Photoreceptors (rods and cones) in the outer nuclear layer (ONL) make connections with horizontal cells (HCs) and bipolar cells (BCs) in the outer plexiform layer (OPL). The BCs, amacrine cell (ACs) and retinal ganglion cells (RGCs or GCs) make connections in the inner plexiform layer (IPL). The HCs, BCs and ACs are in the inner nuclear layer (INL). RGCs and some displaced ACs are in the ganglion cell layer (GCL). Reproduced with permission. Source: http://www2.fz-juelich.de/isb/isb-1//Retina

The thickness of the rat retinas is about 220 µm. For cats and humans, it is about 250 µm and 500 µm respectively (Buttery, Hinrichsen, Weller, & Haight, 1991). In this simplified exposition of retina, photoreceptors are treated as neurons because of the emphasis on their

synaptic connections with the extensions of other neurons (bipolar cells and horizontal cells) in the OPL. In the context of visual transduction, it may be more appropriate to acknowledge their differences from neurons.

The axons of the RGCs comprise the optic nerve, which outputs the visual information processed by the retina to the brain. The amacrine cells have dendrites but usually no identifiable axon. Their dendrites make connections with the RGCs, the bipolar cells and the other amacrine cells in the IPL. Although the functions of most of the amacrine cell types remain uncertain, it is now known that the 'starburst amacrines' play a key role in the generation of directional motion sensitivity. Only the RGCs and a small subset of the amacrine cells that have been studied can generate spikes (Murakami & Shimoda, 1977; Taylor, 1996).

The complete dendritic fields cannot be shown in a retinal slice because the size of the fields is usually greater than the section thicknesses, so dendritic trees are invariably clipped off by the slicing. Entire dendritic fields can be revealed in a whole-mount preparation if suitable stains or dyes are used (Jensen, 1991; Masland, 2001a; Sun, Li, & He, 2002). Whole-cell patch clamping of retinal neurons can be made to reveal the cell morphology and also record the response of the neurons in the retina (Robinson & Chalupa, 1997; Taylor & Wassle, 1995). The patch-clamp technique was developed by Neher and Sakmann to study the electrophysiology of cells (Hamill, Marty, Neher, Sakmann, & Sigworth, 1981). The view of the whole-mount retinal preparation, including the topographic location of the neuron and its dendritic stratification in the IPL, is essential for distinguishing between cell types (Famiglietti & Kolb, 1976).

These primary classes of retinal cells form many parallel microcircuits with unique functions. After light passes through the transparent retinal cells and is transduced by the photoreceptors, the spatiotemporal patterns of the entire image are encoded in a parallel cascade of neuronal circuits. By understanding the fundamental organization of the retinal cell structure, we can hopefully understand how visual information is processed in the retinal network.

1.3 Retinal ganglion cells and others

The human retina contains approximately 104 million photoreceptors. There is space in the optic nerve for only about 1.2 million axons of retinal ganglion cells to carry the output signal streams to the brain. Particular aspects of the visual world are extracted and encoded by the complicated signal processing that occurs in the retina. The convergence from photoreceptors to RGCs involves complex signal processing, which occurs in the retinal network (Dacey, 2000; Field & Chichilnisky, 2007; Gollisch & Meister, 2010; Levick & Dvorak, 1986; Levttvin, Maturana, McCulloch, & Pitts, 1959; Rodieck, 1998; Wassle, 2004; Werblin, 2010). Mammals, such as cat and rat, have 5-10 times fewer RGCs than humans (Masland & Martin, 2007).

For the mammalian retina, there are about 15-20 different RGCs (Masland, 2001a). Although the functions of many RGCs are still unclear, their physiology and morphology have been well characterized in several species, especially in cats (Barlow, Levick, & Yoon, 1971; Boycott & Wassle, 1974; Cleland & Levick, 1972; Enroth-Cugell & Robson, 1966; Fukuda & Stone, 1974; Levick, Cleland, & Dubin, 1972; J. Stone & Fukuda, 1974; Wassle, Cleland, & Levick, 1975).

Retinal cell classification is well-progressed due to the advances in histochemistry, microscopy and pharmacology (Boycott & Wassle, 1974; Dreher, Sefton, Ni, & Nisbett, 1985; Enroth-Cugell & Robson, 1966; Huxlin & Goodchild, 1997; Sun, et al., 2002). The major populations of retinal cell types have been discovered, identified and quantified (Martin & Grunert, 1992; Masland, 2001b; Vaney, 1980). The mammalian retinas consist of a huge diversity of neuronal types, approximately 55 distinct cell types were identified and possibly a few more additional types are yet to be found (Masland, 2001b). The different cell types can be categorized into five major classes: RGCs, amacrine cells, bipolar cells, horizontal cells, and photoreceptors (Dowling, 1987; Kolb, 1994; Masland, 2001a; Rodieck, 1998) (Figure 1.2B and 1.3). These five major cell classes are conserved among vertebrates (Meister & Berry, 1999).

In cats, the RGCs are particularly densely packed in a region named the area centralis. This is the homologue of the human foveal region. The angular distance from the centre of the area centralis defines the origin for cat visual eccentricity. Some structural features of the

RGCs have a well-defined functional relation with eccentricity, such as soma size, dendritic tree size, and dendritic tree coverage (Pasternak & Horn, 1991; Rapaport & Stone, 1988; Stein, Johnson, & Berson, 1996; Wassle, Peichl, & Boycott, 1981). In addition, there are useful scaling constants that relate visual angle in degrees to spherical distance along the retina measured from the centre of the area centralis (or fovea) to the target position on the retina: Cat 1 mm ≈ 4.4° (Bishop, Vakkur, & Kozak, 1962); Human 1 mm ≈ 3.5° (Drasdo & Fowler, 1974).

To identify a RGC, the simplest way is to quantify its morphology. The term morphology includes the size and configuration of the soma, the dendritic tree areal spread, the pattern used by the dendrites to fill the spread, and the dendritic stratification within the IPL (Dreher, et al., 1985; Huxlin & Goodchild, 1997; Rowe & Stone, 1977; Sun, et al., 2002; Tauchi & Masland, 1984). Other criteria for classifying RGCs include studying its responses to electrical stimuli (electrophysiology), identifying its chemical building components (biochemistry) (Siegert et al., 2009), and finding its connectivity (micro-anatomy) (Buhl & Peichl, 1986; Dann & Buhl, 1987; Levick, et al., 1972). The purpose of classification is to partition the large number of RGCs into a more manageable, smaller number of classes. Random minor individual variations of any one particular feature may make it impossible to assign a RGC to a single class. It is therefore essential to take into account morphological, physiological and other characteristics to obtain practical homogeneity within the classes. In turn, these differences may affect the relative suitability of the different RGC types for stimulation by a retinal visual prosthesis.

The neurochemical compositions of RGC plasmalemmas are diverse. Each of the different types of RGCs makes use of different types of ion channels. In addition, the heterogeneity of ion channels among RGCs leads to differences in their intrinsic membrane properties, including the RGC's voltage-current relationship, differing firing rates and firing patterns (Lipton & Tauck, 1987; Robinson & Wang, 1998). A complete survey of the intrinsic properties of 10 morphologically defined cat RGC types was carried out but was conducted in room temperature instead of physiological temperature (O'Brien, Isayama, Richardson, & Berson, 2002). Intrinsic properties do not always correlate precisely with classification based on morphology and visual repertoire.

This variety of ion channels allows visual information to be encoded diversely by different types of ionic transmembrane currents, which result in a significant range of spike shapes (Fohlmeister & Miller, 1997; Kress, Dowling, Meeks, & Mennerick, 2008). The various compositions of the multiple subtypes of ion channels in different cell locations leads to different spatiotemporal RGC responses. The diversity of RGCs across species makes the complete exposition of their responses to stimuli very difficult. This complexity is reflected in the diverse terminologies used by different researchers under various circumstances, which overall are confusing. In the following sections, we will use cat RGCs as the model to introduce the response of RGCs to stimuli.

1.4 RGC - Responses to light

The concept of a receptive field, first introduced by Hartline, sets the stage for visual neuroscientists to describe the response of the optic nerve fibers when the RGCs are stimulated with light (Hartline, 1938, 1940). The 'field' refers to the retinal area where stimulation triggers the response of the neuron. The receptive field depends on the properties of the visual pathways connected to that neuron (Allman, Miezin, & Mcguinness, 1985; Hubel & Wiesel, 1960). However, it is not just the field area that matters, its surroundings and also its synaptic interactions distant from the field are also essential (Derrington, Lennie, & Wright, 1979; Hamasaki & Maguire, 1985; McIlwain, 1966). The receptive field organization is of great importance because it influences how visual information is highly compressed from the photoreceptors to the RGCs.

In the 1950s, Kuffler's experiments on cat retina were devoted greatly to the exposition of the spatiotemporal organization of receptive field (Kuffler, 1952, 1953). He showed that there are two basic types of RGCs, referring to their concentric, centre-surround receptive field organizations: the ON-centre/OFF-surround (or simply referred to as the *ON-cell*), and the OFF-centre/ON-surround (or simply referred to as the *OFF-cell*) (Kuffler, 1953). When light intensity increases at the centre of the receptive field in an ON-cell, it will increase the discharge (firing of spikes) of the RGC. In the same situation, the discharge of an OFF-cell will be decreased. Likewise, when light intensity decreases at the centre of the receptive field,

the discharge of an ON-cell will be decreased and the OFF-cell will be increased. The change of light intensity in intervening zone, the area between the centre and the surround, may increase the discharge as well. A simple diagram illustrating the receptive field of an ON-cell is shown in Figure 1.4.

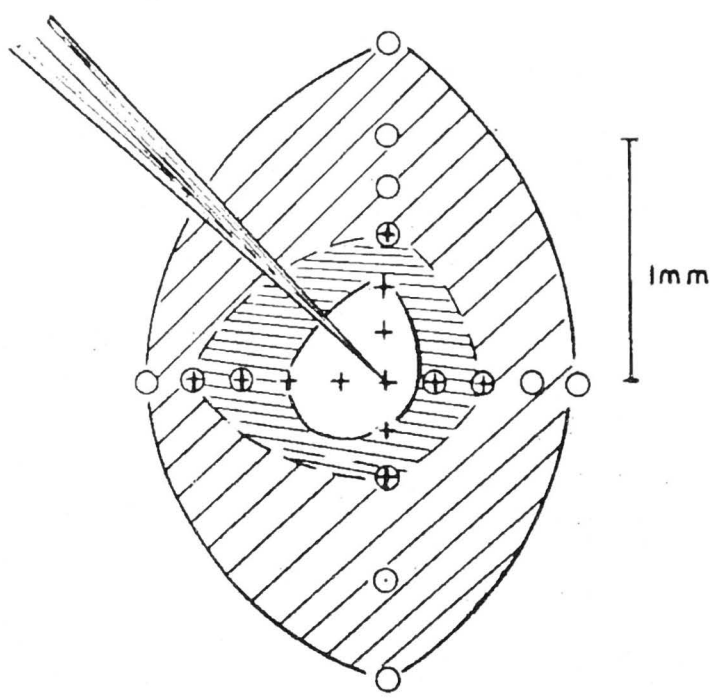

Figure 1.4 A simple illustration of an ON-centre/OFF-surround receptive field from Kuffler (1953). A recording electrode is positioned at the cell body. The discharge of the cell will increase when: 1) increment of light stimuli is presented to the central region (+); 2) decrement of light stimuli is presented to the periphery (◯); 3) Intensity of light changes in the intervening zone (⊕). Reproduced from (Kuffler, 1953).

This centre-surround organization is important for RGC encoding. Light stimuli can vary from starlight to sunlight, a variation of over ten orders of magnitude in luminance. On the other hand, the RGCs can only fire spikes over two orders of magnitude, when the number of spikes per second is considered. It is impossible for most RGCs to encode the absolute value of luminance. What most RGCs do is to encode the 'contrast', which is the normalized percentage of the centre to the surround (Dowling, 1987; Rodieck, 1998). In the first instant, contrast is calculated by divisive gain control in the photoreceptors (light adaptation), but is then enhanced by the surround subtracting low spatial frequency components, which we now understand adds to redundancy reduction (Srinivasan, Laughlin, & Dubs, 1982). One set of RGC types coarsely encode absolute luminance at least at photopic levels. These are the recently discovered melanopsin containing RGCs (Dacey et al., 2005) that possess intrinsic photosensivity based on that photopigment.

1.4.1 W/X/Y

Initial studies showed that both ON- and OFF-cells of cats could be divided into two subtypes: X-cells and Y-cells, based on the linearity of RGC's spatial summation of discharge (Enroth-Cugell & Robson, 1966). They used a full-field stimulus pattern consisting of a spatial sinusoidal grating pattern. The contrast of the grating could be switched abruptly between 32% and 0% periodically at 0.45 Hz. The astonishing result was that the responses dichotomized their recorded sample of Kuffler-type receptive fields into two previously unrecognized classes: X-cells and Y-cells. In X-cells, it was possible to find a position of the stationary grating where the RGC maintained discharge was essentially unaffected when the display switched from 0% contrast (uniform field at the mean intensity of the sinusoid) to 32% (sinusoidal pattern). In other words, when the easily visible grating appeared, it was as though the X-cell was quite 'blind' to the sharp transition. On the other hand, all Y-cells gave a clear response at every transition regardless of the spatial position of the pattern. For X-cells, there were two special positions per cycle of the sinusoid that yielded null responses, namely where the spatial profile of the sinusoid crossed the mean level of the waveform in an up-going or down-going sense. The null response was obtained when either of the positions coincided with an axis of odd symmetry of the entire centre-surround receptive field. At this point of coincidence, each half of the *entire* receptive field (both centre and surround) must have been experiencing strong stimulation: half in a positive sense and the other half in a negative sense. The absence of net response implies linear summation over the entire receptive field, for both the centre and the surround components.

The X-cells exhibit linear spatial summation and their performance substantially obeys the superposition principle. They have comparatively smaller receptive field sizes (Christen, Cohen, & Winters, 1981; Enroth-Cugell & Pinto, 1972). On the other hand, the Y-cells show non-linear spatial summation, and they also have relatively larger receptive field sizes. In addition, the Y-cells respond at twice the temporal frequency of a high contrast, fine, moving grating. This differs strongly from the simple first-harmonic response of the X-cells (Hochstein & Shapley, 1976; Shapley & Victor, 1980). The soma sizes of the Y-cell and the X-cell are approximately 20 microns on average, and increase with eccentricity (Boycott & Wassle, 1974; Stanford, 1987b; Stein, et al., 1996). The soma sizes of the Y-cells are larger than the X-cells at eccentricities away from the area centralis. Some RGCs were found with non-concentric

receptive fields, with very slowly conducting axons (T3) (J. Stone & Hoffmann, 1972). The functional organization of the various receptive field types were related to the axon diameter and related to the soma size, thus the correlation between the receptive field and the axon conducting velocity were studied (Fukada, 1971). Along with some RGCs with concentric receptive fields that have the slowly conducing axons, the RGCs in the T3 group are called W-cells (J. Stone & Fukuda, 1974). The W-cells have soma size less than 15 microns (Stanford, 1987a; Stein, et al., 1996). Of all RGCs in the cat retina, there are about 50% X-cells (Boycott & Wassle, 1974), 5% Y-cells (Wassle, Levick, & Cleland, 1975), and the rest were classed as W-cells (Fukuda & Stone, 1974). In primate, when the same classification is applied, there are only 5% W-cells in the RGC population, which indicated that they might not be as important as the X-cells and the Y-cells (Freeman, 2009; Masland & Martin, 2007). The W-cells are a physiologically diverse group containing feature detectors, color (blue/green) sensitive cells, and sluggish Y-like cells among other things (Levick, 1996).

1.4.2 Transient and Sustained

Two types of concentric RGCs that had dissimilar spiking patterns were introduced as the 'Transient' and the 'Sustained' cells (Cleland, Dubin, & Levick, 1971). Later it was shown that these two classes of RGCs have two subclasses: brisk and sluggish (Cleland & Levick, 1974a). Thus they formed four subclasses in total: Brisk-transient (BT), Brisk-sustained (BS), Sluggish-transient (ST) and Sluggish-sustained (SS). Cleland and Levick also correlated these subclasses to the axon conducting groups. The fast (T1), the medium (T2) and the slow (T3) axon conducting groups were linked to the BT, BS and the sluggish (ST and SS) RGCs respectively. Furthermore, they verified there were non-concentric receptive fields RGCs that were in the T3 group (Cleland & Levick, 1974b). Later this finding were included in the description of W-cells (J. Stone & Fukuda, 1974).

Although there was considerable evidence, such as the axon conduction velocity, showing that the transient and the sustained RGCs are equivalent to the Y-cells and the X-cells respectively, Cleland et al. (1971) believe that it is better to keep their terminologies since these spiking patterns are also dependent on eccentricity. The spike pattern is not absolutely one-sided. For example, the spike pattern of the Y-cells at area centralis contain considerable

amount of tonic component rather than being solely phasic. Like simple and complex cells in the cortex, the use of ratios of tonic/first harmonic, or second on first harmonics, to define cell types has recently been thrown into question (Mechler & Ringach, 2002). It is worth noting that while there has been some debate about the presence of Y-like cells in primates these have recently been identified (Crook, Peterson, Packer, Robinson, Gamlin, et al., 2008; Crook, Peterson, Packer, Robinson, Troy, et al., 2008; Petrusca et al., 2007), making the cat a reasonable model again, except perhaps for the midget RGC system of primates.

The discharge properties of the transient and sustained classes of RGCs vary with their eccentricities and have different functional roles (Ikeda & Wright, 1972). When the RGCs are close to the area centralis, both classes become biased towards relatively stronger sustained components. In the periphery, both classes become more biased towards relatively stronger transient components. Previous studies suggested that the transient and sustained properties might be generated differently due to dissimilar synaptic connections. However, blocking the inhibitory GABAergic and glycinergic feedback from amacrine cells truncates the transient response. It does not change the response of the RGC from phasic to tonic (G. B. Awatramani & M. M. Slaughter, 2000; G. Awatramani & M. M. Slaughter, 2000). In mammals, antagonistic centre-surround receptive field organization is generated in the OPL and the transient-sustained subdivision first appears in the IPL, for review see (Thoreson & Mangel, 2012). The BT RGCs can produce 'sustained' response characteristics in the standing contrast test, by continuously eliciting with the 'Periphery (Shift) effect' (neuron excited by stimuli located far away from its receptive field, (McIlwain, 1966)) at the same time (Hamasaki & Maguire, 1985; Kruger, 1980).

The different terminologies used to describe the receptive field properties (for reviews see (Levick & Thibos, 1983; Rowe & Stone, 1977)) are summarized in Figure 1.5.

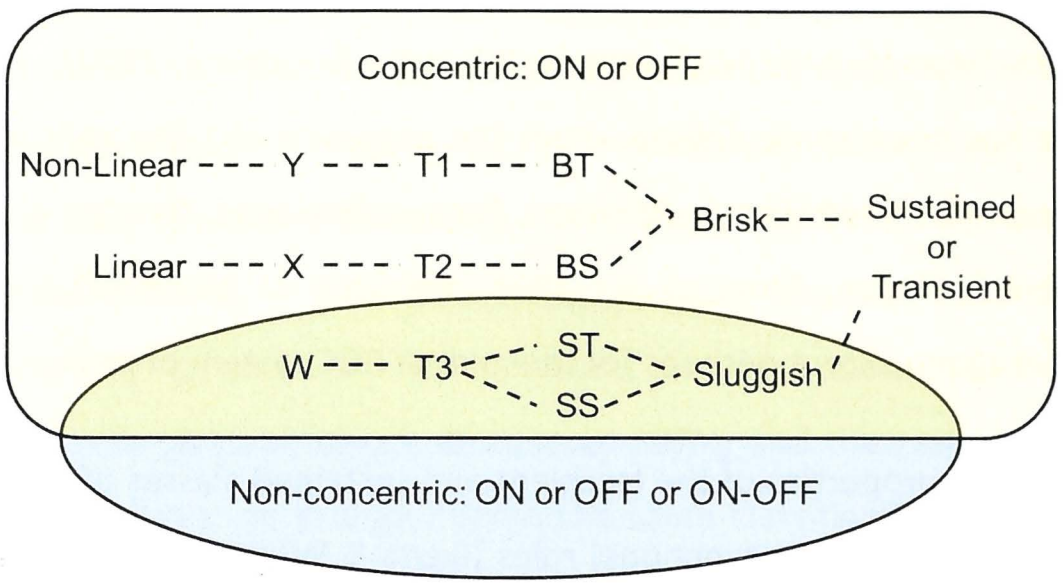

Figure 1.5 Summary of terminologies used to describe the receptive field properties. The dash lines show the possible link of each type to it corresponding counterpart. In a historical perspective, Kuffler (1952, 1953) found the concentric, centre-surround (ON-cell or OFF-cell) organization of receptive fields. Enroth-Cugell and Robson (1966) subdivided the types based on the spatial summation of discharge (Non-linear: Y-cell; Linear: X-cell) of the RGCs. Later Cleland et al. (1971) classified two RGCs spiking patterns (sustained or transient), and they correlated them to the X/Y classification and the axon conduction velocity (Fast: T1; Medium: T2; Slow: T3). The W-cells were added to the X/Y classification by Stone and Hoffmann (1972) after they found the RGCs with non-concentric receptive field, associated with slow conducting axons (T3). Cleland and Levick (1974a) further subdivided the Sustained/Transient classification into brisk and sluggish, and correlated the axon conducting velocity to these classes: Brisk-Transient (BT), Brisk-Sustained (BS), Sluggish-Transient (ST) and Sluggish-Sustained (SS). The BT and BS RGCs are in the axon conducting velocity groups T1 and T2 respectively, while the sluggish RGCs (SS and ST) are in the T3 group. In the T3 group, Cleland and Levick (1974b) also showed there are RGCs with non-concentric fields. Stone and Fukuda (1974a) added RGCs in the T3 group with concentric receptive fields into the W-cell category. The yellow region covers the RGCs with concentric centre-surround receptive fields, with different classification schemes. The blue region covers the RGCs with non-concentric receptive fields (e.g. Uniformity-detector). The green region comprised the RGCs with both concentric and non-concentric receptive fields.

1.5 RGC - Responses to electrical stimulation

In order to study the physiological properties of the RGCs and/or make use of the surviving RGCs in visual prosthesis, we wish to activate the RGCs by electrical stimulation. As mentioned above, one of the foremost questions to ask is if a non-physiological electrically-evoked spike carries the same visual information as a natural light-elicited spike. We can certainly study the physiological properties of the individual RGCs in respect of the electrically-evoked spike. However, the attributes of the spikes generated depend on the physiological properties of the neurons, the electrical stimulus applied, and also the responses of the neighboring neurons in the neural network. Moreover, a single spike on its own contributes

limited perceptual visual information. It is the inter-correlated spike trains of the different neurons in the entire retinal network that provides the perceptual experience of vision as a whole.

The Hodgkin and Huxley model described the ionic mechanism of the excitable membranes (Hodgkin & Huxley, 1952a, 1952b). The basic mechanism of spike generation by electrical stimulation in the RGCs is no different from any other excitable membrane. Once the electrical stimulation opens enough voltage-gate ion channels and reaches the threshold of the excitable cell membrane, the neuron will spike. As described above, the exchange of the ions through the opened channels triggers the 'all-or-none' spike generation mechanism. A number of factors can affect the divergence of the threshold and the efficacy of the electrically-evoked spike generation, for review see (Margalit et al., 2002).

The optic nerve is assembled from the axons of the 15-20 types of RGCs that have different function roles in visual perception (Dacey, Peterson, Robinson, & Gamlin, 2003; Masland, 2012), each of which have distinct anatomical structures and different network connections. The threshold to elicit a spike depends on the heterogeneous and spatially oriented excitability properties of the target neural elements being stimulated. The primary electrical stimulation response is generated by a dense band of voltage-gated sodium channels located within the proximal axon (Fried, Lasker, Desai, Eddington, & Rizzo, 2009). This band is also known as the axon initial segment (AIS), for reviews see (Kole et al., 2008). The anatomic properties of the band are diverse within each RGC types due to the various compositions of ion channels within the band (Fried, et al., 2009), thus generating a wide range of electrically-evoked spikes with various spatiotemporal properties.

The activation threshold is affected by the location of the stimulating and reference electrode pair to the AIS of the target RGC. The position and orientation of the pair determine the amount of current that will flow out of the AIS. The impedance of the tissues between the stimulating electrode and the AIS will increase with their separation distance. In addition, if the electric field is longitudinal to the excitable axon membrane surface, the cell membrane potential will be depolarized with maximum efficiency, thus lowering the threshold (Hille, 1992; Jack, Noble, & Tsien, 1975). On the other hand, if the electric field is transverse, the influence is minimal since the net charge effect on the membrane potential is close to zero.

The current charge transfer efficiency is defined by the stimulating electrode's physical properties, including the material that makes up the electrode and its shape, and the stimulus pulse waveform. Some common biocompatible materials are titanium nitride, tungsten, platinum and iridium oxide, for reviews see (Cogan, 2008). Their charge injection limits are well studied (Beebe & Rose, 1988; Craggs, Donaldson, & Donaldson, 1986; Levick, 1972). Material such as diamond (Hadjinicolaou et al., 2012) is also used. When the charge density is beyond the tolerance of the material used, toxic irreversible reactions might occur in the electrode-tissue interface. The amount of current or charge required is always carefully considered, in order to prevent tissue or electrode damage, and to determine the threshold of the neuronal activation. The current density is based on the surface area of the stimulating electrode and its shape. The primary issue to consider when using an electrode to stimulate the neurons is safety. Two critical concerns are the heat related thermal damage, for review see (Opie et al., 2012), and the neural damage induced by electrical stimulation, for reviews see (McCreery, Agnew, Yuen, & Bullara, 1988; McCreery, Agnew, Yuen, & Bullara, 1990).

Under continuous electrical stimulation, there will be electrochemical reactions between the electrode material and the tissue. The corrosion of the electrode and the dissolution of the electrode material are both unavoidable (Brummer & Turner, 1977). It is just a matter of time until the damage exceeds the tolerance criteria. With the defined stimulating electrode, the current charge distribution is determined by the stimulus pulse. The most common stimulus waveform is a biphasic symmetric charge-balanced rectangular current pulse. A biphasic symmetric waveform consists of two pulses with the same current density and opposite polarity. If the overall net charge is unbalanced, it might trigger irreversible electrochemical reactions and change the pH at the tissue electrode interface. The charge-balanced waveform results in an overall zero net charge, thus avoiding accumulation of electrochemical byproducts that cause tissue or electrode damage. Nonetheless, other forms of stimulus can be used, such as the biphasic asymmetric charge-balanced waveform, sinusoidal waveform or even simple square (charge-unbalanced) pulses (Shepherd & Javel, 1999). For the biphasic asymmetric charge-balanced waveform, there are two charge-balanced pulses with opposite polarity: one phase will have a longer pulse duration and a lower current amplitude, while the other phase will have a shorter pulse duration and a higher current amplitude. There are four possible waveform arrangements by considering the order

of the polarity and the sequence of the pulse duration/amplitude orders (Figure 1.6). Another important parameter is the interphase interval (IPI). It has the effect of lowering the threshold, which makes electrical stimulation more efficient (Weitz, Behrend, Humayun, Chow, & Weiland, 2011).

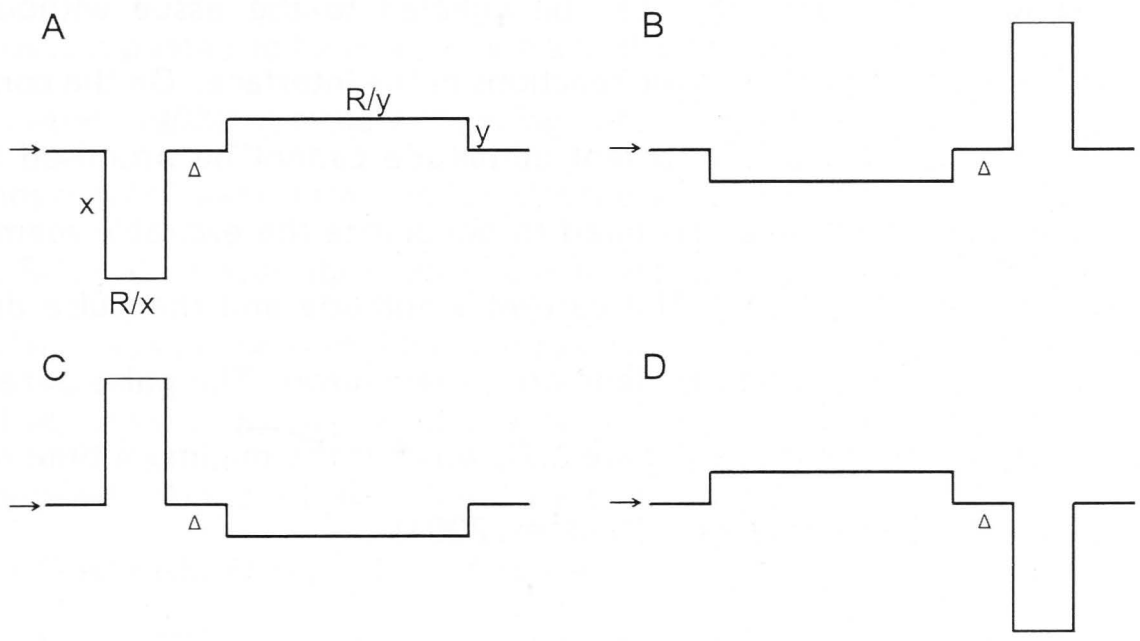

Figure 1.6 Four possible biphasic asymmetric charge-balanced waveform configurations. There are two charge-balanced pulses with opposite polarity. Set the current amplitudes for the first and second pulses as x and y (ampere), and the durations as R/x and R/y (time) respectively. The products (current*duration) of each pulse are R (coulomb) with opposite polarity, therefore the net charge of the waveform is zero. The interphase interval (Δ) is the time period between the two pulses. The arrow (→) is pointing at the baseline, typically at 0 current. **A**) A cathodic higher-current-shorter-duration pulse followed by an anodic lower-current-longer-duration pulse; **B**) A cathodic lower-current-longer-duration pulse followed by an anodic higher-current-shorter-duration pulse; **C**) An anodic higher-current-shorter-duration pulse followed by a cathodic lower-current-longer-duration pulse; **D**) An anodic lower-current-longer-duration pulse followed by an anodic higher-current-shorter-duration pulse.

It is more meaningful to consider the stimulus in the sense of electric charge instead of current. There are three parameters of a stimulus: the polarity, the current amplitude and the pulse duration. A stimulus with a high current amplitude, presented for a very short duration, cannot be guaranteed to activate a neuron because it takes time for the ion channels to react. Stimulation works by charging the local membrane capacitance to the threshold charge value for the AIS. After the end of a very short pulse, the charge redistributes spatially to the adjacent membrane capacitance. The initially high membrane potential smoothly relaxes during the redistribution phase towards resting potential and will continue to recruit activated sodium channels throughout the decay period. When the originally deposited charge is above

charge threshold, the voltage record will go through a minimum (still positive to resting potential) and then swing upward as the activated sodium channels take control. In the case of biphasic waveform, if the entire waveform is shortened so much that the opposite phase of the stimulus turns on before the activation of sodium channels is sufficiently advanced, the spike will be aborted as the opposite phase is now actively removing charge from the membrane capacitance (Tasaki, 1956). Thus, there are constraints for the reaction. In addition, there is a limit on the amount of charge that can be injected to the tissue without damaging the electrode and initiating irreversible toxic reactions in the interface. On the contrary, a stimulus with very long duration and a low current amplitude cannot be promised to elicit a spike. There is a minimum current value required to depolarize the excitable membrane known as the rheobase (Jack, et al., 1975). The current amplitude and the pulse duration together define the quantity of charge that can depolarize the neuron. The pulse duration at twice the rheobase is known as the chronaxie (Figure 1.7), which is the minimum time required to reach the activation threshold, for review see (Geddes, 2004).

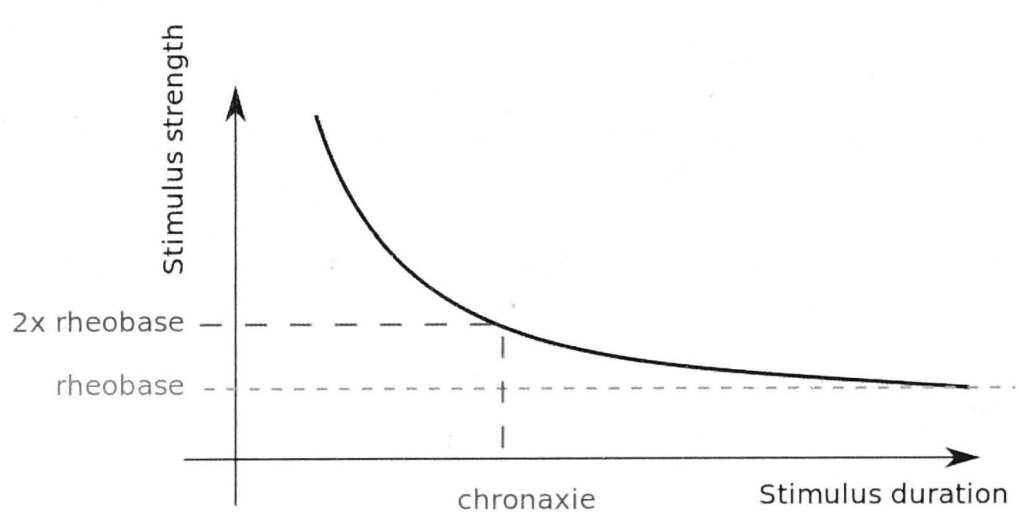

Figure 1.7 Rheobase and Chronaxie. The well-defined relationship between the stimulus strength and the stimulus duration. The minimum strength to reach the threshold of depolarization of an excitable membrane is called the rheobase. The minimum duration required to elicit a spike at twice the rheobase is known as the chronaxie. Source of figure: (Wikipedia Public Domain).

An excitable membrane can be activated by anodic or cathodic pulses, even without charge balancing. For safety reasons a charge-balanced stimulus, with minimum threshold (current and duration) is desirable. In a biphasic stimulus, cathodic phase first is considered as the preferred choice since the threshold is lower compared to anodic phase first (Ranck, 1975). The IPI between the two phases allows time for spread of the charge along the membrane capacitances and avoids loss of membrane charge to the following opposite polarity

component of the stimulus waveform. However, the optimal IPI is still an unknown. After all, there may not be a practical optimal stimulus at the lowest thresholds. There are just too many variables to be satisfied especially when a multi-electrode array (MEA) is used instead of a single stimulating electrode with a return (Shivdasani et al., 2010).

A single stimulus can be set up to elicit a single RGC spike (Ahuja, Behrend, Kuroda, Humayun, & Weiland, 2008; Fried, Hsueh, & Werblin, 2006; Sekirnjak et al., 2006). However, when the stimulus is repeated to form a pulse train, the threshold may be altered (Schmidt et al., 1996; Veraart et al., 1998). A rapidly changing pattern of electrical stimulation can depress the neural responses (McCreery, et al., 1988; McCreery, et al., 1990). The results are diverse among different RGCs at various stimulation frequencies. Fried et al. (2006) showed that a train of pulses (250 pulses per second (PPS)) reliably elicited a train of spikes over a one second period (Fried, et al., 2006). Similar results were demonstrated with a 500 PPS spike train (duration not specified) (Ahuja, et al., 2008). By contrast, some RGCs did not reliably elicit spikes at 100 PPS (Sekirnjak, et al., 2006). A more systematic study was done which showed that brisk transient (BT) RGCs could reliably follow stimulus trains up to 600 PPS while other RGC types (directionally selective (DS): ON-DS and ON-OFF DS; local edge detector; and OFF-delta) failed to follow at 200 PPS and beyond (Cai, Ren, Desai, Rizzo, & Fried, 2011). These experiments were done with different protocols but one common feature is they all used a fixed frequency stimulus train presented over a short period of time. A key question for this thesis is to see if the RGCs can follow a stimulus train that imitates a near continuous natural light-elicited spike pattern, as would be required for a visual prosthesis.

1.6 Thesis aims

Despite the complexity of the brain, where vision is interpreted, the retina by itself has very subtle unsuspected properties. So far, a rather detailed catalogue of retinal performance has been built: a nearly complete set of the retinal ganglion types; some understanding of the encoding in the spikes trains; and some knowledge about how RGCs respond to electrical stimulation. From physiology to the applications of retinal prosthesis, there is much still to be learnt to achieve practical visual recovery.

From an engineering point of view, in order to reconstruct vision with the aid of a prosthesis, RGCs are to be understood as the basic components (such as resistors and capacitors) to an electronic circuit. The challenge is to design and create a truly harmonized hybrid bio-electronic device. We know what the inputs and outputs are, but what we need is a better understanding of the retinal components and to design a blackbox to recreate the lost functions of the retina.

There are four aims in this thesis:

Aim 1: Characterize the intrinsic physiological properties of rat RGCs. Examine the hypothesis that the intrinsic properties of individual RGC types are conserved across mammalian species.

Research Plan 1: Patch-recordings were made of the voltage responses of the rat RGCs over a range of current injections. Evaluation of the intrinsic physiological properties of RGCs was done by subsequent analysis. The recorded RGCs were filled with neurobiotin or biocytin and their morphologies were captured and studied by confocal microscopy. Based on the 3-dimensional images, the RGCs were classified into 16 types as defined in the literature. A few rare types of RGCs were encountered but were not included, owing to limited sample sizes. Intrinsic physiological properties between rat and cat were compared using a cluster analysis for the purpose of checking if the RGC types were conserved across these two species. This study has been published (Wong, Cloherty, Ibbotson, & O'Brien, 2012).

Aim 2: Analyze the spike waveform of rat RGCs. Examine the possibility that RGC types can be identified by their spike characteristics alone.

Research Plan 2: Statistical analysis of the spikes of the rat RGCs recorded in Plan 1. Parameters from the spike waveforms, phase plots, and their first and second time-derivatives were extracted. Unsupervised classifications were done and the clusters were compared with the types as defined by confocal images in Plan 1. Part of this study has been published collaboratively (Accepted in upcoming conferences: (Maturana, Wong, Cloherty, et al., 2013; Maturana, Wong, Kameneva, et al., 2013)).

Aim 3: Quantify the effect of the inner limiting membrane on the thresholds for epiretinal electrical stimulation of RGCs.

Research Plan 3: A pair of bipolar stimulating electrodes was placed above or penetrating the inner limiting membrane of a rat retina. Voltage-clamping recordings were made of the voltage responses of the rat RGCs. The thresholds to elicit spikes under these two conditions were compared. The results have been partially published (Cloherty et al., 2012).

Aim 4: Reconstruct naturalistic scene in cat RGCs by epiretinal electrical stimulation.

Research plan 4: Light stimuli were projected on the whole-mount retina preparation. Patch-recordings were made of the voltage responses of the cat RGCs under three light stimuli: 1) standing contrast; 2) moving gratings with various contrast and spatial frequencies; 3) videos showing what normal human eyes see during saccadic movements across natural scenes. The response of the RGCs to the stimuli, the soma size, the receptive field and the intrinsic properties were used to classify the cat RGC types as defined in the literature. The spike timings from stimulus 3 were used as the blueprint to construct biphasic pulse trains for electrical stimulation. The correlations of the spikes trains obtained from stimulus 3 and electrical stimulation were evaluated. I have reported some of the results in an oral presentation (Australian Neuroscience Society 33rd Annual Meeting 2013, Melbourne, Australia).

1.7 References

Access-Economics. (2004). The Economic Impact and Cost of Vision Loss in Australia. 1-122.

Ahuja, A. K., Behrend, M. R., Kuroda, M., Humayun, M. S., & Weiland, J. D. (2008). An in vitro model of a retinal prosthesis. *Ieee Transactions on Biomedical Engineering, 55*(6), 1744-1753. doi: Doi 10.1109/Tbme.2008.919126

Allman, J., Miezin, F., & Mcguinness, E. (1985). Stimulus Specific Responses from Beyond the Classical Receptive-Field - Neurophysiological Mechanisms for Local Global Comparisons in Visual Neurons. *Annual Review of Neuroscience, 8*, 407-430. doi: DOI 10.1146/annurev.neuro.8.1.407

Awater, H., & Lappe, M. (2004). Perception of visual space at the time of pro- and anti-saccades. *Journal of Neurophysiology, 91*(6), 2457-2464. doi: DOI 10.1152/jn.00821.2003

Awatramani, G. B., & Slaughter, M. M. (2000). Origin of transient and sustained responses in ganglion cells of the retina. *Journal of Neuroscience, 20*(18), 7087-7095.

Awatramani, G., & Slaughter, M. M. (2000). Origin of transient responses of ganglion cells in salamander retina. *Investigative Ophthalmology & Visual Science, 41*(4), S761-S761.

Barlow, H. B., Levick, W. R., & Yoon, M. (1971). Responses to single quanta of light in retinal ganglion cells of the cat. *Vision Res, Suppl 3*, 87-101.

Beebe, X., & Rose, T. L. (1988). Charge Injection Limits of Activated Iridium Oxide Electrodes with 0.2ms Pulses in Bicarbonate Buffered Saline. *Ieee Transactions on Biomedical Engineering, 35*(6), 494-495. doi: Doi 10.1109/10.2122

Bishop, P. O., Vakkur, G. J., & Kozak, W. (1962). Some Quantitative Aspects of Cats Eye - Axis and Plane of Reference, Visual Field Co-Ordinates and Optics. *Journal of Physiology-London, 163*(3), 466-&.

Boycott, B. B., & Wassle, H. (1974). The morphological types of ganglion cells of the domestic cat's retina. *J Physiol, 240*(2), 397-419.

Brummer, S. B., & Turner, M. J. (1977). Electrochemical considerations for safe electrical stimulation of the nervous system with platinum electrodes. *IEEE Trans Biomed Eng, 24*(1), 59-63. doi: 10.1109/TBME.1977.326218

Buhl, E. H., & Peichl, L. (1986). Morphology of Rabbit Retinal Ganglion-Cells Projecting to the Medial Terminal Nucleus of the Accessory Optic-System. *Journal of Comparative Neurology, 253*(2), 163-174. doi: DOI 10.1002/cne.902530204

Buttery, R. G., Hinrichsen, C. F. L., Weller, W. L., & Haight, J. R. (1991). How Thick Should a Retina Be - a Comparative-Study of Mammalian-Species with and without Intraretinal Vasculature. *Vision Research, 31*(2), 169-&.

Cai, C., Ren, Q., Desai, N. J., Rizzo, J. F., 3rd, & Fried, S. I. (2011). Response variability to high rates of electric stimulation in retinal ganglion cells. *Journal of Neurophysiology, 106*(1), 153-162. doi: jn.00956.2010 [pii]10.1152/jn.00956.2010

Christen, W. G., Cohen, H. I., & Winters, R. W. (1981). Summing properties of the surround response mechanism of cat retinal ganglion cells. *Experientia, 37*(8), 857-859.

Cleland, B. G., Dubin, M. W., & Levick, W. R. (1971). Sustained and transient neurones in the cat's retina and lateral geniculate nucleus. *J Physiol, 217*(2), 473-496.

Cleland, B. G., & Levick, W. R. (1972). Physiology of Cat Retinal Ganglion-Cells. *Investigative Ophthalmology, 11*(5), 285-&.

Cleland, B. G., & Levick, W. R. (1974a). Brisk and sluggish concentrically organized ganglion cells in the cat's retina. *J Physiol, 240*(2), 421-456.

Cleland, B. G., & Levick, W. R. (1974b). Properties of Rarely Encountered Types of Ganglion-Cells in Cats Retina and an Overall Classification. *Journal of Physiology-London, 240*(2), 457-492.

Cloherty, S. L., Wong, R. C. S., Hadjinicolaou, A. E., Meffin, H., Ibbotson, M. R., & O'Brien, B. J. (2012). Epiretinal Electrical Stimulation and the Inner Limiting Membrane in Rat Retina. *2012 Annual International Conference of the IEEE Engineering in Medicine and Biology Society (EMBC)*, 2989-2992.

Cogan, S. F. (2008). Neural stimulation and recording electrodes. *Annual Review of Biomedical Engineering, 10*, 275-309. doi: DOI 10.1146/annurev.bioeng.10.061807.160518

Craggs, M. D., Donaldson, N. D., & Donaldson, P. E. K. (1986). Performance of Platinum Stimulating Electrodes, Mapped on the Limit-Voltage Plane .1. Charge Injection Invivo. *Medical & Biological Engineering & Computing, 24*(4), 424-430. doi: Doi 10.1007/Bf02442699

Crapper, D. R., & Noell, W. K. (1963). Retinal Excitation and Inhibition from Direct Electrical Stimulation. *Journal of Neurophysiology, 26*, 924-947.

Crespi, S., Biagi, L., d'Avossa, G., Burr, D. C., Tosetti, M., & Morrone, M. C. (2011). Spatiotopic Coding of BOLD Signal in Human Visual Cortex Depends on Spatial Attention. *PLoS One, 6*(7). doi: ARTN e21661DOI 10.1371/journal.pone.0021661

Crook, J. D., Peterson, B. B., Packer, O. S., Robinson, F. R., Gamlin, P. D., Troy, J. B., & Dacey, D. M. (2008). The Smooth Monostratified Ganglion Cell: Evidence for Spatial Diversity in the Y-Cell Pathway to the Lateral Geniculate Nucleus and Superior Colliculus in the Macaque Monkey. *Journal of Neuroscience, 28*(48), 12654-12671. doi: Doi 10.1523/Jneurosci.2986-08.2008

Crook, J. D., Peterson, B. B., Packer, O. S., Robinson, F. R., Troy, J. B., & Dacey, D. M. (2008). Y-Cell Receptive Field and Collicular Projection of Parasol Ganglion Cells in Macaque Monkey Retina. *Journal of Neuroscience, 28*(44), 11277-11291. doi: Doi 10.1523/Jneurosci.2982-08.2008

Dacey, D. M. (2000). Parallel pathways for spectral coding in primate retina. *Annu Rev Neurosci, 23*, 743-775. doi: 10.1146/annurev.neuro.23.1.743

Dacey, D. M., Liao, H. W., Peterson, B. B., Robinson, F. R., Smith, V. C., Pokorny, J., . . . Gamlin, P. D. (2005). Melanopsin-expressing ganglion cells in primate retina signal colour and irradiance and project to the LGN. *Nature, 433*(7027), 749-754. doi: Doi 10.1038/Nature03387

Dacey, D. M., Peterson, B. B., Robinson, F. R., & Gamlin, P. D. (2003). Fireworks in the primate retina: in vitro photodynamics reveals diverse LGN-projecting ganglion cell types. *Neuron, 37*(1), 15-27. doi: S0896627302011431 [pii]

Dann, J. F., & Buhl, E. H. (1987). Retinal Ganglion-Cells Projecting to the Accessory Optic-System in the Rat. *Journal of Comparative Neurology, 262*(1), 141-158. doi: DOI 10.1002/cne.902620111

Derrington, A. M., Lennie, P., & Wright, M. J. (1979). The mechanism of peripherally evoked responses in retinal ganglion cells. *The Journal of physiology, 289*, 299-310.

Dowling, John E. (1987). *The Retina: An Approachable Part of the Brain*: Belknap Press of Harvard University Press.

Drasdo, N., & Fowler, C. W. (1974). Non-linear projection of the retinal image in a wide-angle schematic eye. *The British journal of ophthalmology, 58*(8), 709-714.

Dreher, B., Sefton, A. J., Ni, S. Y. K., & Nisbett, G. (1985). The Morphology, Number, Distribution and Central Projections of Class-I Retinal Ganglion-Cells in Albino and Hooded Rats. *Brain Behavior and Evolution, 26*(1), 10-48. doi: Doi 10.1159/000118764

Enroth-Cugell, C., & Pinto, L. H. (1972). Properties of the surround response mechanism of cat retinal ganglion cells and centre-surround interaction. *J Physiol, 220*(2), 403-439.

Enroth-Cugell, C., & Robson, J. G. (1966). The contrast sensitivity of retinal ganglion cells of the cat. *J Physiol, 187*(3), 517-552.

Famiglietti, E. V., & Kolb, H. (1976). Structural Basis for on-Center and Off-Center Responses in Retinal Ganglion-Cells. *Science, 194*(4261), 193-195. doi: DOI 10.1126/science.959847

Field, G. D., & Chichilnisky, E. J. (2007). Information processing in the primate retina: Circuitry and coding. *Annual Review of Neuroscience, 30*, 1-30. doi: DOI 10.1146/annurev.neuro.30.051606.094252

Fohlmeister, J. F., & Miller, R. F. (1997). Mechanisms by which cell geometry controls repetitive impulse firing in retinal ganglion cells. *Journal of Neurophysiology, 78*(4), 1948-1964.

Freeman, Daniel. (2009). *MAINTAINED DISCHARGE AND ADAPTATION PROPERTIES OF RAT RETINAL GANGLION CELLS.* PhD, Boston University.

Fried, S. I., Hsueh, H. A., & Werblin, F. S. (2006). A method for generating precise temporal patterns of retinal spiking using prosthetic stimulation. *Journal of Neurophysiology, 95*(2), 970-978. doi: 00849.2005 [pii]10.1152/jn.00849.2005

Fried, S. I., Lasker, A. C. W., Desai, N. J., Eddington, D. K., & Rizzo, J. F. (2009). Axonal Sodium-Channel Bands Shape the Response to Electric Stimulation in Retinal Ganglion Cells. *Journal of Neurophysiology, 101*(4), 1972-1987. doi: DOI 10.1152/jn.91081.2008

Fukada, Y. (1971). Receptive Field Organization of Cat Optic Nerve Fibers with Special Reference to Conduction Velocity. *Vision Research, 11*(3), 209-&. doi: Doi 10.1016/0042-6989(71)90186-6

Fukuda, Y., & Stone, J. (1974). Retinal distribution and central projections of Y-, X-, and W-cells of the cat's retina. *Journal of Neurophysiology, 37*(4), 749-772.

Geddes, L. A. (2004). Accuracy limitations of chronaxie values. *Ieee Transactions on Biomedical Engineering, 51*(1), 176-181. doi: Doi 10.1109/Tbme.2003.820340

Gollisch, T., & Meister, M. (2010). Eye smarter than scientists believed: neural computations in circuits of the retina. *Neuron, 65*(2), 150-164. doi: S0896-6273(09)00999-4 [pii]10.1016/j.neuron.2009.12.009

Granit, R. (1946). The distribution of excitation and inhibition in single-fibre responses from a polarized retina. *J Physiol, 105*, 45-53.

Hadjinicolaou, A. E., Leung, R. T., Garrett, D. J., Ganesan, K., Fox, K., Nayagam, D. A. X., . . . O'Brien, B. J. (2012). Electrical stimulation of retinal ganglion cells with diamond and the development of an all diamond retinal prosthesis. *Biomaterials, 33*(24), 5812-5820. doi: DOI 10.1016/j.biomaterials.2012.04.063

Hamasaki, D. I., & Maguire, G. W. (1985). A neural pathway for the shift response in the cat. [Research Support, U.S. Gov't, P.H.S.]. *Brain research, 337*(1), 51-58.

Hamill, O. P., Marty, A., Neher, E., Sakmann, B., & Sigworth, F. J. (1981). Improved Patch-Clamp Techniques for High-Resolution Current Recording from Cells and Cell-Free Membrane Patches. *Pflugers Archiv-European Journal of Physiology, 391*(2), 85-100. doi: Doi 10.1007/Bf00656997

Hartline, H. K. (1938). The Response of single optic nerve fibers of the vertebrate eye to illumination of the retina. *Am J Physiol*(121).

Hartline, H. K. (1940). The receptive fields of optic nerve fibers. *American Journal of Physiology, 130*(4), 0690-0699.

Hille, Bertil. (1992). *Ionic Channels of Excitable Membranes* (Second ed.): Sinauer Associates Inc.

Hochstein, S., & Shapley, R. M. (1976). Quantitative analysis of retinal ganglion cell classifications. *J Physiol, 262*(2), 237-264.

Hodgkin, A. L., & Huxley, A. F. (1952a). Currents Carried by Sodium and Potassium Ions through the Membrane of the Giant Axon of Loligo. *Journal of Physiology-London, 116*(4), 449-472.

Hodgkin, A. L., & Huxley, A. F. (1952b). A Quantitative Description of Membrane Current and Its Application to Conduction and Excitation in Nerve. *Journal of Physiology-London, 117*(4), 500-544.

Hoffman, J. E., & Subramaniam, B. (1995). The Role of Visual-Attention in Saccadic Eye-Movements. *Perception & Psychophysics, 57*(6), 787-795. doi: Doi 10.3758/Bf03206794

Hubel, D. H., & Wiesel, T. N. (1960). Receptive Fields of Optic Nerve Fibres in the Spider Monkey. *Journal of Physiology-London, 154*(3), 572-580.

Humayun, M. S., Prince, M., de Juan, E., Barron, Y., Moskowitz, M., Klock, I. B., & Milam, A. H. (1999). Morphometric analysis of the extramacular retina from postmortem eyes with retinitis pigmentosa. *Investigative Ophthalmology & Visual Science, 40*(1), 143-148.

Hunziker, Hans-Werner. (2007). *Im Auge des Lesers* Stäubli.

Huxlin, K. R., & Goodchild, A. K. (1997). Retinal ganglion cells in the albino rat: Revised morphological classification. *Journal of Comparative Neurology, 385*(2), 309-323. doi: Doi 10.1002/(Sici)1096-9861(19970825)385:2<309::Aid-Cne9>3.0.Co;2-5

Ikeda, H., & Wright, M. J. (1972). Receptive Field Organization of Sustained and Transient Retinal Ganglion-Cells Which Serve Different Functional Roles. *Journal of Physiology-London, 227*(3), 769-800.

Jack, J.J.B., Noble, D., & Tsien, R.W. (1975). *Electric current flow in excitable cells*: Clarendon Press, Oxford.

Jakobs, T. C., Koizumi, A., & Masland, R. H. (2008). The spatial distribution of glutamatergic inputs to dendrites of retinal ganglion cells. *Journal of Comparative Neurology, 510*(2), 221-236. doi: Doi 10.1002/Cne.21795

Jensen, R. J. (1991). Intracellular recording of light responses from visually identified ganglion cells in the rabbit retina. *J Neurosci Methods, 40*(2-3), 101-112.

Kolb, H. (1994). The Architecture of Functional Neural Circuits in the Vertebrate Retina - the Proctor Lecture. *Investigative Ophthalmology & Visual Science, 35*(5), 2385-2404.

Kole, M. H., Ilschner, S. U., Kampa, B. M., Williams, S. R., Ruben, P. C., & Stuart, G. J. (2008). Action potential generation requires a high sodium channel density in the axon initial segment. [In Vitro Research Support, Non-U.S. Gov't]. *Nature neuroscience, 11*(2), 178-186. doi: 10.1038/nn2040

Kress, G. J., Dowling, M. J., Meeks, J. P., & Mennerick, S. (2008). High threshold, proximal initiation, and slow conduction velocity of action potentials in dentate granule neuron mossy fibers. *Journal of Neurophysiology, 100*(1), 281-291. doi: 90295.2008 [pii]10.1152/jn.90295.2008

Kruger, J. (1980). The Shift-Effect Enhances X-Type and Suppresses Y-Type Response Characteristics of Cat Retinal Ganglion-Cells. *Brain Research, 201*(1), 71-84. doi: Doi 10.1016/0006-8993(80)90776-3

Kuffler, S. W. (1952). Neurons in the Retina - Organization, Inhibition and Excitation Problems. *Cold Spring Harbor Symposia on Quantitative Biology, 17*, 281-292.

Kuffler, S. W. (1953). Discharge Patterns and Functional Organization of Mammalian Retina. *Journal of Neurophysiology, 16*(1), 37-68.

Lamb, T. D., Collin, S. P., & Pugh, E. N. (2007). Evolution of the vertebrate eye: opsins, photoreceptors, retina and eye cup. *Nature Reviews Neuroscience, 8*(12), 960-975. doi: Doi 10.1038/Nrn2283

Levick, W. R. (1972). Another Tungsten Microelectrode. *Medical & Biological Engineering, 10*(4), 510-&. doi: Doi 10.1007/Bf02474199

Levick, W. R. (1996). Receptive fields of cat retinal ganglion cells with special reference to the Alpha cells. *Progress in Retinal and Eye Research, 15*(2), 457-500. doi: Doi 10.1016/1350-9462(96)00011-0

Levick, W. R., Cleland, B. G., & Dubin, M. W. (1972). Lateral Geniculate Neurons of Cat - Retinal Inputs and Physiology. *Investigative Ophthalmology, 11*(5), 302-&.

Levick, W. R., & Dvorak, D. R. (1986). The Retina - from Molecules to Networks. *Trends in Neurosciences, 9*(5), 181-185.

Levick, W.R., & Thibos, L. N. (1983). Receptive Fields of Cat Ganglion Cells: Classification and Construction. *Prog Retinal Res, 2*, 267-319.

Levick, W.R., & Zacks, J. L. (1970). Responses of Cat Retinal Ganglion Cells to Breif Flashes of Light. *Journal of Physiology-London, 206*(3), 677-&.

Levttvin, J.Y., Maturana, H. R., McCulloch, W. S., & Pitts, W.H. (1959). What the Frog's Eye Tells the Frog's Brain. *Proc. Inst. Radio Engr., 47*, 1940-1951.

Lipton, S. A., & Tauck, D. L. (1987). Voltage-Dependent Conductances of Solitary Ganglion-Cells Dissociated from the Rat Retina. *Journal of Physiology-London, 385*, 361-391.

Marc, R. E., Jones, B. W., Watt, C. B., & Strettoi, E. (2003). Neural remodeling in retinal degeneration. *Progress in Retinal and Eye Research, 22*(5), 607-655. doi: Doi 10.1016/S1350-9462(03)00039-9

Margalit, E., Maia, M., Weiland, J. D., Greenberg, R. J., Fujii, G. Y., Torres, G., . . . Humayun, M. S. (2002). Retinal prosthesis for the blind. *Surv Ophthalmol, 47*(4), 335-356. doi: S0039625702003119 [pii]

Martin, P. R., & Grunert, U. (1992). Spatial Density and Immunoreactivity of Bipolar Cells in the Macaque Monkey Retina. *Journal of Comparative Neurology, 323*(2), 269-287. doi: DOI 10.1002/cne.903230210

Martinez-Conde, S., Macknik, S. L., & Hubel, D. H. (2004). The role of fixational eye movements in visual perception. *Nature Reviews Neuroscience, 5*(3), 229-240. doi: Doi 10.1038/Nrn1348

Masland, R. H. (2001a). The fundamental plan of the retina. *Nature Neuroscience, 4*(9), 877-886.

Masland, R. H. (2001b). Neuronal diversity in the retina. *Curr Opin Neurobiol, 11*(4), 431-436. doi: S0959-4388(00)00230-0 [pii]

Masland, R. H. (2012). The neuronal organization of the retina. [Research Support, N.I.H., Extramural Review]. *Neuron, 76*(2), 266-280. doi: 10.1016/j.neuron.2012.10.002

Masland, R. H., & Martin, P. R. (2007). The unsolved mystery of vision. *Curr Biol, 17*(15), R577-582. doi: S0960-9822(07)01419-4 [pii]10.1016/j.cub.2007.05.040

Maturana, M., Wong, R., Cloherty, S., Ibbotson, M. R., Hadjinicolaou, A. E., Grayden, D. B., . . . Kameneva, T. (2013). *Retinal ganglion cells electrophysiology: the effect of cell morphology on impulse waveform*. Paper presented at the 2013 Annual International Conference of the IEEE Engineering in Medicine and Biology Society (Embc), Osaka, Japan.

Maturana, M., Wong, R., Kameneva, T., Cloherty, S., Ibbotson, M. R., Hadjinicolaou, A. E., . . . O'Brien, B. J. . (2013). *Predicting the location of the axon initial segment using spike waveform analysis: Simulations of retinal ganglion cell physiology*. Paper presented at the Computational Neurosciences Conference 2013, Paris, France.

McCreery, D. B., Agnew, W. F., Yuen, T. G., & Bullara, L. A. (1988). Comparison of neural damage induced by electrical stimulation with faradaic and capacitor electrodes. [Comparative Study Research Support, U.S. Gov't, P.H.S.]. *Annals of Biomedical Engineering, 16*(5), 463-481.

McCreery, D. B., Agnew, W. F., Yuen, T. G. H., & Bullara, L. (1990). Charge-Density and Charge Per Phase as Cofactors in Neural Injury Induced by Electrical-Stimulation. *Ieee Transactions on Biomedical Engineering, 37*(10), 996-1001. doi: Doi 10.1109/10.102812

McIlwain, J. T. (1966). Some Evidence Concerning Physiological Basis of Periphery Effect in Cats Retina. *Experimental Brain Research, 1*(3), 265-&.

Mechler, F., & Ringach, D. L. (2002). On the classification of simple and complex cells. *Vision Research, 42*(8), 1017-1033. doi: Pii S0042-6989(02)00025-1Doi 10.1016/S0042-6989(02)00025-1

Meister, M., & Berry, M. J., 2nd. (1999). The neural code of the retina. *Neuron, 22*(3), 435-450. doi: S0896-6273(00)80700-X [pii]

Murakami, M., & Shimoda, Y. (1977). Identification of Amacrine and Ganglion-Cells in Carp Retina. *Journal of Physiology-London, 264*(3), 801-&.

O'Brien, B. J., Isayama, T., Richardson, R., & Berson, D. M. (2002). Intrinsic physiological properties of cat retinal ganglion cells. *Journal of Physiology-London, 538*(3), 787-802. doi: 10.1113/jphysiol.2001.013009

Opie, N. L., Greferath, U., Vessey, K. A., Burkitt, A. N., Meffin, H., Grayden, D. B., & Fletcher, E. L. (2012). Retinal Prosthesis Safety: Alterations in Microglia Morphology due to Thermal Damage and Retinal Implant Contact. *Invest Ophthalmol Vis Sci, 53*(12), 7802-7812. doi: iovs.12-10600 [pii]10.1167/iovs.12-10600

Pasternak, T., & Horn, K. (1991). Spatial Vision of the Cat - Variation with Eccentricity. *Visual Neuroscience, 6*(2), 151-158.

Petrusca, D., Grivich, M. I., Sher, A., Field, G. D., Gauthier, J. L., Greschner, M., . . . Litke, A. M. (2007). Identification and characterization of a Y-like primate retinal ganglion cell type. *Journal of Neuroscience, 27*(41), 11019-11027. doi: Doi 10.1523/Jneurosci.2836-07.2007

Quigley, H. A., & Broman, A. T. (2006). The number of people with glaucoma worldwide in 2010 and 2020. *British Journal of Ophthalmology, 90*(3), 262-267. doi: DOI 10.1136/bjo.2005.081224

Ranck, J. B. (1975). Which Elements Are Excited in Electrical-Stimulation of Mammalian Central Nervous-System - Review. *Brain Research, 98*(3), 417-440. doi: Doi 10.1016/0006-8993(75)90364-9

Rapaport, D. H., & Stone, J. (1988). The Periphery Effect in Cat Retinal Ganglion-Cells - Variation with Functional Class and Eccentricity. *Experimental Brain Research, 70*(1), 73-78.

Robinson, D. W., & Chalupa, L. M. (1997). The intrinsic temporal properties of alpha and beta retinal ganglion cells are equivalent. *Curr Biol, 7*(6), 366-374. doi: S0960-9822(06)00184-9 [pii]

Robinson, D. W., & Wang, G. Y. (1998). Development of intrinsic membrane properties in mammalian retinal ganglion cells. *Seminars in Cell & Developmental Biology, 9*(3), 301-310. doi: DOI 10.1006/scdb.1998.0229

Rodieck, R.W. (1998). *The First Steps in Seeing*: Sinauer Associates.

Rowe, M. H., & Stone, J. (1977). Naming of neurones. Classification and naming of cat retinal ganglion cells. *Brain Behav Evol, 14*(3), 185-216.

Santos, A., Humayun, M. S., deJuan, E., Greenberg, R. J., Marsh, M. J., Klock, I. B., & Milam, A. H. (1997). Preservation of the inner retina in retinitis pigmentosa: A morphometric analysis. *Investigative Ophthalmology & Visual Science, 38*(4), 1443-1443.

Schmidt, E. M., Bak, M. J., Hambrecht, F. T., Kufta, C. V., ORourke, D. K., & Vallabhanath, P. (1996). Feasibility of a visual prosthesis for the blind based on intracortical microstimulation of the visual cortex. *Brain, 119*, 507-522. doi: DOI 10.1093/brain/119.2.507

Sekirnjak, C., Hottowy, P., Sher, A., Dabrowski, W., Litke, A. M., & Chichilnisky, E. J. (2006). Electrical stimulation of mammalian retinal ganglion cells with multielectrode arrays. *Journal of Neurophysiology, 95*(6), 3311-3327. doi: DOI 10.1152/jn.01168.2005

Shapley, R. M., & Victor, J. D. (1980). The Effect of Contrast on the Non-Linear Response of the Y-Cell. *Journal of Physiology-London, 302*(May), 535-547.

Shepherd, R. K., & Javel, E. (1999). Electrical stimulation of the auditory nerve: II. Effect of stimulus waveshape on single fibre response properties. *Hearing Research, 130*(1-2), 171-188. doi: Doi 10.1016/S0378-5955(99)00011-8

Shivdasani, M. N., Luu, C. D., Cicione, R., Fallon, J. B., Allen, P. J., Leuenberger, J., . . . Williams, C. E. (2010). Evaluation of stimulus parameters and electrode geometry for an effective suprachoroidal retinal prosthesis. *J Neural Eng, 7*(3), 036008. doi: S1741-2560(10)47737-X [pii]10.1088/1741-2560/7/3/036008

Siegert, S., Scherf, B. G., Del Punta, K., Didkovsky, N., Heintz, N., & Roska, B. (2009). Genetic address book for retinal cell types. *Nature Neuroscience, 12*(9), 1197-U1130. doi: Doi 10.1038/Nn.2370

Srinivasan, M. V., Laughlin, S. B., & Dubs, A. (1982). Predictive Coding - a Fresh View of Inhibition in the Retina. *Proceedings of the Royal Society B-Biological Sciences, 216*(1205), 427-459. doi: DOI 10.1098/rspb.1982.0085

Stanford, L. R. (1987a). W-cells in the cat retina: correlated morphological and physiological evidence for two distinct classes. *Journal of Neurophysiology, 57*(1), 218-244.

Stanford, L. R. (1987b). X-Cells in the Cat Retina - Relationships between the Morphology and Physiology of a Class of Cat Retinal Ganglion-Cells. *Journal of Neurophysiology, 58*(5), 940-964.

Stein, J. J., Johnson, S. A., & Berson, D. M. (1996). Distribution and coverage of beta cells in the cat retina. *Journal of Comparative Neurology, 372*(4), 597-617.

Stone, J., & Fukuda, Y. (1974). Properties of cat retinal ganglion cells: a comparison of W-cells with X- and Y-cells. *Journal of Neurophysiology, 37*(4), 722-748.

Stone, J., & Hoffmann, K. P. (1972). Very slow-conducting ganglion cells in the cat's retina: a major, new functional type? *Brain Res, 43*(2), 610-616.

Stone, J. L., Barlow, W. E., Humayun, M. S., de Juan, E., Jr., & Milam, A. H. (1992). Morphometric analysis of macular photoreceptors and ganglion cells in retinas with retinitis pigmentosa. *Arch Ophthalmol, 110*(11), 1634-1639.

Sun, W., Li, N., & He, S. (2002). Large-scale morophological survey of rat retinal ganglion cells. *Vis Neurosci, 19*(4), 483-493.

Taira, N., Imazawa, Y., & Motokawa, K. (1965). Electrical Stimulation of on- and Off-Units in Cats Retina. *Tohoku Journal of Experimental Medicine, 85*(1), 89-&.

Tasaki, I. (1956). Initiation and Abolition of the Action Potential of a Single Node of Ranvier. *Journal of General Physiology, 39*(3), 377-395. doi: Doi 10.1085/Jgp.39.3.377

Tatler, B., O'Carroll, D. C., & Laughlin, S. B. (2000). Temperature and the temporal resolving power of fly photoreceptors. *Journal of Comparative Physiology a-Sensory Neural and Behavioral Physiology, 186*(4), 399-407. doi: DOI 10.1007/s003590050439

Tauchi, M., & Masland, R. H. (1984). The Shape and Arrangement of the Cholinergic Neurons in the Rabbit Retina. *Proceedings of the Royal Society B-Biological Sciences, 223*(1230), 101-+. doi: DOI 10.1098/rspb.1984.0085

Taylor, W. R. (1996). Response properties of long-range axon-bearing amacrine cells in the dark-adapted rabbit retina. *Visual Neuroscience, 13*(4), 599-604.

Taylor, W. R., & Wassle, H. (1995). Receptive-Field Properties of Starburst Cholinergic Amacrine Cells in the Rabbit Retina. *European Journal of Neuroscience, 7*(11), 2308-2321. doi: DOI 10.1111/j.1460-9568.1995.tb00652.x

Thoreson, W. B., & Mangel, S. C. (2012). Lateral interactions in the outer retina. *Progress in Retinal and Eye Research, 31*(5), 407-441. doi: DOI 10.1016/j.preteyeres.2012.04.003

Tkalcevic, L. A., & Abel, L. A. (2005). The effects of increased visual task demand on foveation in congenital nystagmus. *Vision Research, 45*(9), 1139-1146. doi: DOI 10.1016/j.visres.2004.11.004

Turi, M., & Burr, D. (2012). Spatiotopic perceptual maps in humans: evidence from motion adaptation. *Proceedings of the Royal Society B-Biological Sciences, 279*(1740), 3091-3097. doi: DOI 10.1098/rspb.2012.0637

Vaney, D. I. (1980). Quantitative Comparison between the Ganglion-Cell Populations and Axonal Outflows of the Visual Streak and Periphery of the Rabbit Retina. *Journal of Comparative Neurology, 189*(2), 215-233. doi: DOI 10.1002/cne.901890202

Veraart, C., Raftopoulos, C., Mortimer, J. T., Delbeke, J., Pins, D., Michaux, G., . . . Wanet-Defalque, M. C. (1998). Visual sensations produced by optic nerve stimulation using an implanted self-sizing spiral cuff electrode. *Brain Research, 813*(1), 181-186. doi: Doi 10.1016/S0006-8993(98)00977-9

Wassle, H. (2004). Parallel processing in the mammalian retina. *Nature Reviews Neuroscience, 5*(10), 747-757. doi: Doi 10.1038/Nrn1497

Wassle, H., Cleland, B. G., & Levick, W. R. (1975). Physiological Identification of a Morphological Class of Cat Retinal Ganglion-Cells. *Experimental Brain Research, 23*, 213-213.

Wassle, H., Levick, W. R., & Cleland, B. G. (1975). The distribution of the alpha type of ganglion cells in the cat's retina. *J Comp Neurol, 159*(3), 419-438. doi: 10.1002/cne.901590308

Wassle, H., Peichl, L., & Boycott, B. B. (1981). Morphology and Topography of on-Alpha and Off-Alpha Cells in the Cat Retina. *Proceedings of the Royal Society B-Biological Sciences, 212*(1187), 157-+. doi: DOI 10.1098/rspb.1981.0032

Weitz, A. C., Behrend, M. R., Humayun, M. S., Chow, R. H., & Weiland, J. D. (2011). Interphase Gap Decreases Electrical Stimulation Threshold of Retinal Ganglion Cells. *2011 Annual International Conference of the Ieee Engineering in Medicine and Biology Society (Embc)*, 6725-6728.

Werblin, F. S. (2010). Circuitry Underlying Visual Processing in the Retina. *Cellular Nanoscale Sensory Wave Computing*, 163-180. doi: Doi 10.1007/978-1-4419-1011-0_8

WHO. (2012). World Health Organization.

Wikipedia Public Domain. In Rheobase chronaxie.png (Ed.): Sav vas.

Wong, R. C. S., Cloherty, S. L., Ibbotson, M. R., & O'Brien, B. J. (2012). Intrinsic Physiological Properties of Rat Retinal Ganglion Cells with a Comparative Analysis. *Journal of Neurophysiology*. doi: jn.01091.2011 [pii]10.1152 / jn.01091.2011

Chapter 2

Intrinsic Physiological Properties of Rat Retinal Ganglion Cells with a Comparative Analysis

2.1 Abstract

The mammalian retina contains 15-20 different retinal ganglion cell (RGC) types, each of which is responsible for encoding different aspects of the visual scene. The encoding is defined by a combination of RGC synaptic inputs, the neurotransmitter systems used, dendritic tree size, location in the visual field and RGCs' intrinsic physiological properties. Each cell's intrinsic properties are defined by its morphology and membrane characteristics, including the complement and localization of the ion channels expressed. In this study, we examined the hypothesis that the intrinsic properties of individual RGC types are conserved among mammalian species. To do so, we measured the intrinsic properties of 16 morphologically defined rat RGC types and compared these data with cat RGC types. Our data demonstrate that in the rat, different morphologically defined RGC types have distinct patterns of intrinsic properties. Variation in these properties across cell types was comparable to that found for cat RGC types. When presumed morphological homologs in rat and cat retina were compared directly, some RGC types had very similar properties. The rat A2 cell exhibited nearly identical patterns of intrinsic properties to the cat alpha cell. In contrast, rat D2 cells (ON-OFF directionally selective) had a very different pattern of intrinsic properties than the cat iota cell. Our data suggest that the intrinsic properties of RGCs with similar morphology and suspected visual function may be subject to natural selection due to the behavioral niche occupied by the species.

2.2 Introduction

The retina has an extraordinary task to perform. It must capture, process and relay all relevant information about the visual scene within one fixation pause (~300ms) before the eye moves on to another target and the process repeats itself. It manages this task through an array of parallel processing networks, each of which is tuned to extract and represent different features of the visual scene (e.g. form, motion, color) and send that information to the appropriate target brain nuclei via the axons of retinal ganglion cells (RGCs). As a result, it is now commonly believed that 15-20 different arrays of RGCs exist in mammalian retina (for review, see (Berson, 2008; Dacey, Peterson, Robinson, & Gamlin, 2003; Masland, 2001), each of which carries a piece of visual information. These elements assemble in the brain as vision.

The visual information carried by RGCs is determined in at least three ways. First, the dendrites of each RGC type sample from the many different types of bipolar (~ 11 types) and amacrine cells (~ 30 types) present in the mammalian retina (for review, see (Masland, 2001; Vaney, 1990; Wässle, 2004). Second, information is filtered differentially by each RGC depending upon the neurotransmitter receptors present. Finally, the intrinsic physiological properties of each RGC type ultimately limit the information they can carry. Prior studies of RGC intrinsic properties have been largely limited to identifying individual ion channel types without regard to an individual cell's morphological type. Only a handful of studies have attempted electrophysiological recordings with complete anatomical reconstruction of each cell and yet fewer studies have sampled the entire cell population (Fohlmeister, Cohen, & Newman, 2010; Fohlmeister & Miller, 1997; Ishida, 1991; Liets, Olshausen, Wang, & Chalupa, 2003; Lipton & Tauck, 1987; Margolis & Detwiler, 2007; O'Brien, Isayama, Richardson, & Berson, 2002; Qu & Myhr, 2008, 2011; Robinson & Chalupa, 1997; Robinson & Wang, 1998; Sheasby & Fohlmeister, 1999; Sucher & Lipton, 1992; Tabata & Kano, 2002; Van Hook & Berson, 2010; Wang, Ratto, Bisti, & Chalupa, 1997; Zeck & Masland, 2007). Moreover, no study has yet compared intrinsic properties for morphologically similar cell types across different mammalian species.

In the present study, we carried out a complete survey of the intrinsic physiological properties of 16 morphologically defined rat RGC types, including both passive (resting membrane potential, time constant, input resistance) and active (maximum firing rates,

frequency adaptation, anomalous rectification and ramping) properties. Our data demonstrate that different types of RGCs in rat, based on anatomical classification alone (Sun *et al.* 2002), vary enormously in both their passive and active intrinsic properties but the properties are consistent within cell types. Moreover, we compared our data with a similar survey previously obtained for the complement of cat RGC types (O'Brien, et al., 2002). Comparing intrinsic properties of rat and cat RGC types that shared similar morphological properties revealed that the agreement was good for some cell types but not for others, suggesting that despite near morphological identity the intrinsic physiological properties of RGCs in a species may be tuned to suit different purposes during evolution. Since the intrinsic properties define not only how each RGC type will respond to its synaptic input, but also how it will respond to extracellular electrical stimulation, our data also suggest that care needs be taken when extrapolating from animal models to humans in the development of retinal prosthetic devices.

2.3 Materials and Methods

2.3.1 Ethical approval

Methods conformed to the policies of National Health and Medical Research Council of Australia and were approved by the Animal Experimentation Ethics Committee of the Australian National University.

2.3.2 Retinal whole mount preparation

Data came from 85 pigmented Long-Evans rats ranging in age from 3 - 15 months. We chose the Long-Evans rat as our animal model for several reasons. First, our aim was to examine whether the intrinsic properties of morphologically similar RGC types are conserved among mammalian species. To do so, we required a species where the complement of morphological types is well established. The rat RGC complement has been examined previously, and we used the most recent and extensive classification scheme for our analysis (Huxlin & Goodchild, 1997; Sun, Li, & He, 2002). In addition, the rat model has been used extensively to study the biophysical properties of neuronal voltage-gated ion channels that underlie many of the physiological properties we describe here. The Long-Evans strain is

pigmented and thus does not have the well-known retinal abnormalities associated with albino animals (Jeffery, 1997). Finally, eye size is substantially greater in rats than mice and thus we were able to record greater numbers of cells in each individual animal and thus reduce overall animal usage.

Animals were initially anaesthetized with isoflurane (5% in O_2) and maintained during enucleation with 3% isoflurane. After enucleation, rats were killed with an overdose of Sodium Pentabarbitone (350mg, intracardiac). After hemisecting the eyes behind the ora serrata, we removed the vitreous body and cut each eyecup into 2 - 4 pieces. Pieces of retinal whole mount were mounted, ganglion cell layer up, on a coverslip which formed the bottom of a perfusion chamber (Warner Instruments, Hamden, CT USA, RC-26GLP) and were held in place with a stainless steel harp fitted with Lycra threads (Warner Instruments, CT USA). Once mounted in the chamber the retina was perfused (4-6 ml min^{-1}) with carbogenated Ames medium (Sigma-Aldrich, St. Louis, MO) at room temperature. Recordings were made at room temperature specifically to allow direct interspecies comparison with data previously obtained for cat RGCs (O'Brien, et al., 2002), and the absolute values obtained may therefore differ from the *in vivo* condition (Fohlmeister, et al., 2010). The chamber was mounted on the stage of an upright microscope (Olympus, BX51WI) equipped with a 40x water immersion lens and visualized with infrared optics on a monitor with 4x additional magnification. Detailed methods have been described previously (O'Brien, et al., 2002).

2.3.3 Physiological data collection and analysis

To obtain a whole cell recording, we first made a small hole in the inner limiting membrane (ILM) and optic fiber layer overlying a ganglion cell (O'Brien, et al., 2002; Robinson & Chalupa, 1997; Taylor & Wässle, 1995). Recordings were limited to RGCs exposed during this procedure that had smooth surfaces and a granular cytoplasm. The pipette internal solution contained (in mM): K-gluconate 115, KCl 5, EGTA 5, HEPES 10, Na-ATP 2, Na-GTP 0.25; (mOsm = 273, pH = 7.3) including Alexa Hydrazide 488 (250 µM) and biocytin (0.5%).

Whole-cell current clamp recordings from retinal ganglion cells were obtained with standard procedures (Hamill, Marty, Neher, Sakmann, & Sigworth, 1981). Initial pipette

resistance ranged between 3 and 7 MΩ. The pipette voltage in the bath was nulled prior to recording. It was also checked immediately at the end of each recording after clearing the pipette tip with a pulse of pressure. If bath potentials before and after recording differed, the latter was taken as ground potential. After obtaining a gigaohm seal and rupturing the cellular membrane, the pipette series resistance was measured and compensated with the bridge balance circuit of the amplifier. Resting potentials were corrected for the change in liquid junction potential that occurs upon break-in and cell dialysis (liquid junction potential was measured directly as -5 mV (Neher, 1992). No capacitance compensation was employed.

Membrane potential was amplified (BA-1S, NPI, Germany) digitized with 16-bit precision at 20 kHz (USB-6221, National Instruments), and stored in digital form. The data collected were analyzed off-line with custom software developed in LabVIEW (National Instruments). Cells were excluded from analysis if they exhibited marked instability of resting potential or if their action potentials did not overshoot 0 mV. We tested each cell with a series of depolarizing and hyperpolarizing current steps. For most cells, the largest depolarizing current step drove the cell into spike block and the largest hyperpolarizing step yielded a membrane potential (V_m) of approximately -90 mV.

Spike widths were measured as the full width at half height. Reported widths for individual cells represent the average of at least 15 of such measurements. To minimize the influence of high spiking frequency on spike width, we restricted our analysis of spike width to spontaneous spikes or those evoked by just-suprathreshold current steps. We calculated the input resistance (R_N) for each cell according to Ohm's law ($V = iR$) from the change in steady-state V_m produced by current injections of known amplitude. We used small amplitude hyperpolarizing currents ($\Delta V_m \sim 5$ mV) to avoid triggering action potentials and other non-linear membrane properties. Membrane time constant (τ) was estimated with the method of "peeling" (Johnston & Wu, 1997). Good fits were determined by limiting the root mean square variation of the fit to less than 0.1 ms. If this criterion could not be achieved, the data were excluded from the analysis.

2.3.4 Statistical analyses

To test whether individual measures were statistically related to morphological type we used (unless otherwise noted) the non-parametric Kruskal-Wallis test for multiple independent samples (SPSS v19, IBM). When a significant relationship was detected, a post-hoc test was applied to determine which pairs of types were significantly different from one another. Error measurements are reported as standard error of the mean (SEM) unless otherwise noted.

We also performed unsupervised hierarchical cluster analyses on the entire dataset (SPSS v. 19, IBM) to examine whether the overall pattern of intrinsic physiological properties for each rat RGC type was predictive of morphological classification. We used a between-groups linkage method for progressive clustering of individual cells, using the squared Euclidean distance as a measure of proximity between individual cells.

In addition, we used the same cluster analysis techniques to examine whether the intrinsic physiological properties of individual morphological types might be conserved among species by comparing our rat data with similar data from cat RGCs (O'Brien et al., 2002). To properly compare cell types between species, z-scores for the mean of each cell type's intrinsic physiological properties were calculated within each species. This within species normalization allows the clustering procedure to examine whether functional relationships among the morphological classes are preserved in the two species.

2.3.5 Immunocytochemistry and morphological identification

After recordings, the tissue was removed from the chamber, mounted onto filter paper, fixed for 30 - 60 minutes in phosphate buffered 4% paraformaldehyde, and stored for up to 2 weeks in 0.1 M phosphate buffered saline (PBS; pH 7.4) at 4 ^{o}C. The tissue was subsequently processed to reveal biocytin-filled cells by immersion in 0.5% Triton X-100 (20 µg/mL streptavidin conjugated to Alexa488; Invitrogen) in PBS overnight. Tissue was washed thoroughly in PBS, mounted onto Superfrost+ slides and coverslipped in 60% glycerol. Cellular morphology was classified after 3-D confocal reconstruction (Zeiss PASCAL).

Cells included in this analysis were ganglion cells rather than displaced amacrine cells. This was immediately apparent for many cells because they had an axon that entered the optic fiber layer. Other cells lacked a discernible axon, presumably having lost it during cell exposure, but were virtually certain to be ganglion cells because their somata were larger than those of amacrine cells, they resembled an established rat RGC type, and they lacked axonal branches in the inner plexiform layer (IPL) and other features typical of displaced amacrine cells. Data from RGCs with and without axons were integrated as no significant differences were observed for any of the parameters measured. Ganglion cells were classified morphologically on the basis of soma size, dendritic field size and structure, and dendritic stratification (% IPL depth, mono- or bi- stratified). Dendritic field diameter was estimated by circumscribing the dendritic tree with concave line segments, measuring the resulting area (Zeiss AIM software) and calculating the diameter of an equivalent circle. Retinal eccentricity was not controlled in this study since it has only a small impact upon cell size (Huxlin & Goodchild, 1997; Peichl, 1989) and is not necessary for morphological classification as it is in other species (e.g. central cat alpha cells and peripheral cat beta cells have similar morphologies). The majority of recorded RGCs could be classified according to previously described morphological types (Huxlin & Goodchild, 1997; Sun, et al., 2002). The remaining cells were excluded from this report.

2.4 Results

2.4.1 RGC morphological types

We recorded the physiological response properties of 229 rat retinal ganglion cells from 85 pigmented Long-Evans rats ranging in age from 3 – 15 months of age. Of those, 125 RGCs were filled well enough for complete confocal reconstruction and subsequent morphological classification. As has been previously described (Huxlin & Goodchild, 1997; Sun, et al., 2002), we encountered 16 different types of RGC (Figure 2.1) that could be clearly identified on the basis of their morphological characteristics (Table 2.1) including soma size, dendritic field size, dendritic field structure and stratification in the IPL.

Table 2.1 Morphological characteristics of rat RGC types.

Cell Type	Soma diameter	Field diameter	% Depth	Predicted Centre Sign
A1	21 (3)	488 (26)	74 (7)	ON
A2i	21 (2)	480 (72)	69 (4)	ON
A2o	22 (1)	362 (26)	33 (1)	OFF
B1	13 (1)	217 (9)	27 (8)	OFF
B2	15 (1)	195 (8)	53 (2)	ON
B3i*	13	266	73	OFF
B3o	11 (4)	238 (13)	23 (4)	OFF
B4	15 (1)	232 (12)	43 (4)	ON-OFF
C1	17 (1)	450 (55)	69 (5)	ON
C2i	15 (1)	355 (43)	58 (4)	ON
C2o	16 (1)	316 (8)	24 (3)	OFF
C3	14 (1)	374 (28)	63 (4)	ON
C4i	15 (1)	377 (24)	71 (7)	ON
C4o	15 (1)	294 (13)	30 (5)	OFF
D1	15 (1)	242 (33)	57 (6); 19 (3)	ON-OFF
D2	17 (1)	364 (21)	61 (2); 27 (2)	ON-OFF

Values are: mean (standard error); * indicated only one sample in type B3i. Field diameter refers to the dendritic field and all diameters are in μm.

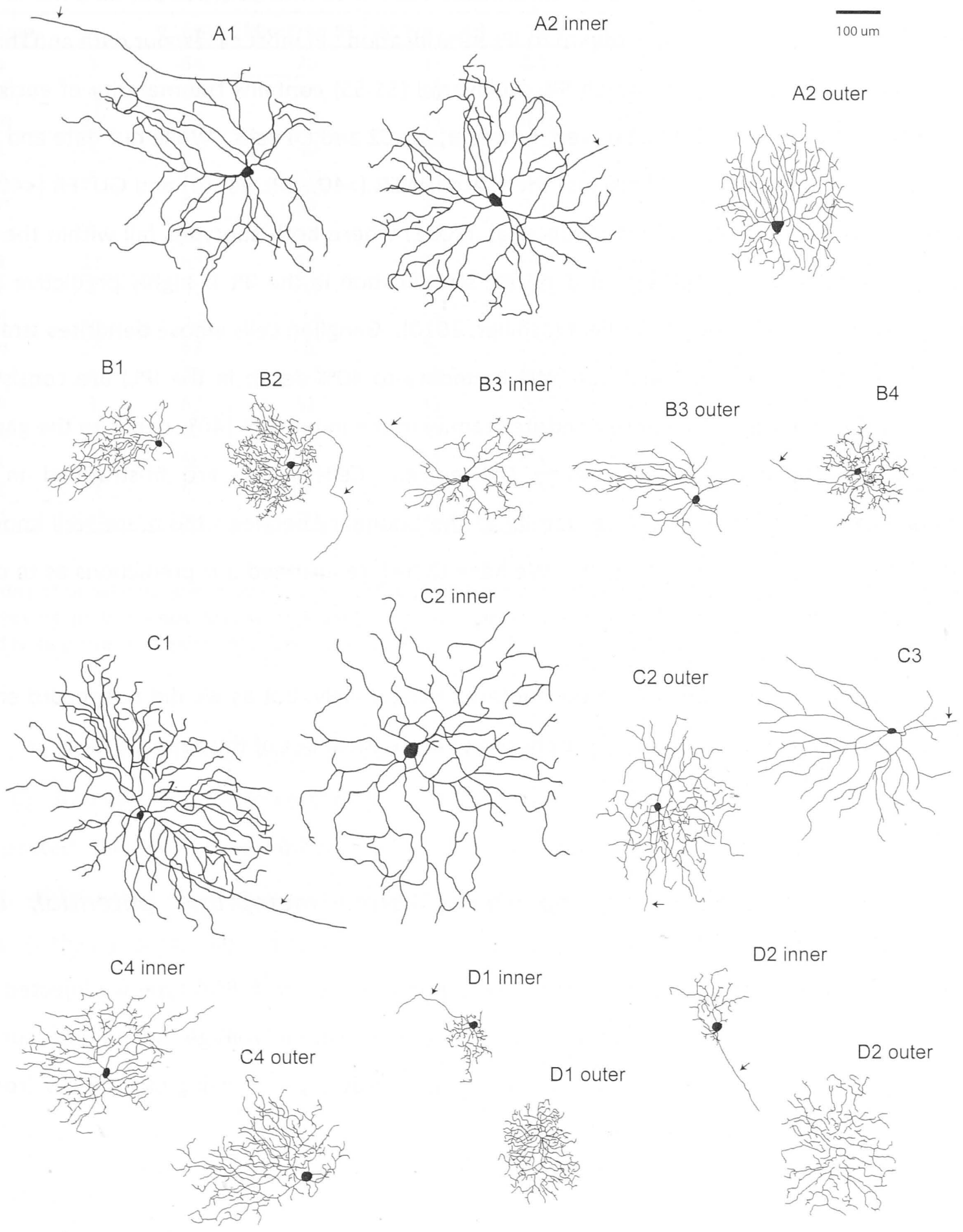

Figure 2.1 Rat retinal ganglion cell (RGC) morphologies. Drawings of individually recorded rat RGCs representative of their type based on soma size, dendritic field size, stratification, and branching pattern. Arrows indicate axonal processes. Inner and outer indicates subtype stratifying in either sublamina a (outer) or b (inner) of the inner plexiform layer. In the case of D types, inner and outer indicate the two levels of a bistratified dendritic arbor. Scale bar = 100 μm.

These data support the prior classification schemes with 16 types but do differ in some of the quantitative details with regard to IPL stratification. In most cases, our data and those of previous studies agree upon which iPL sublayer(s) (S1-S5) contains the majority of each cell's dendrites. Differences were observed, however, for C2 and C4 cells. While our data and those of Huxlin & Goodchild (1997) suggest there are INNER (>40% IPL depth) and OUTER (<40% IPL depth) subtypes, this differs from Sun et al. (2002) where both subtypes fall within the inner IPL (40-100% depth). The level of dendritic stratification in the IPL is highly predictive of the centre sign of a RGC's receptive field (Schiller, 2010). Ganglion cells whose dendrites stratify in the outer 40% (Inner nuclear layer (INL) boundary to 40% depth in the IPL) are consistently OFF-centre, whereas cells whose dendrites ramify in the inner 60% (40% depth to the ganglion cell layer boundary) are consistently ON-centre. Cells which are bi-stratified in both sublaminae or have dendrites that ramify at the boundary between them are well known to have ON-OFF centre receptive fields. We have therefore included our predictions as to centre sign in Table 2.1.

Other morphologies were encountered occasionally, but as we did not record enough for a complete classification, we have chosen to leave them out of this report.

2.4.2 Passive membrane properties (Resting membrane potential, Input resistance, Time constant)

To characterize the passive membrane properties of each RGC type we injected small hyperpolarizing currents to avoid activating or inactivating voltage dependent currents. Resting V_m varied somewhat among the different rat RGC types, ranging over 13 mV from -54 mV (A1) to -67 mV (B4, Figure 2A; Table 2.2).

Table 2.2 Intrinsic physiological properties of rat retinal ganglion cell types.

Cell type	n	V_m (mV)	Max Freq (Hz)	SS Freq (Hz)	FA	SW (ms)	τ (ms)	R_N (MΩ)	Sag (mV)
A1	3	-54	70	31	0.55	1.73	24.5	264	-7.0
A2i	4	-62	165	50	0.69	1.08	11.9	121	-7.5
A2o	21	-59	204	55	0.72	0.85	9.5	98	-4.0
B1	3	-61	30	20	0.32	1.84	48.5	678	-3.7
B2	8	-65	105	34	0.64	1.73	37.6	391	-2.5
B3i*	1	-54	39	24	0.38	1.34	31.2	451	-4.1
B3o	4	-65	74	29	0.50	1.88	34.1	468	-3.5
B4	11	-67	87	38	0.51	1.96	50.9	647	-2.3
C1	4	-61	137	53	0.61	1.53	24.1	233	-8.4
C2i	6	-59	114	53	0.49	1.67	19.8	281	-9.3
C2o	14	-63	120	40	0.63	1.44	22.3	348	-5.4
C3	4	-61	102	42	0.59	1.53	26.5	454	-4.3
C4i	3	-60	62	32	0.45	2.57	34.2	333	-4.9
C4o	15	-62	136	45	0.60	1.73	32.7	384	-2.9
D1	7	-66	103	42	0.53	1.84	31.2	357	-1.7
D2	17	-61	135	63	0.51	1.64	25.4	290	-8.4
ALL	125	-56	101	40	0.53	1.69	30.2	379	-4.8

n: number of sample; V_m: membrane potential; Max Freq: maximum firing rate; SS Freq: steady-state firing rate; FA: frequency adaptation index; SW: spike width; τ: time constant; R_N: input resistance; Sag: rectification of V_m back toward resting level in response to hyperpolarization.

In contrast, R_N and τ varied more than five-fold among the different cell classes (Figure 2.2 B, C). A2o cells had the lowest mean R_N (98 MΩ), while B1 cells had the highest (677 MΩ). As expected, the cellular τ exhibited similar variability among the different RGC types (Figure 2.2 C), which was very closely related to R_N (Pearson's r = 0.78). Where A2o cells had the lowest R_N they also had the shortest τ (9.5ms), while B4 cells had the longest τ (50.9ms).

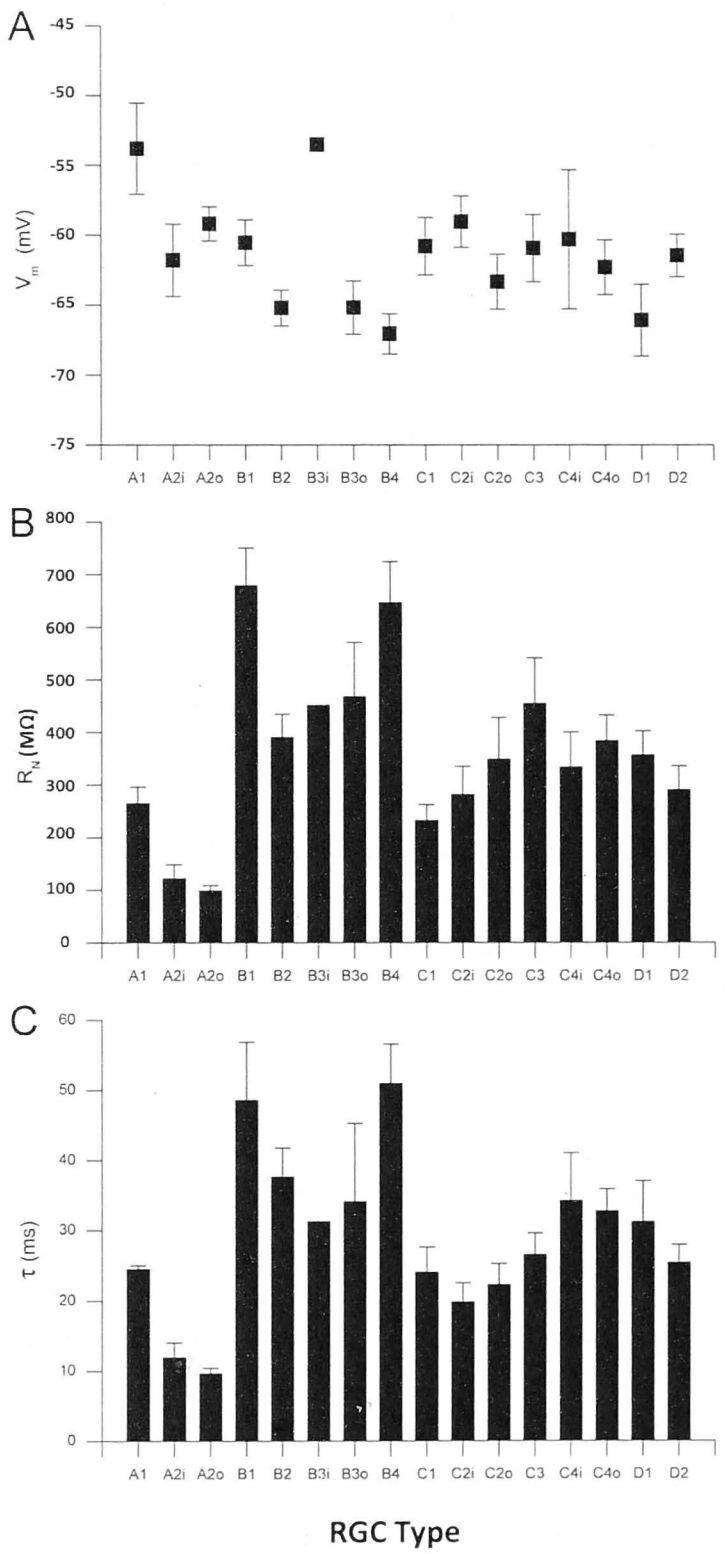

Figure 2.2 Passive membrane properties. **A**) Average resting membrane potential (V_m) for each rat RGC type. **B**) Average input resistance (R_N). **C**) Average time constant (τ). Error bars in this and all subsequent figures represent standard error of the mean (SEM) unless otherwise specified. Horizontal axes: Rat RGC type.

As A2 and B4 types represent some of the largest and smallest RGC types in the rat retina it is possible that both R_N and τ are determined largely by cell size. To get an estimate of how closely these variables are related, we plotted these data for all RGCs recorded (Figure 2.3) and calculated the correlation coefficient for each distribution.

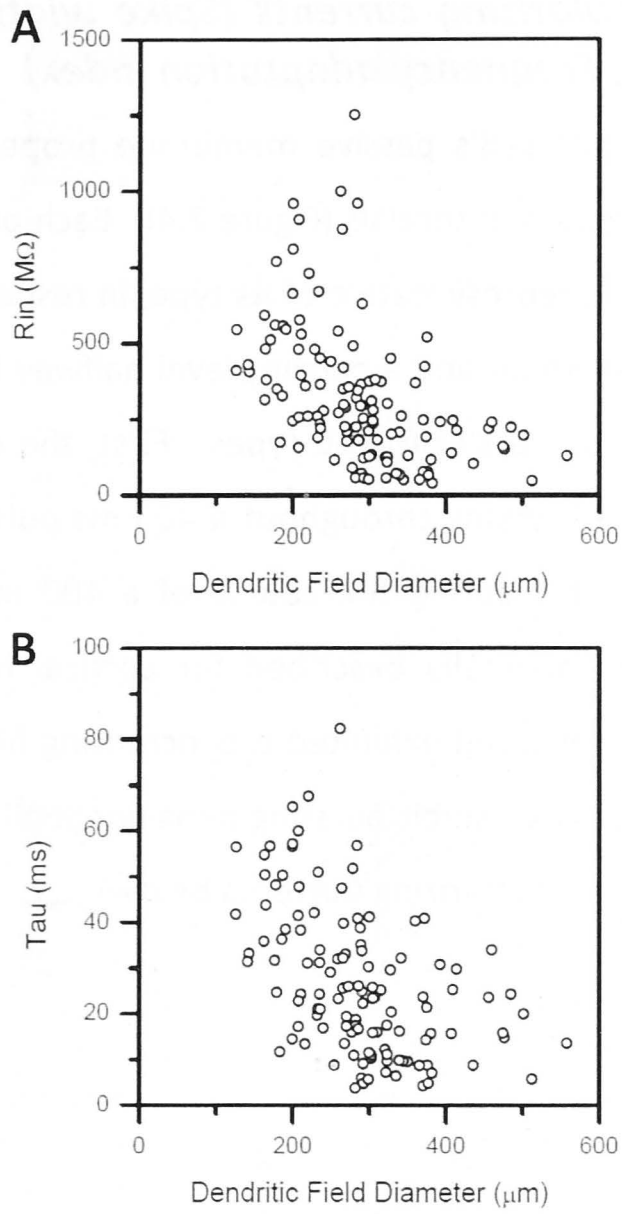

Figure 2.3 Cell size partly accounts for variance in passive properties. **A**) Variation in input resistance (R_N), and **B**) time constant (τ) with dendritic field size for all retinal ganglion cells. There is a small negative trend in both R_N ($r = -0.46$) and τ ($r = -0.47$) with dendritic field size, suggesting that other variables (e.g. leak conductance) also play a large role in defining these parameters.

Both plots in Figure 2.3 demonstrate negative correlations of R_N and τ with increasing cell size as was expected. These relationships, however, account for only a small fraction of the variance in the data (Pearson's $r = -0.46$ (R_N), -0.47 (τ), $p < 0.001$). Thus, R_N and τ are indeed related to cell size, but it is clearly not the only defining variable. Differences in leak conductance(s) as well as spontaneous synaptic input contribute to baseline R_N and τ, but these variables were not measured here.

2.4.3 Responses to depolarizing currents (Spike width, Maximum firing rate, Steady-State firing rate, Frequency adaptation index)

After characterizing each cell's passive membrane properties we injected a series of depolarizing pulses to elicit action potentials (Figure 2.4). Each panel in Figure 2.4 displays the spiking activity of a single cell, representative of its type, in response to three levels of current injection: near threshold, maximum and a current level halfway between these values. There were several features common to all rat RGC types. First, the data demonstrate that all rat RGCs are capable of repetitive spiking throughout a 400 ms pulse. In addition, all RGC types exhibited decreasing firing rates during the course of a 400 ms pulse, most similar to the Regular Spiking (RS) pattern originally described for cortical neurons (Connors & Gutnick, 1990). None of the cells we recorded exhibited the increasing firing rate characteristic of Fast Spiking (FS) neurons, nor did they exhibit bursting behavior similar to Intrinsically Bursting (IB) cells (but see Responses to Hyperpolarizing Currents below).

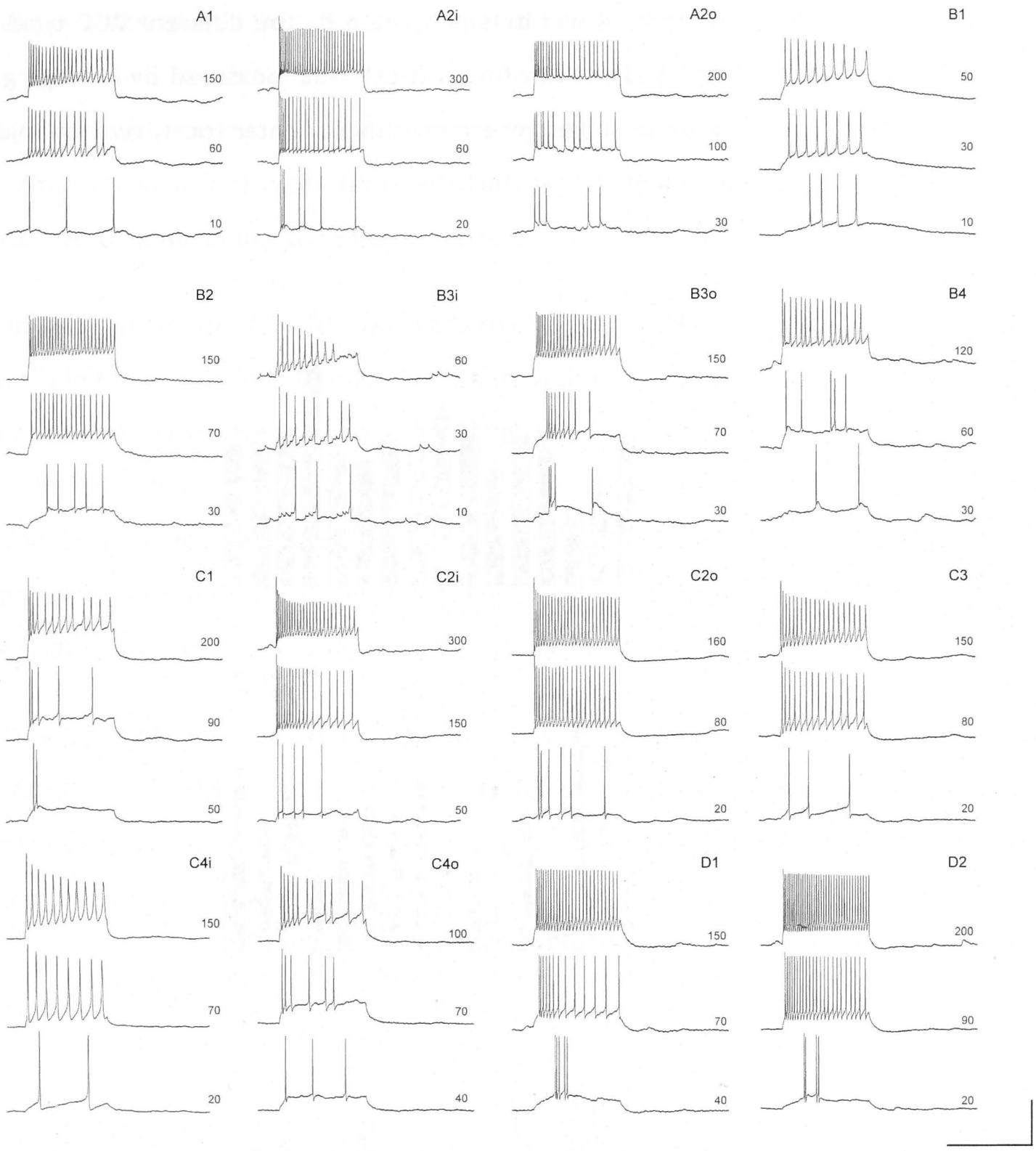

Figure 2.4 Spiking patterns of rat ganglion cell (RGC) types. Representative responses of a single cell from each RGC type to different levels of depolarizing current injected for 400 ms. Number next to each trace indicates current amplitude (pA). The traces for each cell type are organized as follow: at threshold (bottom), midrange (middle), maximum rate (without resulting in spike blockade) (top). All rat RGCs were capable of repetitive spiking and exhibited patterns similar to those of 'Regular Spiking' neurons with varying amounts of frequency adaptation. In addition, most RGC types also exhibited spike amplitude reduction over time, while some were clearly resistant to this even at very high spike rates (e.g. D1, D2). Vertical scale bar, 50 mV; horizontal scale bar, 400 ms.

Quantification of the spike waveforms generated by the different RGC types yielded clear differences (Figure 2.5). Spike width for each cell was measured by averaging the full width at half height of 15 or more spikes generated either spontaneously or from injection of near threshold depolarizing current.

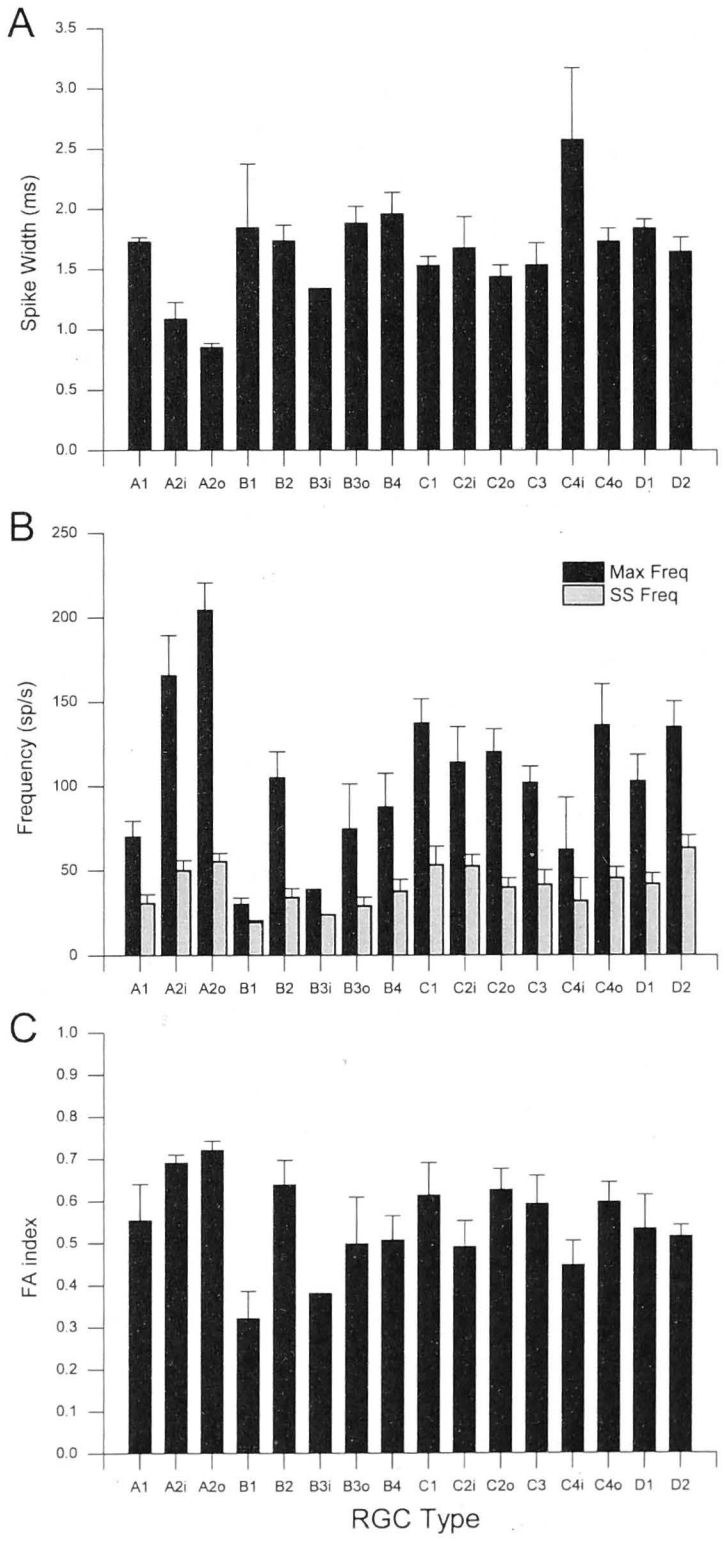

Figure 2.5 Active membrane properties. **A**) Average spike width for each retinal ganglion cell (RGC) type (ms). **B**) Average maximum and steady state firing rate during injection of maximum amplitude depolarizing current for 400 ms. **C**) Average frequency adaptation (FA) index exhibited by each RGC type.

Spike width ranged from 0.9 ms generated by A2o cells up to 2.5 ms characteristic of C4i cells, with much variability in between. Statistical analyses demonstrated that while A2i and A2o spike widths were not significantly different, they both differed significantly from most of the remaining cell types (Kruskal Wallis H (125) = 64.2, $p < 0.05$). No significant differences were found among the other cell classes.

In addition to spike width, the patterns of action potential generation also varied dramatically in the population. Consistent with their short action potentials, A2 cells were also capable of generating the highest firing rates (Figure 2.5B; A2i = 166sp/s; A2o = 204 sp/s). In contrast, B1 cells were the slowest RGC type to generate action potentials (30 sp/s). Correlation analysis demonstrated that spike width did exhibit a negative correlation with maximum firing rate (Pearson's $r = -0.67$, $p < 0.001$) and steady-state firing rate (Pearson's $r = -0.53$, $p < 0.001$), suggesting that numerous factors play a role in defining firing rate.

Moreover, RGC types differed in how well they could sustain their maximum firing rates. To quantify this, we calculated the steady-state firing rate (frequency) by averaging the last three spikes elicited during a 400 ms depolarizing current pulse and calculated the frequency adaptation (FA) index:

$$FA = \frac{Initial\ Frequency \quad - \quad Steady - State\ Frequency}{Initial\ Frequency}$$

The resulting index ranges from 0 (no change in spike rate) to 1 (indicating a decrease in firing rate during the current pulse). As mentioned previously, all RGC types exhibited firing patterns similar to RS cortical neurons (Connors & Gutnick, 1990), and as such all types had positive values of FA index (Figure 2.5C). The FA index also varied among the RGC population with B1 cells being the best at maintaining their maximum frequency (FA = 0.32) while A2 cells exhibited the greatest reduction in firing rate during stimulation (FA = 0.72). Correlation analyses demonstrated a clear positive relationship of maximum firing rate with the strongest reduction in spike frequency over 400 ms (Pearson's $r = 0.87$). Differences among RGC types were also observed in their propensity for action potentials to reduce in amplitude throughout the pulse. Where most RGC types exhibited a slow reduction in spike amplitude during repetitive spiking (e.g. Figure 2.4: B3i, C4i), D1 and D2 cells showed little such reduction, even at maximum spike rates.

2.4.4 Responses to Hyperpolarizing Currents (Sag, Ramping, Rebound bursting)

Figure 2.6 shows the responses of the different rat RGC types to the injection of hyperpolarizing current pulses. Individual cell types exhibited the presence of several different active membrane properties below voltage threshold. Many cell types exhibited varying degrees of anomalous rectification in response to hyperpolarization, also known as "sag" (e.g. Figure 2.6: C1, D2). To quantify the amount of rectification observed, we measured the positive shift in V_m back toward the resting level when the peak hyperpolarization reached -85 mV during 400 ms pulses of negative current (or linearly interpolated when -85 mV was not exactly reached). This difference can be observed by comparing the responses of C3 and D2 cells. Where D2 cells demonstrate a clear sag in V_m even above -85 mV, rectification only occurs in C3 cells when they are substantially hyperpolarized beyond -85 mV. Among the RGC types, C2i cells exhibited the most sag (9 mV) while D1 cells had the least, exhibiting nearly no sag at all. Following the termination of hyperpolarizing pulses, many cells exhibited a subsequent overshoot of the resting V_m, which was capable of generating action potentials. Rebound bursting could be elicited in cells that had either substantial sag (e.g. Figure 2.6: B3o) or no sag at all (e.g. Figure 2.6: B3i, C2o, C4o), suggesting different mechanisms for their generation.

Finally, in a minority of RGCs we observed a phenomenon opposite to bursting - a clear lengthening of the time it took to return to resting V_m after hyperpolarizing pulses. This was most easily observed when the resting potential was held at -85 mV and depolarizing current injections were introduced (Figure 2.6: B4*). Small depolarizing current pulses charged the membrane passively. Larger pulses, however, led to a process that held V_m lower than would be predicted by passive charging, followed by a slow depolarizing ramp of V_m until the pulse ended.

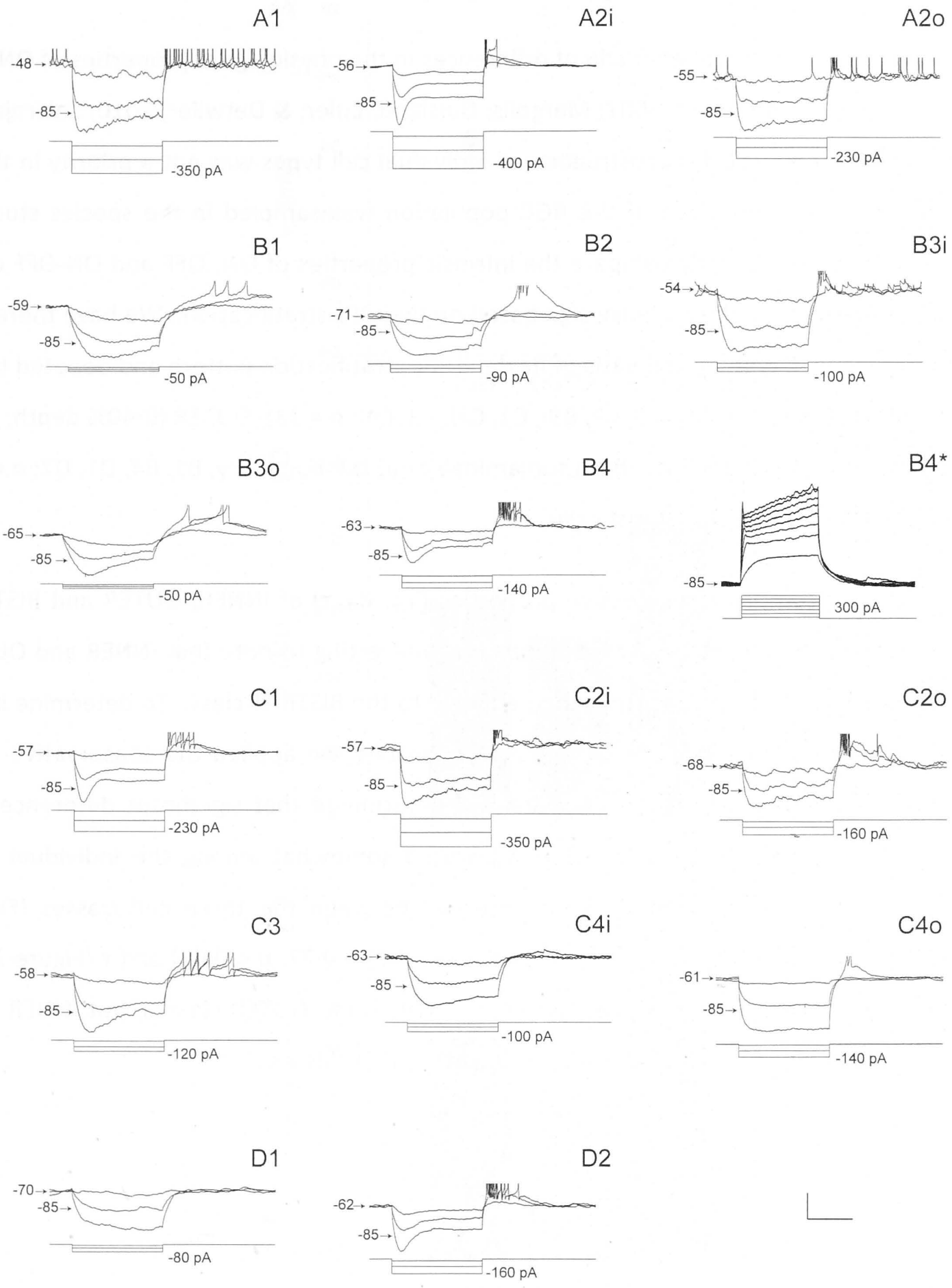

Figure 2.6 Retinal ganglion cell (RGC) responses to hyperpolarizing current injections. Recordings of individual RGCs representative of their morphological type responding to negative current injections of varying amplitude. RGC types differed greatly in their responses to hyperpolarizing currents. Where many cells hyperpolarized in a fairly linear manner with current amplitude (e.g. B3i, C4o) most RGC types exhibited non-linearities. In many cells this took the form of anomalous rectification of membrane potential (V_m) back toward the resting potential (sag, e.g. A2i, D2) that began well positive of potassium equilibrium potential (E_K). In other cells, only very large hyperpolarization close to or beyond E_K led to a very slow rectification (e.g. A1, C2i). At current offset, the majority of cell types responded with an overshoot of V_m leading to rebound spiking. When held at negative membrane potentials and injected with a series of depolarizing pulses, some cells (e.g. B4*) exhibited clear ramping of the V_m. Vertical scale bar, 20 mV; horizontal scale bar, 200 ms.

2.4.5 Is centre sign predictive of intrinsic properties?

Recently, much has been made of differences in the physiological properties of ON and OFF RGCs (Margolis & Detwiler, 2007; Margolis, Gartland, Euler, & Detwiler, 2010; Sekirnjak et al., 2011). As morphological reconstruction of individual cell types was not a priority in these studies, it is unclear how much of the RGC population was sampled in the species studied. While our data cannot directly compare the intrinsic properties of ON, OFF and ON-OFF cells, we can make predictions about centre sign based on their IPL stratification. We have therefore categorized each RGC type on the basis of its dendritic stratification pattern and denoted them as: INNER (40-100% depth, A1, A2i, B2, B3i, C1, C2i, C3, C4i; n = 33), OUTER (0-40% depth, A2o, B3o, C2o, C4o; n = 54), or BISTRAT (both sublaminae or at the boundary, B1, B4, D1, D2; n = 38) and compared their properties statistically.

Figure 2.7 compares the passive properties (V_m, R_N, τ) of INNER, OUTER and BISTRAT RGCs. Comparing the means in all three plots, it is interesting to note that INNER and OUTER cells seem more similar to one another than either is to the BISTRAT class. To determine if the three classes had significantly different passive properties, we applied the conservative non-parametric Kruskal-Wallis H test to the data and determined that significant differences do exist between the groups. Where resting V_m varied somewhat among the individual cells recorded, no significant differences were observed between the three cell classes (Figure 2.7A). Significant differences in both R_N (Figure 2.7B; $H(2) = 9.72$, $p < 0.01$) and τ (Figure 2.7C; $H(2) = 14.34$, $p < 0.01$.) were observed between BISTRAT and OUTER classes, but INNER cells were not significantly different from either of the other two classes.

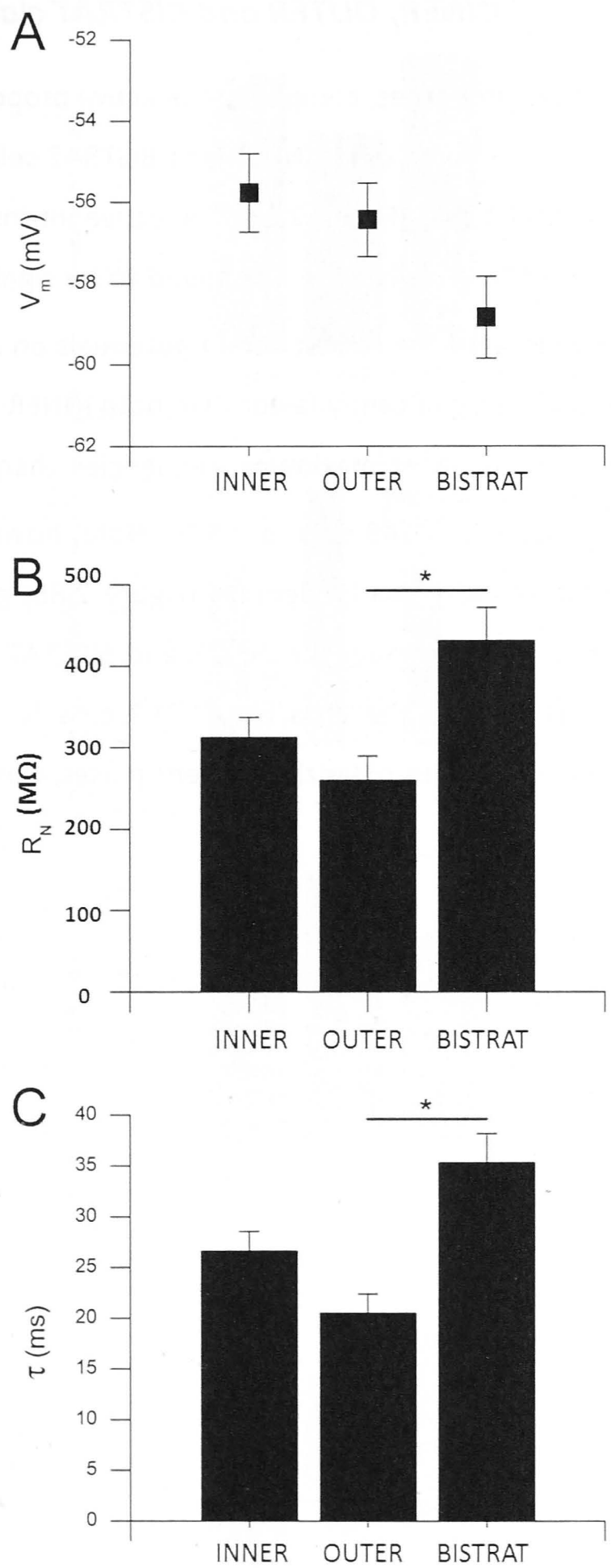

Figure 2.7 Average passive membrane properties of INNER, OUTER and BISTRAT retinal ganglion cell classes. **A**) Average resting membrane potential (V_m). **B**) Average input resistance (R_N). **C**) Average time constant (τ). Significant differences in the means are indicated by comparator bars ($p < 0.01$). Overall INNER and OUTER cells are more similar to each other than they are to BISTRAT cells.

2.4.6 Active properties of INNER, OUTER and BISTRAT classes

In contrast to passive properties, comparing the active properties of INNER, OUTER and BISTRAT classes suggests that in most cases INNER and BISTRAT cells are more similar to each other than either are to OUTER cells (Figure 2.8). The active intrinsic physiological properties of the INNER, OUTER and BISTRAT cells were also found to be significantly different for some variables. OUTER RGCs generated the fastest action potentials on average (Figure 2.8A; $\overline{X}$ = 1.33 ms, σ = 0.54 ms) and were significantly faster than both INNER and BISTRAT RGCs. OUTER RGCs also generated spikes at higher maximum frequencies than either INNER or BISTRAT RGCs. (Figure 2.8B, black bars; $\overline{X}$ = 148 sp/s, σ = 87). Note, however, that the steady-state firing rate for all three classes was nearly identical (Figure 2.8B, grey bars). This led to the observed significant difference in FA index for OUTER and BISTRAT cells (Figure 2.8C). Finally, while a clear trend was present in the data for OUTER cells to have the least anomalous rectification when injected with hyperpolarizing current pulses, this did not reach significance (Figure 2.8D).

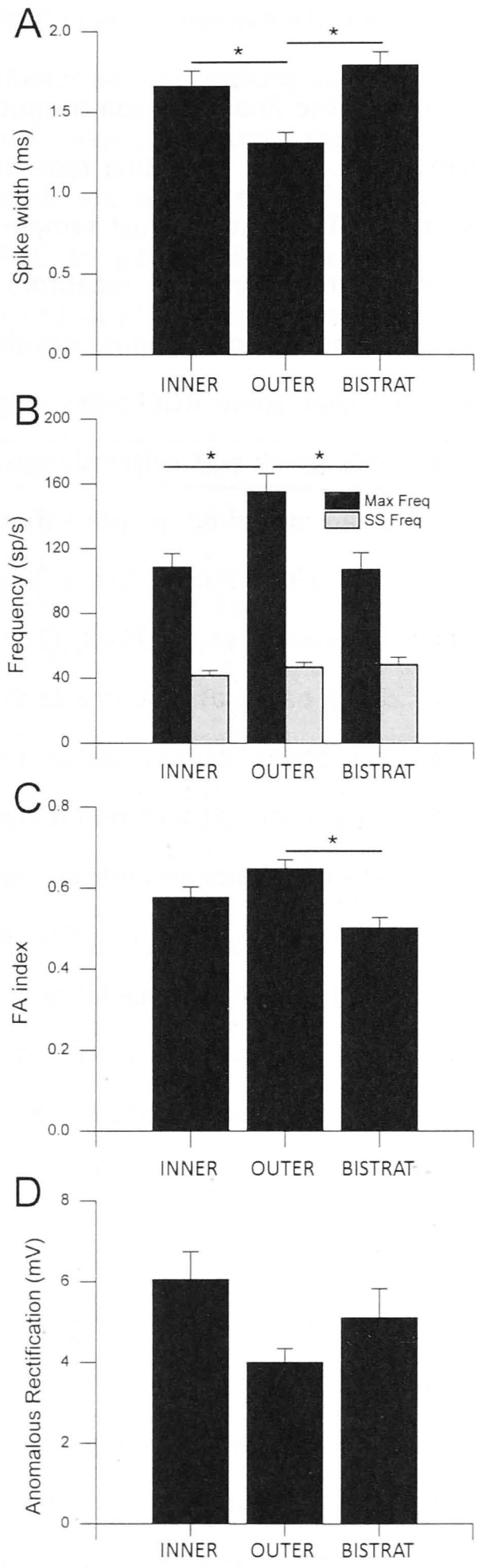

Figure 2.8 Average active properties of INNER, OUTER & BISTRAT retinal ganglion cell (RGC) classes. **A**) Average spike width. **B**) Average maximum and steady-state frequencies. **C**) Average frequency adaptation (FA) index. **D**) Anomalous rectification. Significant differences in the means are indicated by comparator bars ($p < 0.01$). In contrast to passive properties (Figure 2.7), INNER and BISTRAT cells are more similar to each other in their active properties than they are to OUTER cells.

2.4.7 Species comparison

The axons of RGCs represent the final common output of the information processing that occurs in the mammalian retina. Each individual type of RGC is believed to encode a different aspect of the visual scene. To do so, it must sample from the appropriate synaptic partners, express appropriate neurotransmitter receptors, and have an appropriate complement of ion channels. Since the task of vision is considered to be similar among many mammalian species, it is expected that some RGC types might be conserved across these species. For example, the alpha cell, which was originally described in cat retina (Boycott & Wässle, 1974), has subsequently been identified in more than 20 other mammalian species (Peichl, 1989; Peichl, Buhl, & Boycott, 1987; Peichl, Ott, & Boycott, 1987) including primates (Crook, Peterson, Packer, Robinson, Gamlin, et al., 2008; Crook, Peterson, Packer, Robinson, Troy, et al., 2008; Petrusca et al., 2007), based on its characteristic morphology and physiology. The characteristic light-evoked responses of cat alpha cells including centre-surround organization, sensitivity to low contrast stimuli and non-linear spatial summation have also been observed in alpha ganglion cells of rabbits and macaques (Amthor, Takahashi, & Oyster, 1989; Cleland, Levick, & Wässle, 1975; Crook, Peterson, Packer, Robinson, Troy, et al., 2008; Enroth-Cugell & Robson, 1966). Since the alpha or Y-cell is believed to play the same functional role in these species, might it be that its biophysical properties are also conserved? In our analysis we have taken the approach that close morphological similarity between species likely indicates similarity in visual function(s). Therefore, are the intrinsic properties also conserved in morphological homologs or is this unnecessary?

We set out to answer this question using the hierarchical clustering technique. Hierarchical clustering methods calculate the linear distances between individual RGC types using all variables and then proceed iteratively, clustering together at each iteration those RGC types that are most similar. To make comparisons across species, however, we needed first to normalize each species' data set. To preserve quantitative differences among the cell types within a species, we calculated the z-score for each cell type based on its sample mean and the mean for all RGC types. This allowed us to preserve the relationships among the cells within a species, but dissociate their actual values to perform the cluster analysis. For example, the mean R_N of the cat alpha cell was previously reported as 31.3 MΩ (O'Brien, et al., 2002) while the average rat A2 cell is more than 3 times this value (102 MΩ. In contrast, the z-scores are

both the lowest among all the RGC types tested in each species (cat alpha: -1.16, rat A2: -1.86). This methodology avoids the cluster analysis making spurious links between cell types based upon absolute values and instead concentrates upon their relative rank among the RGC types. The results of the cluster analysis are presented in Figure 2.9. Table 2.3 lists the known morphological types of cat RGC to date, their predicted rat RGC equivalent based on morphology, and the closest ranked rat RGC type(s) based on their intrinsic properties.

Table 2.3 Rat and cat RGC homologs.

Cat	Rat	Cluster Result
Alpha	A2	A2
Beta	B2	-
Delta	C2o	C2o, C3
Epsilon	C3	C2o, C3
Zeta	B4	B1, B4
Eta	C4o	A1
Theta	D1	-
Iota	D2	A1
Kappa	C1	C4i
Lambda	B1	C2o, C3

Homologous retinal ganglion cell types present in cat and rat retina as predicted by morphology and cluster analysis of intrinsic properties are shown.

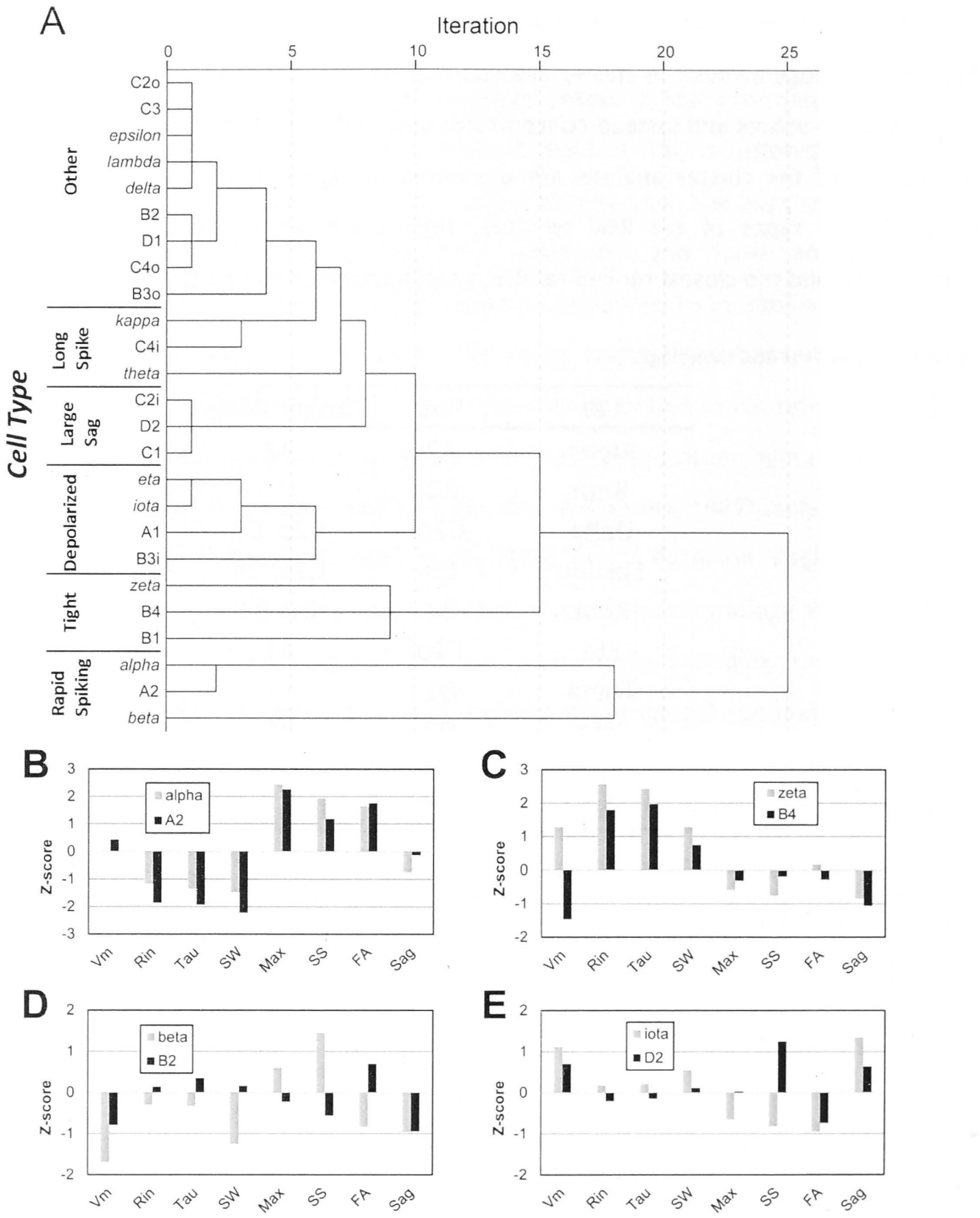

Figure 2.9 Cluster analysis. **A**) Dendrogram of median linkage cluster analysis. Cat retinal ganglion cell (RGC) types are listed in italics. Data from A2i and A2o were combined to be comparable with the cat alpha cell data. Left: RGC categories that have characteristic patterns of intrinsic properties. "Rapid spiking" cells have very short action potentials and are able to spike at high rates. "Tight" cells have very high input resistance (R_N) and long time constant (τ). "Depolarization" cells have an elevated resting membrane potential (V_m). "Large Sag" cells exhibited responded to hyperpolarizing steps with a clear rectification in V_m greater than most other RGC types. "Long spiking" cells generate extremely long action potentials. The remaining cells in the purple group "Other" are clustered together as their intrinsic properties are close to the mean in almost all categories. Head to head z-score comparisons of **B**) cat alpha and rat A2 cells. **C**) cat zeta and rat B4 cells. In B) and C), they both demonstrate a remarkably similar pattern of intrinsic properties. In contrast, very little similarity was found between the predicted morphological equivalents of **D**) the cat beta cell and the rat B2 cell and **E**) the cat iota cell and rat D2 cell.

For some cells, the cluster analysis yielded very clear correspondences. For example, the cat alpha and rat A2 cells (INNER and OUTER varieties combined) were clustered together early in the analysis and remained independent for many more cycles before cat beta cells were added (Figure 2.9A). The striking similarity in the intrinsic properties of these two cell types was quite obvious when plotted together on a histogram (Figure 2.9B). Similarly, the cat zeta cell was found in the cluster analysis to be most similar to the rat B4, then the B1 cell. The histogram illustrating the data obtained from these two cell types was also strikingly similar (Figure 2.9C). In contrast, the cat beta cell was not clustered with any rat RGC type until nearly the end of the analysis when it was added to the rat A2 and cat alpha cell cluster. The predicted morphological equivalent of the cat Beta cell, the rat B2 cell (Huxlin & Goodchild, 1997; Sun, et al., 2002), showed almost no similarity when plotted together on a histogram (Figure 2.9D: beta and B2). The cluster analysis also confirmed morphological predictions for the cat delta (rat C2o) and epsilon (rat C3) cell types, but completely disagreed with predictions for the two direction selective (DS) cells, cat iota (rat D2, ON-OFF DS) and kappa (rat C1 ON-DS) cells.

In addition to comparing the intrinsic properties of morphological homologs, the cluster analysis also demonstrated that the array of intrinsic physiological properties we have characterized is useful when used independently to classify RGCs. While the analysis was not capable of identifying individual morphological types independently, it did generate six categories (labeled as Rapid Spiking, Tight, Depolarized, Large Sag, Long Spike and Other) each with characteristic intrinsic properties. These categories are indicated in Figure 2.9 by the adjacent labels. The "Rapid Spiking" cells exhibit very short action potentials and high frequency spiking. In contrast, the "Long Spike" cells generate action potentials much longer than most other RGC types. The "Tight" cells have unusually large R_N and long τ. These cells should therefore be among the most sensitive to fluctuations in synaptic input. The "Depolarized" cells had a resting V_m more depolarized than other RGC types. Whether this is of biophysical or synaptic origin is not yet established. "Large Sag" cells exhibit greater sag in V_m when hyperpolarized, most likely indicating greater expression of Hyperpolarization-activated cation current (I_h). The remaining "Other" cells had intrinsic properties that were not easily separable. The z-scores for each cell type are presented in Table 2.4, and organized in the

same fashion as in Figure 2.9A. Thus, while the intrinsic properties alone are not capable of differentiating each morphologically defined RGC type, they can narrow it down significantly.

Table 2.4 Retinal ganglion cell categories identified by cluster analysis.

Category	Cell type	V_m	R_N	τ	SW	Max Freq	SS Freq	FA	Sag
Other	C2o	-0.52	-0.20	-0.75	-0.70	0.45	0.01	0.89	0.22
	C3	0.09	0.51	-0.35	-0.43	0.03	0.13	0.56	-0.24
	Epsilon	-0.56	-0.77	-0.67	-0.62	0.27	0.25	0.65	-0.85
	Lambda	-0.12	-0.38	-0.52	-0.11	-0.12	-0.31	-0.21	-0.38
	Delta	0.91	-0.33	-0.35	-0.64	0.15	0.35	0.16	-0.42
	B2	-1.00	0.08	0.70	0.13	0.10	-0.49	1.00	-0.99
	D1	-1.22	-0.15	0.09	0.42	0.05	0.17	-0.02	-1.33
	C4o	-0.26	0.03	0.24	0.11	0.82	0.45	0.61	-0.83
	B3o	-0.99	0.60	0.37	0.53	-0.61	-0.89	-0.36	-0.55
Long Spike	*Kappa*	-1.16	-0.15	0.52	1.46	-1.13	-1.01	-1.32	0.93
	C4i	0.25	-0.31	0.38	2.45	-0.90	-0.66	-0.86	0.02
	Theta	-0.49	0.07	-0.09	0.58	-0.28	-0.63	1.40	1.75
Large Sag	C2i	0.57	-0.65	-0.99	-0.04	0.31	1.03	-0.44	1.87
	D2	-0.04	-0.59	-0.45	-0.12	0.79	1.90	-0.20	1.49
	C1	0.12	-0.98	-0.58	-0.44	0.85	1.08	0.76	1.47
Depolarized	*Eta*	0.71	0.29	0.17	0.24	-0.67	-0.46	-0.70	0.18
	Iota	1.11	0.17	0.21	0.54	-0.66	-0.82	-0.95	1.34
	A1	1.89	-0.76	-0.54	0.11	-0.72	-0.76	0.18	0.90
	B3i	1.96	0.48	0.10	-0.96	-1.44	-1.31	-1.51	-0.33
Tight	*Zeta*	1.28	2.56	2.42	1.28	-0.59	-0.75	0.16	-0.85
	B4	-1.47	1.79	1.97	0.75	-0.31	-0.19	-0.28	-1.07
	B1	0.18	2.00	1.74	0.43	-1.65	-1.65	-2.09	-0.49
Rapid Spiking	*Alpha*	0.01	-1.16	-1.35	-1.48	2.44	1.94	1.64	-0.74
	A2	0.43	-1.86	-1.93	-2.22	2.26	1.18	1.76	-0.13
	Beta	-1.69	-0.30	-0.33	-1.25	0.60	1.45	-0.83	-0.96

Values are z-scores of rat and cat RGC intrinsic physiological properties underlying the categorization by the cluster analysis. Cat RGC types are shown in italics.

2.5 Discussion

This study has produced two major findings of interest: rat RGCs vary extensively in their patterns of intrinsic physiological properties between anatomically distinct cell types, and morphologically homologous RGC types in different species may or may not have conserved intrinsic properties.

2.5.1 RGC morphological types

The cells we observed in this study compared quite closely with those reported previously (Huxlin & Goodchild, 1997; Sun, et al., 2002). Our data support the classification scheme of Sun et al. (2002) as characterizing the vast majority of RGC types present in rat retina. On occasion, we did encounter some RGCs not included in this classification but they were indeed rare. Although not reported in the paper associated with this chapter, data was collected from 4 cells whose exact type was not identifiable. Their morphologies indicated that they were not of the common types. An example is shown in Figure 2.10.

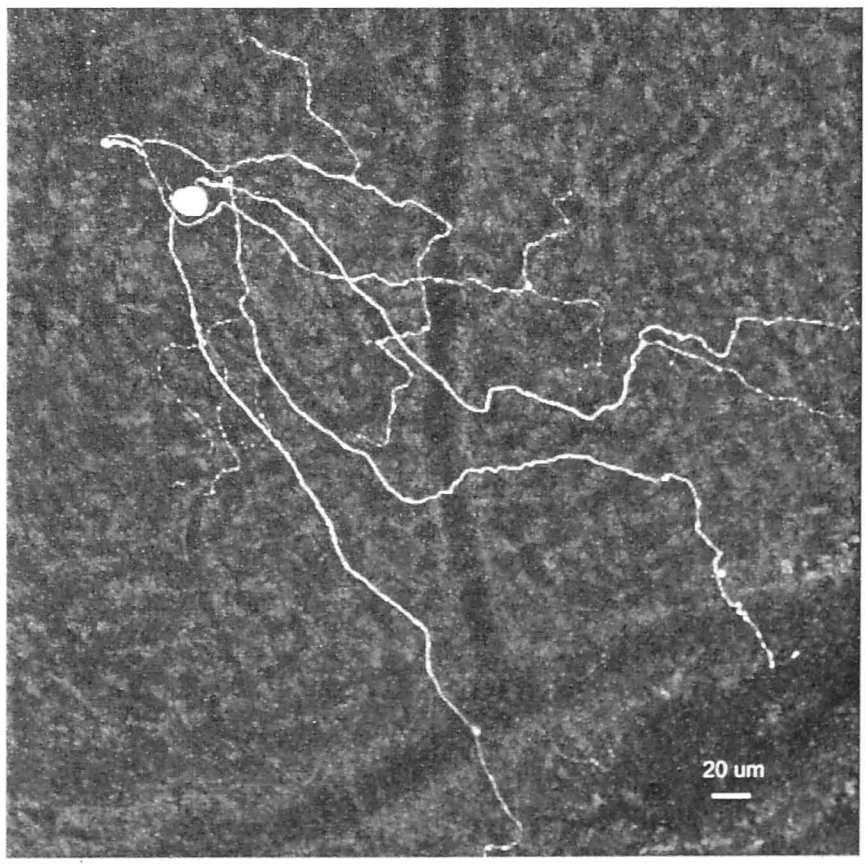

Figure 2.10 The confocal image of a 'rare' type retinal ganglion cell. Its morphology is different from those shown in Figure 2.1.

Direct comparisons of the morphological parameters we quantified for each RGC type with those published previously were largely similar, with some exceptions. Due to the nature of our experiments requiring displacement of the ILM and ganglion cell axon fibers to allow whole cell recording, most of our cells were recorded in more peripheral locations. Cleanly removing the ILM close to the optic disk is made difficult because the large number of fiber bundles. As a result our data over represents the periphery. However, as has been shown previously for rat RGCs (Huxlin & Goodchild, 1997), there is only very little change in soma or dendritic field size with eccentricity.

Comparing IPL stratification of RGC dendrites among the three studies would seem to indicate substantial differences. It is our considered opinion that the quantitative differences observed among the studies are largely artifactual due to the assignation of an entire dendritic field to a single % depth. While we would concur that the majority of RGC types are indeed monostratified, this does not mean that individual dendrites do not waver up and down within the IPL by more than a few percent. Thus, when an entire cell's dendritic field is characterized as occupying a single % depth, on the basis of a small number of local dendritic measurements, something is missed. This may be the root of the differences in stratification when comparing our data with prior studies. When compared with the data of Huxlin and Goodchild (1997) our stratification data are numerically different but nearly all cells are found within the same sublaminae when broken down into the traditional 20% strata (S1-S5). Our stratification results were overall similar to those of Sun et al. (2002) in large part, with exception to types C2 and C4 where our data suggest INNER (> 40% depth) and OUTER (< 40% depth) subvarieties. This is similar to the Huxlin & Goodchild (1997) description for C2 cells; C4 cells were not identified as a separate cell type in their study. Finally, some differences we observed may be due to the strain of rat used. Where both Huxlin & Goodchild (1997) and Sun et al. (2002) used albino rat strains (Sprague Dawley) we chose to use the pigmented Long-Evans strain.

2.5.2 Intrinsic physiological properties

Rat RGCs exhibited a wide variety of intrinsic physiological properties that were correlated with their morphological type. Statistically significant differences among RGC types were found among both passive (R_N, τ) and active properties (spike width, maximum and

steady state frequency, FA index, anomalous rectification). In addition, we carefully evaluated previous claims of statistical differences among RGCs grouped by their likely receptive field centre sign (ON, OFF, ON-OFF) through extensive sampling of all RGC types. Clear differences were observed between our OUTER and BISTRAT cells for most variables, both passive and active. Differences between INNER and OUTER cells were also observed but in most cases did not reach significance. It would appear that INNER cells are more similar to BISTRAT cells than OUTER cells for most variables, but we make this claim cautiously as INNER cells formed the smallest sample among the three groups, so sampling bias may have influenced the statistics. Collectively, our data demonstrate that intrinsic physiological properties of RGCs will indeed shape their responses to synaptic inputs and ultimately limit the information that can be transferred.

The differences we have observed in the intrinsic physiological properties of RGCs are ultimately attributed to many factors including their morphology (Fohlmeister & Miller, 1997; Sheasby & Fohlmeister, 1999) and the complement of ion channels expressed by each cell type. While our data cannot unambiguously identify which channels are present in each cell type, the intrinsic properties we have observed do allow us to predict the relative abundance of certain types of ion channels expressed. In addition, when examined in the context of RGC light evoked responses, we begin to understand how the intrinsic properties are tuned to enhance certain aspects of a cell's light response.

Our data demonstrate nearly a 10-fold difference in the R_N measured among our sample of rat RGCs. Differences in cell size accounts for a portion of this variability (Figure 2.3), but ionic conductances must also play a role. Since we did not introduce pharmacological agents to effect synaptic blockade, the origin(s) of these conductances could potentially be intrinsic to the cell or could also arise from tonic synaptic activity or their combination. Our data demonstrate that, like cat alpha cells (O'Brien, et al., 2002), A2 cells have the lowest R_N and are the largest of all rat RGC types, and should therefore have the greatest input capacitance (C_N). Since the cellular τ represents the product of these two parameters ($\tau = R_N C_N$), and A2/alpha cells also have the fastest τ of all RGC types, it would seem that their passive properties have been tuned to effect a rapid response to synaptic input, despite their large size. This optimization for speed, however, would decrease the alpha cell's relative sensitivity to an equivalent synaptic input to other RGC types, yet they would appear to be among the

most sensitive cells to visual contrast (Kaplan & Shapley, 1986). This apparent paradox implies that A2/alpha cells have either increased synaptic input relative to other RGC types or possibly also employ active dendritic conductances to enhance their sensitivity (Dhingra, Freed, & Smith, 2005; Velte & Masland, 1999). Whether retinal cells receive the same number of synapses per linear micrometer of dendrite is a matter of some disagreement in the literature (Eriköz, Jusuf, Percival, & Grünert, 2008; Jakobs, Koizumi, & Masland, 2008). Indeed, it has been reported that smaller RGCs actually receive a proportionally greater number of excitatory inputs than larger RGCs (Jakobs, et al., 2008). Further experimentation will be required to disentangle these implications.

On the other end of the spectrum, the rat B4 cell is very small, has nearly the largest R_N and the longest τ of all RGC types, a pattern similar to that found for the cat zeta cell (O'Brien, et al., 2002). These data would imply this cell type would be among the most sensitive of all RGCs to synaptic input. As for the cat zeta cell, the B4 cell exhibits ramping of V_m in response to subthreshold depolarizing current. This behavior is indicative of the presence of a slowly inactivating voltage-gated potassium (K^+) current (I_D), a current that activates below spike threshold, originally described in hippocampal neurons (Storm, 1988) and previously observed in isolated RGCs (Barres, Silverstein, Corey, & Chun, 1988; Lukasiewicz & Werblin, 1988; Sucher & Lipton, 1992). The presence of I_D has been demonstrated previously to boost responses to repeated subthreshold stimuli (Storm, 1988). In the retinal context, this would suggest that an initially subthreshold flickering stimulus in the B4 cell's receptive field could eventually evoke a response. Thus, the expression of I_D could further enhance the sensitivity of B4/zeta cells. Some evidence to support this idea has been observed in rabbit local edge detector cells, a possible homologue of the B4/zeta cell (van Wyk, Taylor, & Vaney, 2006).

In all our recordings, adult rat RGCs were capable of repetitive spiking and exhibited a variable amount of frequency adaptation similar to the Regular Spiking pattern originally described for cortical neurons (Connors & Gutnick, 1990). The differences we observed in frequency adaptation among different RGC types may be due to the differential expression of calcium-activated K^+ (K_{Ca}) channels. These channels are well known to play a role in frequency adaptation and have been shown previously to be present in mammalian RGCs (Lipton & Tauck, 1987; Wang, Robinson, & Chalupa, 1998; Weick & Demb, 2011). The high FA index

exhibited by A2/alpha cells may bias the temporal properties of their well-known 'transient' light responses to standing contrast (Cleland, Levick, & Sanderson, 1973).

In addition to frequency adaptation, many RGC types exhibited a clear reduction in spike amplitude over the course of a 400 ms depolarizing current pulse. Prior studies have demonstrated that cat RGC types vary in their rate of voltage-gated sodium channel (VGSC) de-inactivation (Kaneda & Kaneko, 1991; Wang, et al., 1997). As repetitive spiking continues, this would lead to an increasing proportion of inactivated VGSCs and hence a reduction in spike amplitude. It has been demonstrated previously that the alpha subunits of VGSCs are differentially expressed among RGC types (Boiko et al., 2003; Guenther, Schmid, Reiff, & Zrenner, 1999; Miguel-Hidalgo, Snider, Angelides, & Chalupa, 1994; O'Brien et al., 2008; Oesch & Taylor, 2010; Skaliora, Scobey, & Chalupa, 1993). Depending upon which VGSC subunits are expressed in each RGC type, this may define which cells exhibit amplitude adaptation and has also been implicated to underlie contrast adaptation (Kim & Rieke, 2003; Weick & Demb, 2011).

Hyperpolarizing current injections into RGCs implicated the presence of at least two other ion channels that are differentially distributed among RGC types. During hyperpolarizing pulses the amount of membrane potential 'sag' back toward the resting potential varied extensively among the different RGC types (Figure 2.6). Positive to potassium equilibrium potential (E_K), the nonspecific cation current known as I_h is well known to play a major role in the generation of sag (Araki, Ito, & Oshima, 1961; Ito & Oshima, 1965; Pape, 1996) and has been previously identified in RGCs (Lee & Ishida, 2007; Mitra & Miller, 2007a, 2007b; O'Brien, et al., 2002; Tabata & Ishida, 1996; Van Hook & Berson, 2010). Offset of hyperpolarizing current injections also led to overshoot of the resting V_m and the generation of a burst of action potentials. In cells where there is clear sag during the pulse, this is at least partially due to the slow inactivation of I_h, which turns off with kinetics similar to those at onset. In some cells, however, a rebound burst was observed when no sag was present during the pulse. This is most likely due to activation of low threshold calcium currents (Mitra & Miller, 2007a, 2007b). Activation of such currents accelerates repolarization of the membrane potential and leads to a similar overshoot of the resting V_m. In contrast to activation of I_h, however, activation of low threshold calcium currents is much shorter lived and results in a very short, intense burst by comparison.

2.5.3 Species comparison

The second major finding relates to the conservation of intrinsic physiological properties of homologous morphological RGC types across mammalian species. Cluster analysis suggested that rat A2 RGCs were very similar to cat alpha cells while rat B4 and cat zeta cells were also similar (Figure 2.9). Given such varied environmental niches for the two species, it seems likely that the intrinsic properties of these four cell types are very important for cellular information processing and may indeed be fundamental for vision generally, not just their specific ecological niches. If so, then we should expect that recordings of the homologous RGC types in other mammalian species would yield similar findings.

By way of contrast, the intrinsic properties of the D2/iota cell morphological homologues are not at all similar between rats and cats. From these data we can conclude that either the intrinsic properties of these two cell types are irrelevant to the visual behavior of the animal, or that these morphological homologs subserve somewhat different functions in the two species. Interestingly, the cat beta cell does not appear to have a homolog in rat retina with respect to intrinsic physiological properties. Indeed, the cluster analysis revealed that the cat beta cell is more closely related to the cat alpha and rat A2 cells than any other cell type (cat or rat). Given the beta cell's other similarities to cat alpha and rat A2 cells (e.g. ON & OFF subclasses, central alpha and peripheral beta cell morphological similarities, spike generator properties (Robinson & Chalupa, 1997)), we propose that the beta cell first arose in mammalian evolutionary history as a cell type duplication event. A behavioral advantage of higher resolution and an ability to recognize form without motion may then have shaped the modern beta cell's dendritic and receptive field properties. Clearly, this speculation would require careful examination of multiple species in the phylogenetic hierarchy.

2.6 References

Amthor, F. R., Takahashi, E. S., & Oyster, C. W. (1989). Morphologies of rabbit retinal ganglion cells with concentric receptive fields. *J Comp Neurol, 280*(1), 72-96.

Araki, T., Ito, M., & Oshima, T. (1961). Potential changes produced by application of current steps in motoneurones. *Nature, 191*, 1104-1105.

Barres, B. A., Silverstein, B. E., Corey, D. P., & Chun, L. L. (1988). Immunological, morphological, and electrophysiological variation among retinal ganglion cells purified by panning. [Research Support, Non-U.S. Gov't. Research Support, U.S. Gov't, P.H.S.]. *Neuron, 1*(9), 791-803.

Berson, D. M. (2008). Retinal ganglion cell types and their central projections. . In A. I. Basbaum, A. Kaneko, G. M. Shepherd, G. Westheimer & (Eds.), *The Senses: A comprehensive reference* (Vol. 1, pp. 491-520): Academic Press.

Boiko, T., Van Wart, A., Caldwell, J. H., Levinson, S. R., Trimmer, J. S., & Matthews, G. (2003). Functional specialization of the axon initial segment by isoform-specific sodium channel targeting. *J Neurosci, 23*(6), 2306-2313.

Boycott, B. B., & Wässle, H. (1974). The morphological types of ganglion cells of the domestic cat's retina. *J Physiol (Lond), 240*(2), 397-419.

Cleland, B. G., Levick, W. R., & Sanderson, K. J. (1973). Properties of sustained and transient ganglion cells in the cat retina. *J Physiol (Lond), 228*(3), 649-680.

Cleland, B. G., Levick, W. R., & Wässle, H. (1975). Physiological identification of a morphological class of cat retinal ganglion cells. *J Physiol (Lond), 248*(1), 151-171.

Connors, B. W., & Gutnick, M. J. (1990). Intrinsic firing patterns of diverse neocortical neurons. *Trends Neurosci, 13*(3), 99-104. doi: 0166-2236(90)90185-D [pii]

Crook, J. D., Peterson, B. B., Packer, O. S., Robinson, F. R., Gamlin, P. D., Troy, J. B., & Dacey, D. M. (2008). The Smooth Monostratified Ganglion Cell: Evidence for Spatial Diversity in the Y-Cell Pathway to the Lateral Geniculate Nucleus and Superior Colliculus in the Macaque Monkey. *Journal of Neuroscience, 28*(48), 12654-12671. doi: Doi 10.1523/Jneurosci.2986-08.2008

Crook, J. D., Peterson, B. B., Packer, O. S., Robinson, F. R., Troy, J. B., & Dacey, D. M. (2008). Y-Cell Receptive Field and Collicular Projection of Parasol Ganglion Cells in Macaque Monkey Retina. *Journal of Neuroscience, 28*(44), 11277-11291. doi: Doi 10.1523/Jneurosci.2982-08.2008

Dacey, D. M., Peterson, B. B., Robinson, F. R., & Gamlin, P. D. (2003). Fireworks in the primate retina: in vitro photodynamics reveals diverse LGN-projecting ganglion cell types. *Neuron, 37*(1), 15-27. doi: S0896627302011431 [pii]

Dhingra, N. K., Freed, M. A., & Smith, R. G. (2005). Voltage-gated sodium channels improve contrast sensitivity of a retinal ganglion cell. *J Neurosci, 25*(35), 8097-8103.

Enroth-Cugell, C., & Robson, J. G. (1966). The contrast sensitivity of retinal ganglion cells of the cat. *J Physiol (Lond), 187*, 517-552.

Eriköz, B., Jusuf, P. R., Percival, K. A., & Grünert, U. (2008). Distribution of bipolar input to midget and parasol ganglion cells in marmoset retina. [In Vitro Research Support, Non-U.S. Gov't]. *Vis Neurosci, 25*(1), 67-76. doi: 10.1017/S0952523808080073

Fohlmeister, J. F., Cohen, E. D., & Newman, E. A. (2010). Mechanisms and distribution of ion channels in retinal ganglion cells: using temperature as an independent variable. [In Vitro Research Support, N.I.H., Extramural]. *J Neurophysiol, 103*(3), 1357-1374. doi: 10.1152/jn.00123.2009

Fohlmeister, J. F., & Miller, R. F. (1997). Mechanisms by which cell geometry controls repetitive impulse firing in retinal ganglion cells. *J Neurophysiol, 78*(4), 1948-1964.

Guenther, E., Schmid, S., Reiff, D., & Zrenner, E. (1999). Maturation of intrinsic membrane properties in rat retinal ganglion cells. *Vision Res, 39*(15), 2477-2484.

Hamill, O. P., Marty, A., Neher, E., Sakmann, B., & Sigworth, F. J. (1981). Improved patch-clamp techniques for high-resolution current recording from cells and cell-free membrane patches. *Pflugers Arch, 391*(2), 85-100.

Huxlin, K. R., & Goodchild, A. K. (1997). Retinal ganglion cells in the albino rat: revised morphological classification. *J Comp Neurol, 385*(2), 309-323. doi: 10.1002/(SICI)1096-9861(19970825)385:2<309::AID-CNE9>3.0.CO;2-5 [pii]

Ishida, A. T. (1991). Ion channel components of retinal ganglion cells. *Prog. Retinal & Eye Res., 15*, 261-280.

Ito, M., & Oshima, T. (1965). Electrical behaviour of the motoneurone membrane during intracellularly applied current steps. [In Vitro]. *J Physiol (Lond), 180*(3), 607-635.

Jakobs, T. C., Koizumi, A., & Masland, R. H. (2008). The spatial distribution of glutamatergic inputs to dendrites of retinal ganglion cells. *J Comp Neurol, 510*(2), 221-236. doi: 10.1002/cne.21795

Jeffery, G. (1997). The albino retina: an abnormality that provides insight into normal retinal development. [Review]. *Trends in neurosciences, 20*(4), 165-169.

Johnston, D., & Wu, S. M. (1997). *Foundations of Cellular Neurophysiology*. Cambridge, MA USA: MIT Press.

Kaneda, M., & Kaneko, A. (1991). Voltage-gated sodium currents in isolated retinal ganglion cells of the cat: relation between the inactivation kinetics and the cell type. *Neurosci Res, 11*(4), 261-275.

Kaplan, E., & Shapley, R. M. (1986). The primate retina contains two types of ganglion cells, with high and low contrast sensitivity. [Research Support, U.S. Gov't, Non-P.H.S. Research Support, U.S. Gov't, P.H.S.]. *Proceedings of the National Academy of Sciences of the United States of America, 83*(8), 2755-2757.

Kim, K. J., & Rieke, F. (2003). Slow Na+ inactivation and variance adaptation in salamander retinal ganglion cells. [Research Support, Non-U.S. Gov't. Research Support, U.S. Gov't, P.H.S.]. *J Neurosci, 23*(4), 1506-1516.

Lee, S. C., & Ishida, A. T. (2007). Ih without Kir in adult rat retinal ganglion cells. [Research Support, N.I.H., Extramural]. *J Neurophysiol, 97*(5), 3790-3799. doi: 10.1152/jn.01241.2006

Liets, L. C., Olshausen, B. A., Wang, G. Y., & Chalupa, L. M. (2003). Spontaneous activity of morphologically identified ganglion cells in the developing ferret retina. *J Neurophysiol, 23*(19), 7343-7350.

Lipton, S. A., & Tauck, D. L. (1987). Voltage-dependent conductances of solitary ganglion cells dissociated from the rat retina. *J Physiol (Lond), 385*, 361-391.

Lukasiewicz, P., & Werblin, F. (1988). A slowly inactivating potassium current truncates spike activity in ganglion cells of the tiger salamander retina. *J Neurosci, 8*(12), 4470-4481.

Margolis, D. J., & Detwiler, P. B. (2007). Different mechanisms generate maintained activity in ON and OFF retinal ganglion cells. *J Neurosci, 27*(22), 5994-6005. doi: 10.1523/jneurosci.0130-07.2007

Margolis, D. J., Gartland, A. J., Euler, T., & Detwiler, P. B. (2010). Dendritic calcium signaling in ON and OFF mouse retinal ganglion cells. [In Vitro Research Support, N.I.H., Extramural Research Support, Non-U.S. Gov't]. *J Neurosci, 30*(21), 7127-7138. doi: 10.1523/JNEUROSCI.5694-09.2010

Masland, R. H. (2001). The fundamental plan of the retina. *Nat Neurosci, 4*(9), 877-886.

Miguel-Hidalgo, J. J., Snider, C. J., Angelides, K. J., & Chalupa, L. M. (1994). Voltage-dependent sodium channel alpha subunit immunoreactivity is expressed by distinct cell types of the cat and monkey retina. *Vis Neurosci, 11*(2), 219-228.

Mitra, P., & Miller, R. F. (2007a). Mechanism underlying rebound excitation in retinal ganglion cells. *Vis Neurosci, 24*(5), 709-731. doi: 10.1017/s0952523807070654

Mitra, P., & Miller, R. F. (2007b). Normal and rebound impulse firing in retinal ganglion cells. *Visual Neuroscience, 24*(1), 79-90. doi: Doi 10.1017/S0952523807070101

Neher, E. (1992). Correction for liquid junction potentials in patch clamp experiments. *Methods in enzymology, 207*, 123-131.

O'Brien, B. J., Caldwell, J. H., Ehring, G. R., O'Brien, K. M. B., Luo, S. J., & Levinson, S. R. (2008). Tetrodotoxin-resistant voltage-gated sodium channels Na(v)1.8 and Na(v)1.9 are expressed in the retina. *J Comp Neurol, 508*(6), 940-951. doi: 10.1002/cne.21701

O'Brien, B. J., Isayama, T., Richardson, R., & Berson, D. M. (2002). Intrinsic physiological properties of cat retinal ganglion cells. *J Physiol (Lond), 538*(Pt 3), 787-802.

Oesch, N. W., & Taylor, W. R. (2010). Tetrodotoxin-resistant sodium channels contribute to directional responses in starburst amacrine cells. [Research Support, N.I.H., Extramural]. *PloS one, 5*(8), e12447. doi: 10.1371/journal.pone.0012447

Pape, H. C. (1996). Queer current and pacemaker: the hyperpolarization-activated cation current in neurons. *Annu Rev Physiol, 58*, 299-327.

Peichl, L. (1989). Alpha and delta ganglion cells in the rat retina. *J Comp Neurol, 286*(1), 120-139. doi: 10.1002/cne.902860108

Peichl, L., Buhl, E. H., & Boycott, B. B. (1987). Alpha ganglion cells in the rabbit retina. *J Comp Neurol, 263*(1), 25-41. doi: 10.1002/cne.902630103

Peichl, L., Ott, H., & Boycott, B. B. (1987). Alpha ganglion cells in mammalian retinae. [Comparative Study]. *Proceedings of the Royal Society of London. Series B, Containing papers of a Biological character. Royal Society, 231*(1263), 169-197.

Petrusca, D., Grivich, M. I., Sher, A., Field, G. D., Gauthier, J. L., Greschner, M., . . . Litke, A. M. (2007). Identification and characterization of a Y-like primate retinal ganglion cell type. *Journal of Neuroscience, 27*(41), 11019-11027. doi: Doi 10.1523/Jneurosci.2836-07.2007

Qu, J., & Myhr, K. L. (2008). The development of intrinsic excitability in mouse retinal ganglion cells. *Dev Neurobiol, 68*(9), 1196-1212. doi: 10.1002/dneu.20653

Qu, J., & Myhr, K. L. (2011). The Morphology and Intrinsic Excitability of Developing Mouse Retinal Ganglion Cells. *PloS one, 6*(7). doi: e21777 10.1371/journal.pone.0021777

Robinson, D. W., & Chalupa, L. M. (1997). The intrinsic temporal properties of alpha and beta retinal ganglion cells are equivalent. *Curr Biol, 7*(6), 366-374. doi: S0960-9822(06)00184-9 [pii]

Robinson, D. W., & Wang, G. Y. (1998). Development of intrinsic membrane properties in mammalian retinal ganglion cells. *Semin Cell Dev Biol, 9*(3), 301-310.

Schiller, P. H. (2010). Parallel information processing channels created in the retina. [Review]. *Proceedings of the National Academy of Sciences of the United States of America, 107*(40), 17087-17094. doi: 10.1073/pnas.1011782107

Sekirnjak, C., Jepson, L. H., Hottowy, P., Sher, A., Dabrowski, W., Litke, A. M., & Chichilnisky, E. J. (2011). Changes in physiological properties of rat ganglion cells during retinal degeneration. [Research Support, N.I.H., Extramural. Research Support, Non-U.S. Gov't. Research Support, U.S. Gov't, Non-P.H.S.]. *J Neurophysiol, 105*(5), 2560-2571. doi: 10.1152/jn.01061.2010

Sheasby, B. W., & Fohlmeister, J. F. (1999). Impulse encoding across the dendritic morphologies of retinal ganglion cells. *J Neurophysiol, 81*(4), 1685-1698.

Skaliora, I., Scobey, R. P., & Chalupa, L. M. (1993). Prenatal development of excitability in cat retinal ganglion cells: action potentials and sodium currents. *J Neurosci, 13*(1), 313-323.

Storm, J. F. (1988). Temporal integration by a slowly inactivating K+ current in hippocampal neurons. *Nature, 336*(6197), 379-381.

Sucher, N. J., & Lipton, S. A. (1992). A slowly inactivating K+ current in retinal ganglion cells from postnatal rat. *Vis Neurosci, 8*(2), 171-176.

Sun, W., Li, N., & He, S. (2002). Large-scale morophological survey of rat retinal ganglion cells. *Vis Neurosci, 19*(4), 483-493.

Tabata, T., & Ishida, A. T. (1996). Transient and sustained depolarization of retinal ganglion cells by Ih. *J Neurophysiol, 75*(5), 1932-1943.

Tabata, T., & Kano, M. (2002). Heterogeneous intrinsic firing properties of vertebrate retinal ganglion cells. [In Vitro Research Support, Non-U.S. Gov't]. *J Neurophysiol, 87*(1), 30-41.

Taylor, W. R., & Wässle, H. (1995). Receptive field properties of starburst cholinergic amacrine cells in the rabbit retina. *Eur J Neurosci, 7*(11), 2308-2321.

Van Hook, M. J., & Berson, D. M. (2010). Hyperpolarization-activated current (I(h)) in ganglion-cell photoreceptors. [Research Support, N.I.H., Extramural]. *PloS one, 5*(12), e15344. doi: 10.1371/journal.pone.0015344

van Wyk, M., Taylor, W. R., & Vaney, D. I. (2006). Local edge detectors: a substrate for fine spatial vision at low temporal frequencies in rabbit retina. *J Neurosci, 26*(51), 13250-13263.

Vaney, D. I. (1990). The mosaic of amacrine cells in the mammalian retina. In J. J. Osborne & G. Chader (Eds.), *Progress in Retinal Research* (Vol. 9, pp. 49-100). Oxford, UK: Pergamon.

Velte, T. J., & Masland, R. H. (1999). Action potentials in the dendrites of retinal ganglion cells. *J Neurophysiol, 81*(3), 1412-1417.

Wang, G. Y., Ratto, G., Bisti, S., & Chalupa, L. M. (1997). Functional development of intrinsic properties in ganglion cells of the mammalian retina. *J Neurophysiol, 78*(6), 2895-2903.

Wang, G. Y., Robinson, D. W., & Chalupa, L. M. (1998). Calcium-activated potassium conductances in retinal ganglion cells of the ferret. *J Neurophysiol, 79*(1), 151-158.

Wässle, H. (2004). Parallel processing in the mammalian retina. [Review]. *Nature reviews. Neuroscience, 5*(10), 747-757. doi: 10.1038/nrn1497

Weick, M., & Demb, J. B. (2011). Delayed-Rectifier K Channels Contribute to Contrast Adaptation in Mammalian Retinal Ganglion Cells. *Neuron, 71*(1), 166-179. doi: 10.1016/j.neuron.2011.04.033

Zeck, G. M., & Masland, R. H. (2007). Spike train signatures of retinal ganglion cell types. *Eur J Neurosci, 26*(2), 367-380. doi: 10.1111/j.1460-9568.2007.05670.x

Chapter 3

Spike Waveform Analysis of Rat Retinal Ganglion Cells

3.1 Abstract

Different types of rat RGCs generate dissimilar action potentials (spikes) due to the complexity of the site of origin and the heterogeneous compositions of the ion channels. The spike shapes and firing behaviors vary among the types. The subtle variations among spikes can be studied by looking at the plots of temporal derivatives of the membrane potentials. Furthermore, by transforming the spike into a phase plot we can study the events that are independent of the time course, such as the firing of a spike when the membrane potential reaches a threshold. In this study, we extracted 11 parameters from the spike shape, the derivative and the phase plots. We used factor analysis to explore the number of possible hidden variables, so that we can evaluate the possibility of using the observed parameters to form a linear regression model. We concluded that a four-factor model is adequate for usefully classifying RGC types.

3.2 Introduction

The retinal ganglion cells (RGCs) collect mostly analog signals from the preganglionic neurons that represent different aspects of visual information. These signals are encrypted into action potentials (spikes) with a wide range of shapes, frequencies and patterns (Coombs, Curtis, & Eccles, 1957; Kuffler, 1953), for review see (Bean, 2007). Different types of neurons generate spikes with a similar all-or-none mechanism, however, spikes are intrinsically different due to the complexity of the site of origin and the direction of propagation. The spike shapes and firing behaviors vary substantially among different types of rat RGCs. We had looked into some of the characteristics of the spikes and their firing behaviors in 16 morphologically defined RGCs types previously (for details see Chapter 2). However, the subtle variations among the spikes cannot be seen at a glance.

Spikes originate in a region called the axon initial segment (AIS), for review see (Kole & Stuart, 2012), which is densely packed with heterogeneous sodium channels and is located proximally 30-50 μm from the soma (Boiko et al., 2003; Coombs, et al., 1957; Hu et al., 2009; Stuart, Schiller, & Sakmann, 1997). The diversity of the ion channel properties and locations make spike generation a variable non-linear process. Some obvious time-dependent information of the spike can be visualized and understood, such as the spike width. However, some properties are difficult to interpret by inspection of the time course alone. For example, all-or-none spike generation is triggered by the membrane potential (V_m) reaching an operationally defined threshold. The V_m is mainly affected by 3 types of ions: sodium ions (Na^+), potassium ions (K^+), and calcium ions (Ca^{2+}). At threshold, the Na^+ channels are activated (opened) and later inactivated (closed). These changes of ion channel status allow the ions flow in and out of the membrane in the form of trans-membrane ionic currents. The ionic currents depolarize (rise) and hyperpolarize (fall) the V_m thus forming the spiky shape of the action potential. At the end of the falling phase some K^+ channels remain open with an accompanying influx of Ca^{2+} that drives the V_m to more hyperpolarized levels than the resting state (after-hyperpolarization) for a period of time (that includes the absolute refractory period), for review see (Rodieck, 1998). By looking at a spike in the time domain, the relation of the trans-membrane ionic currents to the changes of the V_m, cannot be easily pinpointed. Therefore it is of interest to facilitate the study of the 'hidden' information from the spikes, by

examining the plots of first (dV/dt) and the second (d^2V/dt^2) derivatives of the V_m versus time, and also their phase plots (dV/dt versus V_m) (Fohlmeister & Miller, 1997; Jenerick, 1963; Kress, Dowling, Meeks, & Mennerick, 2008; Meeks & Mennerick, 2007). These plots reveal independent (uncorrelated) information from the RGCs, which are sometimes more comprehensive. For example, the heterogeneous compositions of voltage-gated channels in different RGC types affect the slopes of different spike shapes during the rising phase (Hu, et al., 2009; Meeks & Mennerick, 2007).

The wide variety of ion channels leads to diverse ionic conductances in the membrane, which correspondingly alter the spike shape, firing frequencies and firing patterns. Conversely, we can study the trans-membrane ionic currents and conductances that lead to different spike shapes and firing behaviors. Nevertheless, the spike shape is not apparently correlated to the firing behaviors (Connors, Gutnick, & Prince, 1982; McCormick, Connors, Lighthall, & Prince, 1985). Spikes initiated at the AIS propagate orthodromically away from the soma, and also travel antidromically back to the soma, therefore the somatic spikes recorded sometimes have an obvious small hump in the phase plot at the rising phase before the large hump, for review see (Bender & Trussell, 2012) (see also Figure 3.2B). This small/first hump corresponds to the onset of a low threshold axonal spike initiated at the distal end of the AIS (Hu, et al., 2009; Palmer & Stuart, 2006). The existence of axonal spikes is sometimes not clearly recognizable from the spike shape and perhaps is too small in the phase plots, but it is certainly prominent in the derivative plots (Figure 3.3).

Phase plot trajectories are used to portray dV/dt versus V_m, in which the rate of change of V_m at different V_m can be clearly studied. The fine details, such as the spike initiation threshold at which the V_m changes rapidly (~10 mV ms^{-1}) (Naundorf, Wolf, & Volgushev, 2006), can be easily evaluated from these plots. The first derivatives show the rate of change of the ion currents which indicate the activities of the ion channels. The second derivatives make the characteristic of the *initial segment-soma dendritic* (IS-SD) break become more obvious. The recorded somatic spike is a complex of axonal and somatic spikes. The IS-SD break is the time between the two peaks in the second derivative plot, corresponding to the maximum rate of change of the two humps in the phase plot (Figure 3.3). The small deflection at the rising phase of the spike presumably reflects an attenuated axonal spike as it spreads back along the

axon hillock into the soma (Coombs, et al., 1957; Kress, et al., 2008; Meeks & Mennerick, 2007).

The studies reported here were primary concerned with eleven parameters that were extracted from: 1) the spike shapes, 2) the dV/dt versus time, 3) the d^2V/dt^2 versus time, and 4) the phase plots. We would like to know if these parameters can be used to classify the different rat RGC types. It is reasonable that the eleven parameters are not completely independent, indeed it is likely that they are determined by a smaller set of hidden variables. We used *factor analysis* to explore the number of possible hidden variables and their correlation with the observed parameters. Correlations between the estimated hidden variables (factor scores) and cell features like putative receptive field attributes and cell types (e.g. dendritic stratification: INNER, OUTER, and BISTRAT, see Chapter 2 for details) are also examined. An advantage of factor analysis is that much of the noise in the measurement of the original parameters is split into the unused factors, and so is removed from the data.

3.3 Materials and Methods

This chapter is an extension of Chapter 2 and uses the same raw dataset. Please see section 2.3 for ethical approval, detailed experimental methods and data recording procedures. Briefly, whole-cell patch clamps were made to record rat RGCs (n=125) responses to intracellular stimulation. The stimuli contained a series of current steps each of 400 ms duration. The recording period was 1 second with 3 seconds rest in between repetitions. All recorded RGCs were morphologically classified into 16 types (see Chapter 2 for details).

3.3.1 Data Analysis

Individual spikes were extracted and analyzed with custom-made LabVIEW programs (National Instruments, 2010 and 2011, USA) from the maintained discharges (spontaneous spike trains) or spike trains with minimum current injections (~10-30 pA) that were close to threshold (i.e. one or two spikes elicited during the 400 ms current injection period). For each

RGC, an average spike was computed from at least 15 single spikes that were aligned to their peaks (Figure 3.1). Generally, the individual waveforms of each RGC spike were homogeneous in shape when evoked by the same amount of current.

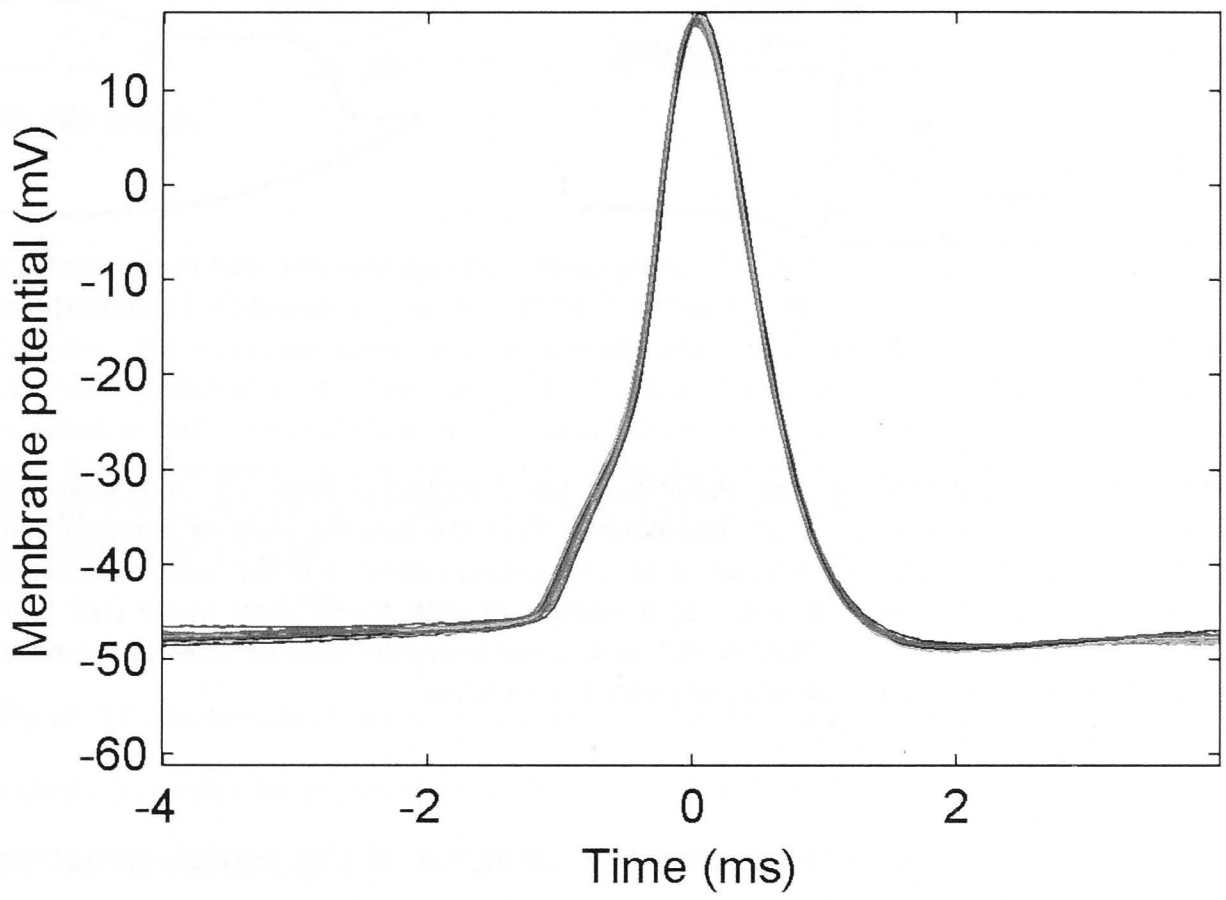

Figure 3.1 An example showing 15 spikes temporally aligned to their peaks. A representative spike is computed by averaging the aligned spikes.

The phase, the dV/dt and the d^2V/dt^2 plots of each of the average spikes were plotted by OriginPro (OriginLab, 8.6, USA) and Matlab (Mathworks, 2012a, USA). A total of 11 parameters were extracted from the spike shapes (n=5) and the phase plots (n=6). The full descriptions of the 11 parameters are given in Table 3.1 and Figure 3.2.

Table 3.1 Brief descriptions of the 11 parameters measured from the spike shape and the phase plot.

Type	Short Name	Full Parameter Name	Brief descriptions
Spike shape	1: rise	Rise time (10-90%) (ms)	The time required for Vm to change from 10% to 90% of the max Vm
	2: max	Max spike amplitude (mV)	Vm peak referenced to the resting potential (baseline)
	3: min	Min after-hyperpolarization amplitude (mV)	Vm nadir referenced to the resting potential (baseline)
	4: diff	Absolute amplitude difference (mV)	Max - Min (mV)
	5: ratio	Ratio of Min to Max	Min / Max
Phase plot	6: break	IS-SD break	presence of the axonal spike, time between the two peaks in d^2V/dt^2 plot
	7: thres	Voltage threshold (mV)	Vm at dV/dt = 10 mV/ms
	8: dMax	Max dV/dt (mV/ms)	highest rate of change of Vm
	9: dMin	Min dV/dt (mV/ms)	lowest rate of change of Vm
	10: tVM	Time_VM	Time from voltage threshold to max dV/dt (ms)
	11: slope	Slope at threshold (1/ms)	Slope of the three data points at threshold

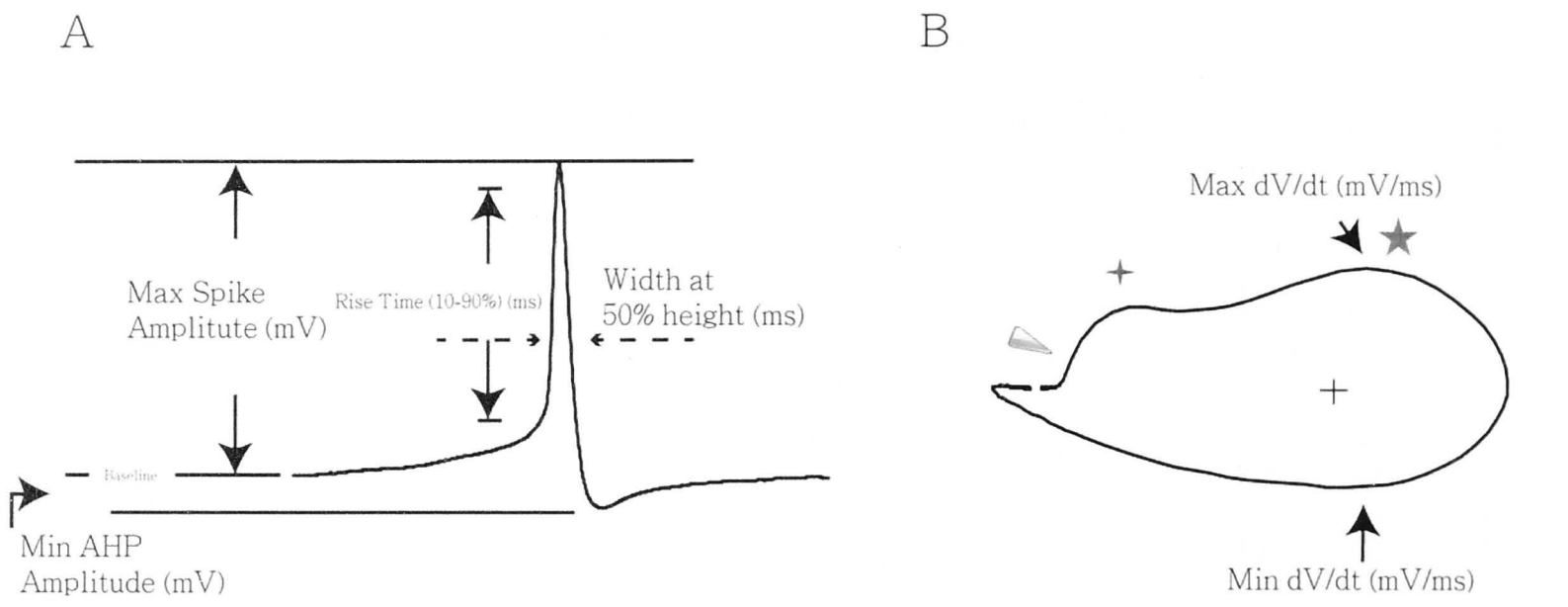

Figure 3.2 Anatomy of a spike and a phase plot. Parameters are described in Table 3.1. **A)** A spike with a general shape, where the membrane potential (V_m) rises (depolarizes) from the baseline (resting potential) and then falls (hyperpolarizes). The V_m drops to below the baseline to a minimum potential (after-hyperpolarization potential, AHP) and gradually reinstates to the resting level. **B)** A phase plot with a small/first hump (red four-point star) indicating the presence of the axonal spike. The second hump (blue five-point star) denotes the somatic spike. The threshold (green triangle) is where dV/dt approximately equals 10 mV/ms.

The hump in the phase plot denotes the presence of the axonal component of the spike. The evidence is clearer in the two peaks seen in the derivative plots (Figure 3.3). The peaks in the dV/dt plot represent the maximum rates of change of the V_m at the AIS and the soma respectively. In the d^2V/dt^2 plot, the first peak indicates the maximum rate of Na^+ channel recruitment at the AIS. Once the threshold is reached, spikes will propagate from the AIS in opposite directions. The antidromic axonal spike takes some time (IS-SD break) to propagate to the soma and affect the somatic ion channels. The second peak shows the maximum rate of Na+ recruitment at the soma (Coombs, et al., 1957; Kress, et al., 2008; Meeks & Mennerick, 2007). The time between the two peaks in the d^2V/dt^2 plot is generally more discernible than the two peaks in the dV/dt plot.

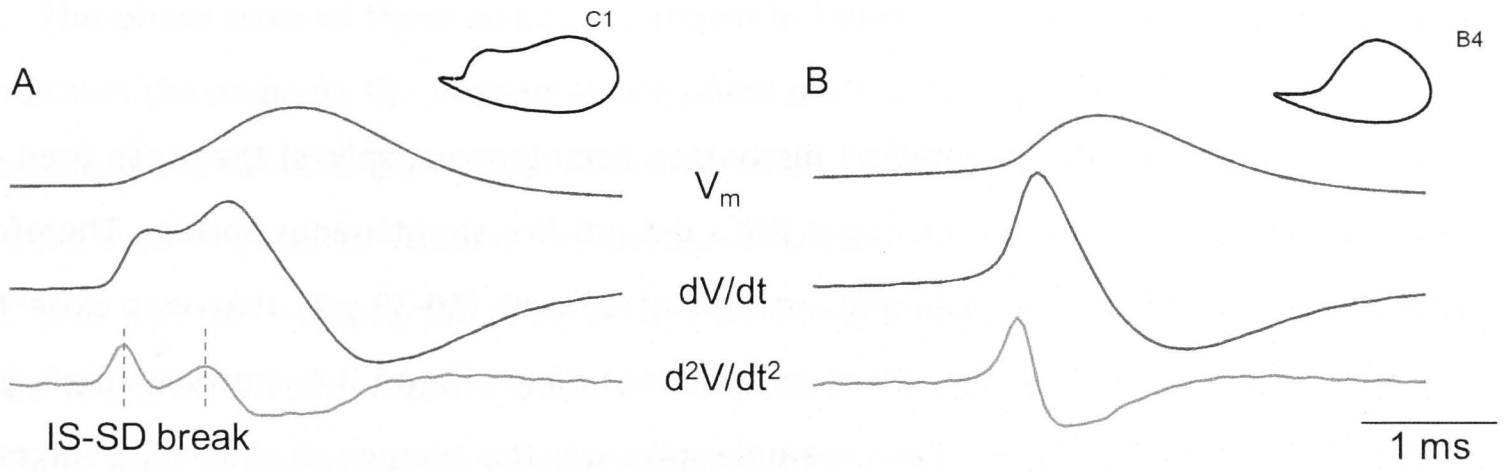

Figure 3.3 Comparison of two different spikes in three plots. The plots demonstrate the membrane potential (V_m) (i.e. the spike), and the first (dV/dt) and second (d^2V/dt^2) derivatives of V_m over time. The plots have been scaled for easier observation. The insets show the associated phase plots (dV/dt vs. V_m). The time coordinate is the implicit parameter, increasing clockwise. **A)** Plots from a C1 RGC. The existence of an axonal spike is not clear in the V_m plot but the two peaks in both the dV/dt and d^2V/dt^2 plots show its presence. The first hump in the phase plot also makes evident the axonal spike. The IS-SD break is defined as the time difference between the two peaks in the d^2V/dt^2 plot. **B)** The plots from a B4 RGC have only one hump and one peak, therefore, an axonal spike is presumably 'absent' (see Discussion).

These 11 parameters were evaluated by a principal component analysis (PCA) based Factor Analysis in order to estimate the number of uncorrelated factors (i.e. hidden variables), that might be determining the parameters we measured. The estimates of the hidden variables, the Factor Scores, were also examined for their correlation with the rat RGC type classifications.

3.4 Results

We examined the maintained discharges (spontaneous spikes) that cells fired in the absence of a stimulus. However, some RGCs did not fire spontaneous spikes. Therefore, in those cases, we injected a minimum amount of current (10-30 pA) that was close to the threshold to obtain one or two spikes in each recording. Figure 3.4 shows exemplary spike shapes from the 16 RGC types. Each example spike was the average of at least 15 spikes. Five related parameters were extracted from the spike shape and are recorded in Table 3.2.

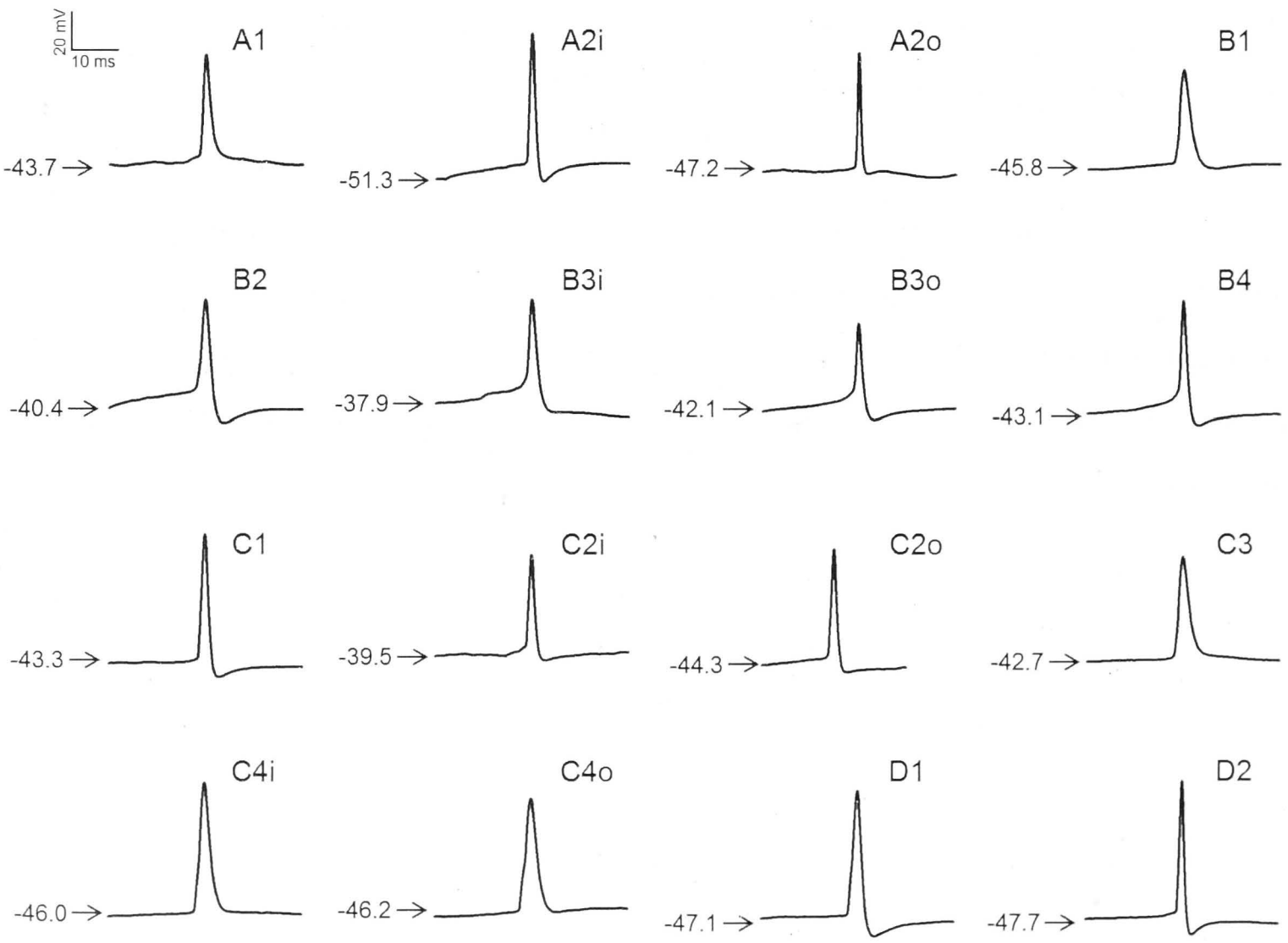

Figure 3.4 Example spike shapes for the 16 morphologically defined rat RGC types. Each panel shows a representative spike (an average of at least 15 spikes from the same RGC) of a rat RGC type. The arrows (→) indicate the resting potentials.

The phase plots of these spikes are shown in Figure 3.5. The cross inside each phase plot indicates the origin (0, 0). In general, the phase plots contained either one or two humps. In some cases the first humps were perhaps too small to recognize, therefore the derivatives plots were used in order to visualize the peaks. In cases where there were two peaks in the d^2V/dt^2 plot (i.e. two humps), the IS-SD breaks were measured. The numbers of phase plots that had the IS-SD breaks were recorded in the column 'm' of Table 3.2 (also Tables 3.4 and 3.5). There were 6 related parameters measured from the phase plots (Table 3.2).

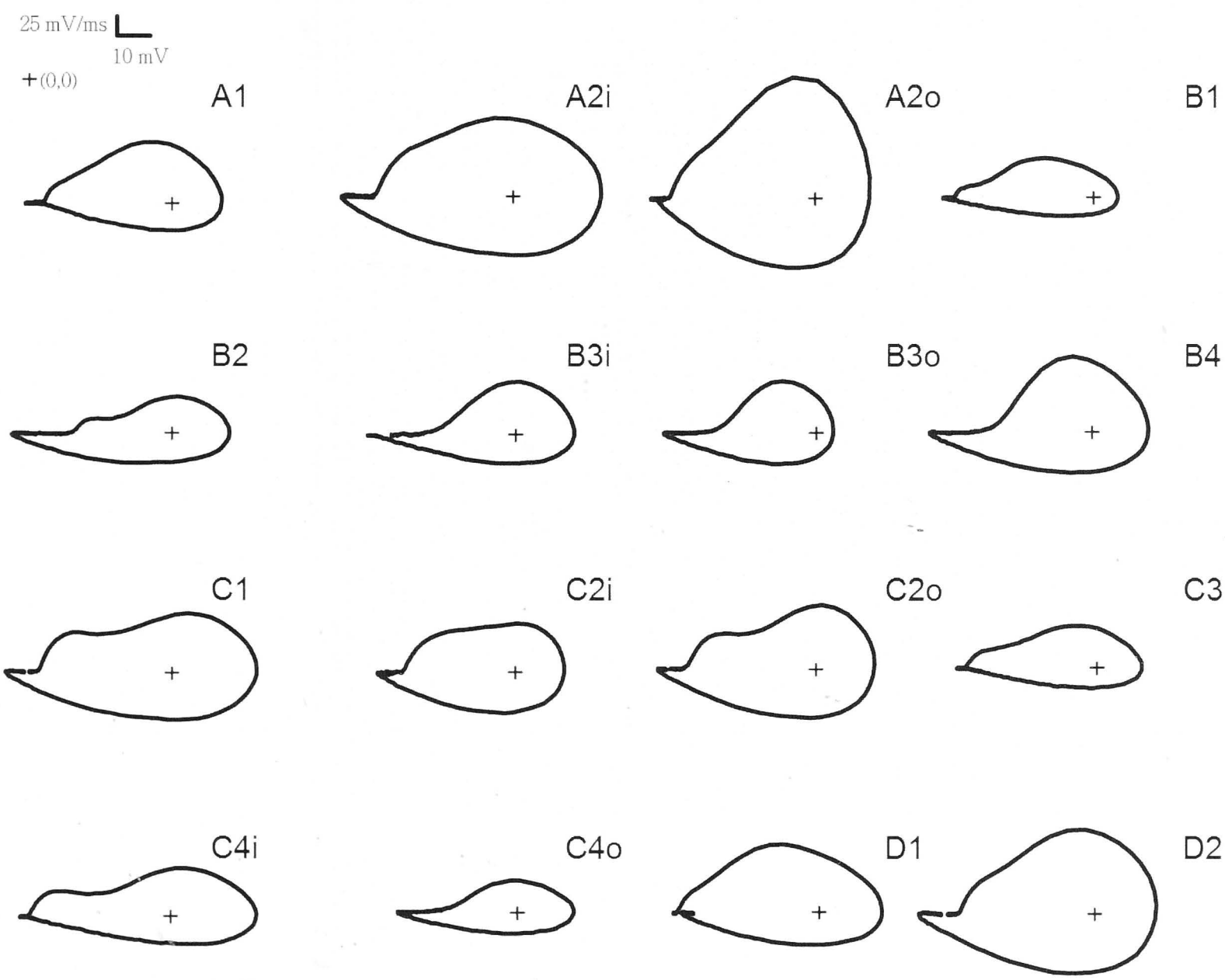

Figure 3.5 Phase plot samples of the 16 morphologically defined rat RGC types. Each panel contains a phase plot transformed from the corresponding spike in Figure 3.4. The crosses (+) denote the origin (0, 0) of the plots. Some of them have very obvious double humps caused by axonal (first hump) and somatic (second hump) spikes (e.g. B2 and C1), and some of the phase plots had only one hump from putative, simultaneous axo-somatic spikes (e.g. B3i and C4o).

All the 11 parameters extracted are listed in Table 3.2. The values were listed as means with standard deviations in the parentheses. Some of the values were clearly distinguishable within the individual parametric groups. For example, the rise times of B type cells were all larger than the rest of the RGC types.

Table 3.2: Spike shape and phase plot parameters of rat RGC types.

		Spike shape						Phase Plot					
Cell type	n	rise (ms)	max (mV)	min (mV)	diff (mV)	ratio	m	break (ms)	thres (mV)	dMax (mV/ms)	dMin (mV/ms)	tVm (ms)	slope (ms^-1)
A1	3	1.22 (0.38)	59.6 (8.44)	-7.21 (4.31)	66.8 (12.5)	0.11 (0.05)	2	0.32 (0.08)	-38.3 (0.86)	75.6 (14.1)	-42.3 (9.77)	0.75 (0.11)	4.51 (1.45)
A2i	4	1.03 (0.45)	57.8 (11.7)	-4.48 (2.06)	62.3 (12.2)	0.08 (0.05)	1	0.26 (0)	-38.2 (2.73)	98.2 (24.6)	-57.8 (16.6)	0.55 (0.08)	6.14 (2.17)
A2o	21	0.86 (0.60)	66.6 (10.3)	-2.47 (1.93)	69.0 (10.6)	0.04 (0.03)	11	0.31 (0.08)	-43.0 (3.45)	147.1 (40.6)	-88.9 (26.8)	0.58 (0.18)	6.92 (2.37)
B1	3	3.51 (1.44)	53.8 (6.59)	-5.16 (2.96)	59.0 (8.37)	0.10 (0.05)	1	0.17	-39.9 (1.18)	48.6 (7.35)	-26.8 (6.37)	0.85 (0.22)	2.50 (0.84)
B2	8	3.91 (2.43)	53.8 (10.1)	-6.93 (5.19)	60.7 (13.1)	0.13 (0.08)	2	0.41 (0.05)	-39.1 (1.15)	56.3 (12.2)	-40.0 (11.3)	0.77 (0.26)	3.91 (1.64)
B3i*	1	4.05279	61.043413	-7.039837	68.08325	0.115757	0	0	-36.70197	89.351646	-49.103634	0.6625	2.503536
B3o	4	3.07 (1.20)	58.5 (13.6)	-5.80 (1.55)	64.3 (12.6)	0.11 (0.04)	1	0.56 (0)	-39.8 (2.40)	61.8 (11.6)	-38.6 (8.89)	0.78 (0.21)	3.20 (0.81)
B4	11	2.57 (1.38)	61.7 (8.70)	-6.41 (2.84)	68.1 (7.88)	0.11 (0.06)	5	0.37 (0.08)	-39.5 (2.47)	72.5 (24.5)	-42.5 (18.8)	0.96 (0.65)	4.89 (2.35)
C1	4	1.12 (0.33)	62.0 (9.24)	-6.37 (4.80)	68.4 (9.87)	0.11 (0.08)	3	0.31 (0.08)	-39.9 (2.56)	77.6 (12.8)	-51.7 (10.6)	0.66 (0.07)	6.19 (2.38)
C2i	6	1.79 (0.58)	56.7 (6.82)	-6.41 (2.69)	63.2 (6.76)	0.12 (0.05)	2	0.42 (0.01)	-38.0 (0.96)	70.2 (22.9)	-46.4 (12.9)	0.80 (0.30)	4.89 (1.92)
C2o	14	1.76 (1.34)	61.5 (12.6)	-4.37 (4.44)	65.8 (14.4)	0.07 (0.06)	9	0.36 (0.07)	-41.7 (3.59)	89.7 (31.2)	-55.5 (23.5)	0.75 (0.22)	5.68 (1.87)
C3	4	1.14 (0.32)	54.3 (7.60)	-2.45 (3.51)	56.7 (10.6)	0.04 (0.05)	2	0.37 (0.06)	-38.7 (1.16)	72.2 (16.7)	-39.9 (14.8)	0.78 (0.36)	5.00 (0.66)
C4i	3	2.24 (0.82)	63.9 (14.3)	-7.16 (5.84)	71.0 (10.2)	0.14 (0.14)	1	0.44 (0)	-41.6 (3.18)	61.3 (1.86)	-36.3 (11.3)	1.01 (0.30)	3.40 (1.70)
C4o	15	2.03 (1.40)	59.1 (8.04)	-6.13 (3.94)	65.2 (8.80)	0.11 (0.07)	9	0.35 (0.05)	-39.8 (2.49)	75.1 (26.7)	-45.8 (16.1)	0.91 (0.57)	4.86 (2.14)
D1	7	1.60 (1.13)	63.6 (3.72)	-4.45 (4.61)	68.1 (7.93)	0.07 (0.07)	6	0.33 (0.09)	-40.6 (2.10)	81.4 (16.2)	-43.4 (10.4)	1.48 (1.17)	6.14 (1.44)
D2	17	1.57 (1.13)	61.0 (9.42)	-7.09 (2.81)	68.0 (10.1)	0.12 (0.05)	9	0.35 (0.08)	-40.0 (1.72)	78.3 (31.9)	-54.1 (22.2)	1.13 (1.26)	5.25 (1.95)
ALL	125	1.85 (1.47)	60.8 (10.4)	-5.31 (3.93)	66.1 (11.0)	0.09 (0.07)	64	0.34 (0.09)	-40.4 (3.06)	87.4 (39.7)	-53.9 (25.5)	0.86 (0.67)	5.28 (2.25)

*Only one record for B3i; n: number of sampled cells; m: number of samples that had two humps; brief parameter descriptions can be found in Table 3.1; values are mean (standard deviation).

We converted the whole set of 11 parameters into a set of uncorrelated principal components with PCA. The inputs were the means for each cell type to insure that the parameters for each class were well measured. We then converted the means to z-scores to reduce the effects of the different scales of some of the parameters. The four largest components account for 90.5% of the variance (and the remaining 7 factors 9.5%, Figure 3.6A) and so we decided to use them for our Factor Analysis, describing them as F1 to F4. We also examined the proportion of variance in the original 11 parameters explained by the four-factor model, the *communalities*. The median communality was 93.3%. Hence the four-factor model seemed to account for all 11 parameters very well (Figure 3.6B).

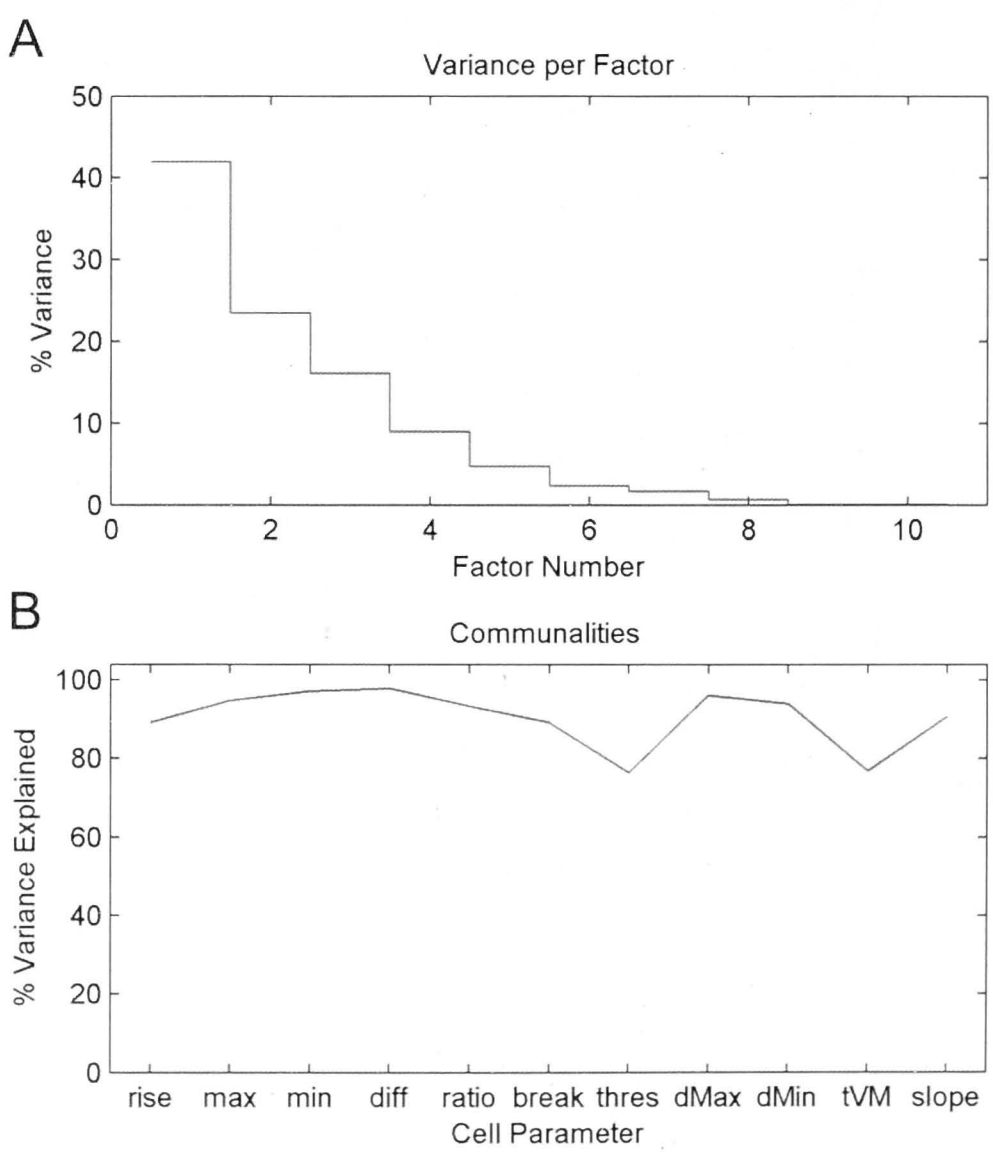

Figure 3.6 Rationale for a four-factor model. The Factors represent the major axes of variation in the data, sorted from greatest to smallest (i.e. ordered by %Variance). **A)** The proportion of the 11 parameters accounted for by the major axes of variation (factors), the first factor (Principal Component Analysis component) accounts for 42% of the data. **B)** The proportion of the variance of the original 11 parameters explained by a factor model containing just the four largest factors (F1 to F4). All the variables are well accounted for by the model except perhaps the threshold value (thres) and the time to Vmax (tVM).

We then calculated Factor Scores as estimates of the hidden variables, and then compared these with the cell types. Specifically, we examined the correlations between the Factor Scores and the original parameters (Table 3.3). For example the first factor (F1) was mainly correlated with the spike rise-time (r^2 = 0.906), the IS-SD break (r^2 = 0.847), and the slope at threshold (r^2 =0.832).

We also examined the correlation between the Factor Scores and two sets of cell classifiers: a quite related retinal layer classifier with the categories INNER, OUTER, BISTRAT; and a cell-type classifier with four categories A to D. The retinal layer classifier was based on dendritic stratification and gave the categories: (INNER - A1, A2i, B2, B3i, C1, C2i, C3, C4i; OUTER - A2o, B3o, C2o, C4o; and BISTRAT - B1, B4, D1, D2) (for details see Chapter 2; INNER: 40-100% depth; OUTER: 0-40% depth; BISTRAT: bistratified or at boundary ~40%). For the cell type classifier: A included A1, A2i, A2o; B included all the B subtypes, and so on.

F3 was correlated with cell-type (A to D) at r^2 = 0.61 (p=0.01), and was mainly associated with max and min dV/dt (dMax, dMin), and time to max dV/dt (tVM). F3 was also correlated with retinal layer, but with marginal significance (p=0.07). There were no other significant correlations between the factors and the cell type classifiers. Interestingly F1, the largest of the factors with its 42% of the variance, was not useful for classifying cells into these categories.

Table 3.3 Results from Factor analysis. Four uncorrelated factors (F1 to F4) were found. For each component, the associated correlation coefficients for each parameter were computed. The scale bar shows the colour code of correlation coefficients, colour scaled from 0 (white, no correlation) to 1 (dark green, perfect correlation).

Param	F1	F2	F3	F4	Scale
1: rise	0.906	0.094	0.170	0.184	0
2: max	0.224	0.939	0.118	0.045	0.1
3: min	0.209	0.124	0.187	0.937	0.2
4: diff	0.119	0.892	0.033	0.409	0.3
5: ratio	0.325	0.106	0.215	0.878	0.4
6: break	0.847	0.187	0.348	0.135	0.5
7: thres	0.116	0.642	0.253	0.524	0.6
8: dMax	0.253	0.448	0.738	0.391	0.7
9: dMin	0.277	0.449	0.754	0.305	0.8
10: tVM	0.151	0.333	0.797	0.008	0.9
11: slope	0.832	0.229	0.267	0.303	1

Table 3.4 Spike shape and phase plot parameters of rat RGC types according to their dendritic stratifications. The three defined groups are putative ON (INNER), OFF (OUTER) and ON-OFF (BISTRAT) cells. Values are mean (standard deviation).

		Spike shape						Phase Plot					
Cell type	n	rise (ms)	max (mV)	min (mV)	diff (mV)	ratio	m	break (ms)	thres (mV)	dMax (mV/ms)	dMin (mV/ms)	tVm (ms)	slope (ms^-1)
INNER	33	2.11 (1.73)	57.5 (10.2)	-5.98 (4.45)	63.5 (11.6)	0.11 (0.08)	13	0.33 (0.12)	-38.9 (2.57)	71.6 (21.1)	-44.9 (14.1)	0.75 (0.27)	4.74 (2.02)
OUTER	54	1.58 (1.30)	62.6 (11.2)	-4.23 (3.67)	66.8 (11.6)	0.07 (0.06)	30	0.34 (0.08)	-41.5 (3.45)	105.9 (47.3)	-64.6 (30.0)	0.73 (0.37)	5.75 (2.37)
BISTRAT	38	2.01 (1.38)	61.1 (8.55)	-6.25 (3.39)	67.3 (9.31)	0.11 (0.06)	21	0.34 (0.09)	-39.9 (2.04)	74.8 (27.4)	-46.6 (20.2)	1.12 (1.06)	5.09 (2.12)

Table 3.5 P-value results from the two-tail t-test between the dendritic stratification defined RGC types. P-values that were statistically significant (< 0.05) were highlighted in orange.

		Spike shape						Phase Plot					
t-test	n	rise (ms)	max (mV)	min (mV)	diff (mV)	ratio	m	break (ms)	thres (mV)	dMax (mV/ms)	dMin (mV/ms)	tVm (ms)	slope (ms^-1)
INNER / OUTER	33	0.143	0.037	0.066	0.210	0.038	13	0.213	0.000	0.000	0.000	0.754	0.039
INNER / BISTRAT	54	0.806	0.125	0.777	0.140	0.985	30	0.271	0.084	0.585	0.676	0.047	0.476
OUTER / BISTRAT	38	0.139	0.480	0.008	0.804	0.010	21	0.953	0.007	0.000	0.001	0.036	0.171

Note: INNER: A1, A2i, B2, B3i, C1, C2i, C3, C4i; OUTER: A2o, B3o, C2o, C4o; BISTRAT: B1, B4, D1, D2

Given that the factor analysis highlighted that several variables were heavily loaded onto the uncorrelated factors, and that some of these were useful for cell classification, it was decided to look at the significance of ratios the original variables when they were grouped by retinal stratification. The means (and standard deviations) are shown in Table 3.4. A two-tail t-test for unequal variances was used to evaluate the statistical significance among the three groups (Table 3.5). The p-values indicating important differences ($p<0.05$) are highlighted in orange.

3.5 Discussion

In this study we examined the spike shapes, their first and second order derivatives, and their associated phase plots. Since the V_m were directly related to the voltage-gated ion channels, extending the inspection from the time domain to the voltage domain gave us a more intuitive assessment of the RGC characteristics.

We found that just relying on the measured intrinsic properties of the 16 morphologically defined rat RGC types to classify the cells was inadequate. The exception was possibly for cell type (A to D), where the third factor (F3), which was significantly correlated ($p = 0.01$) with the phase plot parameters with max and min dV/dt (dMax, dMin), and time to max dV/dt (tVM). F3, and its associated parameters, were also somewhat correlated with dendritic stratification. The dendrites of the RGCs that ramify throughout the inner plexiform layer (IPL) have been reported to be related to the receptive field properties (Nelson, Famiglietti, & Kolb, 1978). The RGCs stratify in different sublaminae of the IPL and made connections to the bipolar cells of the ON and OFF pathways. Therefore, the INNER, OUTER and BISTRAT groups were putative ON, OFF and ON-OFF cells correspondingly. Notice that the B1 and B4 cells are not strictly morphologically bistratified cells, their dendrites are at the boundary. The currently examined parameters did not distinguish the stratification well.

The second factor (F2) was mainly correlated with the spike shape parameters: maximum spike amplitude (max), and the difference between max and the after polarization level (min). At the very least the factor analysis indicates many of the spike shape and phase

plot variables are independent measures. Given that F2 and F3 are uncorrelated this suggests that perhaps some set of parameters related to the five mainly associated with F2 and F3 would do a better job of categorizing the cells, and this could form the basis of future research. The PCA based factor analysis insured that the factors found were orthogonal. There is nothing to say that the true hidden variables are orthogonal, they only need to span the space of factors 2 and 3. We did also attempt an alternative method that yields non-orthogonal factors, a maximum likelihood method that produces the best estimate of the correlation matrix between the input variables (Reyment & Joreskog, 1996). It produced poorer communalities and so we did not pursue it. Alternative methods like Independent Components Analysis could also be used in a further investigation.

The plots we used in this study facilitated the study of rat RGC type classification. Parameters such as the thresholds were more recognizable and quantifiable in the phase plot with the defined rate of change of V_m, rather than looking at the turning point (so-called the 'kink') in the spike shape. Visualization of the axonal and the somatic spikes were a lot easier in the d^2V/dt^2 plot than the spike shape or the phase plots. In addition, from previous study we knew that the slope at threshold had a close relationship with the distance of the AIS from the soma (Kress, et al., 2008).

When the RGCs were regrouped into INNER, OUTER, and BISTRAT, the differences among them perhaps became more noticeable. The t-tests showed that the parameters extracted from the phase plots were very useful (6 out of 11 parameters) for classifying the differences between the INNER-OUTER, and the OUTER-BISTRAT groups. These results were consistent with the findings in Chapter 2. On the other hand, the INNER-BISTRAT comparison was not as outstanding as the others. Only one parameter (tVM) showed significance, however, tVM was one of the variables that had a high correlation coefficient with F3 from the PCA. Combined with the other parameters, it appears to be a fairly critical component for classification of the RGC types in this study.

From the results in Table 3.2, some of the variations between different RGC types were obvious. However, the number of cells showing a two-peak appearance (m) was only half the size of the total number recorded (n). The confocal image reconstructions (see Chapter 2, figure

2.1) indicated that the majority of the RGCs recorded had axons extending toward the optic disc head. Occasionally there were possibly 'missing' or 'damaged' axons that we could not identify from the images. One of the protocols that we planned to do but failed to complete (mostly due to human error) was to label the AIS Na^+ channels with ankyrin-G (Goldberg et al., 2008; Hu, et al., 2009; Kress, et al., 2008). Without staining the AIS, we couldn't measure the distance from the AIS to the soma, nor to know if the axon was still intact, or at least if the AIS was still present in those recorded RGCs. If we know the distance of the AIS from the soma, we can compute the conduction velocity as well. Adding an extra protocol to block the synaptic connections with pharmacological agents (e.g. tetrodotoxin to block Na^+ channels) would certainly facilitate further trans-membrane conductance studies (Kress, et al., 2008; Meeks & Mennerick, 2007).

It is hard to imagine how there could be a soma-dendritic component *without* an initial segment-soma component, under normal conditions. The physical distance between the soma and the AIS is only 20-30 microns of a rather large-core cable (axon hillock). There might be other possibilities: 1) the somatic and axonal spikes might be simultaneously activated and so overlapped; 2) the axonal spike was present but didn't travel antidromically towards the soma; 3) the high-frequency response of the recording amplifier was so limited that critical details of the waveform have been smoothed out; 4) the time derivatives were inadequate to show the finer details.

Another issue was the temperature because the V_m and synaptic activities were certainly affected by thermal and kinetic energy. Despite the imperfections in this dataset, nonetheless, the parameters found here expanded the dataset for rat RGC type classification by using the response of the cells independent of the morphologies. These parameters are still useful for the development of RGC modeling. Ongoing RGC modeling study is being carried out with collaborators.

During this study, it was noticed that some of the cell properties varied with the amount of current being injected. Some of those data suggest candidates with which to expand the variable set with independent parameters. One of the most critical factors is the temperature. A preliminary study (detailed not reported here) of 18 RGCs (mixed types) were conducted after the normal recordings in room temperature, by changing the temperature to 33°C and repeating

the whole procedures on the same cell. The results from t-tests showed that there were no significant statistical differences in the parameters: rise, min, ratio and break. Nevertheless, all the other parameters were significantly affected. Examples showing the effect of temperature are shown in Figure 3.7.

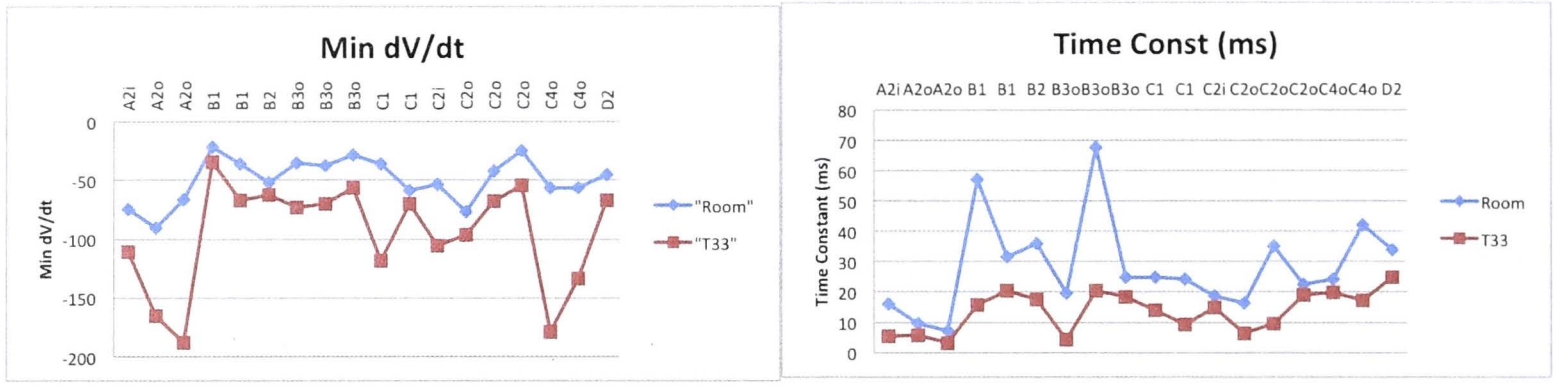

Figure 3.7 Temperature effects on RGC parameters. Examples of two parameters, minimum dV/dt from waveform analysis (left) and time constant from intrinsic properties (right), which are affected by temperature. The horizontal axis shows the cell types of the recorded cells in the preliminary study. The blue and red curves are data recorded at room temperature and 33^{o}C respectively.

Unfortunately, the 18 cells recorded did not unveil all the 16 common types and in particular 5 types (A1, B3i, B4, C4i and D1) were missing. The existing data showed that temperature is an important variable but as aforesaid, the current dataset on this separate aspect was incomplete and thus we need more data to support the findings. In future RGC modeling studies, it will be necessary to take account of the temperature as an important variable to be investigated.

3.6 References

Bean, B. P. (2007). The action potential in mammalian central neurons. *Nature Reviews Neuroscience, 8*(6), 451-465. doi: Doi 10.1038/Nrn2148

Bender, K. J., & Trussell, L. O. (2012). The Physiology of the Axon Initial Segment. *Annual Review of Neuroscience, Vol 35, 35*, 249-265. doi: DOI 10.1146/annurev-neuro-062111-150339

Boiko, T., Van Wart, A., Caldwell, J. H., Levinson, S. R., Trimmer, J. S., & Matthews, G. (2003). Functional specialization of the axon initial segment by isoform-specific sodium channel targeting. *Journal of Neuroscience, 23*(6), 2306-2313.

Connors, B. W., Gutnick, M. J., & Prince, D. A. (1982). Electrophysiological properties of neocortical neurons in vitro. [In Vitro Research Support, U.S. Gov't, P.H.S.]. *Journal of Neurophysiology, 48*(6), 1302-1320.

Coombs, J. S., Curtis, D. R., & Eccles, J. C. (1957). The Interpretation of Spike Potentials of Motoneurones. *Journal of Physiology-London, 139*(2), 198-231.

Fohlmeister, J. F., & Miller, R. F. (1997). Mechanisms by which cell geometry controls repetitive impulse firing in retinal ganglion cells. *Journal of Neurophysiology, 78*(4), 1948-1964.

Goldberg, E. M., Clark, B. D., Zagha, E., Nahmani, M., Erisir, A., & Rudy, B. (2008). K+ channels at the axon initial segment dampen near-threshold excitability of neocortical fast-spiking GABAergic interneurons. *Neuron, 58*(3), 387-400. doi: DOI 10.1016/j.neuron.2008.03.003

Hu, W. Q., Tian, C. P., Li, T., Yang, M. P., Hou, H., & Shu, Y. S. (2009). Distinct contributions of Na(v)1.6 and Na(v)1.2 in action potential initiation and backpropagation. *Nature Neuroscience, 12*(8), 996-U961. doi: Doi 10.1038/Nn.2359

Jenerick, H. (1963). Phase Plane Trajectories of the Muscle Spike Potential. *Biophysical journal, 3*, 363-377.

Kole, M. H. P., & Stuart, G. J. (2012). Signal Processing in the Axon Initial Segment. *Neuron, 73*(2), 235-247. doi: DOI 10.1016/j.neuron.2012.01.007

Kress, G. J., Dowling, M. J., Meeks, J. P., & Mennerick, S. (2008). High threshold, proximal initiation, and slow conduction velocity of action potentials in dentate granule neuron mossy fibers. *Journal of Neurophysiology, 100*(1), 281-291. doi: 90295.2008 [pii]10.1152/jn.90295.2008

Kuffler, S. W. (1953). Discharge Patterns and Functional Organization of Mammalian Retina. *Journal of Neurophysiology, 16*(1), 37-68.

McCormick, D. A., Connors, B. W., Lighthall, J. W., & Prince, D. A. (1985). Comparative Electrophysiology of Pyramidal and Sparsely Spiny Stellate Neurons of the Neocortex. *Journal of Neurophysiology, 54*(4), 782-806.

Meeks, J. P., & Mennerick, S. (2007). Action potential initiation and propagation in CA3 pyramidal axons. *Journal of Neurophysiology, 97*(5), 3460-3472. doi: 01288.2006 [pii] 10.1152/jn.01288.2006

Naundorf, B., Wolf, F., & Volgushev, M. (2006). Unique features of action potential initiation in cortical neurons. *Nature, 440*(7087), 1060-1063. doi: Doi 10.1038/Nature04610

Nelson, R., Famiglietti, E. V., & Kolb, H. (1978). Intracellular Staining Reveals Different Levels of Stratification for on-Center and Off-Center Ganglion-Cells in Cat Retina. *Journal of Neurophysiology, 41*(2), 472-483.

Palmer, L. M., & Stuart, G. J. (2006). Site of action potential initiation in layer 5 pyramidal neurons. *Journal of Neuroscience, 26*(6), 1854-1863. doi: Doi 10.1523/Jneurosci.4812-05.2006

Reyment, R. A., & Joreskog, K. G. (1996). *Applied Factor Analysis in the Natural Sciences*.

Rodieck, R. W. (1998). *The First Steps in Seeing*: Sinauer Associates.

Stuart, G., Schiller, J., & Sakmann, B. (1997). Action potential initiation and propagation in rat neocortical pyramidal neurons. *Journal of Physiology-London, 505*(3), 617-632. doi: DOI 10.1111/j.1469-7793.1997.617ba.x

Chapter 4

Epiretinal Electrical Stimulation and the Inner Limiting Membrane in Rat Retina

4.1 Abstract

In this study, we aim to investigate the difference between the activation thresholds of two extracellular stimulating electrode positions: above or below the inner limiting membrane (ILM), using rat type-A retinal ganglion cells (RGCs). The objective is to obtain information for the design of an epiretinal prosthesis. A pair of bipolar stimulating electrodes was placed on the retina, one on the surface of the inner retina as a reference electrode, and the other one either placed above the inner retinal surface or penetrating into the ILM. Then we made whole-cell patch-clamp recordings from type-A RGCs in an isolated rat retinal whole-mount preparation. Across our cell population (n=15), we found no significant difference in the median threshold stimulus amplitudes when the stimulating electrodes were placed below as opposed to above the ILM ($p = 0.08$). However, threshold stimulus amplitudes did tend to be lower when the stimulating electrodes were placed below the ILM (30 μA vs 56 μA). Furthermore, in 6 of the recordings it was noticed that single electrical stimulation led to the production of a closely timed second spike.

4.2 Introduction

According to the World Health Organization, approximately 20 million people are blind due to diseases that cause degeneration of the retina (WHO, 2012). One of the leading causes of blindness is Retinitis Pigmentosa (RP), which affects more than 1.5 million people globally (Hartong, Berson, & Dryja, 2006). This disease causes progressive loss of photoreceptors and thus eliminates vision at the initial step of visual processing in the retina. In addition, RP causes degeneration of other neurons in the retina. Approximately 30% retinal ganglion cells (RGCs) survive (Santos et al., 1997; Stone, Barlow, Humayun, de Juan, & Milam, 1992) , which carry visual information to the brain via their axons. If we can make use of these remaining output neurons of the retina, partial vision recovery may become possible.

A retinal prosthesis bypasses the signal processing in the retinal network and starts the artificial vision by way of other retinal neurons. There are several approaches to the design of a retinal prosthesis. Depending on the location of implantation and stimulation strategies, they are named differently, for review see (Dowling, 2005). Among these prostheses, the epiretinal approach targets surviving RGCs and activates them by the implantation of a prosthetic device across the inner surface of the retina. The objective is to directly stimulate the RGCs with electrical current so that they generate spike patterns resembling those normally evoked by light. This approach is particularly attractive owing to the close proximity of the device to the target tissue, which in theory should reduce the threshold for RGC activation. Moreover, it minimizes the undesired modulation of other non-spiking pre-ganglionic neurons in the retina thus preserving the accuracy of the output signal. However, placement of a device on the epiretinal surface poses a number of engineering and physiological challenges.

One of the challenges is the uncertainty regarding the relationship between the position of the stimulating electrode and the physiological thresholds for efficacious electrical stimulation of the target RGCs. This question has received considerable attention, for review see (Sekirnjak et al., 2006). The multi-electrode array (MEA) of the epiretinal implant will normally be surgically attached to the surface of the inner retina, close enough to the RGCs in

order to ensure that the array is firmly attached and far enough away to assure that the RGCs underneath are not damaged. When the MEA, typically encapsulated in a rigid biocompatible package, is implanted on the curved retinal surface in a seamless fashion, some electrodes will just touch the surface of the inner retina while some other electrodes will penetrate through the inner limiting membrane (ILM).

Here, we are interested in the threshold for activating a RGC in two practical stimulating electrode positions, one is at the surface of the inner retina (above ILM) and the other is minimally penetrating into the retina (below ILM). The depth of the penetration was restricted since the pressure of a deeper penetration into the retina means the MEA may cause deformation of the retinal surface and increase the chance of neuronal damage. The restriction is associated with the physical size of the stimulating electrode tip. Once penetrated, the tip will be located in the ganglion cell layer, i.e. below ILM.

4.3 Materials and Methods

4.3.1 Ethical approval

All experimental procedures were approved by the institutional Animal Experimentation Ethics Committee at the Australian National University and were performed in strict compliance with the Australian Code of Practice for the Care and Use of Animals for Scientific Purposes from the Australian National Health and Medical Research Council.

4.3.2 Retinal whole-mount preparation

Whole-cell patch-clamp recordings were made from retinal ganglion cells in isolated whole-mount preparations from four pigmented Long Evans rats (*Rattus norvegicus*) of 11 months of age. Animals were anaesthetized by inhalation of gaseous isoflurane (5% for induction, 3-5% during enucleation) in oxygen. After enucleation rats were killed by intracardiac injection of an overdose of lethabarb (sodium pentobarbitone, 150 mg kg^{-1}).

After enucleation, each eye was hemisected behind the ora serrata and the vitreous body was removed. The resulting eyecup was then dissected into 2 to 4 pieces. The piece of retina for a first experiment was isolated from the sclera; others were stored in the culture storage with continuous perfusion of oxygenated Ames' medium (Sigma-Aldrich, St. Louis, MO USA). The isolated retinal whole-mount was then placed, with ganglion cell layer up, on a cover slip, which formed the bottom of a perfusion chamber (RC-26GLP, Warner Instruments, Hamden, CT USA). Once in the chamber, the tissue was held in place with a stainless steel harp fitted with Lycra threads (Warner Instruments, Hamden, CT USA) and perfused (4-6 mL min^{-1}) with oxygenated Ames' medium at room temperature (~20 ^{o}C) under normal room light condition. The chamber was mounted on the stage of an upright microscope (Olympus BX51WI, Japan) equipped with water immersion lens (20x and 40x). To aid visualization, the tissue was trans-illuminated with infrared light (> 700 nm) and viewed on a monitor with 4x additional magnification.

4.3.3 Whole-cell patch-clamp recordings

Before setting-up a whole-cell recording, we placed the bipolar stimulating electrodes so that a target RGC was positioned approximately halfway between them (Figure 4.1). The target RGC, a putative type-A (A1, A2i or A2o) was recognizable due to its soma size (~ 20 µm in diameter, see Chapter 2, Table 2.2 for details; see also Figure 4.2). Then we made a small hole in the ILM and an optic fiber layer overlaid the target RGC. Very often more than one RGC was exposed. Whole-cell patch clamping was attempted on the target RGC exposed in the opening. Whole-cell current-clamp recordings from retinal ganglion cells were made according to standard procedures (Hamill, Marty, Neher, Sakmann, & Sigworth, 1981) using an intracellular amplifier (BA-1S, NPI, Germany). Initial pipette resistance ranged between 4 and 5 MΩ. The pipette conductance in the bath was compensated with the bridge balance circuit of the amplifier. Once the RGC was patched, intracellular stimulation was carried out to validate the quality of the patch and healthiness of the cell. A small brief positive current (~ 20 pA) was injected to elicit a spike. The membrane potentials and the spike overshoots of the RGC were used to ascertain the health of the spike generating mechanism. A small negative

current (~ -20 pA) to verify that the input resistance of the RGC was within the range of the target type. In this case, we targeted type-A RGCs with input resistance less than the other RGC types, in the range of 98 to 264 MΩ (see Chapter 2, Table 2.2 for details) (Wong, Cloherty, Ibbotson, & O'Brien, 2012).

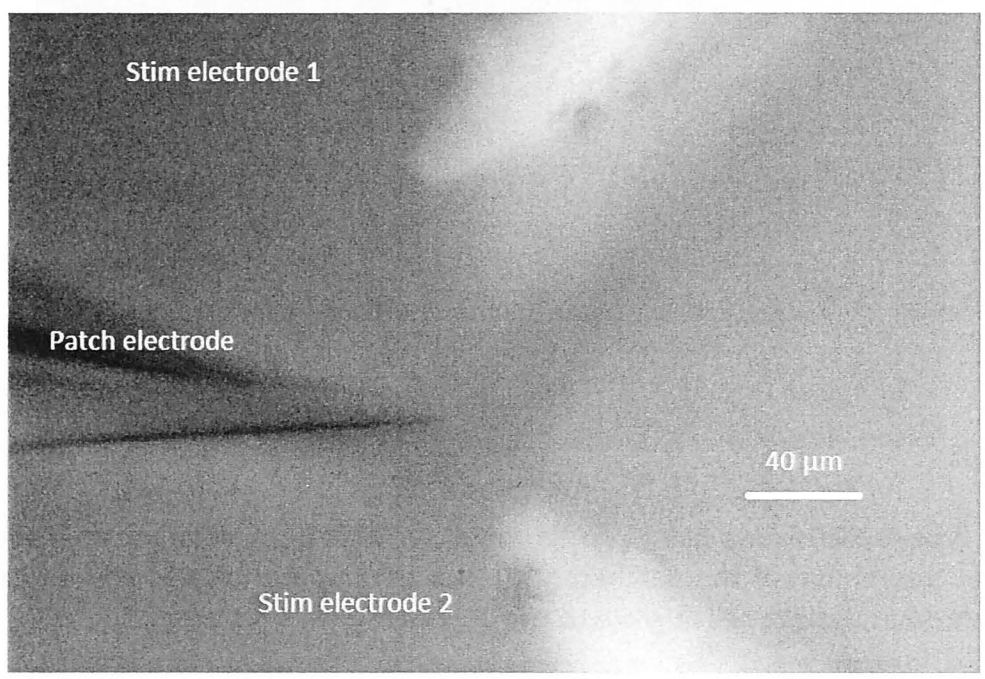

Figure 4.1 A demonstration of the configurations of the three electrodes. The two stimulating electrodes will be placed approximately the same distance away from the target RGC. Then the patch (recording) electrode will make whole-cell patch-clamp to the target RGC. One of the stimulating electrodes will be the reference and the other one will be placed in the 'above ILM' or 'below ILM' position.

Non type-A RGCs or unhealthy cells were rejected. An indicator of unhealthy cells was chromatolysis, where the nucleus of the RGC migrates to the periphery (Watson, 1968). The nucleus was normally observable under the microscope or on the monitor after magnification. Figure 4.2 illustrates visualization of a cell. The outline of the nucleus was difficult to recognize because of the optical sectioning effect of the microscope optics and the limited quality of the camera. In this case the nucleus was considerably larger and it was about half the diameter of the cell-body profile and it appeared as a rather smooth region because the deoxyribonucleic acid (DNA) was in a finely dispersed state, rather than condensed into chromosomes. The nucleus was surrounded by a definitely granular cytoplasm made up of rough endoplasmic reticulum and ribosomes: the protein synthesis machinery. Inside the patched RGC, the small circle near the patch electrode was the nucleolus. This was a condensation of nuclear material

within the nucleus, often eccentrically located within the nucleus itself (Hughes, 1975). The location of the nucleolus also indicated the effect of chromatolysis if there was any.

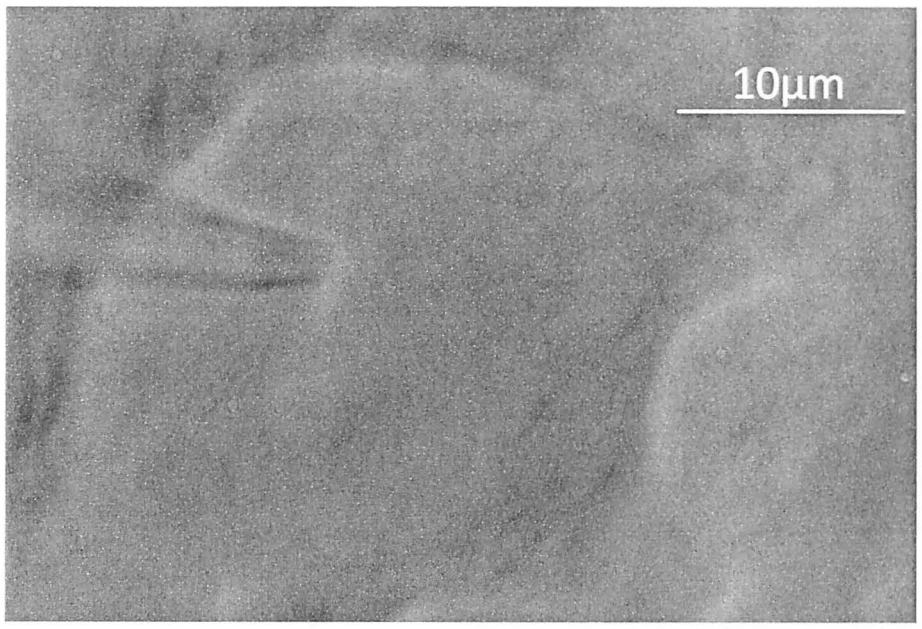

Figure 4.2 A putative type-A RGC being patched. Its soma size was a much larger than the RGCs beside it. The nucleolus (small disc in the middle of the patched RGC) was observable. It was eccentrically located within the nucleus. If there was chromatolysis, it will migrate to the periphery.

The patch pipette internal solution consisted of (in mM): K-gluconate 115, KCl 5, EGTA 5, HEPES 10, ATP-Na 2, GTP-Na 0.25 (mOsm = 282, pH = 7.3) including Alexa Hydrazide 488 (0.25%) and biocytin-HCl (0.25%). Resting potentials were corrected for the change in liquid junction potential after experiments. No capacitance compensation was employed.

4.3.4 Bipolar Electrodes and Electrical Stimuli

Electrical stimuli were delivered by way of a pair of iridium electrodes (MicroProbes for Life Science, Gaithersburg, MD USA) fabricated from 125 µm diameter wire insulated with Parylene-C. The electrode was tapered (25:1) to a tip diameter of 5 µm and the insulation removed to expose 20 µm at the tip (Figure 4.3). The bipolar iridium electrodes with a 5 um tip are readily available in the market and made of a well-known recording electrode material. The small tip size allows easier penetration into the ILM with minimal damage to the retinal. The bipolar configuration was adopted with a view to using the minimum amount of current to

activate neurons. We tested the impedance of each bipolar electrode pair by sending a test current pulse with known amplitude (typically 1 mA) while the pair is totally immersed in saline (1 M NaCl), and measured the resulting voltage from the oscilloscope. Then, we used Ohm's law (Impedance = Voltage / Current) to calculate the impedance. Resulting electrode impedances ranged from 200-300 kΩ at 1 kHz. The two electrodes forming the bipolar pair were typically placed approximately 150 µm apart as shown in Figure 4.1.

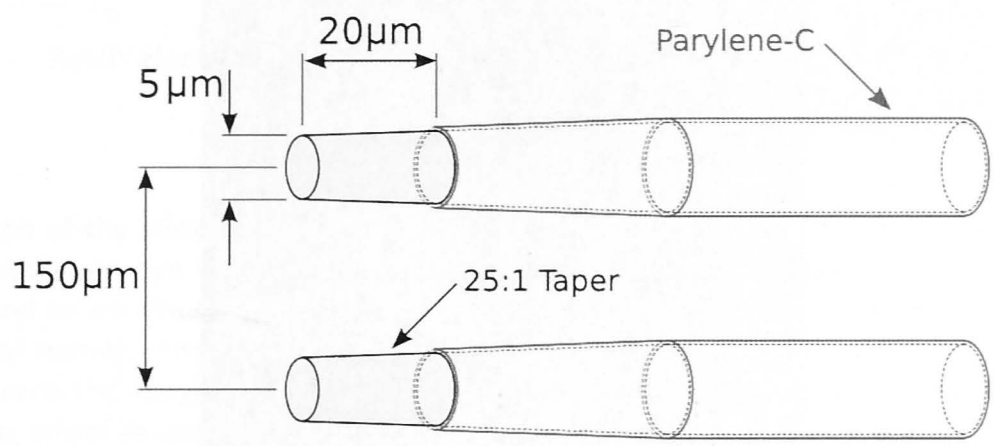

Figure 4.3 Schematic diagram showing the tip profile of the iridium stimulating electrodes (the exposed tips are shown shaded in gray).

Before obtaining a whole-cell patch recording, the stimulating electrodes were positioned by way of a micromanipulator (MP-325, Sutter Instruments, Novato, CA USA) such that the tips and the target cell's soma were approximately collinear. The target cell soma was centred between the tips of the two stimulating electrodes (Figure 4.1). One electrode served as the reference electrode. The other electrode was placed either above the inner retina (above ILM) or penetrated through the ILM (below ILM). The coordinates shown on the micromanipulator monitored the depth of the penetration. The penetrating electrode was set on the holder controlled by the micromanipulator with an angle of 30 degree. Since the ILM is elastic, the penetrating electrode was pushed 'hard' into the inner retinal surface until punctured through the ILM. After penetration, the electrode was retracted to relieve the strain (Figure 4.4).

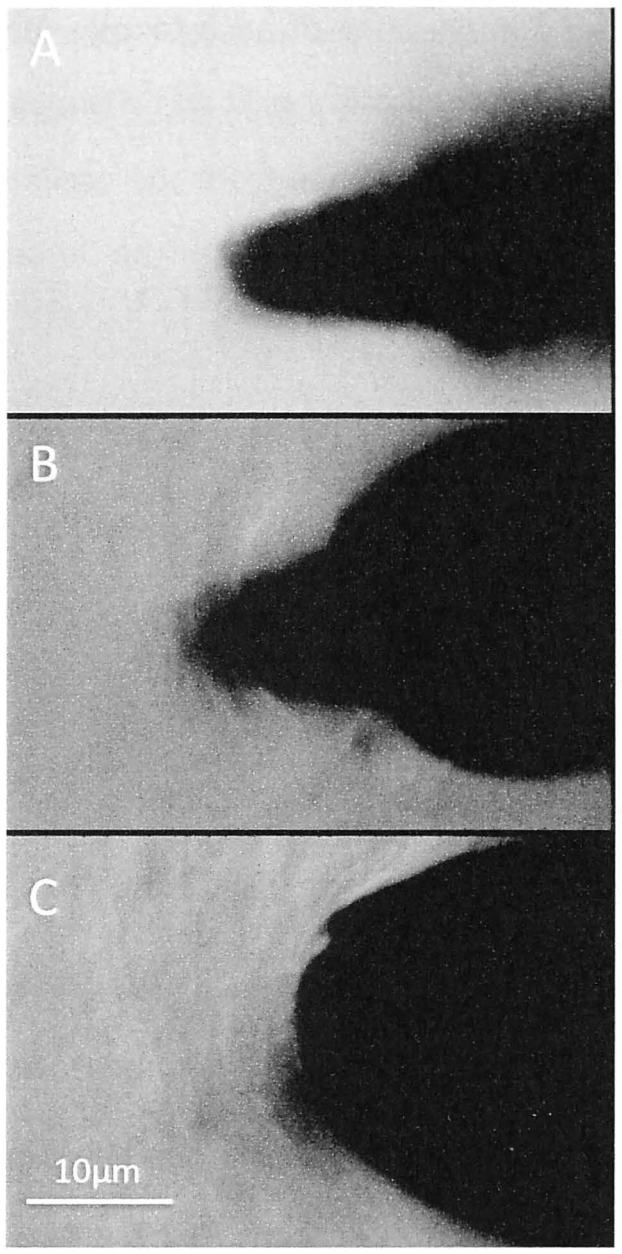

Figure 4.4 Different positions of the stimulating electrode at the inner retinal surface. **A**) At the surface. **B**) Penetrating into the surface. The 'arcs' formed at the retinal surface shows the elastic membrane is under pressure. **C**) Penetrated into the surface, and retracted to relieve strain.

Electrical stimuli consisted of single biphasic charge-balanced current pulses (200 µs per phase) of varying amplitude (2-200 µA). There was no inter-phase interval. The cathodic pulse was sent first, followed by the anodic pulse with the same amplitude. Each stimulus was repeated at least 10 times with an inter-stimulus interval of 3 seconds or more. The current range covered the dynamic range (0-100% efficacy) of spike activation. The biphasic pulses were used to ensure that the net charge was zero in order to avoid from causing any possible damage to the retina by irreversible electrochemical reaction. The RGC were automatically filled with florescence dye (Alexa 488 hydrazide) by diffusion from the recording pipette during the experiment. This enabled the morphology (cell body, dendritic tree and axon) of the RGCs to be recognized and recorded (Figure 4.5) during the live experiment.

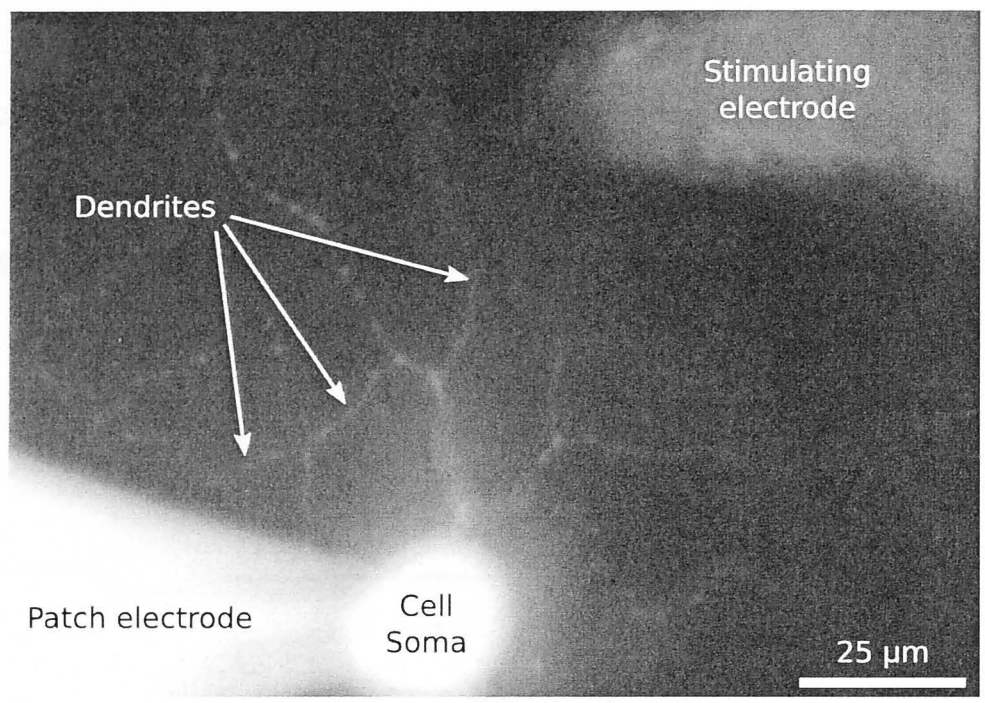

Figure 4.5 Photograph of the stimulating and recording configuration. Here the patch electrode internal solution contains Alexa488 hydrazide dye to enable visualization of the cell morphology. The cell soma is clearly visible (bottom of frame), and so are a number of dendrites (centre of frame). One of the two stimulating electrodes is also visible (upper right of frame). The other stimulating electrode lies out of frame, a similar distance below the cell soma. For this exposure, the imaging optics was focused on the dendrites, blurring the cell soma, patch pipette and stimulating electrode, which lie closer to the objective, such that they appear overly large.

4.3.5 Data Acquisition and Analysis

Both the stimulation time and RGC membrane potential time-course were recorded with a custom-developed application in a commercially available LabVIEW system (NI USB-6221, National Instruments, Austin, TX USA). The signals were sampled at 20 kHz with 16-bit precision and stored for off-line analysis.

The efficacy (***E***) of each stimulus was quantified as the percentage of trials on which the stimulus elicited action potentials from the recorded cell, i.e.,

$$E = \frac{n_s}{N} \tag{4.1}$$

where n_s is the number of trials in which single action potentials at short latency (~0.5 ms) were elicited from the recorded cell and ***N*** is the total number of trials.

For each cell, the threshold stimulus amplitude was determined by fitting a two-parameter logistic function to the efficacy data (fitted parameters controlled the position and slope of the function at 50% efficacy). We thus defined threshold stimulus amplitude as that stimulus amplitude which elicited action potentials on at least 50% of trials. A parametric bootstrap procedure was used to generate a distribution of thresholds from which 95% confidence intervals were calculated.

4.4 Results

Figure 4.6 shows recordings of membrane potential from a representative cell. Figure 4.6A shows the membrane potential during stimulation with a single biphasic stimulus (42 μA, 200 μs per phase) at t_0 (stimulation start time, t=0). In this recording, the stimulating electrodes were positioned above the ILM, touching the surface of the inner retina. The stimulus artifact at $\boldsymbol{t_0}$ is clearly identifiable. However, this stimulus was sub-threshold, failing to elicit action potentials on any of the 15 trials. Figure 4.6B and 4.6C show comparable recordings of membrane potential from the same cell during stimulation with single biphasic stimuli (200 μs per phase) of different amplitudes (51 μA and 70 μA respectively). As stimulus amplitude was increased, the stimulus elicited action potentials with short latency on an increasing proportion of trials. In addition, a second spike was elicited from a single electrical stimulation. This occurred in 6 out of 15 cells. A potential third spike, in the form of a big bump was observed in two of those cells (data not shown here). The latencies were approximately 350 and 400 ms, respectively. However, with only two cells currently available, no conclusion could be drawn. Thus, this additional revelation was not further elaborated in the thesis.

Figure 4.6D shows the efficacy of the stimulus as a function of stimulus amplitude for the same cell. Filled circles indicate the efficacy of each of the stimulus amplitudes tested. The solid line shows a two parameter logistic function fitted to the data, the coefficient of determination, $R^2 = 0.99$, indicating a good fit. The horizontal bar indicates the 95% confidence interval for the threshold stimulus amplitude. In this case, the current threshold was 53.8 μA.

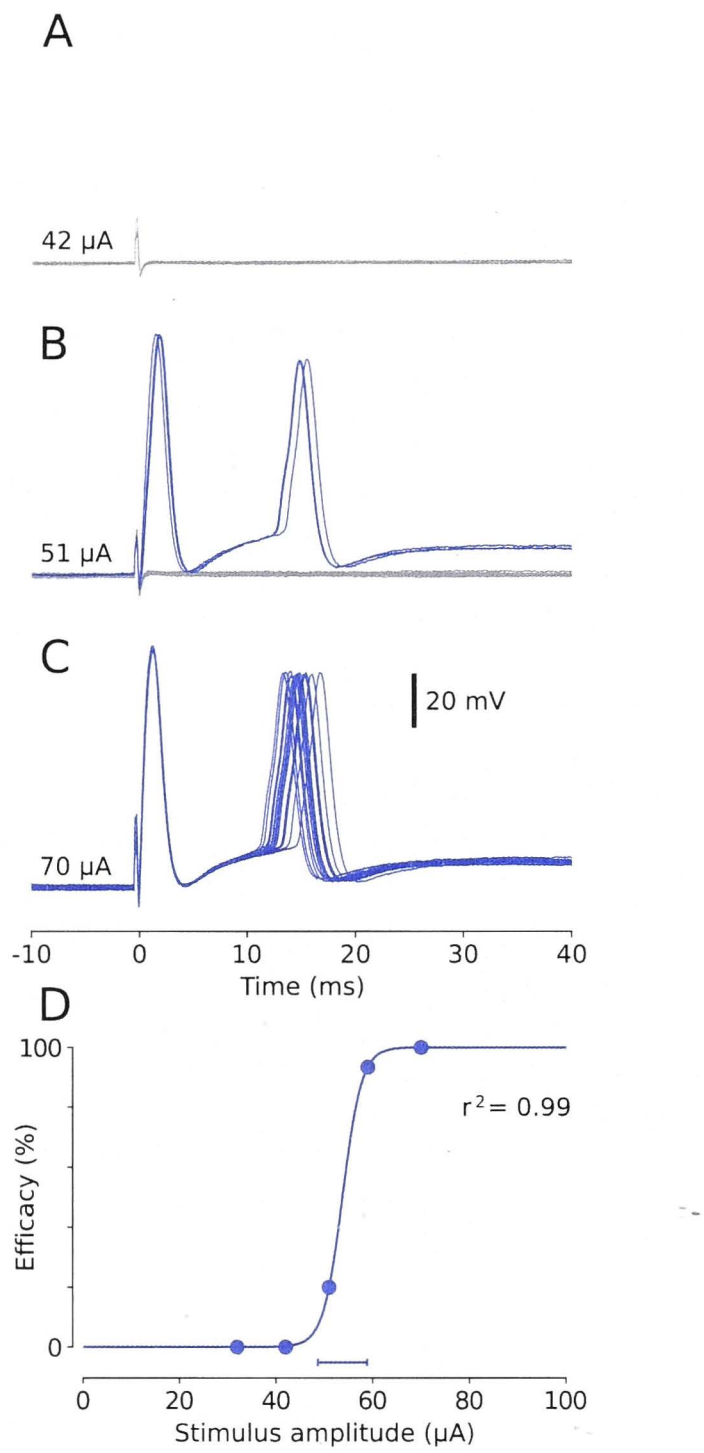

Figure 4.6 Response of a representative cell to biphasic current pulses (200 µA per phase) delivered via a pair of bipolar stimulating electrodes placed above the inner limiting membrane (ILM). **A-C**) Membrane potential for stimulus amplitudes of: 42, 51 and 70 µA (n=15). As stimulus amplitude was increased, the stimulus elicited action potentials with short latency (blue traces) on an increasing proportion of trials. Note that a second spike was observed. **D**) Efficacy of the stimulus as a function of stimulus amplitude for the same cell. Filled circles indicate the efficacy at each of the stimulus amplitudes tested.

We made recordings from 15 putative type-A RGCs (see Discussion). To assess the effect of the ILM on the physiological stimulus thresholds of two electrodes at different positions, the stimulating electrodes were placed above the ILM in eight recordings, while in the remaining seven recordings the stimulating electrodes were penetrated into the ILM. Figure 4.7A shows efficacy curves fitted to the responses of each cell. In all cases, R^2 of the fit

was > 0.96. Blue and red curves indicate placement of the stimulating electrodes above and below the ILM, respectively. Figure 4.7B compares the distribution of threshold stimulus amplitudes across the two groups of cells (i.e., stimulation above versus below the ILM). While the median threshold stimulus amplitude was lower when the stimulating electrodes were placed below the ILM (30 µA vs 56 µA), this difference was not significant across our cell population (Kruskal-Wallis, p = 0.08). Similarly, we found no significant difference between the slopes of the efficacy curves at threshold for the two cell groups (Figure 4.7C; Kruskal-Wallis, p = 0.91).

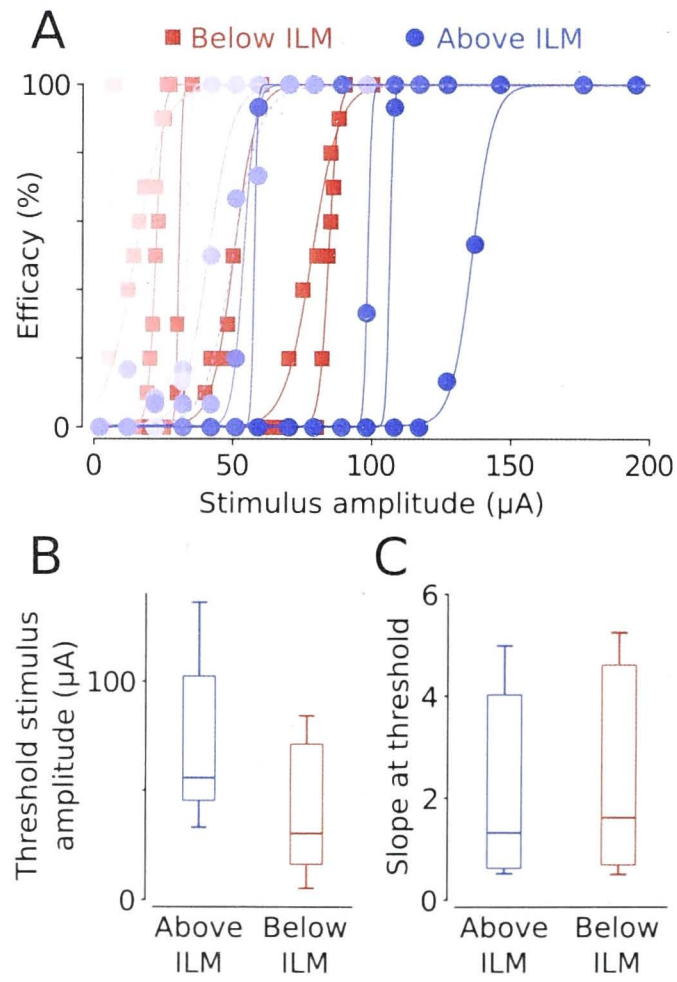

Figure 4.7 Efficacy curves and threshold comparison. **A**) Efficacy curves fitted to the responses of each cell. Blue and red curves indicate cells for which the stimulating electrodes were placed above and below the inner limiting membrane (ILM), respectively. In all cases, R^2 of the fit was > 0.96. **B**) Comparison of the threshold stimulus amplitudes for the two groups of cells – blue (above ILM) versus red (below ILM). Data from individual cells in each group are indicated by different shades of blue or red respectively. The dashed blue line indicates the efficacy curve for the confirmed A2o retinal ganglion cell. **C**) Comparison of the slope of the efficacy curves at threshold for the two cell groups. In B) and C) the horizontal lines indicate the medians of the distributions; the rectangles indicate the 25th and 75th percentiles and the whiskers encapsulate 100% of the data.

4.5 Discussion

The mammalian retina is believed to contain 15-20 different types of RGCs, the dendritic fields of each of them tiles the retina, for review see (Masland, 2001). Each cell type is characterized by its anatomical morphology and its functional properties. While the morphology of many rat RGC types has been described (Huxlin & Goodchild, 1997; Sun, Li, & He, 2002), a comprehensive survey of their intrinsic physiological properties is complete but is limited to 16 morphologically defined types (Wong, et al., 2012) (see also Chapter 2). It is certain that different RGC types in the rat retina exhibit different intrinsic physiological properties and it is therefore likely that they will respond differently to extracellular electrical stimulation and require different stimulation parameters. The one thing that is conserved across different types is the generation of the electrically evoked spikes at the most sensitive zone in a band of densely packed voltage-gated sodium channels located within the proximal axon (Behrend, Ahuja, Humayun, Weiland, & Chowe, 2009; Fried, Lasker, Desai, Eddington, & Rizzo, 2009; Sekirnjak et al., 2008). This band is also known as the axon initial segment (AIS), for review see (Kole et al., 2008). The varied composition of the ion channels in the AIS leads to the diversity of response to electrical stimulation (Fried, et al., 2009).

When making our recordings, we have endeavored to target type-A RGCs. This was achieved primarily based on their larger soma sizes, and then confirmed by their intrinsic properties later. In one of the recordings, we performed three-dimensional confocal reconstruction of the cell's morphology. We confirmed this cell as an A2o RGC according to established morphological criteria (i.e., soma size, spatial extent and stratification of the dendritic arborization in the inner plexiform layer etc.). Despite this, there was an uncomfortably wide range of stimulus thresholds within our cell population. It is plausible that some of this variability may be attributable to unrecognized differences in cell type. Nevertheless, it is important to consider other sources of threshold variation.

One of the critical factors will be the relation between the orientation of the stimulus bipole and the direction of the target RGC's axon. The stimulus bipole determines the electric field, and thus defines the direction of the current that affects the membrane potentials. If the

electric field is transverse to the direction of the axon, the influence will be minimal as the net effect on the membrane potential is close to zero. Membrane potentials will still be altered inefficiently since the electric fields are not absolutely straight. On the other hand, the effect is maximized if the field is longitudinal to the axon. The electrical field along the axon will depolarize the membrane efficiently, and result in a lower stimulation threshold. These differences might explain the wide range of stimulation thresholds as showed in Figure 4.7A. If that is the case, then the choice of the reference electrode in the MEA of the epiretinal prosthesis should closely follow the orientation of the RGC's axon. Apparently, different positions would have implications on the threshold from the results of our preliminary trials. In order to maintain consistency, the reported cells, the stimulating and the reference electrode were always lined up consistently in the same orientation.

4.5.1 Patch-clamp clamp versus other recording techniques

We employed whole-cell patch-clamp recordings to observe activation of RGCs in isolated rat retinas. This technique has the advantage over extracellular recording techniques for providing direct access to the intracellular space of the recorded cell. This in turn facilitates filling of the cell with fluorescent dye and subsequent reconstruction of the cell's morphology and identification of the cell type. The disadvantage is that there may be some loss of cytosolic components of the RGC by diffusion into the pipette. Although it is not the focus of the present study, this technique will in future facilitate a more detailed correlation of efficacious stimulus parameters with the known RGC types. However, patch–clamp recordings are highly selective, yielding information mainly about activation of the recorded cell plus activity of neighboring neurons. The extracellular potentials produced by the activity of the neighboring neurons were much smaller, compared to the intracellular spike, but knowledge of the extracellular potentials generated by closely associated neighbors can be very informative.

4.5.2 Effect of the inner limiting membrane

We investigated the effect of the two different positions, above and below ILM, of the stimulating electrode on the threshold stimulus amplitude required for activation of RGCs in the rat retina. Threshold stimulus amplitudes tended to be lower when stimulating electrodes were placed below as opposed to above the inner limiting membrane. However, with our small sample, the difference was not statistically significant. It remains an open question in the rat model as to whether the stimulating electrode position (above or below the ILM) represents a significant impediment to efficacious activation of RGCs by epiretinal prosthesis.

4.5.3 Two impulses elicited by a single electrical stimulus

The extracellular electrical stimulation is most likely activating a population of RGCs, and possibly neurons other than RGCs, such as the amacrine and bipolar cells. Some of these neurons might inhibit the depolarization of the target RGC. It is therefore likely that absolute threshold stimulus amplitudes derived from patch-clamp recordings do not reveal the stimulus required for activation of the visual pathway. Our thresholds are correspondingly higher than previous estimates obtained using extracellular recordings from large scale microelectrode arrays to characterize activation of rat retina in response to epiretinal electrical stimulation (Sekirnjak, et al., 2006).

Neurons follow the 'All-or-None Law', similar to a nerve or muscle fiber stimulation established by Henry Pickering Bowditch in 1871. The 'All-or-None Law' is a principle describes the relationship between a single, brief stimulus and the response of a neuron: the spike event is a binary function of the strength of the stimulus: either no spike is elicited or a spike of maximum amplitude will be evoked. The amplitude of a generated spike is independent of the intensity of the inducing stimulus.

Several groups had shown that a short duration (~0.1 ms) stimulus elicited a single spike from a RGC (Ahuja, Behrend, Kuroda, Humayun, & Weiland, 2008; Fried, Hsueh, & Werblin, 2006; Sekirnjak, et al., 2006). We observed the same phenomenon in our

experiments except a second spike occasionally (n=6) appeared after the first spike, in a 'Two-or-None' fashion (Figure 4.6 A-C). A similar observation was mentioned previously (Sekirnjak, et al., 2006). Moreover, a third 'spike' (n=2) was seen in the form of a bump. The "reflected" spike was only suggested as a possible explanation for the observations. This opinion was based on the experimental observations and circumstantial evidences presented in Sekirnjak et al. (2006). At this stage our hypothesis is not supported by any data but may be worth investigating further.

As we are measuring the membrane potential with current-clamp technique, a gigaOhm seal was formed followed by the obvious potential 'jump' to the resting potential after 'break-in'. There is no question that the patch electrode was recording the membrane potential of a single RGC. The spike generated has remarkably large amplitude comparing to the neuronal activities picked up by the recording electrode from the surround. In other words, the second spike is not from neurons other than the one we had patched. When a recording is attempted, minimal disturbance was maintained. Any damage to other neural and glial elements in the close vicinity may cause abnormalities, such as plasmalemmal defects in adjacent cells or axons repairing themselves in cytoplasmic continuity. If unrecognized damage occurred, such as two structurally independent elements were 'joined' unexpectedly, then it should be recognizable as the spike waveform would change to an unexpected shape.

The spiking of RGCs under electrical stimulation is a basic property of excitable membranes that should be reasonably consistent across species. Similar electrical stimulation experiments have been done but they didn't report any second spikes (Jensen, Rizzo, Ziv, Grumet, & Wyatt, 2003). We noticed that the results might arise from a different method of tissue preparation. In their experiment, they kept a large portion (~ 1 x 2 cm) of the retina, and the axons of most of the RGC axons studied were preserved to the optic nerve head. By contrast, Sekirnjak et al. (2006) used pieces of retina 1-2 mm in diameter (similar to the size of our preparations). In both cases where a second spike was observed, the unmyelinated intraocular axons of all the RGCs would have been transected. We certainly removed the optic nerve head. In addition, from past experience (Chapter 2), the confocal reconstructed images

confirmed that axons of the RGCs were damaged occasionally. Unfortunately we didn't reconstruct the image of the RGCs in this study.

The spike-interval histograms of spontaneous and the evoked second spikes (Figure 3B of (Sekirnjak, et al., 2006)) showed a close match of particular time intervals for each of the pair. The probability of such matching happening by chance is very low since the intervals in the RGC maintained discharge are normally described as a Gamma process (Kuffler, Fitzhugh, & Barlow, 1957). In other words, the inter-spike intervals are expected to be 'random' instead of 'regular'. The fact that an excess of a particular inter-spike intervals appeared in both the maintained discharged and electrically stimulated spike trains suggested that the second spike was generated by a mechanism that is non-physiological. A possible explanation for the second spike was that an impulse was being regenerated at the cut end of the axon after the first impulse was stalled there. It would then propagate in the antidromic direction (reflected) back to the recorded cell, where it would appear as the second spike. Because conduction velocity is the same in each direction, the interval between the first and second spikes would be twice the conduction time from AIS to the cut end plus a variable extra time for regenerating the second spike at the cut end. This hypothesis is further supported by the observed rapid reduction of second spike appearance at stimulus repetition rates faster than 5 Hz (Figure 7C of (Sekirnjak, et al., 2006)). It is to be expected that fast stimulus repetition would not allow sufficient recovery time at the damaged cut end of the axon to permit the possibility of the second / reflected spike generation.

There are subtle differences between the shapes of the first and the second spikes. In Chapter 3 we had discussed the spike shape revealed the states of the ion channels when a RGC depolarized. The inflected rising phase and modest jitter of the second spike indicate the second spike was not the product of direct electrical stimulation. The evidence indicates that axonal events in the vicinity of the transection are responsible for the observation of the two impulses from a single electrical stimulus. It is possible that the second spike is 'reflected' from the damaged end of the axon. The reflective spike transverses back along the axon in the opposite direction of the original and thus have a different spike shape. A close examination of representative examples of the waveform of the second spike does in fact show a point of

inflection on the rising phase of the spike at about the half-amplitude point. This is in agreement with the generally accepted notion that impulses propagating in the retrograde direction along the axon of an RGC experience a reduced safety factor when invading the soma-dendritic compartment.

4.6 References

Ahuja, A. K., Behrend, M. R., Kuroda, M., Humayun, M. S., & Weiland, J. D. (2008). An in vitro model of a retinal prosthesis. *Ieee Transactions on Biomedical Engineering, 55*(6), 1744-1753. doi: Doi 10.1109/Tbme.2008.919126

Behrend, M. R., Ahuja, A. K., Humayun, M. S., Weiland, J. D., & Chowe, R. H. (2009). Selective labeling of retinal ganglion cells with calcium indicators by retrograde loading in vitro. *Journal of Neuroscience Methods, 179*(2), 166-172. doi: DOI 10.1016/j.jneumeth.2009.01.019

Dowling, J. (2005). Artificial human vision. *Expert Review of Medical Devices, 2*(1), 73-85. doi: Doi 10.1586/17434440.2.1-73

Fried, S. I., Hsueh, H. A., & Werblin, F. S. (2006). A method for generating precise temporal patterns of retinal spiking using prosthetic stimulation. *Journal of Neurophysiology, 95*(2), 970-978. doi: 00849.2005 [pii]10.1152/jn.00849.2005

Fried, S. I., Lasker, A. C. W., Desai, N. J., Eddington, D. K., & Rizzo, J. F. (2009). Axonal Sodium-Channel Bands Shape the Response to Electric Stimulation in Retinal Ganglion Cells. *Journal of Neurophysiology, 101*(4), 1972-1987. doi: DOI 10.1152/jn.91081.2008

Hamill, O. P., Marty, A., Neher, E., Sakmann, B., & Sigworth, F. J. (1981). Improved Patch-Clamp Techniques for High-Resolution Current Recording from Cells and Cell-Free Membrane Patches. *Pflugers Archiv-European Journal of Physiology, 391*(2), 85-100. doi: Doi 10.1007/Bf00656997

Hartong, D. T., Berson, E. L., & Dryja, T. P. (2006). Retinitis pigmentosa. *Lancet, 368*(9549), 1795-1809. doi: Doi 10.1016/S0140-6736(06)69740-7

Hughes, A. (1975). A quantitative analysis of the cat retinal ganglion cell topography. *The Journal of comparative neurology, 163*(1), 107-128. doi: 10.1002/cne.901630107

Huxlin, K. R., & Goodchild, A. K. (1997). Retinal ganglion cells in the albino rat: Revised morphological classification. *Journal of Comparative Neurology, 385*(2), 309-323. doi: Doi 10.1002/(Sici)1096-9861(19970825)385:2<309::Aid-Cne9>3.0.Co;2-5

Jensen, R. J., Rizzo, J. F., 3rd, Ziv, O. R., Grumet, A., & Wyatt, J. (2003). Thresholds for activation of rabbit retinal ganglion cells with an ultrafine, extracellular microelectrode. *Invest Ophthalmol Vis Sci, 44*(8), 3533-3543.

Kole, M. H., Ilschner, S. U., Kampa, B. M., Williams, S. R., Ruben, P. C., & Stuart, G. J. (2008). Action potential generation requires a high sodium channel density in the axon initial segment. [In Vitro Research Support, Non-U.S. Gov't]. *Nature neuroscience, 11*(2), 178-186. doi: 10.1038/nn2040

Kuffler, S. W., Fitzhugh, R., & Barlow, H. B. (1957). Maintained Activity in the Cats Retina in Light and Darkness. *Journal of General Physiology, 40*(5), 683-702. doi: Doi 10.1085/Jgp.40.5.683

Masland, R. H. (2001). The fundamental plan of the retina. *Nature Neuroscience, 4*(9), 877-886.

Santos, A., Humayun, M. S., deJuan, E., Greenberg, R. J., Marsh, M. J., Klock, I. B., & Milam, A. H. (1997). Preservation of the inner retina in retinitis pigmentosa: A morphometric analysis. *Investigative Ophthalmology & Visual Science, 38*(4), 1443-1443.

Sekirnjak, C., Hottowy, P., Sher, A., Dabrowski, W., Litke, A. M., & Chichilnisky, E. J. (2006). Electrical stimulation of mammalian retinal ganglion cells with multielectrode arrays. *Journal of Neurophysiology, 95*(6), 3311-3327. doi: DOI 10.1152/jn.01168.2005

Sekirnjak, C., Hottowy, P., Sher, A., Dabrowski, W., Litke, A. M., & Chichilnisky, E. J. (2008). High-resolution electrical stimulation of primate retina for epiretinal implant design. *Journal of Neuroscience, 28*(17), 4446-4456. doi: Doi 10.1523/Jneurosci.5138-07.2008

Stone, J. L., Barlow, W. E., Humayun, M. S., de Juan, E., Jr., & Milam, A. H. (1992). Morphometric analysis of macular photoreceptors and ganglion cells in retinas with retinitis pigmentosa. *Arch Ophthalmol, 110*(11), 1634-1639.

Sun, W., Li, N., & He, S. (2002). Large-scale morophological survey of rat retinal ganglion cells. *Vis Neurosci, 19*(4), 483-493.

Watson, W. E. (1968). Observations on the nucleolar and total cell body nucleic acid of injured nerve cells. *The Journal of physiology, 196*(3), 655-676.

WHO. (2012). World Health Organization.

Wong, R. C. S., Cloherty, S. L., Ibbotson, M. R., & O'Brien, B. J. (2012). Intrinsic Physiological Properties of Rat Retinal Ganglion Cells with a Comparative Analysis. *Journal of Neurophysiology*. doi: jn.01091.2011 [pii]10.1152 / jn.01091.2011

Chapter 5

Naturalistic Vision Reconstruction in Cat Retinal Ganglion Cells by Electrical Stimulation

5.1 Abstract

People with severe retinal degeneration can still retain about 30% of their retinal ganglion cells (RGCs). Epiretinal prostheses could therefore bypass the signal processing in the retinal network and make use of the surviving RGCs to recreate vision by reconstructing realistic outputs of the RGCs with an implant. The reconstructed outputs would be electrically-evoked responses (ERs) that closely resemble the light-elicited responses (LRs). It is therefore important to know how different types of RGCs respond to electrical stimulation, and if they are capable of reproducing ERs that match real LRs. Whole-cell patch clamp recordings were made from individual cat RGCs *in vitro*, with micro-scale nitrogen doped ultra-nanocrystaline diamond (N-UNCD) electrodes (200 μm x 200 μm) placed at approximately 50 μm from the target RGC for extracellular stimulation. The light stimuli included standing contrasts; moving gratings with various contrasts, spatial and temporal frequencies; and videos of naturalistic scenes as viewed via saccadic eye movements. A train of asymmetric charge-balanced biphasic pulses were then built according to the spike time of the LR for each individual RGC. This impulse train was then used to stimulate the same RGC that produced the LR. The expectation was that the RGC would reproduce an ER with the 'same' pattern, i.e. a pattern that contains the 'same' visual information. We compared the cross-correlation coefficient (r) between the LRs and the ERs to determine how well our reconstructions worked. Our data suggested that, for example in the naturalistic video response reconstruction, the brisk-transient (BT) RGCs (n=17) were more capable of reconstructing the LRs ($r = 0.72 \pm 0.27$), and the brisk-sustained (BS) RGCs (n=16) could not ($r = 0.35 \pm 0.20$). There was statistically significant difference of the following competency between the BT and BS types ($p=0.0001$). The OFF-centre BT RGCs had the best performance ($r = 0.86 \pm 0.21$). These results we mirrored when LPs and ERs obtained to moving gratings were compared. In addition, the BS RGCs were almost completely silenced and suppressed by high frequency electrical stimulation. Furthermore, unexpected firing patterns were observed approximately 5 seconds after high frequency (400 Hz) stimulation.

5.2 Introduction

Retinal degenerative diseases, such as retinitis pigmentosa (RP) and age-related macular degeneration (AMD), cause progressive loss of photoreceptors. The photoreceptors are our input receivers to the visual world, which capture the light entering our eyes and convert it into electrical signals. These electrical signals are processed by the retinal network and output to the brain in the form of action potentials, also known as spikes. Spike trains therefore encode aspects of visual information sent to the higher visual centres in the brain via the axons of the retinal ganglion cells (RGCs). When spikes reach the brain, they are interpreted as a dynamic representation of the external visual scene. Once the photoreceptors are gone, the retina eventually becomes deafferented and vision is lost. Progressive loss of photoreceptors will also trigger remodelling in the retinal network: both changes in neuronal structure and large-scale reorganization (Marc, Jones, Watt, & Strettoi, 2003). Nonetheless, post-mortem morphometric analysis of retina of RP patients has shown that there are retinal neurons surviving (RGCs:29.7%; Bipolar cells and others: 78.4%) even with severe photoreceptors loss (95.1 % gone) (Humayun et al., 1999; Santos et al., 1997; J. L. Stone, Barlow, Humayun, de Juan, & Milam, 1992). Similar results have been obtained in AMD patients: a different degree of retinal degeneration with somewhat greater RGC survival (~70%) (Kim et al., 2002).

The idea of a retinal prosthesis is to help people recover vision from blindness, by making use of the surviving retinal neurons (Humayun et al., 1996; Rizzo & Wyatt, 1997). One approach is to bypass the retinal processing, and directly stimulate the remaining RGCs with a device implanted on the inner retina. If these RGCs are still responsive, it may be feasible to restore vision to a certain degree by activating them with electrical stimulation. Ideally, if the electrically-evoked spike trains match perfectly with the light-elicited spike patterns, vision may be recovered since the brain will receive the 'same' signal inputs.

Substantial effort has been made in order to understand the retinal response under electrical stimulation, for examples see (Cai, Ren, Desai, Rizzo, & Fried, 2011; Margalit & Thoreson, 2006; Sekirnjak et al., 2006; Stett, Barth, Weiss, Haemmerle, & Zrenner, 2000; Ye, Ryu, Kim, & Goo, 2008). Many experiments have shown that RGCs can be excited by

extracellular electrical stimulation by a prosthesis, for examples see (Crapper & Noell, 1963; Fried, Kubow, & Werblin, 2004; Sekirnjak, et al., 2006). However, the heterogeneity of RGCs should not be ignored. The understanding of the cellular response properties of individual RGCs is often limited because electrical stimulation is normally carried out with many restrictions: physiologically by the cell properties and neuronal interactions in the retinal network; and technically by the design of the prosthesis. There are about 20 different types of RGCs in human eyes, each having its own physiological properties and response selectivity (Masland, 2012). The receptive field of each RGC encodes a unique representation of its own small patch of the visual scene. Relatively, little is known about how these individual RGCs respond to electrical stimulation, especially when the retina is simultaneously stimulated at many points with a multi-electrode array (MEA).

It has been shown that a single, short duration stimulus pulse can elicit a single RGC spike (Ahuja, Behrend, Kuroda, Humayun, & Weiland, 2008; Cai, et al., 2011; Fried, Hsueh, & Werblin, 2006; Sekirnjak, et al., 2006). When these single pulses are extended into a pulse train, less consistent results were seen. Fried et al. (2006) showed that a train of pulses (250 pulses per second (PPS)) reliably elicited a train of spikes over a one second period. Similar results were showed by Ahuja et al. (2008) with a 500 PPS spike train (duration not specified). By contrast, Sekirnjak et al. (2006) found that some RGCs couldn't reliably elicit spikes even at 100 PPS. A more systematic study was done by Cai et al. (2011). They showed that brisk-transient (BT) RGCs could reliably follow a spike train up to 600 PPS while other RGC types (directionally selective (DS): ON-DS and ON-OFF DS; local edge detectors; and OFF-deltas) failed to follow at 200 PPS and above. We need to bear in mind however, that these stimuli were applied as a regular train with a fixed inter-pulse period. Therefore, they do not properly imitate how the retinas are 'excited' naturally.

There are three eye movement classes in general: saccades, pursuit movements, and vergence movements, for reviews see (Hoffman & Subramaniam, 1995; Martinez-Conde, Macknik, & Hubel, 2004; Schutz, Braun, & Gegenfurtner, 2011). Saccades rapidly orientate the eye to the focus of interest; pursuit movements track the moving objects in order to keep their images on the central retinal region (human: fovea; cat: area centralis); vergence movements adjust the viewing angle of the eyes so that binocular vision is maintained, including

stereoscopic (depth) vision. During natural saccadic movement of the eyes, that is to say: when the eyes are switching gaze-fixations approximately three times per second and with an ocular rotational speed of up to 400 degree per second (App & Delous, 1998) during each switch, the retinas will receive different visual input at each fixation pause. Furthermore, the rapid global shifts themselves in the retinal image of the natural scene have a significant excitatory and/or inhibitory effect on the spiking of the RGCs as a group (Roska & Werblin, 2003). That study reported that certain RGC types are transiently suppressed during scene shifts, suggesting that the inhibition of RGCs during encoding should not be ignored in the design of the pattern of electrical stimulation.

The objective of the present study was to attempt a replication of the spike train obtained as naturalistic light-elicited responses (LRs), with an electrical stimulus pattern (SP) matching it. To do so, we made a video with an eye tracker device to record a natural scene, together with the relative position of the focus of the eye at the scene, while a human volunteer navigated within the natural environment. The video thus contained the actual input to a substantial patch of the retina for a 14-second period. Then we projected the video onto an isolated cat retina, recorded the RGC spike responses and constructed an electrical pulse train based on the LR pattern. The test for fidelity was to compare the spike timings of the electrically-evoked responses (ERs) and the LRs.

5.3 Materials and Methods

The subtle correlations of the eye movements and the responses of the RGC were not investigated in the present work. In general, saccades refer to rapid eye movements that re-position the retinal centre to the point of interest. The causes of the movements were not examined. The goals of the standing and moving grating tests (see below) were to map the receptive field and identify the RGC types at this point. The light stimuli were used to decide if the recorded RGC was an ON-cell (ON-centre-OFF-surround) or an OFF-cell (OFF-centre-ON-surround), by forming a quick map of the receptive field centre. Only the receptive field centre component was mapped because that is known to 'match' to the dendritic tree size and shape (Peichl & Wassle, 1983). The sole purpose of this study is about the reproduction of the LRs of

the RGCs when electrical stimulus trains are used. Due to limited resources, adjustments were made during the experiment period. Therefore, the protocols are not exactly the same for all RGC recordings (see Section 5.3.3).

5.3.1 Ethical approval

Methods conformed to the policies of the National Health and Medical Research Council of Australia (NHMRC), and were approved by the Animal Experimentation Ethics Committee of the University of Melbourne.

5.3.2 Naturalistic scene video preparation

The videos containing the naturalistic scenes were acquired with an eye tracker at 50 frames per second (SMI iView XHED, Germany). A subject was asked to wear the eye tracker and voluntarily kept his head stable without using any head-fixation equipment (chin rest, forehead pad etc.), while looking at a natural scene. The eye tracker recorded the direction coordinates of the primary line of sight of the subject's right eye during saccadic movements to the scene captured by the head-fixed camera on the eye tracker. The eye actually rotates around a centre of rotation approximately at the centre of curvature of the posterior segment of the eyeball. *Therefore*, the coordinates of that point *do not significantly change* during a rotation. In principle, the eye tracker output should report the *direction cosines of the vector* that coincides with the primary line of sight of the eye, namely: the vector originating at the fovea and passing out through the centre of rotation of the eye and centre of the pupil. A convenient reference frame is a head-fixed set of coordinates with the origin corresponding to the centre of rotation of the eye. The direction cosines are calculated from images captured by a *head-fixed camera* showing displacements of features at the front of the eye (e.g. outline of pupil or outline of cornea) that move as the eye rotates. The videos were then modified by extracting a portion from the full scene around the *current eye direction* vector on every frame (i.e. the small patch of the scene to which the right eye was directed). This portion corresponds to a landscape orientated image (aspect ratio 4:3), 18.6° (width) by 13.9° (high)

when projected onto the retina. If the coordinates led to a portion that was out of range, the frame was skipped. The dropping of frames did not cause any noticeable visual effects. We made three videos:

video-1 was taken when the subject was looking at the faces of three people from approximately two meters away;

video-2 was recorded when the subject was listening and looking at a person talking at a close distance (face to face);

video-3 was made when the subject was asked to sit down and look at some distant trees outside a window.

The first two videos (video-1 and video-2) were used for the first 8 experiments and the rest of the experiments (n=25) were done with video-3. The durations of the videos, from the first to the third, were 8 seconds, 14 seconds and 14 seconds respectively. The video production was done using Matlab (The Mathworks, 2012a and 2012b, USA). The full viewed static scene of video-3 with the saccadic traces and example snapshots of the extracted portions are shown in Figure 5.1.

Previous surveys conducted by Bionic Visual Australia suggested that most blind patients want to see the faces of their loved ones. Therefore videos-1 and -2 were made to see faces; video-1 seeing faces of 3 people from distance and video-2 seeing face during a personal conversation. We found that eye movements under both videos would probably be affected heavily (along with head movement), as between-people interactions were involved. Therefore we made video-3, which simply involved looking at trees from a window. While we did not go into details about the different effects arising from these three different visual scenes, we primarily looked at the possibility of replicating the light response patterns of the RGCs by electrical stimulation.

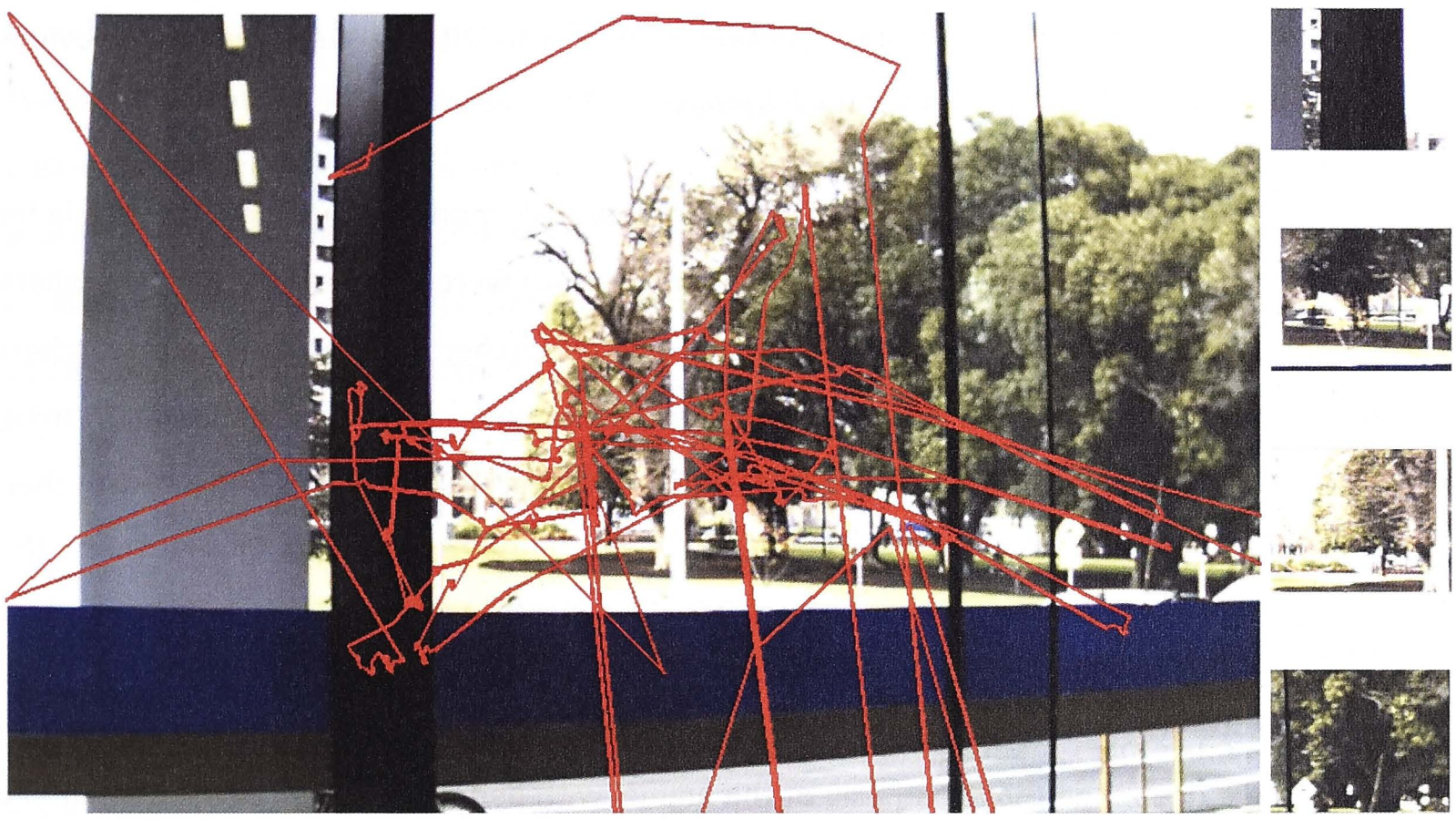

Figure 5.1 Traces of saccades of the subject's eye on a natural scene. This scene was from video-3. The subject looked out from a window and kept his head stable while looking at the trees outside. Left: The eye tracker recorded the directional coordinates of the subject's primary line of sight. These traces are plotted in the figure in red. Right: examples of snapshots at several locations from the modified video that was projected onto the retina centred on the location of the RGC recording.

5.3.3 Retinal whole-mount preparation

Experiments were performed on retinas of 27 cats, average weight 2.9 kg, and ranging in age from 4 to 24 months. Data came from animals that were classified into two groups according to the sources that provided the animals: Group-A animals were prepared in other labs and Group-B animals were prepared in-house. Group-A animals (11 out of 27) were cats obtained after cortical experiments in other labs (Bionic Vision Australia (2), Visual and Cognitive Neuroscience Laboratory (1), Bionic Ear Institute (5), and The National Vision Research Institute of Australia, NVRI (3)). The retinas of 6 (out of 11) cats in Group-A had robust light responses. Group-B animals were cats obtained particularly for this experiment (16 out of 27), which were donated or purchased from other institutes (ANU (5), CSL biotherapies (2), University of New South Wales (9)). The retinas of 9 (out of 16) cats in Group-B had robust light response. A total of 33 light responsive RGCs were recorded from Group-A (9) and Group-B (24). The retinas with no robust light response were used for other electrical

stimulation experiments that are not reported in this thesis. There were no other obvious differences between Group-A and Group-B retinas.

The animals in Group-A had been under continuously monitored general anesthesia for between 1 to 5 days for cortical recording. The enucleations were completed at the labs where anaesthesia was done according to the corresponding researchers' protocols. The researchers called us about an hour before they finished their experiments. After enucleation (~ 15 min), the animals were euthanased immediately by the researchers in accordance with their approved protocols.

Before enucleations, we checked the eye blink reflex, pedal withdrawal and respiration rate to ensure the cats were still under stable anaesthesia. If there were any trace of responses, we deepened the anesthesia of the animal with pentobarbitone (20 mg kg^{-1}) until a deep surgical stage of anesthesia was reached.

After enucleation, the eyeballs were immersed into incubation-Ames solution: Ames' medium, 8.8 g L^{-1}, Sigma-Aldrich), 23 mM $NaHCO_3$ (Sigma-Aldrich), 10 mM D-Glucose (Sigma-Aldrich), 1% Pen-strep Glutamine (GIBCO), 1% N2 supplement (GIBCO), 1% horse serum (Sigma-Aldrich), 0.1% phenol-red (Sigma-Aldrich) and bubbled with carbogen (95% O_2 and 5% CO_2). The incubation-Ames wash cleaned up the surface of the eyeball and the antibiotic components protected against bacterial infection. Then the eyes were hemisected behind the ora serrata. The vitreous body was removed with a pair of No. 5 tweezers. One tweezer held the optic nerve head at the back of the eyecup and the other one gripped the vitreous body and gradually peeled it away from its regional attachments at the ora serrata and optic nerve head. The dissected eyes were put into HEPES-Ames solution: Ames' medium (8.8 g L^{-1}, Sigma-Aldrich), 10 mM HEPES (Sigma-Aldrich), 5 mM NaCl (Sigma-Aldrich), 10 mM D-Glucose (Sigma-Aldrich), bubbled with oxygen. The HEPES-Ames solution provided nutrient supplies with a buffered pH ~7.2 to the dissected eyes. The bottle containing the dissected eyes was placed into a polystyrene box and transferred back to the NVRI laboratory. The transportation time was about 15 min.

Group-B animals were anesthetized at the NVRI lab with a mixture of Ketamine (20 mg kg^{-1}) and Xylazine (1 mg kg^{-1}). Pentobarbitone (20 mg kg^{-1}) were used for the last 9 animals

from UNSW after the initial anesthetization with Ketamine and Xylazine, due to a change of the anaesthetic protocol for the purpose of extending the anaesthesia time for another experiment post-enucleation (with ethics approval from the University of Melbourne). The dissection procedures were similar as described above except no HEPES-Ames was used. After enucleation, animals were euthanized with an overdose of Lethabarb (pentobarbital sodium 150 mg kg^{-1}) intracardiac injection.

The dissected eyes (from Group-A after transportation, and from Group-B dissected on site) were placed into Ames solution (pH = ~7.2, room temperature ~20°C) equilibrated with carbogen under dim room light. We cut a piece containing the area centralis (one sector from each eye, the apical angle of the sector was approximately 60°). Then the sclera was removed from each piece. The retinal piece remained attached to the pigment epithelium and choroid. It was mounted onto a cover slip with the RGC side up. The slip with the retina on it formed the bottom of a perfusion chamber (RC-26GLP, Warner Instruments, Hamden, CT). The retinal piece was held in place with a stainless steel harp fitted with Lycra threads spaced at 1 mm intervals (Warner Instruments SHD-25GH, USA).

With the retinal piece now stably mounted, the chamber was placed on the stage of an upright microscope (Olympus BX51WI, Japan). It was continuously superfused with Ames solution at 9 to 11 ml per minute, equilibrated with carbogen and kept under dim red illumination at 34 ± 0.5 °C. The reservoir of Ames solution was maintained in a water bath (Stuart SWBD) at about 34 °C and a dual automatic temperature controller (Warner Instrument TC-344B, USA) was used to regulate the final temperature at the inlet of the chamber. Before use, the various solutions (incubation-Ames, HEPES-Ames and superfuse-Ames) had their pH checked (~7.2) with a digital pH meter and were filtered (Millipore Stericup, pore size 0.22 micron) but not chilled (see Discussion).

Normally the retinal piece was held in the chamber for about 12-16 hours. The longest period was about 30 hours and the RGCs still had robust light responses. In the first few experiments, each patched RGC was kept for about 4 hours (for multiple protocols) and still maintained robust light and electrical responses. Later, the experimental protocols were reduced to those described in this chapter and each successful recording took approximately 2

hours. Adjustments were made during the experiment period. The main adjustment was made to the anesthesia protocol. The initial protocol was set to inject the drug (Ketamine and Xylazine) in the thigh to anesthetize the cat and terminate the cat immediately after enucleation (both eyes within ~15 min). Subsequently, we changed the protocol (with ethics approval) concerning the drug composition (Ketamine, Xylazine, and Pentobabitone) in order to extend the anesthetization period so that the cat was kept alive after the removal of one eye pending another student removing the other eye 12 hours later. It turned out it didn't work and thereafter we changed the protocol to inject the drug (Ketamine, Xylazine and Pentobabitone) at the neck (following a protocol from the Bionics Institute), and terminated the cat right after enucleation. Some minor changes were also made, such as to use different equipment for surgery and minor re-adjusting the lab equipment before every experiment. No obvious impact on the results was found caused by the changes. Data from patched RGCs that did not fit any of the classification criteria, or did not meet the recording standards, or failed to complete the protocols (see below for detailed descriptions) were discarded from this analysis. The successful rate was very low, only about 1 full recording out of 8 attempts due to various reasons (see Discussion).

5.3.4 Light and electrical stimulation preparation

Static and moving contrast visual stimuli were generated with Vision Egg (Straw, 2008) installed in a desktop computer (Dell Pentium Dual Core E6500@2.93 GHz, with 3GB RAM, Window XP SP3; Video Card: NVIDIA GeForce GT 220 with 1 GB RAM). Vision Egg allows the adjustments of size, contrast, temporal frequency and spatial frequency of the stimuli. The stimuli were transferred from the computer to a monochrome organic light-emitting diode (OLED) projector (e-Magin EMA 100301-01, white luminance maximum ~ 140 cd/m^2. The OLED projector was mounted onto the microscope's video port. The projection system had to conform to the configuration of the microscope. The light stimuli went through a mirror unit within, were magnified by the objective lens (typically 10x during experiment, see below for details), and projected onto the retina mounted in a chamber on the fixed stage. The actual intensity of the projected light was not measured.

A photodiode (Vishay BPW34, Australia: Dark current 2 nA, Wavelength 900 nm, Rise Time 0.05 μs) was attached to a display monitor presenting a copy of the stimuli to the experimenter. For standing contrast and moving grating recordings (see below), the photodiode was attached at the centre of the mapped receptive field. The voltage of the photodiode was recorded and normalized to represent the time course of the light. For the video response recordings (see below), the photodiode was placed at the corner of the monitor. The frame of the VLC media player changed the frame colour when the movie started, and the photodiode detects this change. The time at the transient change of the photodiode voltage was recorded as the video stimulus start time.

Electrical stimuli (current pulses, see below) were produced with an electrical stimulator (Multichannel Systems STG4004-1.6mA, Germany) operated with its associated software (Multichannel Systems MC_Stimulus II, Germany). Custom made programs, LabVIEW (National Instruments, 2010 and 2011, USA) and Matlab (The Mathworks, 2012a, USA), were used to convert the spike times into a multichannel system input file format. The output current pulses were sent out from the channel (channel-1) that was connected to the stimulating electrode. The output from the stimulator was monitored by the channel (channel-4) synchronized with channel-1, which output the same train of current pulses. A resistor (10 kΩ) was connected to channel-4 and the voltage across the resistor was recorded with a LabVIEW device (National Instruments, NI USB-6221, USA) digitized at 40 kHz. This extra recording channel provided a visible indication of the stimuli, and recorded the actual time of every biphasic pulse (see section 5.3.5). There was a delay (5 μs) for every biphasic pulse generated. This error is cumulative. Therefore the actual time of the biphasic pulse generated was not exactly the same as the expected LR spike on which it was based, over the duration of the stimulation (15 seconds) the total error was on the order of milliseconds (maximum error = 2.4 ms, 471 spikes).

5.3.5 The stimulating electrode and biphasic pulse

The reference electrode was handmade by melting silver wire into a small sphere and coating it with chloride. The stimulating electrodes used were microscale nitrogen doped

ultra-nanocrystaline diamond (N-UNCD) electrodes (200 μm x 200 μm) developed by Garrett et al. (Hadjinicolaou et al., 2012). On the experiment day, the impedance of the stimulating electrode was tested before use in order to ensure the impedance was within the recommended range (8 to 10 kΩ). A test symmetric charge balanced biphasic current pulse (typically 1 mA, phase duration 100 μs, interphase interval (IPI) 40 μs) was sent from the stimulator while the N-UNCD electrode and the reference electrode were immersed into the saline solution (~1M NaCl). The output voltage was measured with an oscilloscope. The impedance was calculated by Ohm's law (Impedance = Voltage / Current).

The electrical stimulation patterns were composed of asymmetric charge-balanced biphasic pulses (simply referred to as biphasic pulses). A single biphasic pulse consisted of opposite-polarity rectangular phases (pulses) separated by a short interphase interval (IPI) of zero current. A cathodic phase came first, followed by an anodic phase. The respective current-duration products (i.e. charge) were set up so that the net charge over the whole biphasic pulse was zero. The duration of the phases and the IPI were fixed to 100 μs (cathodic), 40 μs (IPI), and 400 μs (anodic) respectively (Figure 5.2). Thus, the magnitudes of the cathodic and anodic phases were always in a 4:1 ratio. For example, if the current amplitude delivered in the cathodic phase was -400 μA, then the amplitude of the anodic phase will be +100 μA. These parameters are similar to the one shown in Shawn K. Kelly's masters thesis, which revealed the largest cortical response among the four possible waveform shapes (varying polarity and sequence) (Kelly, 1998). A few preliminary trials (not reported) showed that the present asymmetric arrangement reduced the threshold relative to symmetric biphasic pulses, but a thorough study has not yet been completed. The maximum deliverable current amplitude for the cathodic phase was set to 1 mA. The surface area of the electrode is $4x10^{-4}$ cm^2. The maximum charge injection capacity converges to a value around 250 μC cm^{-2} at the maximum deliverable current. These values were chosen carefully so that the electrode surface voltage will not exceed 1 V. This is below the voltage (1.3 V) at which water begins to be electrolysed.

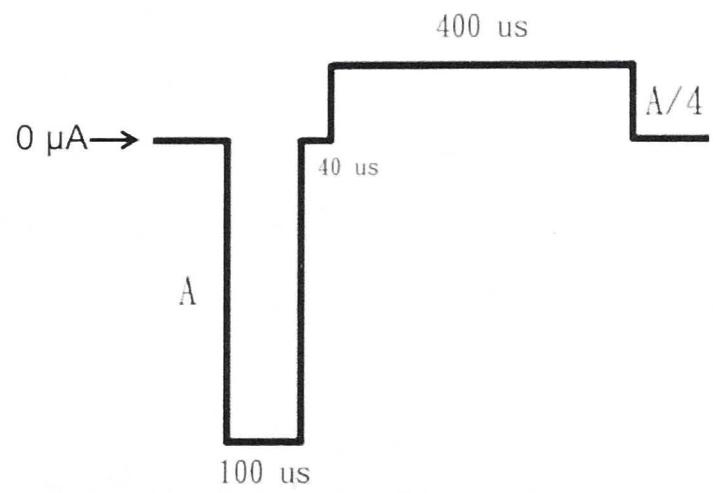

Figure 5.2 An asymmetric charge-balanced biphasic pulse. The durations are fixed: cathodic pulse (100 μs), inter-phase interval (40 μs), and anodic pulse (400 μs). The magnitudes of the cathodic (A) and the anodic (A/4) currents are always in 4:1 ratio.

5.3.6 Electrophysiology data collection

The microscope was equipped with 40x and 10x water immersion lenses (Olympus, Japan). Once the chamber was on the stage, 20 μl acridine orange (1 mM) was added drop-by-drop at the inlet of the chamber to assist visualization. Acridine orange is a non-toxic fluorescent dye that stains the RGC bodies and renders the RGCs visually recognizable (Jensen, 1991). Under the 10x lens, the area centralis was readily located since the region was densely packed with acridine orange-stained somata of RGCs. These stained RGCs were fluoresced green under the mercury exciting lamp (Olympus U-RFL-T, Japan) and were very easily noticed. The acridine orange stain faded away within a few minutes. All data were acquired from the RGCs located within the area centralis and approximately 5 mm distal (away from the optic disc, ~22°; 1 mm = ~4.4° (Bishop, Vakkur, & Kozak, 1962)) from it. Exact locations of the recorded RGCs were not recorded.

The patching procedure was done under the 40x lens. A small hole was made in the inner limiting membrane, by carefully pricking the inner retinal surface with the tip of the electrode. When the tip hooked the surface, the electrode was moved upwards (away from the surface) and sideways until the surface was torn gently and slowly (similar procedures as described in the previous chapters). The target RGC was exposed in the resultant small hole for whole-cell patch clamp recording (Robinson & Chalupa, 1997; Taylor & Wassle, 1995). Typically a few other RGCs were disclosed but the target was the RGC with the biggest soma

among the exposed RGCs. After the target RGC was located, the stimulating electrode was placed ~ 50 µm proximal to it. The reference electrode was also placed as close to the target RGC as possible but on the opposite side. The placement of the electrodes affects the RGC activation threshold (for details see Chapter 4). The closer the reference electrode was placed to the target RGC, the smaller the stimulus artefact.

The RGC membrane potentials were recording using an intracellular bridge mode amplifier (NPI BA-1S, Germany) and data were acquired with a LabVIEW device and the custom made LabVIEW programs. The data acquisition setup was similar to the previous chapters except more channels were involved, including connections to the stimulator. The light stimuli were generated by a separate computer that was connected to the OLED projector.

Acridine orange stained RGCs with soma diameters over 20 µm were identified with the aid of a scale bar marked on the monitor. Whole-cell current clamp recordings from RGCs were obtained with standard procedures (Hamill, Marty, Neher, Sakmann, & Sigworth, 1981). Initial pipette resistance ranged between 3 and 7 MΩ. The pipette voltage in the bath was nulled prior to recording. It was also checked immediately at the end of each recording after clearing the pipette tip with a pulse of pressure. If bath potentials before and after recording differed, the latter was taken as the reference potential. The pipette series resistance was measured and compensated with the bridge balance circuit of the amplifier. Resting potentials were corrected for the change in liquid junction potential that occurs upon obtaining a gigaseal and break-in. Diffusional exchange between cytoplasm and pipette contents (liquid junction potential was measured directly as -5 mV (Neher, 1992)). No capacitance compensation was employed. Occasionally negative current was applied to maintain the baseline membrane potential in the range -60 to -70 mV.

The membrane potential was amplified and digitized with 16-bit precision at 40 kHz (National Instruments USB-6221, USA) and stored in digital form. The data collected were analysed off-line with Matlab. At the beginning of the experiment, RGCs were excluded if they exhibited marked instability of resting potential, or if their action potentials did not overshoot 0 mV.

RGC classifications were done along with the electrophysiology data collection using a set of tests. According to the soma sizes, the selected RGCs were either alpha or beta RGCs (Figure 5.3), for review see (Boycott & Wassle, 1974; J. Stone & Clarke, 1980). Further classifications were confirmed by the following procedures.

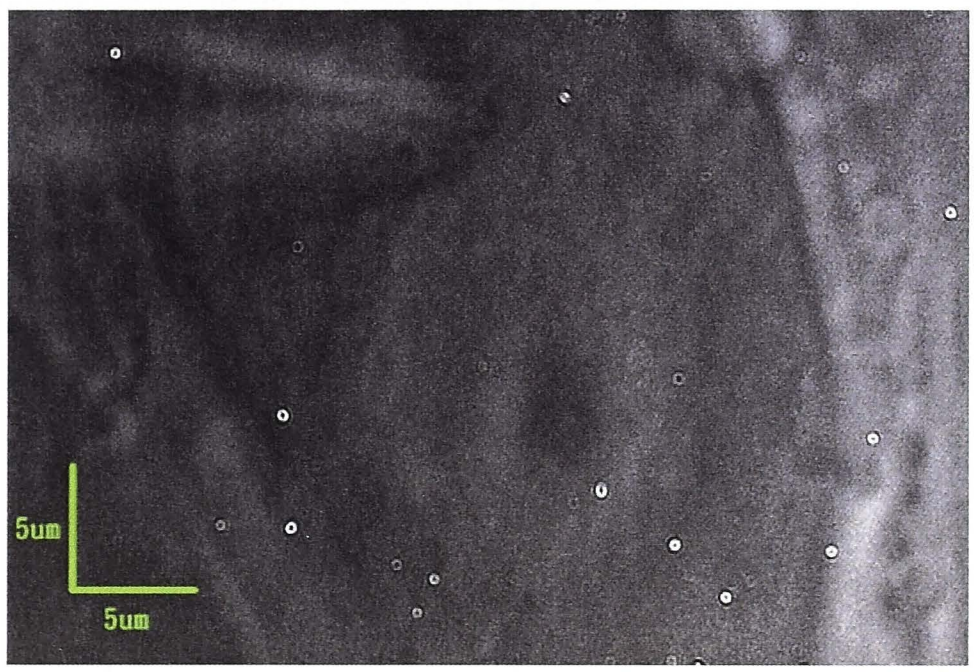

Figure 5.3 A putative alpha RGC. Example of a RGC for an experiment with an estimated average soma diameter larger than 20 μm. It should be either an alpha or a beta cell. The cell type can be verified by evaluation of the intrinsic properties, and the receptive field properties, of the cell.

5.3.7 Recordings

The responses from the amplifier were displayed on the monitor and oscilloscope, and also connected to an audio speaker. There are three types of recordings associated with three different kinds of stimuli: intracellular electrical stimuli, light stimuli, and extracellular stimuli. The duration of each recording was 15 seconds. The recordings were repeated at least 10 times with a recovery period between the repetitions (1 min to 5 min) and different types of recordings (5 min to 15 min). Spike height and shape is strongly influenced by the amount of maintained discharge at the instant of the measurement and in the recent past history of discharge. After the RGC was patched, we switched to the 10x lens and focused onto the photoreceptors (see Discussion). We closed the curtain around the experimental setup to keep the inside in darkness. We allowed approximately 10 min dark adaptation before the recordings began.

5.3.7.1 Intracellular stimulation

Each patched RGC was injected with depolarizing and hyperpolarizing current steps at several strengths (similar procedures as described in Chapter 2). Depolarizing steps led to spike generation for strengths above a definite threshold level. The spike width at half height of the spike was extracted and compared to the values listed in Table 1 of O'Brien et al. (2002). The former values were measured at room temperature instead of physiological temperature; nevertheless, they gave us insight into the expected values. The full spike width at half height of alpha and beta cells are distinguishable (< 0.9 ms) from the rest of the listed RGC types (> 1.3 ms). Furthermore, the input resistance of alpha cells is about 8 times less than that of beta cells. The combination of these two intrinsic properties provided a preliminarily differentiation of alpha and beta cells from other types of RGCs.

5.3.7.2 Light responses

A small circular spot (~ 1^{o} in diameter; generated with 'Vision Egg', Straw (2008)) was used to map the receptive field of the patched RGC. For ON-RGCs, we used a white spot presented on a dark background (100% contrast) and for OFF-RGCs we used a dark spot with a uniform grey background instead (50% contrast). Thus the adaptation state of the retina was quite different for ON-cells and OFF-cells, it would have been more suitable to use a uniform grey background for both cell types. However, since the goal was to map the receptive field centre quickly, we used 100% contrast to get a robust visual/audio response from ON-cells. It seemed that the OFF-cells were relatively more robust. That is, the responses of the ON-cells were 'dull' at low contrasts, especially when there were many spontaneous spikes. Cells with ON-OFF responses were omitted (n=2).

5.3.7.3 Standing contrast

The receptive fields were not perfectly circular in shape. After the full receptive field was mapped, the spot was enlarged to approximately the size of the centre of the receptive

field mapped. The spot was turned on and off, wherein off being the background state. We recorded the responses of the RGCs to the resulting change of contrast (Figure 5.4).

Figure 5.4 An OFF RGC recording under the standing (flickered) contrast test. Left: A spot approximately the full size of the receptive field centre produced with Vision Egg. Right: The response of the RGC showed an increased discharge for over the 5 seconds when the OFF stimulus was present.

Essentially, the purposes of these tests were to determine the ON or OFF receptive field properties, map the receptive field, and roughly assess the spatial summation of responses of the RGC.

5.7.3.4 Moving gratings

Initially the width of the bars of the moving grating was set at about the same size as the diameter of the receptive field centre of the patched RGC. The responses of the RGCs were recorded to different Michelson contrasts (Michelson, 1927), ranging from 10% to 100% (Figure 5.5). Assessing the response/contrast functions is important for testing the linearity of responses, and for observing the emergence of second harmonic nonlinearity when an ostensibly 'linear' RGC is driven 'softly' into saturation at the top and bottom of its response range. Occasionally the spatial frequency and temporal frequency were adjusted to achieve more optimal stimulus conditions. These adjustments provide the basic data for characterising the performance of RGCs in the domains of spatial frequency and temporal frequency. The goal was to define the linear domain of the response/contrast functions, because performance can be evaluated most easily where linearity applies.

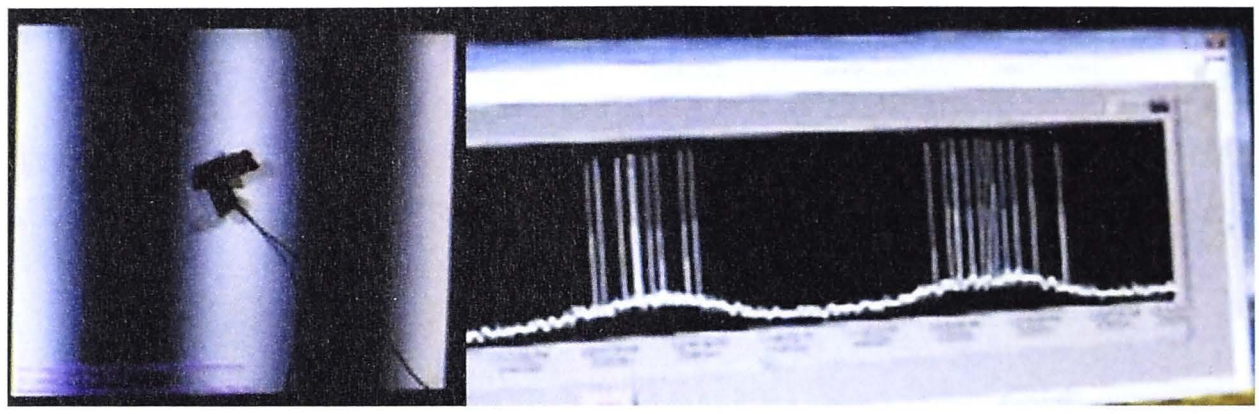

Figure 5.5 An OFF RGC undergoing the moving grating test (100% contrast). Left: The width of the grating was approximately the size of the diameter of the receptive field centre Right: The response of the RGC showed bursts of spikes when the OFF stimulus was presented to the receptive field centre and no spikes during the ON stimulus.

The evidence from soma size, spike width, input resistance and receptive field sizes of the RGCs indicated that the recorded cells were either alpha or beta cells. The concentric receptive field properties, either ON or OFF, were clearly disclosed during the mapping. The spiking patterns of the RGCs should have both sustained and transient components in their light evoked responses. It is the balance between these components that has to be assessed (Cleland, Dubin, & Levick, 1971). Cell classification was made based on the results of both the standing contrast and moving grating recordings. The spiking patterns were either classified as BT or BS (Cleland & Levick, 1974; W.R. Levick & Thibos, 1983). If the RGCs responded with high frequency and transient bursts of spiking to stimuli centred in their receptive field, then they were classified as BT RGCs. The RGCs responding continuously with a tonic firing rate were classified as BS RGCs (Cleland & Levick, 1974). Overall, we classified the recorded RGCs into four groups: ON-centre brisk-transient (ON-BT), OFF-centre brisk-transient (OFF-BT), ON-centre brisk-sustained (ON-BS), and OFF-centre brisk-sustained (OFF-BS). Two examples of spiking trains for transient and sustained responses were shown in Figure 5.6.

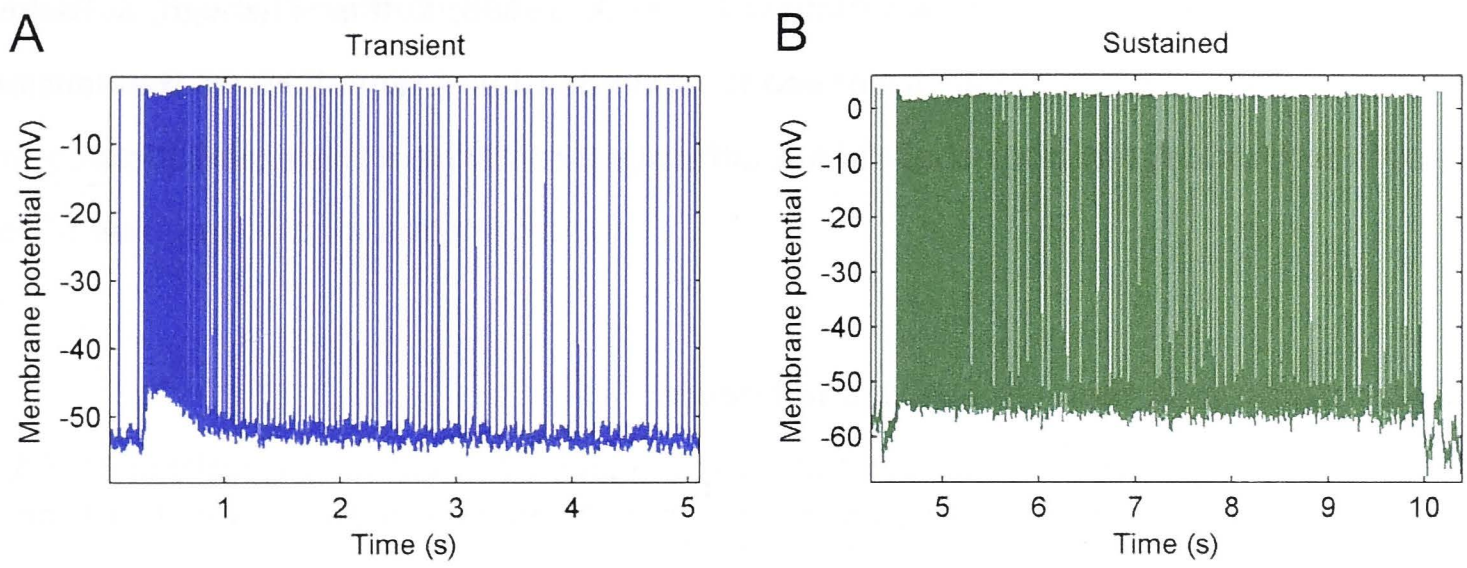

Figure 5.6 The two spiking patterns of the RGCs. A) A typical RGC transient spiking pattern sometimes described as phasic. A burst of spikes was generated when the stimulus was present, and the spike frequency quickly returned to the normal maintained discharge level even though the stimulus remained on. **B)** A typical RGC sustained spiking pattern. The RGC spike firing rate remained substantially elevated (> 5 seconds) while the stimulus was present.

5.3.7.5 Naturalistic video

The projected naturalistic videos covered the receptive fields of the target RGCs completely. Since we positioned the target RGC at the centre of the visual field for patching, the receptive fields were normally positioned at the centre of the projection. The exact topographic RGC locations were not specified (Figure 5.7).

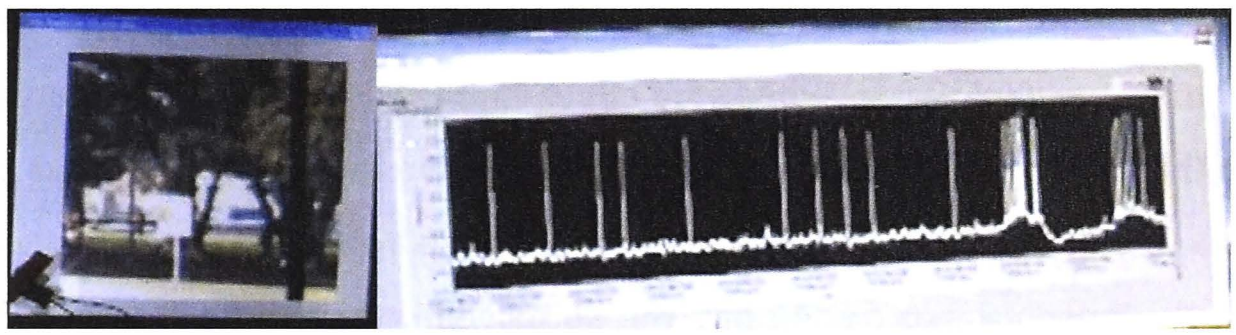

Figure 5.7 An OFF RGC under the naturalistic video test. The receptive field centre was approximately at the centre of the projected video stimulus. Left: A snapshot of the video that was being projected onto the retina. The photodiode recorded the start time of the video. Right: The first few spikes represent the spontaneous activity of the RGC. The last two bursts at right were responses of the RGC to the video stimulus.

5.3.7.6 Maintained discharge (spontaneous spike)

Some RGCs had a maintained discharge in the absence of intentional visual stimulation. The discharge was recorded and the inter-spike interval histogram was compiled. The shape of

the interval histogram *in vivo* is known (Barlow & Levick, 1969b; Kuffler, Fitzhugh, & Barlow, 1957) to be usually well matched by a *Gamma* function density. Examination of the densities for the cells in this study indicated they did not differ significantly from this expectation.

5.3.7.7 Electrical stimulation – threshold and latency

All electrical SPs were constructed with a train of biphasic pulses. The start time of each biphasic pulse was defined as the time of the peak of the spikes in the LRs. Before applying the SP trains of 10 biphasic pulses at 1 Hz or 2 Hz (SP_{10}) was sent to stimulate the RGCs to assess the threshold current. For each test train, the amplitude of the cathodic phase of the biphasic pulse varied in the range from 10 μA to 1 mA. Normally we started at 100 μA, progressively increasing or decreasing the current (coarse step: 100 μA; fine step 20 μA) until the points for the efficacy curve were established. The threshold stimulus amplitude was determined by fitting a two-parameter logistic function to the efficacy data (fitted parameters controlled the position and slope of the function at 50% efficacy). We thus defined the threshold stimulus current (I_{thresh}) as that stimulus amplitude which elicited action potentials on at least 50% of trials. The current amplitude for subsequent testing was set to the level of pulse train that would successfully evoke a spike for every stimulus (I_{max}). In some cells, not all stimuli were able to successfully evoke a spike, but these cells passed the 50% efficacy margin (n=8, mean efficacy = 67.5%). So, we set the upper limit for I_{max} to 1 mA for safety purpose in these cases (see Discussion). The time from the onset of the cathodic phase to the peak of the evoked spike was defined as the delay time (t_{delay}). A close approximation of the conventional latency can be found by subtracting half the spike width (at half height) from t_{delay}. The underlying idea is that the end-point of the latency period ought to correspond to the time at which the spike mechanism has become regenerative. In other words, it should be the point at which the in-rush of sodium ions has become self-sustaining and would need no further assistance from the stimulus current. The inflexion point, which based upon the temporal derivatives of the rising phase, is one of the ways to identify this time point.. At this point, the rate of rise of membrane potential (first time derivative, dV/dt) has reached its peak value. It is also the time at which the second time derivative (d^2V/dt^2) is changing sign from positive to

negative. This derivative measures the trans-membrane current, so the change of sign marks the point at which the net membrane current has first become inward. A rough estimate of the point of inflection is at half height of the spike. Therefore, the half spike width at half height was used to compute the latency.

5.3.7.8 Electrical stimulation – Moving grating and Naturalistic video

The SP generation procedures for the moving grating and naturalistic video were similar except that the source of the LRs are different: one used the LR generated from the RGC responses from the moving grating (SP_{mg}) and the other one use the LR generated from the RGC responses from the naturalistic video (SP_{nv}). If the RGC had spontaneous activity, both types of LRs were filtered to remove spikes appearing at the maintained discharge rate. With a few exceptions, RGCs have a maintained discharge in the absence of intentional visual stimulation (Barlow & Levick, 1969a; Kuffler, et al., 1957; W. R. Levick, 1973). The maintained discharges are important for the development of neuronal connections (Blankenship & Feller, 2010). However, it is not the intention here to delve into the many ways in which maintained discharge affects the interpretation of visually generated signals. We consider the maintained discharge as background noise and the responses of the RGC due to stimuli were represented by firing at higher frequencies (bursts). From preliminary work, we found the time between two spikes in the bursts is usually lower than the time between two spontaneous spikes. From the spike time histogram (not reported), the spikes in bursts that were treated as those beyond the mean plus one standard deviation (t_{m1std}). Therefore we filtered the LRs with t_{m1std} to reduce the 'noise'. In other words, the filtered LRs to represent mainly the spikes generated by the light stimuli with greatly reduced influence from any spontaneous activity (see Discussion). The cathodic amplitude of the biphasic pulses in the SPs was set to the predetermined I_{max}. The resulting patterns, for both the moving grating (SP_{mg}) and the naturalistic videos (SP_{nv}), were used to stimulate the same RGC which produced the ERs (Figure 5.8). The electrical stimulation responses of the RGCs were recorded at least 10 times for statistical analysis.

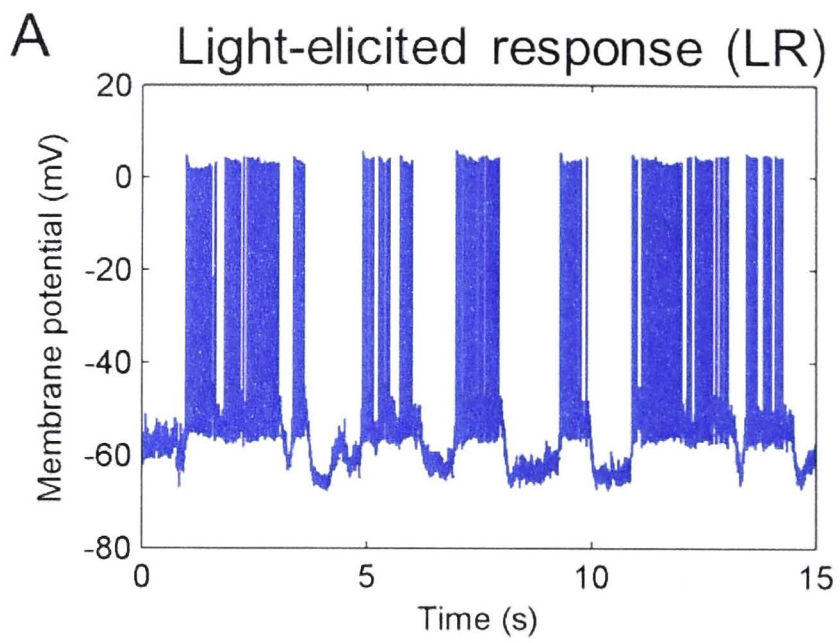

Figure 5.8 Vision reconstruction trilogy: record light-elicited response to a naturalistic stimulus (LR), generated stimulus pattern (SP), and the produce electrical-evoked response (ER). **A)** The LR was generated by projecting the naturalistic movie onto the retina. **B)** The SP was produced according to the spike times from the LR. Each stimulus in SP is an asymmetric charge balanced biphasic pulse. **C)** The ER from the results of SP stimulation. There are spontaneous spikes included in this ER. Furthermore, some stimuli failed to evoked spikes.

5.3.8 Data Analysis

The main purpose of the data analysis in this chapter was to look into the degree to which the ERs matched the LRs. In order to quantify the level of resemblance between the two response patterns (LRs and ERs), we looked at the cross-correlation between them. The data analyses were done offline with custom-made Matlab programs.

5.4 Results

In this section, the preliminary experimental results from 33 cat RGCs were reported. Each RGC was classified according to its physical properties, intrinsic properties and its responses to the light stimuli. The RGCs were categorized into four groups: ON-BT, OFF-BT, ON-BS and OFF-BS. The ERs of each RGC were compared to the SP, which was equivalent to the LR of the same RGC with most of the maintained discharge removed. Each ER often contained some spontaneous (non-electrically evoked) spikes. The level of resemblance was quantified by the correlation coefficient of the SP/ER cross-correlograms (simply referred as correlograms). Subsequent analysis indicated that the mean correlation within the window 0 to 2 ms was used (see the text for Figures 5.11 to 5.14).

5.4.1 RGC classification

The retinal recording area included the area centralis and about 5 mm (~22°) peripheral to it. After a current clamp was made, a current pulse (duration: 400 ms) was sent to stimulate the RGC from the recording electrode. The recorded RGC was depolarized with a positive current injection (~ 10 to 50 μA) until a few spikes appeared. The average spike width at half height was measured from 10 - 15 spikes of each RGC. The RGCs were hyperpolarized with a negative current injection (~ -10 to -50 μA) for the input resistance calculation. A summary of the mean values of the spike widths and input resistance of the recorded RGCs is listed in Table 5.1.

Table 5.1 Properties of the RGCs. Values are: mean (standard deviation).

Type	n	soma dia. (um)	Spike width (ms)	Input resistance (MΩ)	Receptive field size (Visual deg.)
ON-BT	11	25.7 (4.43)	0.45 (0.07)	81.6 (24.6)	3.66 (0.73)
OFF-BT	6	24.6 (5.87)	0.37 (0.03)	54.3 (26.1)	2.75 (1.06)
ON-BS	11	23.2 (1.89)	0.50 (0.09)	131.8 (29.0)	3.44 (0.84)
OFF-BS	5	21.5 (1.44)	0.59 (0.08)	161.0 (54.9)	3.09 (0.76)

From Table 1 of O'Brien et al. (2002), the full spike width at half height of alpha (0.6 ± 0.03 ms) and beta (0.8 ± 0.02 ms) cells were distinguishable from the rest of the listed cat RGCs ranging from 1.34 ± 0.15 ms to 3.20 ± 0.15 ms. The difference of the input resistance between alpha (31.3 ± 4.8 MΩ) and beta (267.2 ± 35.3) cells was marked. The alpha RGCs' input resistances were different compared to the rest of the RGC resistances ranging from 137.3 ± 39.5 MΩ to 1048 ± 176.7 MΩ. However, the values for the alpha cells found from our experiment were not in the range listed by O'Brien et al. (2002), except for the two cells they measured furthest away from the area centralis.

Of the 33 RGCs for which all experiment protocols were completed, 22 were ON-cells and 11 were OFF-cells. Based on the spiking patterns from the standing contrast and moving grating recordings, they were further classified as BT or BS (see Methods). There were 11 ON-BT, 6 OFF-BT, 11 ON-BS, and 5 OFF-BS RGCs recorded. The estimated geometric mean of the receptive field widths were measured and are listed in Table 5.1.

5.4.2 Electrical stimulation

The evoked spikes (red circles) were discernible from the spontaneous spikes (Figure 5.9). The responses to the stimuli began at a fixed time and they were signified by the obvious artefact. The evoked spikes appeared after the stimuli and the peaks of the spikes were generally higher than the spontaneous spikes since they normally arose on the anodic phase of the biphasic pulses. We extracted two parameters, I_{max} and t_{delay}, from the results of ER_{10}. The spikes were determined to be evoked spikes if they appeared consistently at about the same time after three repeated SP_{10} stimulations (30 stimuli). That consistent time period was

considered to be the t_{delay}. For RGCs that didn't have spontaneous spikes, spikes that appeared after the stimulations were presumed to be due to electrical stimulation. A spike may occur that does not have anything to do with the previous electrical stimulus within t_{delay}, but the chance of that happening 30 times in a row is very low. The consistency of the spikes evoked by the stimuli can be visualized by a raster plot (see Figure 5.11A).

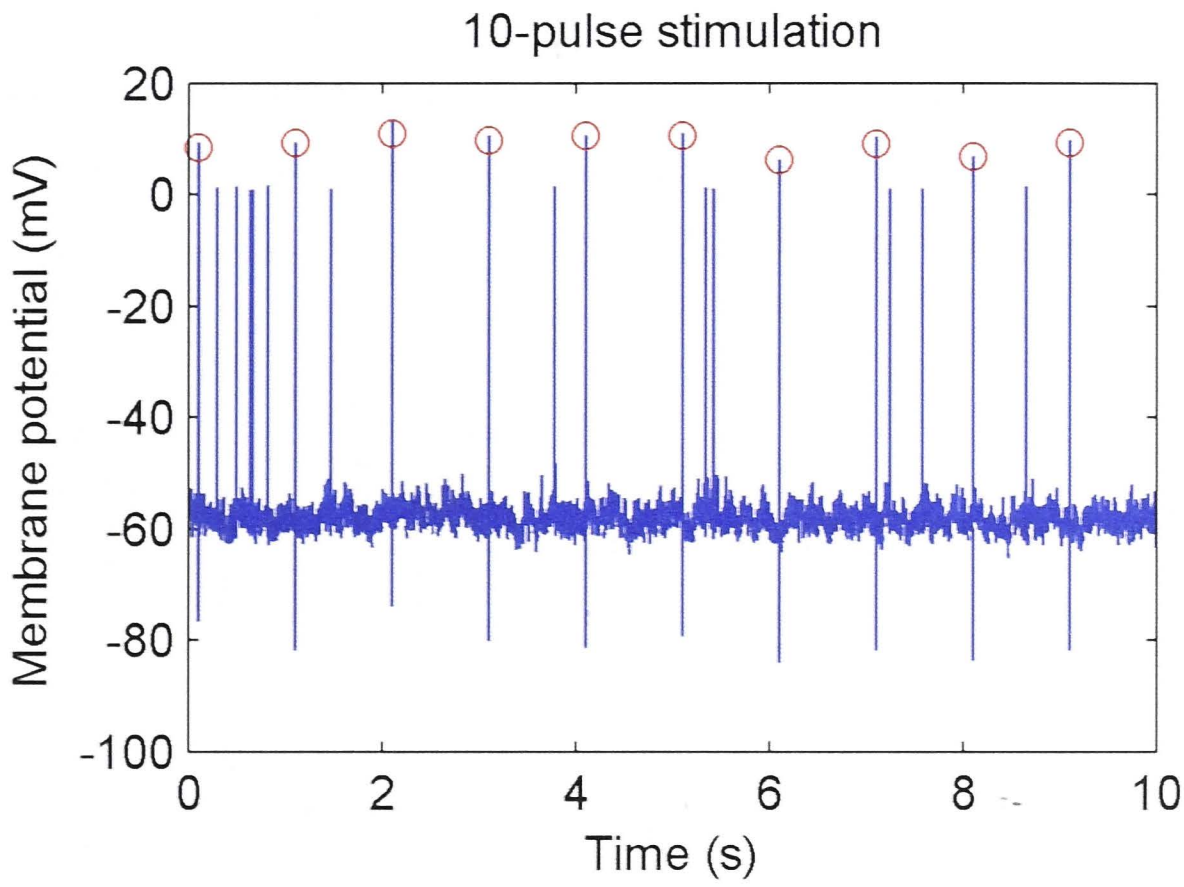

Figure 5.9 An example of a 10-pulse stimulus sequence. The evoked spikes (peaks indicated by the red circles) are distinguishable from the spontaneous spikes. The evoked spikes appear after the stimuli (fixed time with relatively large artefacts) are delayed. The peaks of the evoked spikes are generally higher than the spontaneous spikes.

The t_{delay} was calculated from the average of three repetitions (total 30 spikes) of SP_{10} at I_{max}. The stimulus times were known and verified from the recordings on channel-4. The mean values of I_{max} and t_{delay} were listed in Table 5.2. The conventional latency can be estimated by reducing the BT t_{delay} by 0.211 ms and the BS t_{delay} by 0.266 ms, overall average result in approximately 416.4 ± 175.0 μs, which is close to ~0.5 ms reported by the others for rabbits (Fried, et al., 2006) and monkeys (Sekirnjak et al., 2008).

Table 5.2 The current I_{max} and the spike latency t_{delay}. Values are: mean (standard deviation).

Type	I_{max} (μA)	t_{delay}(μs)
ON-BT	731.8 (345.3)	611.9 (167.9)
OFF-BT	375.0 (299.6)	649.7 (167.9)
ON-BS	809.1 (242.9)	677.4 (242.0)
OFF-BS	740.0 (332.3)	680.5 (122.0)

We used I_{max} of each individual RGC to set up the stimuli SP_{mg} and SP_{nv} to stimulate the same RGC from which we had the LR_{mg} and LR_{nv}. The number of stimuli in a SP varied in the range of 10 to 471. The evoked spikes in ERs were distinguishable from misses (stimuli with no evoked spikes) and the spontaneous spikes (Figure 5.10).

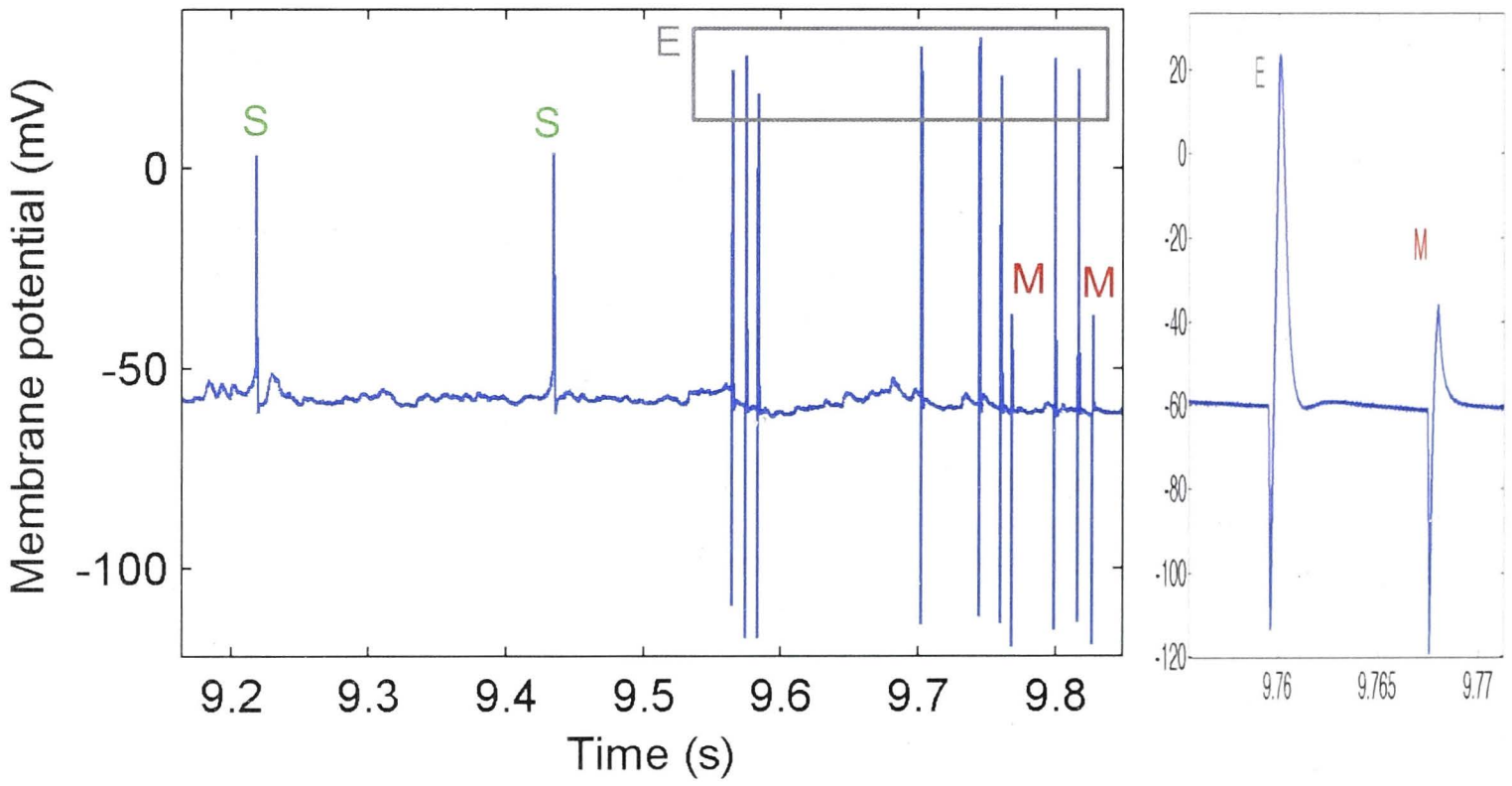

Figure 5.10 An example of an electrically-evoked response (ER). A portion of the ER showing: stimuli that successfully evoked spikes (grey 'E'); two stimuli that failed to evoke a spike (red 'M' for miss); and two spontaneous spikes (green 'S') are shown. The inset at the right-hand side shows the differences between 'E' and 'M' for instance.

5.4.3 Raster plots and correlograms

The stimulations were repeated at least 10 times for each ER. To visualize the resemblance of the SP to the ERs, we used raster plots and the correlograms. In the raster plots, each stem (vertical line segment) represented a spike. The red stems in the first row represent the SP. Each subsequent row denotes a trial and each stem within a row represents a spike, either evoked or spontaneous. The example of the raster plot (Figure 5.11A) shows the SP_{nv} of 13 trials aligned with the ER_{nv} of an OFF-BT RGC.

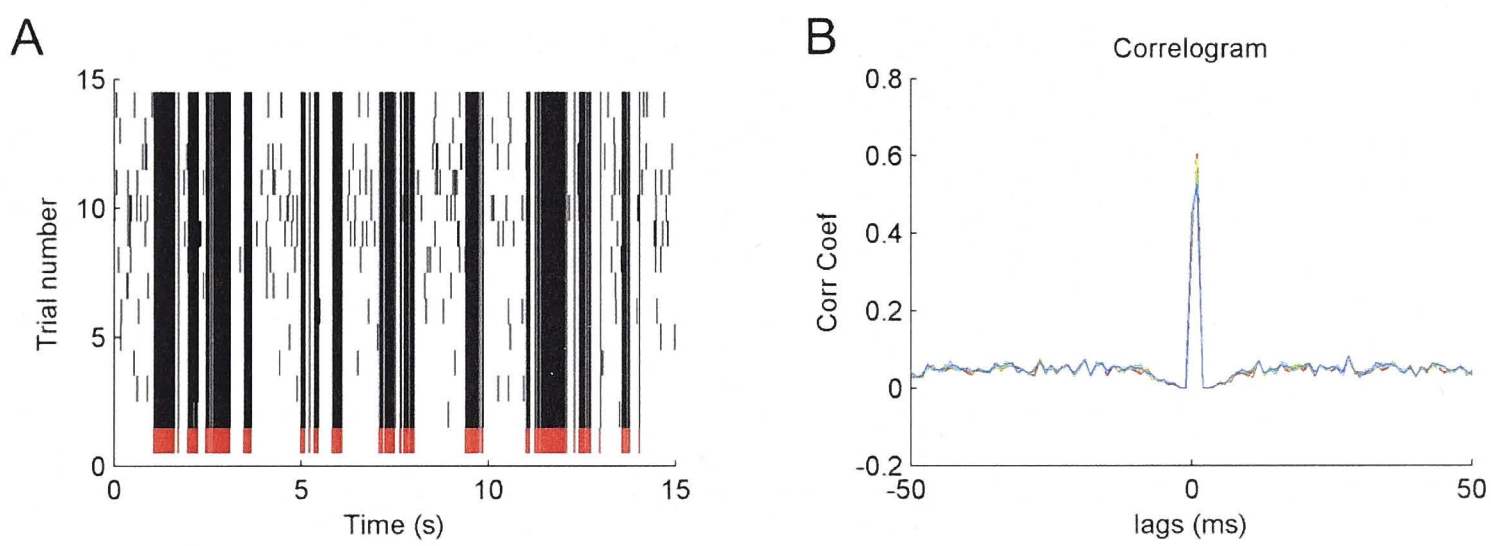

Figure 5.11 A high correlation case. Visualization of the correlation of the naturalistic video stimulus patterns (SP_{nv}) and the associated electrically-evoked responses (ER_{nv}) (13 trials) for a case where one highly resembles the other. **A)** A raster plot of the SP_{nv} and the ER_{nv} of an OFF-BT RGC. The red stems at the bottom represent the spikes in the SP_{nv} and the black stems represented spikes (evoked or spontaneous) in each trial of the ER_{nv}. Spikes in the ER_{nv} were consistently aligned with the SP_{nv} in this example, suggesting that the spikes were evoked by the stimuli. **B)** Correlograms of the SP_{nv} and all the ER_{nv} (plotted in different colours, legend omitted) showing that the correlations were consistently high (~0.6).

A contrary example of a raster plot of an ON-BS RGC (Figure 5.12) showing the ER_{nv} were not aligned with the SP_{nv}. Almost all stimuli failed to evoke a spike. When we examined the ER more closely, at each burst of the SP, the first stimulus was able to evoke a spike successfully, however, the following stimuli could not. In this example, there were a large number of spontaneous spikes. These spontaneous spikes did not appear during the period when the stimuli failed to evoke spikes. It seems that the stimulation suppressed the RGC and spiking was inhibited.

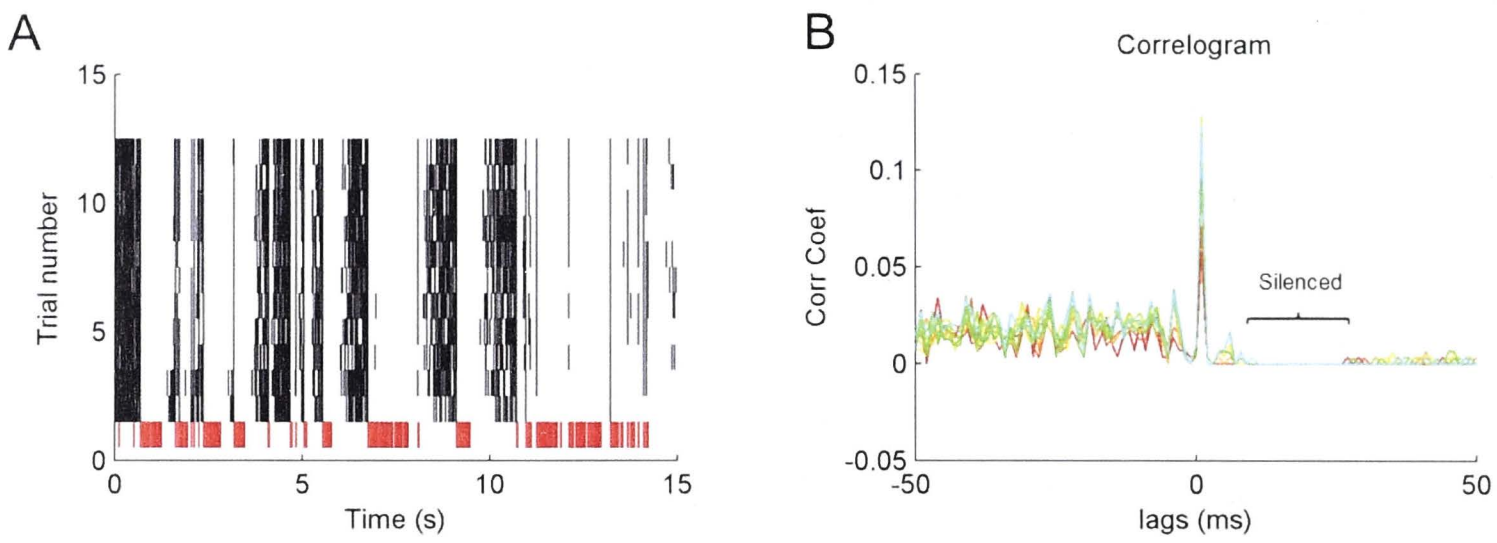

Figure 5.12 A low correlation case. Visualization of the correlation of naturalistic video stimulus patterns (SP_{nv}) and associated electrically-evoked responses (ER_{nv}) (11 trials) that were highly non-correlated. **A)** The raster plot of the SP_{nv} and the ER_{nv} of an example of an ON-BS RGC. Conventions as in Fig. 5.11. There were a great many spontaneous spikes during the non-stimulus period but there were almost none during the stimulus period. Most stimuli failed to evoke a spike except the first one of every SP burst. **B)** Correlogram of the SP_{nv} vs. the ER_{nv} (plotted in different colours, legend omitted) showed that the mean correlation at short delays was low (~0.12).

There were still some matches (first spike of every burst) leading to the low, but non-zero, correlation. The flat period (bracketed area in Figure 5.12B, from lags 10-25 ms) indicated the RGC was completely silenced soon after any electrical stimulation. Extending the time scale of Figure 5.12, we saw a cleft (Figure 5.13B indicated by the arrow →), which suggested that the activity of the RGC was suppressed after electrical stimulation and then the spontaneous spiking recovered later (Figure 5.13B). By contrast, Figure 5.13A shows no cleft.

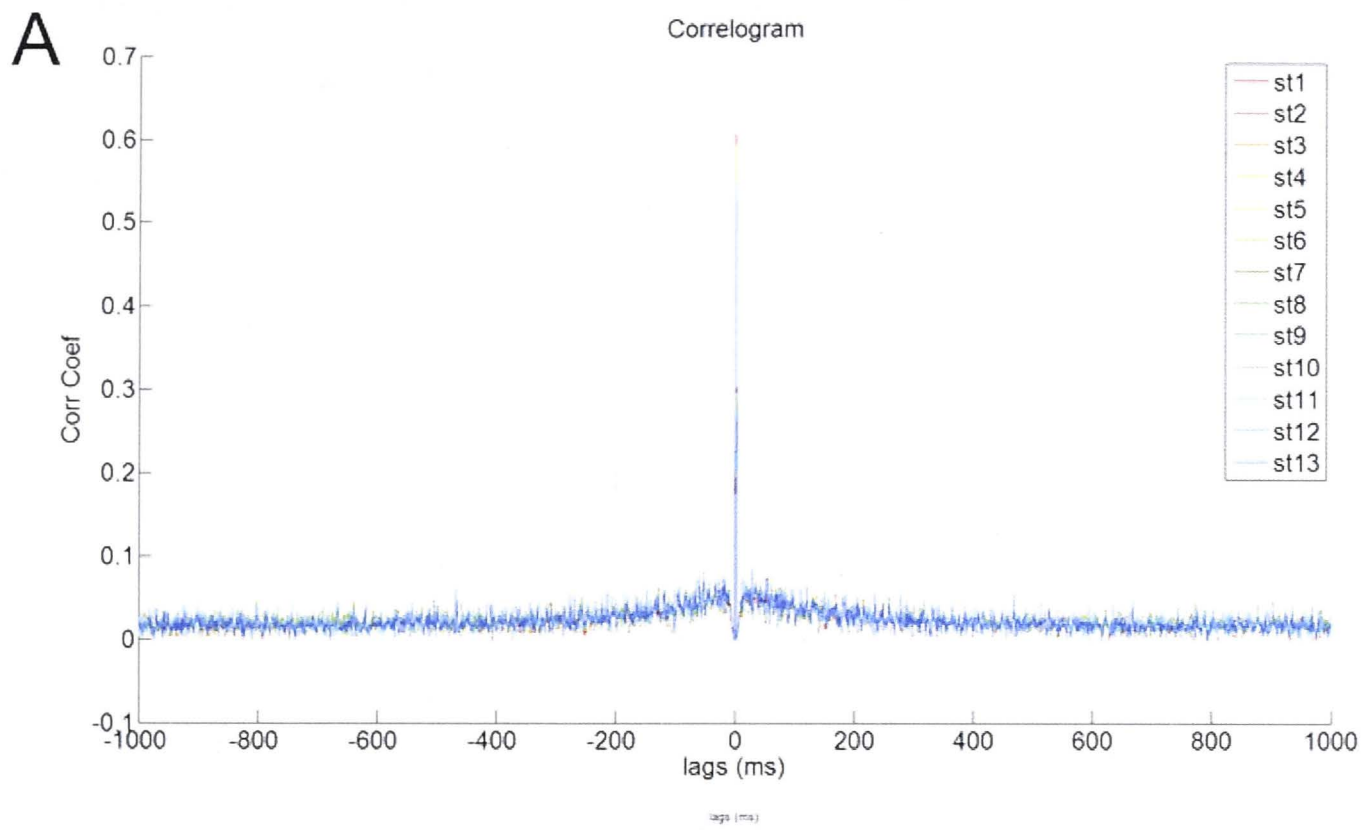

Figure 5.13 Correlograms of the two examples compared. These are the same correlograms in Figure 5.11B and Figure 5.12B respectively, except the time scale has been extended to 1ms. **A)** High correlation example, the correlation coefficients are pretty much 'mirrored' abut 0 lag time. **B)** Low correlation example, the RGC was almost completely silenced for 15 ms (see Figure 5.12B for details), and then spiking gradually recovered post-stimulus. The cleft (→) where the arrow is pointing suggests that the activity of the RGC was suppressed.

By taking a closer look at the correlograms of the examples, we found that the correlations were low after 2 ms (Figure 5.14). That suggested the spikes that were found 2 ms after each stimulus were probably not electrically evoked.

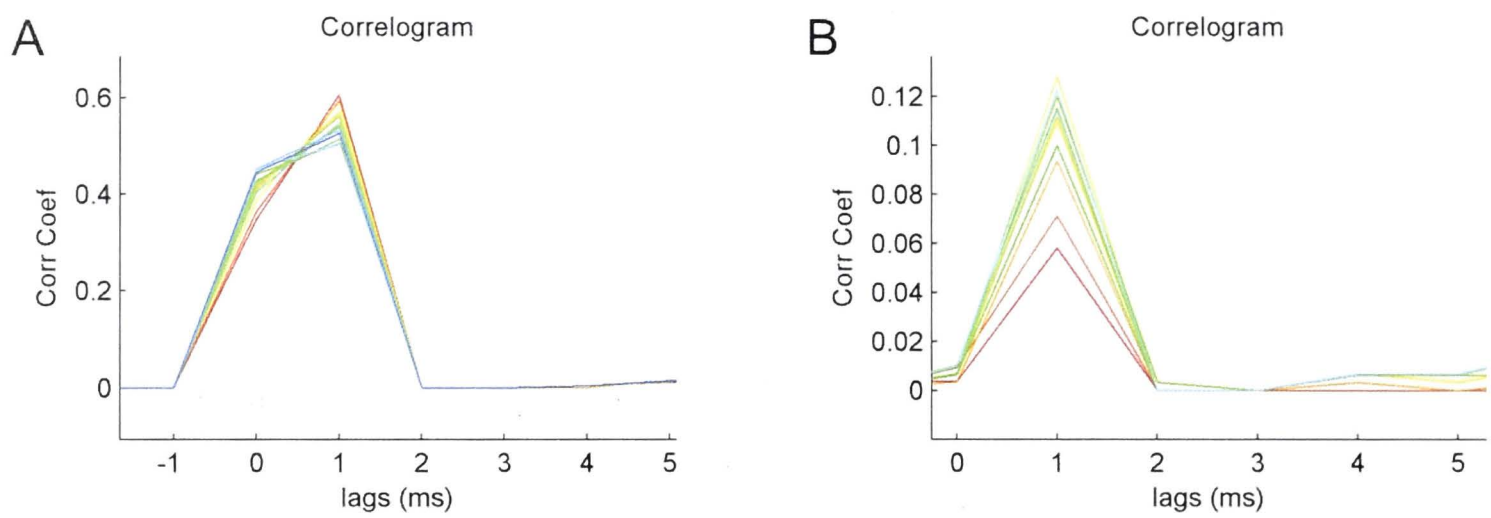

Figure 5.14 Correlograms of the previous examples at a finer time scale. In both cases, the correlations were reduced to near zero at 2 ms. **A)** From Figure 5.13A, and **B)** From Figure 5.13B.

The maximum spike frequency found in the dataset for all LRs was 328.8 Hz, which was close to the maximum spike frequency (325.9 Hz) found by intracellular stimulation for all cat RGC types at room temperature (O'Brien, Isayama, Richardson, & Berson, 2002). We did not examine the maximum spike frequency of the RGCs activated by extracellular electrical stimulation. Based upon the maximum spike frequency, the RGCs were apparently only capable of generating another spike after approximately 3 ms. In the correlogram, albeit that the chance of having two spikes within any bin (1 ms) is very low. The correlation in each bin was relatively independent, thus we took the mean correlation coefficient from lags 0 to 2 ms to represent the overall resemblance of the SR and the ERs (Table 5.3).

Table 5.3 Correlation coefficients of the SP and the ERs, averaged for lags between 0 and 2 ms. Values are means (standard deviations), the maximum mean correlation value is 1.

Type	Grating	Video
ON-BT	0.581 (0.239)	0.649 (0.262)
OFF-BT	0.850 (0.254)	0.861 (0.212)
ON-BS	0.318 (0.178)	0.336 (0.200)
OFF-BS	0.397 (0.210)	0.380 (0.185)

Among the different groups, t-tests showed that there were statistically significant differences between the ON-BT and ON-BS correlations (Grating: p=0.036; Video: p=0.00736), OFF-BT and ON-BS (Grating: p=0.0038; Video: p=0.00129), OFF-BT and OFF-BS (Grating: p=0.0294; Video: p=0.0055). Moreover, there was also statistical significance between the overall BT and BS groups (Grating: p=0.0014; Video: p=0.0001).

We next scrutinized the histograms of the correlation coefficient for both the ER_{mg} (n=26, some moving grating stimulations were not included from the early experiments) and ER_{nv} (n=33) (Figure 5.15). From the histograms, the RGCs with relatively higher correlations were mainly BT RGCs. By contrast, those with lower correlations are mainly BS RGCs. In between the high and low range was a mix of all RGC types except the OFF-BT RGCs.

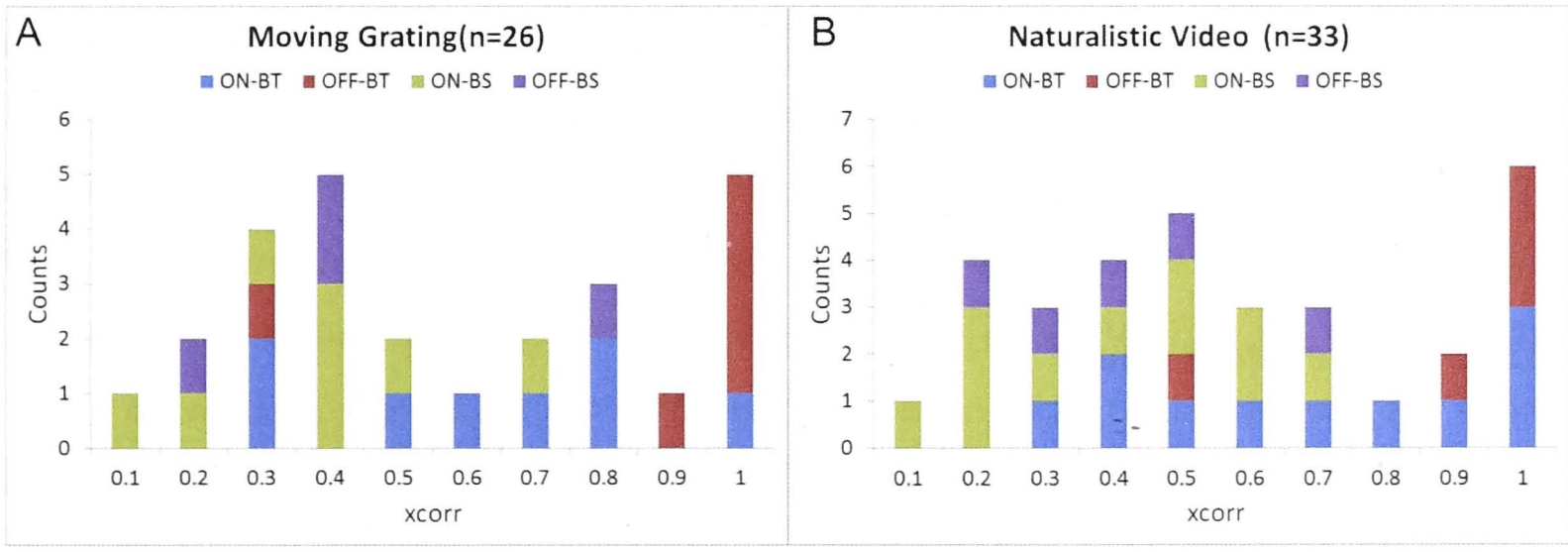

Figure 5.15 Histograms of the correlation coefficients (xcorr) of the RGCs. A) xcorr results comparing the light-elicited responses (LR) and the electrically-evoked responses (ER) from the moving grating test. **B)** xcorr results comparing the LRs and the ERs from the naturalistic video tests. The majority of RGCs that had relatively high xcorr were BT RGCs. By contrast, the RGCs with the lowest xcorr were BS RGCs.

5.5 Discussion

The overall low recording success rate was mainly due to surgical difficulties early on in the study and this was later improved. The removal of the vitreous body tends to have a substantial impact on the healthiness of the RGCs (diminished gas exchange of oxygen etc.) and for effective patching. Since more than half of the tissue came from animals after experiments, plus extra transportation time, the quality of the tissue was also less than optimal. Nevertheless, there weren't any obviously differences between Groups A and B.

5.5.1 Species mismatch

Evaluation of the responses of cat RGCs by projecting human saccadic video projection onto the cat's retina may represent a significant species mismatch. Compared to humans, the cat's saccade amplitude (~15°) is about 3-fold larger; the cat's fixation duration (~130 ms) is about 3 times longer; and the peak saccadic velocity (~150 °/s) is about 50% slower (Crommelinck & Roucoux, 1976; Evinger & Fuchs, 1978; Moeller, Kayser, Knecht, & Konig, 2004). The most critical issue is probably the spatial resolution and cell type distribution, in which cat (~ 8 cycle/°) is much poorer than human (~ 60 cycle/°) (Cleland, Crewther, Crewther, & Mitchell, 1982; Kaplan & Benardete, 2001). Moreover, there may be relatively more W-cells in cats. However, the receptive field organization of the two species seems similar, and it was expected that the characteristics of the RGCs are closely correlated (Enroth-Cugell & Robson, 1966). Nevertheless, it might be more suitable to use a cat saccadic video instead, or perhaps convert the human-seeing images to suit the cat's eye/brain.

5.5.2 Temperature effect

The rate of oxygen demand is important for the cat retina; it is as important as for the brain. We tried to use chilled solutions for transportation in order to slow down the metabolism, but the result was negative. For example the retinas from some of these Group-A cats were somewhat shrunken by the time we got them back to the lab. Therefore, we left the solutions at room temperature, except during experiment when the solution was maintained at ~34°C. The experiment temperature (~34°C) is lower than the normal cat body temperature (~38°C), which has some influences on the spike generation mechanism. However, while the rates of both sodium ion channel activation and inactivation are dependent on temperature, the respective Q10 coefficients (a measure of a 10 °C change in a biological system) are sufficiently closely matched to permit spike generation and propagation to occur over the range from 20 to 37 °C (Schwarz & Eikhof, 1987). The effect at the lower end is probably greater (see Chapter 3 Discussion) but at the higher temperature end might be minor.

5.5.3 Classification

The area centralis was located readily because the density of RGCs in this region was clearly noticeable under the microscope with the aid of acridine orange. Selections of the RGCs were based on the estimated soma sizes. The putative alpha and beta cells were larger than the other types of RGCs. The beta cells can also be recognised easily because they were arranged in a closely packed pattern in the retina. Away from the area centralis, the soma size differences were more obvious. We tried to support the classification from two known intrinsic properties of the RGCs. In a related study (O'Brien, et al., 2002), the spike widths and the input resistances were measured at room temperature, and those for alpha and beta cells were different from the other RGC types. In this study, those two intrinsic parameters were used as references. However, we were aware that they can be remarkably different at physiological temperature (on the order of twofold in rat RGCs, see Chapter 3). Compared to room temperature, at physiological temperature the increased thermal energy will certainly enhance the diffusional movements of ions and thus change the intrinsic properties of the RGCs. A comparative study of cat RGC intrinsic properties at physiological temperature might facilitate future studies. The cells (n=33) in this Chapter were collected from the area centralis. On the other hand, the values (n=77) reported in O'Brien et al. (2002) spanned the entire retina, and the ON and OFF RGC types were combined in each of the alpha and beta cell types. Therefore, the results might have some statistical differences. In addition, the expedient transient vs. sustained classification used here is not conventional. There is an extra step to superimpose the brisk/sluggish dichotomy on the sustained/transient dichotomy according to the Cleland and Levick (1974) but might not be suitable for our protocols. Ideally, all the RGCs should be filled and indentified anatomically.

Nonetheless, our target area for implanting prostheses is the macular region. We are therefore more interested on the responses of the RGCs in this region where RGCs are densely packed. The primary goal of this study was to look at the capability of reconstructing the LR of the RGCs by electrical stimulation. The video simulated saccadic eye movements, which provided a background imitating the normal natural scene viewing conditions. The responses of the RGCs were complicated since the stimulating electrode will non-physiologically activate a population of RGCs. The target RGC and its neighbours would be all activated at once, and

the network consequences were unknown. It was unrealistic when both the ON- and OFF-systems were activated by the electric stimulation simultaneously. The periphery effect (W. R. Levick, Oyster, & Davis, 1965; McIlwain, 1966) was also substantially neglected, especially when we explored only the central area of the retina with light stimuli.

5.5.4 Light stimuli

The generated light stimuli may have been rather strong, especially given that the lens was focused on the photoreceptor layer to elicit a more robust responses. Therefore they were likely to produce strong activity in the automatic gain control and shift effects in the inner and outer plexiform layers. These are not directly experienced in vision because they operate automatically and are not controllable directly. Indirectly, they can be experienced as transient 'after-images'.

Of all the properties studied, the one that carried the greatest certainty was the ON-centre or OFF-centre characteristic of the receptive field. The mapping of the surround was skipped in order to speed up the overall analysis process. Some of the phasic and tonic spike firing patterns were distinguishable for identifying the type of the RGC. We could not clearly see the dendritic patterns during the experiment. Therefore it was preferable to categorize the recorded RGCs into the four groups based on their receptive field properties rather than using the alpha vs. beta terminology.

5.5.5 Maintained discharge

Maintained discharge arises in discussions of visual responses in two main contexts. In the first, it is supposed that there is simply *a constant additive excitatory noise source* inherent in the process of combining synaptic input from the region covered by the dendritic tree. This is the context assumed in the present work. An alternative context is to suppose that the maintained discharge is the end-point result of transduction of the inherent Poisson noise of the light stimulus itself, after processing by *automatic gain control and shift effect* in the outer

and inner plexiform layers have been applied. In this view, the noise is a transformed, *irreducible* remnant of the original stochastic photon rate that encoded the imposed signal light. At the RGC level, the signal is split between the ON- and OFF-systems: the ON-system represents increments above the ambient background (roughly, the mean illumination of the scene); the OFF-system represents decrements below the ambient background. In this second context, the noise is not simply an additive constant. It is an inherent component of the signal. *How it should be formulated is still not experimentally resolved.*

The analysis is an attempt to develop an empirical approach to divide the spikes of the discharge into two sets: those ostensibly elicited by the transitions of the light stimuli where bursts of spikes were common, and those supposedly associated with the 'maintained discharge' and therefore governed by the Gamma densities of inter-spike intervals (see 5.3.7.6). Published examples of interval histograms of a spike discharge elicited by a periodically flashing light have been presented by Ogawa et al (1966) (e.g. their Fig. 8) (Ogawa, Bishop, & Levick, 1966). They are typically bimodal or multimodal for frequencies of flicker below the 'Critical Fusion Frequency'. The short interval peak corresponds with the bursts at transitions of the light stimulus. The long interval peak corresponds with the gap in the discharge at the 'inhibitory' transition of the light stimulus coupled with the slow recovery of the maintained discharge. This demonstration supports the idea of an empirical 'filtering' procedure for removing the maintained discharge.

The main rationale for removing the maintained discharge is as follows. The goal is to test the accuracy of the electrically-driven version of the natural vision pattern against the original light-driven version by using the method of cross-correlation of the two spike-train instances. The power of the test is increased by stripping off the 'maintained' spikes that are considered to be independent of the photic-forcing stimulus.

5.5.6 Uniqueness of encoding

We represented the spike train of the LR using the spontaneous spike time characteristic (t_{m1std}, see section 5.3.7.8). In this way, we reduced the 'noise' but at the same

time we might also have lost some visual information. One interesting thing is, when the same light stimuli are repeated, the RGCs do not generate 'exactly' the same LR. The time for the burst may be nearly the 'same'. However, the individual spike times within the burst are slightly different every time. If the RGCs convey the same stimuli with the same set of coding methods, then the LR should be unique (Troy, 2012). Clearly, this is not borne out by a sufficiently fine temporal analysis. The unexpected timing variations observed actually lend support to the notion that the 'noise' component of the discharge is a reflection of the inherent noise embedded in the light stimulus itself, even at photopic levels (Barlow, 1958).

The brain can decode these spikes with variances and understand them, which suggests that there is some kind of fuzzy method of communication between the retina and the brain. The communication between the retina and the brain is not a one-to-one correspondence. Even with the same stimulus, each time responses of the RGCs will not be exactly the same. The brain can still 'see' the same object with the non-exact information provided by the RGCs. That is to say that the brain is specifically tuned to the output from the RGCs during retinal development. If the electrical stimulation forces the RGC to produce a more 'regular' spike trains and disturb the rest of the retinal network, can it be understood by the fine-tuned brain? Nevertheless, this might all suggest that we should perhaps generate stochastic stimuli based on the statistics of a collection of LR responses to repeated presentations of same stimulus train, rather than cull presumed noise spikes as a way of generating realistic LRs and SPs.

5.5.7 Electrical stimulation

There were imperfections in our electrical stimulation as well, especially when both ON and OFF pathway were unavoidably stimulated simultaneously. This could be improved by increasing the selectivity of the stimulating electrode. The stimulating electrode we used here is still under development for use in retinal prostheses.

We were able to replicate the ER in some RGCs but we do not know what the result will represent when it reaches the brain. What we wanted to achieve is to understand the

responses of different types of RGC under electrical stimulation so that we can devise a conjugate stimulation strategy. As long as we can get a single RGC of some kind under full control from a single stimulus, we should be able to improve the overall quality of any prosthesis when we expand to MEA stimulation.

5.5.8 Biphasic pulse parameters

One critical component for this study was setting the optimal parameters of the biphasic pulse. We used asymmetric charge balanced biphasic pulses to construct the SPs. With the four possible setups, we picked the cathodic phase first, followed by a short period of IPI and then an anodal phase last. The durations were set to constants so that we only varied the current amplitude. At this point we do not know which setup is the most efficient to activate the RGCs safely. The physical properties and the placement of the stimulating electrode used have some critical effects. As we tested the impedance of the N-UNCD electrode on every experiment, we found that the electrode degraded substantially in a few days. We had to discard data from some of the patched RGCs because they could not evoke spikes at the maximum extracellular stimulation output current (1 mA). Most of these RGCs spiked normally under intracellular stimulation. The RGCs reported here were those for which we completed all the experimental protocols with minimal deterioration of the quality of the stimulating electrode and with reasonable homogeneity of the cells' performance.

In the present chapter, the SP_{10} procedure was utilized to find the efficacy curve so as to determine I_{max} and t_{delay}. These two parameters were used to set up the other SPs. There were RGCs (n=8; 2 ON-BT; 3 ON-BS; 3 OFF-BS) that were not able to give 100% efficacy even at the maximum per stimulus current of 1 mA. These were not discarded because they still passed I_{thresh} to 67.5% efficacy. Not surprisingly, their LR/ER correlations were low (grating:0.245 ± 0.124; video:0.245 ± 0.115). The study of the inhibition in Figure 5.12B (the silenced period) and 5.13B (the cleft) indicated that the handicapped efficacy probably wasn't due to the current not being large enough to evoke a spike. Instead, the cells were indeed inhibited for unknown reasons. Note that none of the OFF-BT RGCs had this problem. We suspect that the inhibition might be type or connection related.

5.5.9 Adaptation issues

Although it was already known that the RGC activation thresholds vary with different stimulation frequencies (Cai, et al., 2011), we did not develop a dynamic scheme to change the parameters for different sections of the LR that had different firing rates. This situation was actually more complicated than first expected. We tried stimulating the RGCs (those that after the regular protocols were still responding robustly) with different frequencies (50, 100, 200, 400 Hz) for a short interval (20, 40, 80ms). Two unexpected effects were observed for 14 of the 33 cells here and so some additional experiments were done after the standard protocol was completed. One was the occurrence of a 'suppression interval' after the stimulation; the other was a 'delayed adaptation' of the firing rate. The suppression interval increased proportionally with the stimulus frequency. In other words, the higher the stimulus frequency, the longer the time for the spikes to reappear after the stimulation. The 'delayed adaptation' of the firing rate (Figure 5.16) occurred some time (~5s) after the completion of the high frequency (400 Hz) stimulation. The firing rate slowed down for approximately five seconds and then returned to normal. We confirmed these observations in 14 RGCs, and all showed the same changes in their responses. However, the additional experiments were performed on RGCs after the regular (2-hour plus) electrical stimulation experiment on top of the culture time, and hence, the RGCs may not be in their best condition. Besides, the additional protocol took at least 1.5 hours to complete, which would have adversely affected the regular experiment if it were done first. Though no conclusive results could be drawn at this stage, the phenomenon is worth mentioning.

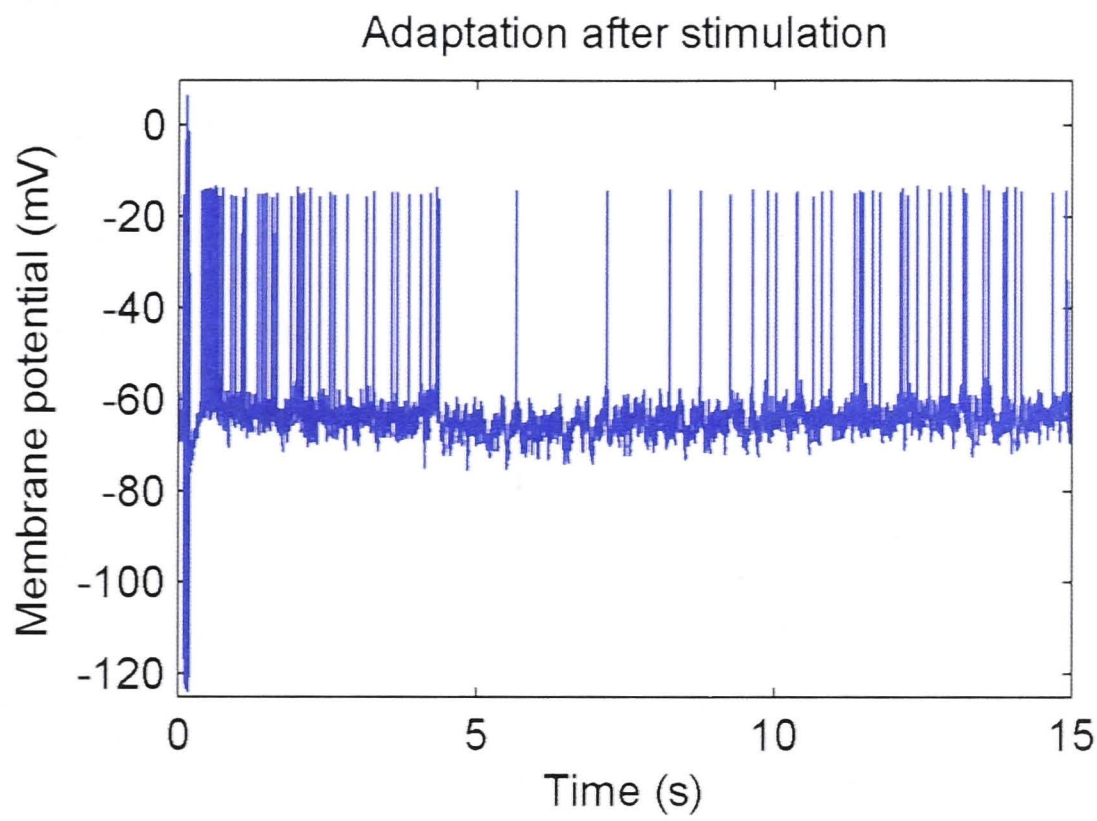

Figure 5.16 The adaptation effect after high frequency stimulation (unpublished). In this example the electrical stimulation frequency was 400 Hz, and the duration of stimulation was 80 ms. The firing rate after the stimulation increased for about 300 ms and then returned to normal. Five seconds after stimulation the firing rate of the RGC rapidly slowed down for about five seconds. Afterwards the firing rate slowly returned to normal. This experiment was performed on a RGC after the regular protocol. The peak of the spike overshoot was reduced to about -20 mV from over 0 mV (at the beginning of the regular experiment).

In this study, we used retinas from healthy animals. The spike train formation of a single RGC is a combinatorial action of the retinal network rather than a single response on its own. The naturally formed LRs were due to different inputs, for example, the inputs from the bipolar cells and the amacrine cells. In some cases, the SPs successfully evoked quite accurate reconstructions of their LRs. We do not know that the visual information contained in this single spike train can be represented in the brain correctly without the information from the other neurons in the network. Certainly, we can see the effect of the unsuccessful cases, where the RGCs were inhibited by the realistic SPs instead of being excited. As shown in Table 5.3 these cells did not follow SPs for gratings drifted at supposedly near optimal spatial and temporal frequencies. These results were probably due to the effects of the inappropriate activation of the surrounding neurons by the rather gross SP stimulation. In a degenerated retina, the consequences of these effects are still unknown to us. Perhaps the effects would be less in a poorly interconnected degenerate retina, but this is completely unknown. The plasticity of the brain might allow it to estimate bounds on the *range* of responses that may be

accepted as a valid representation of the particular event that occurred in the external world, giving rise to the particular set of responses that are experienced.

5.5.10 Correlations

The results we found to broadly agree with those that have been reported earlier: the BT RGCs seem to be able to follow SPs having high stimulation rates (up to 600 Hz), and the BS RGCs could not (failing from 200 Hz and up). Some BS RGCs followed every other pulse; some generated a few consecutive pulses then no responses as previously reported (Cai, et al., 2011). The correlogram is a simple and powerful tool to analyse the temporal structure of two spike trains. We use it to evaluate the degree of match between the ERs and the LRs. We can simply interpret the results from Table 3 and visualizing Figures 5.12 and 5.13: highly correlated indicates a good match, poorly correlated is a bad match. The correlation coefficients among the different types of cells were from as low as 0.071, to as high as 1. The abstract values depend on the bin size. We knew that the latency jitter was within a millisecond period (Table 2). Perhaps we can investigated the short and long latency components in the future (Jensen, Ziv, & Rizzo, 2005).

As expected, some RGCs were capable of replicating their LRs. We are more interested as to why some of them could not. In Figure 5.12B and 5.13B, the silenced period and the cleft indicated there are some critical events which lead to inhibition. This unknown inhibition mechanism might be the reason for some of the medium level correlations showed in Figure 5.15 as well. The causes are most likely a combination of the activation of other retinal neurons, stimulus parameters, and electrode properties. Interestingly, the OFF-BT RGCs gave the best performance among all the RGCs and the current required (I_{max}) to fully activate them was also the least (Table 2). The lower currents would mean less costimulation of other cell types. If we can fully control the OFF-BT RGCs, we certainly can come up with a better stimulus strategy. In other words, it may be possible to form a phosphine-based image with better quality by just using the OFF-BT RGCs.

5.6 References

Ahuja, A. K., Behrend, M. R., Kuroda, M., Humayun, M. S., & Weiland, J. D. (2008). An in vitro model of a retinal prosthesis. *Ieee Transactions on Biomedical Engineering, 55*(6), 1744-1753. doi: Doi 10.1109/Tbme.2008.919126

App, E., & Delous, G. (1998). Saccadic velocity and activation: Development of a diagnostic tool for assessing energy regulation. *Ergonomics, 41*(5), 689-697. doi: Doi 10.1080/001401398186856

Barlow, H. B. (1958). Temporal and Spatial Summation in Human Vision at Different Background Intensities. *Journal of Physiology-London, 141*(2), 337-350.

Barlow, H. B., & Levick, W. R. (1969a). 3 Factors Limiting Reliable Detection of Light by Retinal Ganglion Cells of Cat. *Journal of Physiology-London, 200*(1), 1-&.

Barlow, H. B., & Levick, W. R. (1969b). Changes in Maintained Discharge with Adaptation Level in Cat Retina. *Journal of Physiology-London, 202*(3), 699-&.

Bishop, P. O., Vakkur, G. J., & Kozak, W. (1962). Some Quantitative Aspects of Cats Eye - Axis and Plane of Reference, Visual Field Co-Ordinates and Optics. *Journal of Physiology-London, 163*(3), 466-&.

Blankenship, A. G., & Feller, M. B. (2010). Mechanisms underlying spontaneous patterned activity in developing neural circuits. *Nature Reviews Neuroscience, 11*(1), 18-29. doi: Doi 10.1038/Nrn2759

Boycott, B. B., & Wassle, H. (1974). The morphological types of ganglion cells of the domestic cat's retina. *J Physiol, 240*(2), 397-419.

Cai, C., Ren, Q., Desai, N. J., Rizzo, J. F., 3rd, & Fried, S. I. (2011). Response variability to high rates of electric stimulation in retinal ganglion cells. *Journal of Neurophysiology, 106*(1), 153-162. doi: jn.00956.2010 [pii]10.1152/jn.00956.2010

Cleland, B. G., Crewther, D. P., Crewther, S. G., & Mitchell, D. E. (1982). Normality of Spatial-Resolution of Retinal Ganglion-Cells in Cats with Strabismic Amblyopia. *Journal of Physiology-London, 326*(May), 235-249.

Cleland, B. G., Dubin, M. W., & Levick, W. R. (1971). Sustained and transient neurones in the cat's retina and lateral geniculate nucleus. *J Physiol, 217*(2), 473-496.

Cleland, B. G., & Levick, W. R. (1974). Brisk and sluggish concentrically organized ganglion cells in the cat's retina. *J Physiol, 240*(2), 421-456.

Crapper, D. R., & Noell, W. K. (1963). Retinal Excitation and Inhibition from Direct Electrical Stimulation. *Journal of Neurophysiology, 26*, 924-947.

Crommelinck, M., & Roucoux, A. (1976). Characteristics of Cats Eye Saccades in Different States of Alertness. *Brain Research, 103*(3), 574-578. doi: Doi 10.1016/0006-8993(76)90458-3

Enroth-Cugell, C., & Robson, J. G. (1966). The contrast sensitivity of retinal ganglion cells of the cat. *J Physiol, 187*(3), 517-552.

Evinger, C., & Fuchs, A. F. (1978). Saccadic, Smooth Pursuit, and Optokinetic Eye-Movements of the Trained Cat. *Journal of Physiology-London, 285*(Dec), 209-229.

Fried, S., Hsueh, H. A., & Werblin, F. S. (2006). A method for generating precise temporal patterns of retinal spiking using prosthetic stimulation. *Journal of Neurophysiology, 95*(2), 970-978. doi: 00849.2005 [pii]10.1152/jn.00849.2005

Fried, S., Kubow, T., & Werblin, F. (2004). Complex synaptic activation of bipolar, amacrine and ganglion cells is elicited with biphasic electrical stimulation. *2004 Ieee International Joint Conference on Neural Networks, Vols 1-4, Proceedings*, 469-469. doi: Doi 10.1109/Ijcnn.2004.1379952

Hadjinicolaou, A. E., Leung, R. T., Garrett, D. J., Ganesan, K., Fox, K., Nayagam, D. A. X., . . . O'Brien, B. J. (2012). Electrical stimulation of retinal ganglion cells with diamond and the development of an all diamond retinal prosthesis. *Biomaterials, 33*(24), 5812-5820. doi: DOI 10.1016/j.biomaterials.2012.04.063

Hamill, O. P., Marty, A., Neher, E., Sakmann, B., & Sigworth, F. J. (1981). Improved patch-clamp techniques for high-resolution current recording from cells and cell-free membrane patches. *Pflugers Arch, 391*(2), 85-100.

Hoffman, J. E., & Subramaniam, B. (1995). The Role of Visual-Attention in Saccadic Eye-Movements. *Perception & Psychophysics, 57*(6), 787-795. doi: Doi 10.3758/Bf03206794

Humayun, M. S., deJuan, E., Dagnelie, G., Greenberg, R. J., Prost, R. H., & Phillips, D. H. (1996). Visual perception elicited by electrical stimulation of retina in blind humans. *Archives of Ophthalmology, 114*(1), 40-46.

Humayun, M. S., Prince, M., de Juan, E., Barron, Y., Moskowitz, M., Klock, I. B., & Milam, A. H. (1999). Morphometric analysis of the extramacular retina from postmortem eyes with retinitis pigmentosa. *Investigative Ophthalmology & Visual Science, 40*(1), 143-148.

Jensen, R. J. (1991). Intracellular recording of light responses from visually identified ganglion cells in the rabbit retina. *J Neurosci Methods, 40*(2-3), 101-112.

Jensen, R. J., Ziv, O. R., & Rizzo, J. F. (2005). Responses of rabbit retinal ganglion cells to electrical stimulation with an epiretinal electrode. [In Vitro Research Support, U.S. Gov't, Non-P.H.S.]. *Journal of neural engineering, 2*(1), S16-21. doi: 10.1088/1741-2560/2/1/003

Kaplan, E., & Benardete, E. (2001). The dynamics of primate retinal ganglion cells. *Vision: From Neurons to Cognition, 134*, 17-34.

Kelly, S. K. (1998). *A System for Electrical Retinal Stimulation for Human Trials.* Master, MIT.

Kim, S. Y., Sadda, S., Humayun, M. S., De Juan, E., Melia, B. M., & Green, W. R. (2002). Morphometric analysis of the macula in eyes with geographic atrophy due to age-related macular degeneration. *Retina-the Journal of Retinal and Vitreous Diseases, 22*(4), 464-470. doi: Doi 10.1097/00006982-200208000-00011

Kuffler, S. W., Fitzhugh, R., & Barlow, H. B. (1957). Maintained Activity in the Cats Retina in Light and Darkness. *Journal of General Physiology, 40*(5), 683-702. doi: Doi 10.1085/Jgp.40.5.683

Levick, W. R. (1973). Variation in Response Latency of Cat Retinal Ganglion-Cells. *Vision Research, 13*(4), 837-853.

Levick, W. R., Oyster, C. W., & Davis, D. L. (1965). Evidence That Mcilwains Periphery Effect Is Not a Stray Light Artifact. *Journal of Neurophysiology, 28*(3), 555-&.

Levick, W. R., & Thibos, L. N. (1983). Receptive Fields of Cat Ganglion Cells: Classification and Construction. *Prog Retinal Res, 2*, 267-319.

Marc, R. E., Jones, B. W., Watt, C. B., & Strettoi, E. (2003). Neural remodeling in retinal degeneration. *Progress in Retinal and Eye Research, 22*(5), 607-655. doi: Doi 10.1016/S1350-9462(03)00039-9

Margalit, E., & Thoreson, W. B. (2006). Inner retinal mechanisms engaged by retinal electrical stimulation. *Investigative Ophthalmology & Visual Science, 47*(6), 2606-2612. doi: Doi 10.1167/Iovs.05-1093

Martinez-Conde, S., Macknik, S. L., & Hubel, D. H. (2004). The role of fixational eye movements in visual perception. *Nature Reviews Neuroscience, 5*(3), 229-240. doi: Doi 10.1038/Nrn1348

Masland, R. H. (2012). The neuronal organization of the retina. [Research Support, N.I.H., Extramural Review]. *Neuron, 76*(2), 266-280. doi: 10.1016/j.neuron.2012.10.002

McIlwain, J. T. (1966). Some Evidence Concerning Physiological Basis of Periphery Effect in Cats Retina. *Experimental Brain Research, 1*(3), 265-&.

Michelson, A. (1927). *Studies in Optics*: U. of Chicago Press.

Moeller, G. U., Kayser, C., Knecht, F., & Konig, P. (2004). Interactions between eye movement systems in cats and humans. *Experimental Brain Research, 157*(2), 215-224. doi: DOI 10.1007/s00221-004-1835-z

Neher, E. (1992). Correction for liquid junction potentials in patch clamp experiments. *Methods in enzymology, 207*, 123-131.

O'Brien, B. J., Isayama, T., Richardson, R., & Berson, D. M. (2002). Intrinsic physiological properties of cat retinal ganglion cells. *Journal of Physiology-London, 538*(3), 787-802. doi: 10.1113/jphysiol.2001.013009

Ogawa, T., Bishop, P. O., & Levick, W. R. (1966). Temporal Characteristics of Responses to Photic Stimulation by Single Ganglion Cells in Unopened Eye of Cat. *Journal of Neurophysiology, 29*(1), 1-&.

Peichl, L., & Wassle, H. (1983). The Structural Correlate of the Receptive-Field Center of Alpha-Ganglion Cells in the Cat Retina. *Journal of Physiology-London, 341*(Aug), 309-&.

Rizzo, J. F., & Wyatt, J. (1997). Prospects for a visual prosthesis. *Neuroscientist, 3*(4), 251-262. doi: Doi 10.1177/107385849700300413

Robinson, D. W., & Chalupa, L. M. (1997). The intrinsic temporal properties of alpha and beta retinal ganglion cells are equivalent. *Curr Biol, 7*(6), 366-374. doi: S0960-9822(06)00184-9 [pii]

Roska, B., & Werblin, F. (2003). Rapid global shifts in natural scenes block spiking in specific ganglion cell types. *Nat Neurosci, 6*(6), 600-608. doi: 10.1038/nn1061nn1061 [pii]

Santos, A., Humayun, M. S., deJuan, E., Greenberg, R. J., Marsh, M. J., Klock, I. B., & Milam, A. H. (1997). Preservation of the inner retina in retinitis pigmentosa: A morphometric analysis. *Investigative Ophthalmology & Visual Science, 38*(4), 1443-1443.

Schutz, A. C., Braun, D. I., & Gegenfurtner, K. R. (2011). Eye movements and perception: A selective review. *Journal of Vision, 11*(5). doi: Artn 9 doi 10.1167/11.5.9

Schwarz, J. R., & Eikhof, G. (1987). Na Currents and Action-Potentials in Rat Myelinated Nerve-Fibers at 20-Degrees-C and 37-Degrees-C. *Pflugers Archiv-European Journal of Physiology, 409*(6), 569-577. doi: Doi 10.1007/Bf00584655

Sekirnjak, C., Hottowy, P., Sher, A., Dabrowski, W., Litke, A. M., & Chichilnisky, E. J. (2006). Electrical stimulation of mammalian retinal ganglion cells with multielectrode arrays. *Journal of Neurophysiology, 95*(6), 3311-3327. doi: DOI 10.1152/jn.01168.2005

Sekirnjak, C., Hottowy, P., Sher, A., Dabrowski, W., Litke, A. M., & Chichilnisky, E. J. (2008). High-resolution electrical stimulation of primate retina for epiretinal implant design. *Journal of Neuroscience, 28*(17), 4446-4456. doi: Doi 10.1523/Jneurosci.5138-07.2008

Stett, A., Barth, W., Weiss, S., Haemmerle, H., & Zrenner, E. (2000). Electrical multisite stimulation of the isolated chicken retina. *Vision Research, 40*(13), 1785-1795. doi: Doi 10.1016/S0042-6989(00)00005-5

Stone, J., & Clarke, R. (1980). Correlation between Soma Size and Dendritic Morphology in Cat Retinal Ganglion-Cells - Evidence of Further Variation in the Gamma-Cell Class. *Journal of Comparative Neurology, 192*(2), 211-217. doi: DOI 10.1002/cne.901920203

Stone, J. L., Barlow, W. E., Humayun, M. S., de Juan, E., Jr., & Milam, A. H. (1992). Morphometric analysis of macular photoreceptors and ganglion cells in retinas with retinitis pigmentosa. *Arch Ophthalmol, 110*(11), 1634-1639.

Straw, A. D. (2008). Vision egg: an open-source library for realtime visual stimulus generation. *Front Neuroinform, 2*, 4. doi: 10.3389/neuro.11.004.2008

Taylor, W. R., & Wassle, H. (1995). Receptive-Field Properties of Starburst Cholinergic Amacrine Cells in the Rabbit Retina. *European Journal of Neuroscience, 7*(11), 2308-2321. doi: DOI 10.1111/j.1460-9568.1995.tb00652.x

Troy, J. B. (2012). *The Uniqueness of the Message in a Retinal Ganglion Cell Spike Train and its Implication for Retinal Prostheses*. Paper presented at the 34th Annual International Conference of the IEEE EMBS, San Diego, California USA.

Ye, J. H., Ryu, S. B., Kim, K. H., & Goo, Y. S. (2008). Functional connectivity map of retinal ganglion cells for retinal prosthesis. *Korean J Physiol Pharmacol, 12*(6), 307-314. doi: 10.4196/kjpp.2008.12.6.307

Chapter 6

Conclusions

There were two main objectives in this thesis covering basic and applied science research on retinal ganglion cells (RGCs). The first objective was to understand the physiology of the RGCs starting with the investigation of 8 intrinsic properties of the 16 defined rat RGC types (Chapter 2). The work was then extended to the disclosure of the hidden information (variables) in the action potentials (spike), in which spike waveforms, their phase plots, and their associated derivatives were analysed (Chapter 3). The second objective was to discover information to aid in the design of visual prostheses to permit people to recover from blindness. That task began by evaluating whether the RGC activation threshold varies depending upon whether the electrode was placed above or below the inner limiting membrane (ILM) in rat retinas (Chapter 4). The core work on vision recovery was done on cat retinas by reproducing the RGC light-elicited responses (LRs) with electrical stimuli (Chapter 5).

The mammalian retina contains many different RGC types, each of which has its unique functional role for encoding different aspects of the visual scene. Each cell's intrinsic properties are defined by its morphology and membrane characteristics, including the complement and localization of the ion channels expressed. There were two major findings in Chapter 2. The first finding was the diversity of the intrinsic properties among different RGC types. Rat RGCs exhibited a wide variety of intrinsic physiological properties that were correlated with their morphological type. Statistically significant differences among RGC types were found on both passive (threshold, input resistance, time constant) and active properties (spike width, maximum and steady state frequency, frequency adaptation index, anomalous rectification). When RGCs were grouped according to their dendritic stratifications (INNER, OUTER, BISTRAT), we found clear differences between OUTER and BISTRAT cells for most of the intrinsic variables.

Different retinas have developed during evolution but the sole purpose of vision is similar, which is to survive. The anatomy of retinas are diverse, however, they all at least have the same rudimentary functions such as to detect contrast, colours and motion in order to find food and avoid predictors. Therefore, we suspected that the morphologically homologous RGC types in different species might be functionally similar, hence have conserved intrinsic

properties. The second finding was the conservation of the intrinsic properties between the morphological homologs in rat and cat RGCs. We found the rat A2 cells exhibited nearly identical patterns of intrinsic properties to the cat alpha cells, whereas rat D2 cells have very different patterns than the putative cat homolog, the iota cell. Rat B2 cells and beta cells were somewhat in between despite their morphological resemblance. Nonetheless, we are not satisfied with the RGC classification by only the morphology identification or with the intrinsic properties alone. Perhaps a better way to identify RGCs is to find their genetic nametags (Siegert et al., 2009).

RGCs communicate using spikes, therefore spike waveforms and spike firing patterns are informative. Spikes are initiated in the axon initial segment that contains a heterogeneous collection of voltage-gated ion channels. In Chapter 3, we extended the studies from the previous chapter by examining details of the spike waveform dynamics. Spike shapes give us an insight into the independent information of the RGCs. Along with the first and second order derivatives of the membrane potential vs. time plots, we assessed the effect of trans-membrane properties by examining 5 parameters. The phase plots showed us the change of the membrane potential due to specific membrane voltage by examining another 6 parameters, and provided evidence of the existence of axonal and somatic spikes in the two-hump phase plots. We used a principal component analysis based factor analysis to study the 11 parameters, and concluded that a four-factor model is possibly adequate for RGC classification. The correlations between the four factors and the original variables provide some evidence as to what parameters one might measure in future to achieve better classification, or at least identify which intrinsic variables are not useful.

The parameters in Chapter 2 and 3 (total 19) were used for RGC modelling (not reported here). Together with the 3-D RGC images (from Chapter 2), they might be useful for more advanced RGC classifications (not reported here). We were aware of the temperature effects, which affected the kinetics of the RGC responses. The rat data were acquired at room temperature, so that we could compare with the previously published cat intrinsic data (O'Brien, Isayama, Richardson, & Berson, 2002). After the regular protocols were completed,

the experiments in Chapter 2 were repeated with the temperature increased to ~33 °C in 18 RGCs (unpublished data), and the influences were up to 2-fold. As the dataset expands in the future, we can have a better assessment of the temperature effect.

Then we moved on to the engineering part of this thesis. We would like to learn more about the stimulus environment (i.e. the inner retina) for the design of an epiretinal prosthesis. Chapter 4 was a transitional chapter where we studied the stimulating electrode positions and worked on comparing preparations for the final chapter. First, we wanted to know the variances of the activation threshold in two extracellular stimulating positions: one was at the surface of the inner retina (above ILM) and the other was minimally penetrating into the retina (below ILM). We found that the threshold stimulus amplitudes were lower when the electrode was placed below the ILM, compared to above. However, the median thresholds between those two positions have no significant difference. In addition, we noticed that the relation between the orientation of the stimulus bipole and the direction of the target RGC's axon is a critical factor that affected the threshold. Furthermore, we observed two spikes being evoked by a single biphasic impulse, which was different from the usual 1-stimulus-1-spike scheme. It is possible that the second spike was 'reflected' from the damaged ends of some of the axons, unfortunately we only have circumstantial evidence. If that was the case, the damaged/unhealthy RGCs might respond inconsistently to the electrical stimulation of the prosthesis. That will increase the difficulty of obtaining precise temporal electrically-evoked responses (ERs).

There were many decisions to make (some with no choices) before the final mission of studying vision recreation in Chapter 5. We chose cats as our model because we knew quite a few things about cat retinas and RGCs; for example, the well-established receptive field properties. It might not be the ideal preparation for a human retinal prosthesis but the cats were the best available model at that time. In addition, we sacrificed fewer animals by obtaining the retinas from other labs after their experiments. The choice of micro-scale nitrogen doped ultra-nanocrystaline diamond (N-UNCD) electrodes instead of other types of commercially available electrodes was because our collaborators are planning to use the N-

UNCD electrodes in an implant. The effectiveness of the N-UNCD electrodes was not discussed in this thesis but we suspect that some of the results might be disturbed by the deficiency of the electrodes, which proved to be quite easily damaged.

The idea of a retinal prosthesis is to help people recover vision from blindness, especially those suffering from retinitis pigmentosa, by making use of the surviving retinal neurons. The goal of chapter 5 was to replicate the LRs produced by assorted light stimuli: standing contrasts, moving gratings, and naturalistic videos that comprise saccadic eye movements. We constructed the stimulus patterns (SPs) with a train of asymmetric charge-balanced biphasic pulses according to the spike times of the LRs. To find the optimal parameters of the biphasic waveform is a difficult task since the performance depends on many factors, such as the biophysics of the target RGC, the orientation of the axon, and the healthiness of the tissue at the stimulus location. Therefore we set the phases of the cathodic first biphasic pulse and its interphase interval to fixed durations, but made the current amplitudes of the phases variable in a 4 to 1 ratio to maintain net zero charge. We evaluated the results by finding the cross-correlations between the SPs (essentially the LR) and the ERs of each RGC recorded. Our data suggested that, the brisk-transient (BT) RGCs were more capable of reconstructing the LRs than the brisk-sustained (BS) RGCs. There was a statistically significant difference of the following competency between the BT and BS types. The OFF-centre BT RGCs had the best performance

For those RGCs with low performance, 8 RGCs failed to evoke 100% efficacy during the preliminary 10-pulse stimulation tests. By examining the raster plots, we noticed that these RGCs were not just incapable of evoking spikes, they were almost completely inhibited by the electrical stimulation for unknown reasons. We speculate that this was due to mass activation of many cell types at once. Another possibly related observation was that of the postponed firing adaptation. This requires further study but in 14 RGCs, this adaptation appeared consistently after high frequency (400 Hz) stimulation (unpublished data). The firing rate reduced approximately 5 seconds after the stimulation, and continuing to slow down for another 5 seconds and then gradually recovered. The cause of that adaptation phenomenon is

uncertain. One possibility is that the electrical stimulation activated the rest of the retinal neurons, such as the amacrine cells and the bipolar cells, hence indirectly altered the RGC responses. Perhaps in later experiments we can try dual patching of abutting BT and BS RGCs, and compare their concurrent ERs under approximately the same SP.

We are interested in implanting a prosthesis onto the high visual acuity area (fovea), therefore the size of any multi-electrode array (MEA) is restricted. The spatial resolution of the artificial vision is in general proportional to the square root of number of electrodes in the MEA, and also the selectivity of the electrodes (slightly better for hexagonal arrays (Mersereau, 1979; Petersen & Middleton, 1962)). An ideal stimulus strategy is to have one electrode that stimulates one (and only one) RGC and produces one output to the brain. This is not practical as we have ~1.2 million RGCs in the human retina, and their receptive fields are overlapping with each other. Each electrode covers thousands of RGCs (i.e. low selectivity). However, since we are dealing with degenerate retinas, we can only make use of the surviving RGCs. It was suggested that a 25 by 25 MEA is good enough to form a recognisable pixelated image (Cha, Horch, & Normann, 1992). For each electrode in the MEA, perhaps we can target the more controllable/capable BT RGCs to output our desired spike trains, and form a fully configurable phosphene-based image in the brain? That image will probably contain 'noise' generated from the rest of the surrounding RGCs but the image should be dominated by the outputs of the target RGCs. Just a thought.

There are other interesting vision recovery approaches, not investigated here but worth mentioning. One of these is to replace the photoreceptors with stem cells. This technique has been studied in animal models (Ali et al., 2000; Canola et al., 2007; Lamba, Gust, & Reh, 2009). Such an approach preserves the signal processing within the retina, however, it is not yet determined if the newborn photoreceptors connect to the appropriate secondary neurons (horizontal cells and bipolar cells). Another issue arising from this approach is the consequential degeneration of retinal circuits after the loss of photoreceptors. Some of the retinal circuitry might be disconnected (Marc, Jones, Watt, & Strettoi, 2003).

Another way is to activate the remaining intact RGCs directly is by delivering proteins that act as light-gated ion channels onto the target RGCs, a method employing both integrated optics and genetics called optogenetics (Miesenbock, 2011; Zhang et al., 2010). The proteins will act as artificial light-gated ion channels, which can be activated by specific wavelengths of light and allow exchange of ions in or out of the neurons (Boyden, Zhang, Bamberg, Nagel, & Deisseroth, 2005). Thus, the neurons can be excited or inhibited by light, depending on what kind of protein is delivered to them. Some researchers have started to develop optogenetics tools to make the RGCs become photosensitive and controllable by specific wavelengths of light (Busskamp, Picaud, Sahel, & Roska, 2011; Cronin & Bennett, 2011; Deisseroth, 2011; Grossman et al., 2009; Thyagarajan et al., 2010).

The diversity of the RGC types and the low selectivity of the MEA limits the spatial resolution of phosphene-based images in the currently proposed generation of electrical retinal prostheses. With the aid of optogenetics, perhaps we can focus on just one type of retinal neuron. Besides BT RGCs, another suitable candidate might be the A-II amacrine cells (personal communication with Professor William Levick, based on Professor Heinz Wassle's talk). Targeting the A-II amacrine cells has some advantages since they are set up with a pre-wired push-pull output to the inner plexiform layer: the excitatory output goes through the ON-cone-bipolar synapses to the ON-centre RGCs, and the simultaneous inhibitory output inhibits the OFF-cone-bipolar synapses that drive the OFF-centre RGCs. This preserves the natural push-pull output of the RGC layer and covers both the ON and OFF pathways. Furthermore, there are many more A-II amacrines that can be transduced by a targeted virus vector than the relatively few RGCs of a particular sub-set (Auricchio et al., 2001; Hellstrom & Harvey, 2011). So the resulting photosensitivity would have a much greater effect on vision, and effective photic stimulation would be well below the damage threshold. The topographic resolution of the A-II amacrine population is potentially finer than that of the RGC arrays as well.

6.1 References

Ali, R. R., Sarra, G. M., Stephens, C., de Alwis, M., Bainbridge, J. W. B., Munro, P. M., . . . Thrasher, A. J. (2000). Restoration of photoreceptor ultrastructure and function in retinal degeneration slow mice by gene therapy. *Nature Genetics, 25*(3), 306-310. doi: Doi 10.1038/77068

Auricchio, A., Kobinger, G., Anand, V., Hildinger, M., O'Connor, E., Maguire, A. M., . . . Bennett, J. (2001). Exchange of surface proteins impacts on viral vector cellular specificity and transduction characteristics: the retina as a model. *Human Molecular Genetics, 10*(26), 3075-3081. doi: DOI 10.1093/hmg/10.26.3075

Boyden, E. S., Zhang, F., Bamberg, E., Nagel, G., & Deisseroth, K. (2005). Millisecond-timescale, genetically targeted optical control of neural activity. *Nature Neuroscience, 8*(9), 1263-1268. doi: Doi 10.1038/Nn1525

Busskamp, V., Picaud, S., Sahel, J. A., & Roska, B. (2011). Optogenetic therapy for retinitis pigmentosa. *Gene Ther*. doi: gt2011155 [pii] 10.1038/gt.2011.155

Canola, K., Angenieux, B., Tekaya, M., Quiambao, A., Naash, M. I., Munier, F. L., . . . Arsenijevic, Y. (2007). Retinal stem cells transplanted into models of late stages of retinitis pigmentosa preferentially adopt a glial or a retinal ganglion cell fate. *Investigative Ophthalmology & Visual Science, 48*(1), 446-454. doi: Doi 10.1167/Iovs.06-0190

Cha, K. H., Horch, K., & Normann, R. A. (1992). Simulation of a Phosphene-Based Visual-Field - Visual-Acuity in a Pixelized Vision System. *Annals of Biomedical Engineering, 20*(4), 439-449. doi: Doi 10.1007/Bf02368135

Cronin, T., & Bennett, J. (2011). Switching on the lights: the use of optogenetics to advance retinal gene therapy. *Mol Ther, 19*(7), 1190-1192. doi: mt2011115 [pii] 10.1038/mt.2011.115

Deisseroth, K. (2011). Optogenetics. *Nat Methods, 8*(1), 26-29. doi: nmeth.f.324 [pii] 10.1038/nmeth.f.324

Grossman, N., Nikolic, K., Poher, V., McGovern, B., Drankasis, E., Neil, M., . . . Degenaar, P. (2009). Photostimulator for Optogenetic Retinal Prosthesis. *2009 4th International Ieee/Embs Conference on Neural Engineering*, 68-71. doi: Doi 10.1109/Ner.2009.5109236

Hellstrom, M., & Harvey, A. R. (2011). Retinal Ganglion Cell Gene Therapy and Visual System Repair. *Current Gene Therapy, 11*(2), 116-131.

Lamba, D. A., Gust, J., & Reh, T. A. (2009). Transplantation of human embryonic stem cell-derived photoreceptors restores some visual function in Crx-deficient mice. *Cell Stem Cell, 4*(1), 73-79. doi: S1934-5909(08)00538-9 [pii] 10.1016/j.stem.2008.10.015

Marc, R. E., Jones, B. W., Watt, C. B., & Strettoi, E. (2003). Neural remodeling in retinal degeneration. *Progress in Retinal and Eye Research, 22*(5), 607-655. doi: Doi 10.1016/S1350-9462(03)00039-9

Mersereau, R. M. (1979). Processing of Hexagonally Sampled 2-Dimensional Signals. *Proceedings of the Ieee, 67*(6), 930-949. doi: Doi 10.1109/Proc.1979.11356

Miesenbock, G. (2011). Optogenetic Control of Cells and Circuits. *Annual Review of Cell and Developmental Biology, Vol 27, 27*, 731-758. doi: DOI 10.1146/annurev-cellbio-100109-104051

O'Brien, B. J., Isayama, T., Richardson, R., & Berson, D. M. (2002). Intrinsic physiological properties of cat retinal ganglion cells. *Journal of Physiology-London, 538*(3), 787-802. doi: 10.1113/jphysiol.2001.013009

Petersen, D. P., & Middleton, D. (1962). Sampling and Reconstruction of Wave-Number-Limited Functions in N-Dimensional Euclidean Spaces. *Information and Control, 5*(4), 279-&. doi: Doi 10.1016/S0019-9958(62)90633-2

Siegert, S., Scherf, B. G., Del Punta, K., Didkovsky, N., Heintz, N., & Roska, B. (2009). Genetic address book for retinal cell types. *Nature Neuroscience, 12*(9), 1197-U1130. doi: Doi 10.1038/Nn.2370

Thyagarajan, S., van Wyk, M., Lehmann, K., Lowel, S., Feng, G. P., & Wassle, H. (2010). Visual Function in Mice with Photoreceptor Degeneration and Transgenic Expression of Channelrhodopsin 2 in Ganglion Cells. *Journal of Neuroscience, 30*(26), 8745-8758. doi: Doi 10.1523/Jneurosci.4417-09.2010

Zhang, F., Gradinaru, V., Adamantidis, A. R., Durand, R., Airan, R. D., de Lecea, L., & Deisseroth, K. (2010). Optogenetic interrogation of neural circuits: technology for probing mammalian brain structures. *Nature Protocols, 5*(3), 439-456. doi: DOI 10.1038/nprot.2009.226